

**DTIC FILE COPY**

AFOSK-IR. 88-1252

ΣΧΗΜΑ 2

# Control of Flexible Structures: Model Errors, Robustness Measures, and Optimization of Feedback Controllers

# aerospace engineering department



***John L. Junkins***      ***S. Rao Vadali***

# TEXAS A&M UNIVERSITY

**October 31, 1988**

**Final Report Contract No. F496-86-K-0014DEF**  
**Air Force Office of Scientific Research**

Approved for public release  
Distribution unlimited.

**AIR FORCE OFFICE OF SCIENTIFIC RESEARCH (AFSC)**  
**ATTENTION: TRANSMITTAL TO DTIC**  
 This document has been reviewed and is  
 approved for release IAW AFR 190-12.  
 No further action required.  
**MANUAL NUMBER**  
**COPY CONTROL AND INFORMATION DIVISION**

DEC 08 1988

TEXAS ENGINEERING EXPERIMENT STATION

unclassified

SECURITY CLASSIFICATION OF THIS PAGE

ADA202234

## REPORT DOCUMENTATION PAGE

Form Approved  
OMB No. 0704-0188

1a. REPORT SECURITY CLASSIFICATION <u>Unclassified</u>			1b. RESTRICTIVE MARKINGS	
2a. SECURITY CLASSIFICATION AUTHORITY			3. DISTRIBUTION / AVAILABILITY OF REPORT <u>Approved for public release, distribution unlimited</u>	
2b. DECLASSIFICATION / DOWNGRADING SCHEDULE				
4. PERFORMING ORGANIZATION REPORT NUMBER(S)			5. MONITORING ORGANIZATION REPORT NUMBER(S) <b>AFOSR-TR- 88-1252</b>	
6a. NAME OF PERFORMING ORGANIZATION Texas A&M University	6b. OFFICE SYMBOL (If applicable) AERO	7a. NAME OF MONITORING ORGANIZATION <u>AFOSR</u>		
6c. ADDRESS (City, State, and ZIP Code) Aerospace Engineering Department College Station, Texas 77843-3141		7b. ADDRESS (City, State, and ZIP Code) <u>same as 8c.</u>		
8a. NAME OF FUNDING / SPONSORING ORGANIZATION AFOSR	8b. OFFICE SYMBOL (If applicable) N/A	9. PROCUREMENT INSTRUMENT IDENTIFICATION NUMBER <u>F49600-86-K-0014</u>		
8c. ADDRESS (City, State, and ZIP Code) Bolling AFB, DC 20332-6648		10. SOURCE OF FUNDING NUMBERS		
		PROGRAM ELEMENT NO. <u>1011024</u>	PROJECT NO. <u>230</u>	TASK NO. <u>B1</u>
11. TITLE (Include Security Classification) Control of Flexible Structures: Model Errors, Robustness Measures, and Optimization of Feedback Controllers" <u>(U)</u>				
12. PERSONAL AUTHOR(S) John L. Junkins and S. Rao Vadali				
13a. TYPE OF REPORT FINAL	13b. TIME COVERED FROM <u>6/1/86</u> TO <u>8/31/88</u>	14. DATE OF REPORT (Year, Month, Day) October 31, 1988	15. PAGE COUNT 301	
16. SUPPLEMENTARY NOTATION				
17. COSATI CODES			18. SUBJECT TERMS (Continue on reverse if necessary and identify by block number)	
FIELD	GROUP	SUB-GROUP	Active Control, Structural Analysis, spacecraft Maneuvers, Robust Control	
19. ABSTRACT (Continue on reverse if necessary and identify by block number)  This report summarizes new methods for flexible structures' dynamic analysis, system identification, and maneuver controls. New control design methods are introduced for considering several competing performance measures simultaneously. A new attitude control method using single gimbal control moment gyros is introduced. New results and insights on singularity avoidance are presented. A method is given for simultaneous optimization of structural design parameters and a feedback controller.				
20. DISTRIBUTION / AVAILABILITY OF ABSTRACT <input checked="" type="checkbox"/> UNCLASSIFIED/UNLIMITED <input checked="" type="checkbox"/> SAME AS RPT. <input checked="" type="checkbox"/> DTIC USERS			21. ABSTRACT SECURITY CLASSIFICATION unclassified	
22a. NAME OF RESPONSIBLE INDIVIDUAL Dr. A. K. Amos			22b. TELEPHONE (Include Area Code) (202) 767-4931	22c. OFFICE SYMBOL AFOSR/NA

**Control of Flexible Structures:  
Model Errors, Robustness Measures, and Optimization  
of Feedback Controllers**

**John L. Junkins  
S. Rao Vadali**

**Department of Aerospace Engineering  
Texas A&M University  
College Station, Texas 77843**

**October, 1988**

**Final Report  
Contract No F49620-86-K-0014DEF  
Air Force Office of Scientific Research**

**8 8 12 8 099**

## **CONTRIBUTORS**

### **Principal Investigators:**

**John L. Junkins  
S. Rao Vadali**

### **Research Assistants:**

**R. Byers  
N. G. Creamer  
G. H. James, Jr.  
Y. Kim  
K. B. Lim  
H-S. Oh  
D. W. Rew  
G. Tallant  
R. C. Thompson**



## SUMMARY

This document constitutes the final report on research performed at Texas A&M University under Air Force Office of Scientific Research Contract No. F49620-86-K-0014DEF. This program was coordinated by Dr. A. K. Amos of AFOSR and Dr. Alok Das of AFAL; their technical liason and support are gratefully acknowledged.

The research project addressed a family of coupled research topics:

- (1) Optimal Control of Large Angle Maneuvers
- (2) Design of Robust Feedback Controllers
- (3) Unified Structure/Controller Optimization
- (4) System Identification and Optimal Estimation
- (5) Scaling Laws for Flexible Structure Experiments

In each of the above areas we have made one or more significant research contributions during the past two years. Each contribution is discussed in detail in an attachment. In the text, we provide an executive summary of the main features of our contributions in each area. Accordingly, this report is organized in six subsections; one subsection for each of the above topics and a conclusions section.

Accession For	
NTIS GRA&I	<input checked="" type="checkbox"/>
DTIC TAB	<input type="checkbox"/>
Unannounced	<input type="checkbox"/>
Justification	
By _____	
Distribution/	
Availability Codes	
Dist	Avail and/or Special
A-1	



## CONTENTS

SECTION	TOPIC	PAGE
1.0	Optimal Control of Large Angle Maneuvers	4
2.0	Design of Robust Feedback Controllers	5
3.0	Unified Structure/Controller Optimization	6
4.0	System Identification and Optimal Estimation	7
5.0	Scaling Laws for Flexible Structure Experiments	8
6.0	Conclusions	10
	References	11
	Attachment Index	12
	Attachments	13 - 300
	Report Documentation Form	301

## **1.0 Optimal Control of Large Angle Maneuvers**

In Attachment 1, we present a new method for near-minimum time control of flexible vehicles. This paper introduces open loop torque shaping methods which allows the engineer to replace the sharp on/off control discontinuities and sign switches (typical of minimum time bang-bang controllers) by smoothed torque profiles. Examples are presented in which we demonstrate the feasibility of directly trading off residual structural vibration versus modest increases in the maneuver time. Our approach allows explicit, non-iterative satisfaction of controller saturation bounds. In Reference 1, this method is presented in greater detail and several additional examples are presented.

In Attachment 2, we present a closed loop control law which captures the attractive features of the torque-shaped open loop control, while gaining the convenience and robustness of a closed loop law. Prior to achieving the neighborhood of the target state, the control resembles the corresponding near-bang-bang smoothed open loop control, but smoothly transitions into a fine pointing and vibration suppression control in the end-game. In Reference 2, this approach is considered in more detail and several examples are considered, including a two-body system.

In Attachment 3, we discuss a novel scheme for steering Single Gimbal Control Moment Gyros (SCMG) in order to maneuver spacecraft. The new formulation is based on improved detailed modeling of the SCMG system including often neglected gimbal and rotor transverse moments of inertia. A new discovery that for a given maneuver, there exists an optimal set of initial gimbal angles (of many such sets) can dramatically reduce the effect of intrinsic singularities. The validity of the method is illustrated through a simulation study, and several issues for further study are identified in Attachment 3.

## **2.0 Design of Robust Feedback Controllers**

In Attachments 4-7, we present several new methods for designing and analyzing robust feedback controllers for flexible structures. In attachments 4-5, we present parameterizations of feedback gains which permit non-iterative assignment of closed loop eigenvalues and subject to these eigenvalue constraints, op-

ment of closed loop eigenvalues and subject to these eigenvalue constraints, optimization of a measure of robustness with respect to model errors. We believe these methods are important new tools for design of high-dimensioned feedback controllers. Reference 3 provides a detailed presentation of the theoretical issues and places these ideas into the context of existing literature on design of feedback controllers.

In Attachment 6, we present a novel analytical formulation for determining the sensitivity of eigenvalues and eigenvectors for non-self-adjoint problems. We correct a significant conceptual misunderstanding and formulation error made in several existing publications on this subject and verify the analytical formulations, to seven digits, by a finite difference method. The essence of the conceptual and formulation error, which we corrected, is that the projection of the gradient of an eigenvector onto itself is non-zero except for the special case of a self-adjoint system. Assumptions to the contrary have been routinely published, as discussed in Attachment 6. Since self-adjoint systems are almost invariably obtained for mechanical systems with feedback control loops closed, and since eigensolution sensitivity is an important issue in robust control, this result is of widespread significance.

In Attachment 7, we present an analytical treatment of an interesting question: The probability of stability in the presence of model errors. We introduce a methodology for calculating *the probability of stability* and address the issue of optimizing free parameters (such as control gains) to maximize the probability of stability. These results are primarily of conceptual and analytical significance, however they do provide an analytical justification for the robustness index introduced in Reference 4.

### 3.0 Unified Structure/Controller Optimization

In Attachment 8, we introduce several important new ideas. We develop a method for considering several performance indices simultaneously in designing a family of control laws which display the tradeoff (eg. control effort versus performance errors versus sensitivity with respect to model errors).

We also develop and apply an algorithm for simultaneous design of selected structural parameters, sensor locations, actuator locations, and control gains.

In this optimization example, (a 55 dimensioned parameter space) we consider three performance measures: (i) Minimum mass, (ii) Minimum sum square eigenvalue sensitivity, and (iii) Maximum robustness (Patel-Toda index). In this example, we found over 30% improvement in actual stability margins (in the 55 dimensional parameter space) with respect to parameter variations as a consequence of robustness optimization, as compared to the minimum mass design. In Reference 4, this subject is developed in detail along with a thorough discussion of the literature.

#### **4.0 System Identification and Optimal Estimation**

In Attachments 9 and 10, we present two significant contributions to system identification and optimal estimation. In Attachment 9, we summarize a new method for structural identification. The method introduces a general way to parameterize large flexible structures by re-scaling the nominal contributions of a prescribed set of substructures to the global mass, stiffness, and damping matrices. A modal energy partitioning method is used to guide the selection of substructures. The scaling parameters are estimated considering the measured and modeled free vibration parameters (a subset of the eigenvalues and eigenvectors) and the measured and modeled forced vibration parameters (frequency response functions, over a frequency bandwidth of interest). The free and forced model parameters are brought simultaneously into least square agreement with their measured values by adjusting the mass, stiffness, and damping parameters. These ideas are applied to several examples in Attachment 9; in Reference 5, additional examples and an expanded discussion of the analytical details are presented.

In Reference 6, we present a Kalman Filter estimation algorithm and simulation results for spacecraft attitude estimation. Attitude is parameterized using the Rodriguez parameters and orthogonal components of angular velocity.

In Attachment 10, we consider the situation that large non-random errors are believed present between the best available mathematical model and the actual physical system. We present a novel approach which estimates the smallest (integral sum square) additive model acceleration error which, when incorporated into the system differential equations, causes the revised model prediction of the

system response to "agree statistically" with the measured response. Statistical agreement is defined by the the fit residuals' covariance matrix matching the assumed known covariance matrix of the measurement process. This simple idea has led to good results on several low dimensioned examples, but the algorithms have not been successfully demonstrated on systems of moderate or high dimensions. Several difficult issues have been encountered associated with how large the measurement sample should be before it is meaningful to enforce the implicit equality of two covariance matrices. In spite of these unresolved issues, this method appears promising. In several examples, we have found the method superior to the conventional Kalman Filter estimators, which makes provision only for process-noise (stochastic model errors), and does not explicitly estimate the model error history.

## **5.0 Scaling Laws for Flexible Structure Experiments**

In Attachment 11, we report on our work on development of scaling laws for ground-based testing of large space structures. We have examined some concepts regarding the scaling of large spacecraft to laboratory sized models, while preserving the dynamic behavior of the system. Proportional changes only in physical dimensions could result in a stiffer system, and consequently, a frequency response radically different from the response of the actual large-scale structure. Some simple formulae were developed for scaling structural mass and material properties such that the modal frequencies are preserved. Our ultimate goal was to include experimental results obtained from testing scale models of thin-walled tubing proposed for space based laser configurations; however, components in the correct sizes and materials were not readily available. In the attachment, we discuss the derivation of the scaling formulae, and the difficulties encountered in the experimental verification of the concepts.

Another topic, unrelated to the scaling concepts, but nevertheless of utmost importance to the experimental testing of large flexible structures, pertains to the use of accelerometers to measure local accelerations of the structure. It was observed during experiments on the AFAL grid structure, that accelerometer data indicated a phase shift of  $\pi$  radians at specific locations on the structure. Knowing that such a phase shift does not occur (structurally at least), we investigated this

behavior analytically and experimentally for simple beam structures. We found an apparently unknown result, or at least a heretofore unpublished truth: rotational motion of the accelerometers in a gravity field causes an error in the output signal, due to the perceived change in gravity as the sensor rotates. The importance of this observation is clear: In order to obtain full benefit from the accelerometer measurements, we must predict and compensate for the gravity-induced accelerometer measurement errors in order to obtain accurate knowledge of the motion of the structure. This is particularly true when the accelerometer measurements are employed in the determination of active controls applied to the structure. In Attachment 12, we briefly present the underlying principle regarding accelerometer measurement errors and discuss experimental procedures used to verify the analytical predictions. A more complete treatment of the response of accelerometers in a gravity field, is given in the attached paper entitled "Low-Frequency Response of Accelerometers for Observer Design in a Gravity Environment." Compensation for the gravity effect is incorporated into an observer design for the AFAL grid structure, with both analytical and experimental results included. This paper has been peer-reviewed and accepted for publication in AIAA JGCD.

## 6.0 Conclusions

During the course of this research project, we have been fortunate to have developed a number of significant results which promise to impact future applications as well as define avenues for further research. Throughout this project, we have emphasized balance between careful analytical developments and pragmatic experimentation and numerical demonstrations to evaluate the practical potential of the ideas under study. The above executive summaries and the attachments detail these contributions. It is significant that nine excellent graduate students' theses and dissertation research were partially supported by the funds of this contract. Seven of these students completed M. S. or Ph. D. degree programs during the course of this project. These excellent students, the Principal Investigators, and Texas A&M University have been significantly accelerated by the performance of this research. It is evident that the project has produced an excellent return on AFOSR's investment in our research program.



## REFERENCES

1. Thompson, R. C., Solution of Two-Point Boundary Value Problems in Optimal Manuevers of Flexible Vehicles, Ph. D. Dissertation, Engineering Mechanics, Virginia Tech, 1987.
2. Byers, R. M., Feedback Control Design for Smooth Near-Minimum Time Rotational Maneuvers of Flexible Spacecraft, M. S. Thesis, Department of Aerospace Engineering, Texas A&M University, 1987.
3. Rew, D. W., Robust Control of Large Flexible Structures: A Multi-Criterion Approach, Ph. D. Dissertation, Engineering Mechanics, VA Tech, 1987.
4. Lim, K. B., A Unified Approach to Simultaneous Structure and Controller Design Optimizations, Ph. D. Dissertation, Engineering Mechanics, Virginia Tech, 1986.
5. Creamer, N. G., Identification of Flexible Structures, Ph. D. Dissertation, Engineering Mechanics, Virginia Tech, Blacksburg, VA, 1987.
6. Tallant, G. S., A Kalman Filtering Technique for Spacecraft Attitude Determination and Control Using Gibbs Vector, M. S. Thesis, Department of Aerospace Engineering, Texas A&M University, 1988.

## ATTACHMENT INDEX

ATTACHMENT NUMBER	TITLE	PAGE
1	Near Minimum Time Open Loop Control of Dynamic Systems	13
2	Feedback Control Design for Smooth, Near-Minimum Time Rotational Maneuvers of Flexible Spacecraft	25
3	Feedback Control and Steering Laws for Spacecraft Using Single Gimbal Control Moment Gyros	56
4	Robust Eigenstructure Assignment by a Projection Method: Applications Using Multiple Optimization Criteria	129
5	Robust Eigensystem Assignment for Flexible Structures	167
6	Re-Examination of Eigenvector Derivatives	185
7	Probability of Stability: New Measures of Stability Robustness for Linear Dynamical Systems	194
8	Unified Optimization of Structures and Controllers	210
9	An Identification Method for Flexible Structures	243
10	Minimum Model Error Estimation for Poorly Modeled Dynamic Systems	253
11	Ground-Based Testing of Large Flexible Spacecraft	262
12	Low Frequency Response of Accelerometers for Observer Design in a Gravity Environment	280

## **ATTACHMENT 1**

# **Near Minimum Time Open Loop Control of Dynamic Systems**

Paper No. AIAA 87-0958-CP

**NEAR MINIMUM TIME OPEN LOOP CONTROL  
OF DYNAMIC SYSTEMS**

**R. C. Thompson, J. L. Junkins, and S. R. Vadali**  
Texas A & M University  
College Station, TX

AIAA Dynamics Specialists Conference  
April 9-10, 1987  
Monterey, CA

## NEAR MINIMUM TIME OPEN LOOP CONTROL OF DYNAMIC SYSTEMS

R. C. Thompson<sup>1</sup>

J. L. Junkins<sup>2</sup>

and

S. R. Vadali<sup>3</sup>

### Abstract

Minimum time, open loop, optimal controls are calculated for single axis maneuvers of a flexible structure. By shaping the control profile with two independent and arbitrary parameters, a wide variety of control shaping can be accomplished. Based upon the dynamics of the model, with a normalized time scale, the resulting Pontryagin's necessary conditions yield a fully nonlinear fixed final time, fixed final state, Two-Point Boundary Value Problem. Upon generating numerical solutions to the problem, the final maneuver time and residual flexural energy are compared to the bang-bang solution as a measure of the success of a given maneuver. Examples presented illustrate the control of flexible modes in addition to the rigid body mode, as well as the qualitative and quantitative effect of the torque shape parameters.

### Introduction

Near-minimum time attitude control of flexible spacecraft with active vibration suppression is a topic of current research. Although true minimum time maneuvers have been examined (Ref. 8), such bang-bang controls cause spillover effects which induce high residual flexural energy. Furthermore,

the control profiles generated in true minimum time problems are impossible to implement perfectly with any hardware due to the instantaneous and multiple switching required by the control theory. Consequently, minimum time optimal control problems are of academic interest only for producing a theoretical lower bound for the maneuver time.

Upon modifying the control profile with a smoothing function and transforming the independent variable (time), a near minimum time problem is generated with the mathematical form of a fixed time nonlinear optimal control problem. The resulting boundary-value-problem yields to a number of established methods of numerical solution. The controls are attenuated in such a way that the magnitude of the control rises smoothly from zero to the bounded maximum at the initiation of the maneuver, and typically has an identically shaped reduction to zero at the final time. In addition, any instantaneous switch during the maneuver is shaped using a smooth continuous function. The sharpness of the control trajectory is determined by a set of arbitrary parameters such that we can produce profiles with low control rates as well as controls which approach, to any desired degree, the bang-bang minimum time solution. The independent variable is transformed such that a linear free final time optimal control problem is converted to a nonlinear fixed time problem, where the maneuver time is contained explicitly as a state variable in the transformed system. This augmented fixed time problem can then be solved numerically for the controls and the corresponding minimum time required to complete the maneuver.

The behavior of the system in response to the optimal controls specified by the set of parameters can be examined to determine tradeoffs necessary to accomplish certain mission objectives. For example, near bang-bang controls offer the shortest maneuver time, however control spillover into the flexible modes will induce structural vibration, perhaps to an unacceptable degree. Conversely, a smoothly varying control reduces the spillover, but may drastically increase the time required to complete the maneuver. We examine issues such as the minimum time required and residual structural energy for various representative control profiles.

<sup>1</sup>Research Associate, Aerospace Engineering,  
Texas A&M University, College Station,  
Texas 77843, Member AIAA

<sup>2</sup>Professor of Aerospace Engineering,  
Texas A&M University, College Station,  
Texas 77843 Fellow AIAA

<sup>3</sup>Assistant Professor of Aerospace Engineering,  
Texas A&M University, College Station, Texas  
77843 Member AIAA

Numerical examples for a low order flexible body are included to demonstrate the implementation of the algorithm and to support our development of a general, effective, and practical approach to producing near minimum time open-loop control of flexible vehicles.

### True Minimum Time Optimal Control Problem

Consider a flexible body described by a set of linear, undamped, ordinary differential equations of motion of the form

$$M\ddot{x} + Kx = Gu \quad (1)$$

where  $M$  is an  $n$  by  $n$  positive definite mass matrix,  $x$  is an  $n$  by 1 vector of configuration coordinates,  $K$  is an  $n$  by  $n$  positive semidefinite stiffness matrix,  $G$  is an  $n$  by  $m$  control influence matrix, and  $u$  is an  $m$  by 1 control vector. The admissible controls  $u(t)$  must satisfy saturation bounds  $|u(t)| \leq u_{\max}$  (every element of  $u(t)$  is bounded). We shall transform Eq. (1) into a set of uncoupled equations in order to reduce the complexity of the optimal control problem. For low order models, or models of discrete systems, this procedure may be unnecessary, although it will greatly simplify the coding effort. However, we must recognize that a discrete representation of any continuous system given by Eq. (1) involves some degree of approximation, which typically means that a number of the higher frequency modes will be inaccurately predicted by this model of the structure. Therefore, there is a practical reason for restricting our attention to the modes (typically some lower few) that are accurately represented for the system under consideration.

By solving the algebraic eigenvalue problem associated with the unforced equations of motion for the diagonal eigenvalue matrix,  $\Lambda$ , and the eigenvector (modal) matrix,  $E$ ; the equations of motion may be uncoupled such that

$$\ddot{\eta} + \Lambda\eta = Bu \quad (2)$$

where

$$E^T M E = I, \quad E^T K E = \Lambda$$

$$x = E\eta, \quad \eta = E^T M x$$

$$B = E^T G, \quad |u(t)| \leq u_{\max}$$

In the development of the near minimum time optimal control problem, we shall seek to control only a subset of the modal coordinates, chosen from the lower frequency modes contained in Eq. (2). Since our work is primarily addressed to an examination of the effect of controlling just the rigid body modes (as opposed to actively controlling some of the flexible body modes, the number of controlled modes in the examples shall be limited to either one or two (for illustrative purposes only). However, the derivation of the optimal control formulation contains no restrictions, and the number of controlled modes is discretionary.

To continue the derivation, we shall choose to control a set of  $M$  modes, and form the vector,  $z$ , to represent the state of the controlled modal system,  $\eta_c$ , which gives

$$\dot{z} = Az + Du, \quad |u| \leq u_{\max} \quad (3)$$

where

$$z = \text{col}(\eta_c, \dot{\eta}_c) \quad (2N \text{ by } 1)$$

$$A = \begin{bmatrix} 0 & I \\ -\Lambda_c & 0 \end{bmatrix} \quad (2N \text{ by } 2N)$$

$$D = \begin{bmatrix} 0 \\ B_c \end{bmatrix} \quad (2N \text{ by } m)$$

and we seek the control that will drive the system from a given initial state to a specified target state

$$z(0) = z_0 \quad (2N \text{ by } 1)$$

$$Vz(t_f) = z_f \quad (2N \text{ by } 1)$$

within the time limit ( $t_f$ ), an unknown constant. The problem defined by Eq. (3) is a fixed final state, free final time two-point boundary value problem (Ref. 5). We shall transform this system into a fixed final state, fixed final time problem, which can be solved by a number of numerical methods, Ref. (1-3), by defining the normalized time variable

$$\tau = \frac{t}{t_f} \quad (4)$$

so that when  $t=0$ ,  $\tau=0$  and when  $t=t_f$ ,  $\tau=1$ . Differentiating both sides of Eq. (4) leads to the identity

$$\frac{d(\quad)}{d\tau} = t_f \frac{d(\quad)}{dt} \quad (5)$$

or

$$(\quad)' = t_f (\quad)' \quad (6)$$

Using the identity and notation given in Eq. (6) and operating on Eq. (3), the fixed final time two-point boundary value problem (TPBVP) is given by

$$\dot{\underline{z}} = t_f (A\underline{z} + D\underline{u}) \quad (7)$$

with the corresponding boundary conditions given by

$$\underline{z}(\tau = 0) = \underline{z}_0 \quad (8a)$$

$$V\underline{z}(\tau = 1) = \underline{z}_f \quad (8b)$$

The optimal control problem is to determine the controls applied to Eq. (7) which will satisfy these boundary conditions and minimize the performance index

$$J = \int_{t_0}^{t_f} dt = \int_0^1 t_f d\tau = t_f \quad (9)$$

The Hamiltonian, formed from the integrand of Eq. (9) and the right hand side of Eq. (7), is

$$H = t_f + \underline{\lambda}^T (t_f (A\underline{z} + D\underline{u})) \quad (10)$$

where the  $2N$  costates,  $\underline{\lambda}$ , are a set of undetermined Lagrange multipliers. Pontryagin's principle, acting upon Eq. (10) produces the equations governing the states and costates

$$\dot{\underline{z}} = \frac{\partial H}{\partial \underline{\lambda}} = t_f (A\underline{z} + D\underline{u}) \quad (11a)$$

$$\dot{\underline{\lambda}} = - \frac{\partial H}{\partial \underline{z}} = -t_f A^T \underline{\lambda} \quad (11b)$$

and  $\underline{u}$  is chosen such that Eq. (10) is minimized for all time. To accomplish this, the last term of Eq. (10) must be negative, a requirement which

is mathematically stated for each element ( $u_i$ ) of the control vector

$$u_i = -U_{\max} \text{sign} \left( \sum_{j=1}^{2N} D_{ji} \lambda_j \right) \quad (12)$$

where the subscripts indicate the elements of the corresponding vectors and matrices.

Equations (11-12) are the necessary conditions for the true minimum time optimal control problem. Except for the unusual singular arc case (characterized by vanishing of the switch function over finite intervals), we note from Eq. (12) that the controls are instantaneously "switched" on and off as well as from positive to negative. Although this leads to the minimum time maneuver, such controls are impossible to implement exactly by any actual hardware. Therefore, true minimum time maneuvers serve only as a minimum bound for the actual time required to maneuver the given body.

Since the controls depend only upon the sign of the argument in Eq. (12), the magnitude of the costates will not effect the value ( $\pm U_{\max}$ ) determined for the controls. From Eq. (11), we see that the costates appear linearly in an unforced first-order, ordinary differential equation (ODE). Consequently, the costates do not have a unique magnitude, and we are free to impose any arbitrary condition which "normalizes"  $\underline{\lambda}(\tau)$  in some convenient way. We shall then introduce a constraint that the undetermined initial costates satisfy the normalization condition

$$\underline{\lambda}^T(0)\underline{\lambda}(0) = C \quad (13)$$

where  $C$  is an arbitrary positive constant. With this constraint, the search for suitable initial costates is restricted to a scaled hypersphere of initial conditions. The magnitude of  $C$  shall be chosen such that numerical behavior of the solution is enhanced, which for most applications implies that  $C \ll 1$ .

#### Profile Shaping of the Optimal Control

We propose to alter the switch functions in the optimal control, given by Eq. (12), in such a way that the control applied to the system is smooth and continuous throughout the entire maneu-

ver. Admissible controls must be smooth functions with values between zero and  $U_{\max}$  (zero near the endpoints of the maneuver) and which switch smoothly from positive to negative or negative to positive, depending upon the switch function argument ( $D_1^T$ ). The arctangent can be used to approximate the switch functions and thereby develop control profiles that meets these criteria and maintains a similarity to the sign function.

Consider the approximation of the sign function of a scalar variable to be expressed by

$$\text{sign}(s(\tau)) = w(\tau, \Delta\tau) \frac{2}{\pi} \tan^{-1}\left(\frac{s(\tau)}{1-\alpha}\right) \quad (14)$$

where the arctan function simulates the sign function (Ref. 7) with the parameter  $\alpha$  determining the degree of approximation and consequently the sharpness of the switch and the multiplier  $2/\pi$  is used to bound the arctan between  $\pm 1$ . As  $\alpha$  approaches 1, the arctan function in Eq. (14) approaches the ideal sign function, however the approximation is smooth and continuous (as shown in Fig. 1 for several values of  $\alpha$ ). The applied weight  $w(\tau, \Delta\tau)$ , is an arbitrary device that is introduced to "shape" the approximation as necessary for specific applications. For example, we note that the arctan approximation still has an "instant on-off" character despite the fact that any interior switches are smooth and continuous. We can arbitrarily smooth the terminal on-off conditions of Eq. (14) by choosing the weight function to attenuate the approximation at the endpoints ( $\tau = 0, 1$ ).

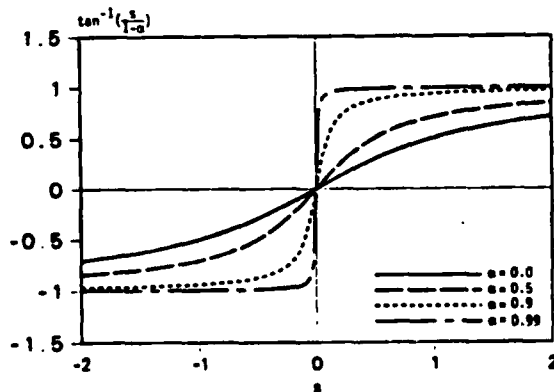


Figure 1 Approximation of sign function

Let the weight function be given by

$$w(\tau, \Delta\tau) = \frac{1}{4} \left[ \tanh\left(\frac{2r(\tau - \frac{\Delta\tau}{2})}{\Delta\tau}\right) + 1 \right] \left[ 1 - \tanh\left(\frac{2r(\tau - 1 + \frac{\Delta\tau}{2})}{\Delta\tau}\right) \right] \quad (15)$$

where  $\Delta\tau$  is a "rise-time" for the function and  $r$  is a positive constant chosen such that the weight function obtains a prescribed value ( $0 < w(\tau, \Delta\tau) < 1$ ) for  $\tau = \Delta\tau$  and  $\tau = 1 - \Delta\tau$ . For our work we shall choose  $r = 2.6$  which insures that  $w(\Delta\tau, \Delta\tau) = w(1 - \Delta\tau, \Delta\tau) = 0.9945$ . This guarantees that the weight function is within one percent of maximum (no attenuation) when  $\Delta\tau \leq \tau \leq 1 - \Delta\tau$ . Although Eq. (15) appears complicated, it allows us to apply a single weight function to the approximation given by Eq. (14) with the effect of prescribing zero slope and zero magnitude to the endpoints of the sign approximation, as shown in Fig. 2. In addition the rise time is a parameter that provides another method of "tuning" the control shaping concept for specific mission requirements.

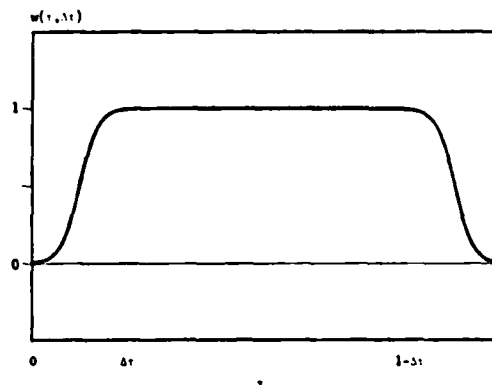


Figure 2 Weight function applied to controls

Therefore the approximation given by Eqs. (14) and (15) is smooth and continuous, with two parameters,  $\alpha$  and  $\Delta\tau$ , available for shaping the profile as required. Since this approximation is applied to a scalar variable, to introduce the approximation into the optimal control formulation requires that each element of the control vector be treated independently. Substituting the approximation from Eq. (14) into Eq. (12) gives the  $i^{\text{th}}$  element of the control vector



$$u_1 = -w(\tau, \Delta\tau) U_{\max} \frac{2}{\pi} \tan^{-1} \frac{\sum_{j=1}^{2N} D_j \lambda_j}{1-\alpha} \quad (16)$$

where  $w(\tau, \Delta\tau)$  is given by Eq. (15). The near minimum time optimal control problem is then given by Eqs. (11), (13), and (16) which includes the as yet undetermined final time  $t_f$ , and the boundary conditions given by Eq. (8).

#### Near Minimum Time Optimal Control Formulation

At this point, we have determined all of the equations and boundary conditions required to produce a minimum time, open loop maneuver with control shaping. The optimal control problem is, as usual, a two point boundary value problem with a partial set of initial conditions specified, and a corresponding set of given final conditions. We form the near minimum time optimal control problem by defining the augmented state vector

$$\underline{X} = \text{col}(\underline{z}, t_f, \underline{\lambda}) \quad (4N + 1 \text{ by } 1) \quad (17)$$

where the unknown final time is now a state variable. Therefore, the two-point boundary value problem may be written as a single first order equation

$$\dot{\underline{X}} = \begin{cases} t_f [A \underline{z} - w(\tau, \Delta\tau) \frac{2}{\pi} U_{\max} D (\tan^{-1} (\frac{\sum_{j=1}^{2N} D_j \lambda_j}{1-\alpha}))] \\ 0 \\ t_f A^T \underline{\lambda} \end{cases} \quad (18)$$

where by definition,  $t_f = X_{2N+1}$ . The boundary conditions and constraints remain unchanged

$$\underline{z}(0) = \underline{z}_0 \quad (19a)$$

$$V \underline{z}(1) = \underline{z}_f \quad (19b)$$

$$\underline{\lambda}^T(0) \underline{\lambda}(0) = C \quad (19c)$$

Note that Eq. (18) is a nonlinear function of the state variables; a consequence of the transformation given by Eq. (4). The optimal control problem has now been "reduced" to a single nonlinear, TPBVP of order  $4N + 1$  with  $2N$  initial conditions  $2N$  final conditions, and one constraint specified. We treat the unknown maneuver time as

a "costate," since our task is to solve Eq. (18) subject to Eq. (19) for the unknown initial costates.

Because the problem is completely nonlinear, we must rely on numerical methods to complete the solution. We elect to solve the near minimum time optimal control formulation through the use of the Method of Particular Solutions (Ref. 2), an iterative procedure for nonlinear equations, since the method relies on the principle of superposition. We must first linearize the equations governing the optimal control problem by using quasilinearization (Ref. 1). Let us define the right hand side of Eq. (18) as a vector function,  $\underline{f}$ , so that

$$\dot{\underline{X}} = \underline{f}(\underline{X}, \tau) \quad (20)$$

Expanding Eqs. (19) and (20) in a Taylor's series to first order for a trial vector  $\underline{X}_k$  gives

$$\dot{\underline{X}}_k + \Delta \dot{\underline{X}}_k = \underline{f}(\underline{X}_k, \tau) + \frac{\partial \underline{f}(\underline{X}_k, \tau)}{\partial \underline{X}} \Delta \underline{X}_k \quad (21a)$$

$$\underline{\lambda}_k^T(0) \underline{\lambda}_k(0) + 2 \underline{\lambda}_k^T(0) \Delta \underline{\lambda}_k(0) = C \quad (21b)$$

in terms of the corrections  $\Delta \underline{X}_k(\tau)$  and  $\Delta \underline{\lambda}_k(0)$ . Note that  $\Delta \underline{\lambda}_k$  is by definition a part of the vector  $\Delta \underline{X}_k$ . The corrected  $k+1$  solution is then given by

$$\underline{X}_{k+1} = \underline{X}_k + \Delta \underline{X}_k \quad (22)$$

Solving Eq. (22) for  $\Delta \underline{X}_k$  and substituting into Eq. (21) gives the quasilinearized optimal control formulation in terms of the  $k+1$  trial solution

$$\dot{\underline{X}}_{k+1} = F_k(\tau) \underline{X}_{k+1} + D_k(\tau) \quad (23)$$

$$\underline{z}_{k+1}(0) = \underline{z}_0 \quad (24a)$$

$$V \underline{z}_{k+1}(1) = \underline{z}_f \quad (24b)$$

$$\underline{\lambda}_k^T(0) \underline{\lambda}_{k+1}(0) = \frac{1}{2} (C + \underline{\lambda}_k^T(0) \underline{\lambda}_k(0)) \quad (24c)$$

where we have defined

$$F_k(\tau) = \frac{\partial \underline{f}(\underline{X}, \tau)}{\partial \underline{X}} \bigg|_{\underline{X}_k(\tau)} \quad (4N+1 \text{ by } 4N+1) \quad (25a)$$

$$\underline{D}_k(\tau) = f(\underline{X}_k, \tau) - F_k(\tau) \underline{X}_k(\tau) \quad (4N+1 \text{ by } 1) \quad (25b)$$

The  $k$  trial solution is known (we are solving for the  $k+1$  solution) and therefore  $F_k$ ,  $\underline{D}_k$ , and  $\underline{\lambda}_k$  are implicit functions of time,  $\tau$ .

The  $k+1$  trial solution of the problem given by Eqs. (23-25) is assumed to be a linear combination of a set of nominal trajectories found by integrating the governing equations with a particular set of initial costates. Each set of initial costates is specified such that it is linearly independent of all other sets. Since we must solve for  $2N+1$  initial costates (which includes the maneuver time), we shall produce  $2N+2$  nominal trajectories  $\underline{X}^j(\tau)$ ,  $j=1,2,\dots,2N+2$  with the initial conditions

$$\underline{X}^j(0) = \begin{Bmatrix} \underline{e}_0 \\ (\delta_{ij}) \end{Bmatrix} \quad \begin{matrix} (2N \text{ by } 1) \\ i=1,2,\dots,2N+1 \end{matrix} \quad (26)$$

where  $\delta_{ij}$  is the Kronecker Delta, and  $(\delta_{ij})$  indicates a vector consisting of elements,  $\delta_{ij}$ , with  $i$  denoting the element number. The  $k+1$  trial solution is then given by

$$\underline{X}_{k+1}(\tau) = \sum_{j=1}^{2N+2} q_j \underline{X}^j(\tau) \quad (27)$$

We determine the coefficients in Eq. (27) such that the trial solution satisfies the boundary conditions and constraint given by Eq. (24). Substituting Eq. (27) into each of the conditions yields

$$\sum_{j=1}^{2N+2} q_j \underline{X}^j(0) = \underline{e}_0 \quad (28a)$$

$$\sum_{j=1}^{2N+2} q_j \underline{X}^j(1) = \underline{e}_f \quad (28b)$$

$$\underline{\lambda}_k^T(0) \left( \sum_{j=1}^{2N+2} q_j \underline{X}^j(0) \right) = \frac{1}{2} (C + \underline{\lambda}_k^T(0) \underline{\lambda}_k(0)) \quad (28c)$$

The first condition may be simplified by realizing that each  $\underline{X}^j(0)$  is equal to  $\underline{e}_0$  as defined in Eq. (26), so Eq. (28a) reduces to

$$\sum_{j=1}^{2N+2} q_j = 1 \quad (29)$$

Note that Eq. (29) gives one relationship for the coefficients, and upon closer examination, it is clear that Eq. (28b) produces  $2N$  equations and Eq. (28c) provides one; therefore, the  $2N+2$  equations

produce a linear system that uniquely determines the coefficients. In matrix form, the coefficients are found by solving

$$\begin{bmatrix} 1 & 1 & \dots & 1 & 1 \\ \underline{V}_z^1(1) & \underline{V}_z^2(1) & \dots & \underline{V}_z^{2N+1}(1) & \underline{V}_z^{2N+2}(1) \\ 0 & \lambda_k^{(1)}(0) & \dots & \lambda_k^{(2N)}(0) & 0 \end{bmatrix} \underline{q} = \underline{d} \quad (30)$$

where  $\lambda_k^{(i)}(0)$  indicates the  $i$ th element of  $\underline{\lambda}_k(0)$  and  $\underline{q} = \text{col}(q_j)$ . The right hand side of Eq. (30) is determined to be

$$\underline{d} = \begin{Bmatrix} 1 \\ \underline{e}_f \\ \frac{1}{2} [C - \underline{\lambda}_k^T(0) \underline{\lambda}_k(0)] \end{Bmatrix} \quad (31)$$

The solution of the near minimum time optimal control is a multi-step procedure. We start with an initial guess in the form of a trial solution,  $\underline{X}_k(\tau)$ . Next, integrate Eq. (23) with the definitions given by Eq. (25) for each nominal trajectory, the neighboring trajectories  $\underline{X}^j(\tau)$ , using the initial conditions specified in Eq. (26). When this has been completed for all  $2N+2$  trajectories, the linear system given by Eq. (30) is formed and solved for the coefficients,  $q_j$ . The  $k+1$  trial solution is calculated by Eq. (27) and compared to the  $k$  solution to determine whether convergence has been achieved. If necessary, the  $k+1$  solution now becomes the new nominal solution,  $\underline{X}_k(\tau)$ , and the procedure is repeated until the system approaches an acceptable degree of precision, based upon a relative displacement convergence test.

#### Application to a Low Order System

To demonstrate the near minimum time optimal control formulation, we apply the method to a simple structure which is composed of a rigid hub and one cantilevered flexible appendage. The hub is pinned to allow only a single axis rotational degree of freedom, and the motion of the appendage is restricted to the plane perpendicular to the rotational axis. The spacecraft structural param-

eters are:

Hub Mass:	16 kg.
Hub Radius:	0.3 m
Appendage Stiffness:	$7 \times 10^9 \text{ N/m}^2$
Appendage Density:	$2700 \text{ kg/m}^3$
Appendage Length:	4 m
Appendage Height:	0.1524 m
Appendage Thickness:	$3.175 \times 10^{-3} \text{ m}$

Using the method of assumed modes (Ref. 9), where the mode shape is described by the function

$$\phi_1(x) = 1 - \cos \frac{1\pi x}{L} - \frac{1}{2}(-1)^1 \left(\frac{1\pi x}{L}\right)^2 \quad (32)$$

the mass and stiffness matrices can be calculated. We shall restrict this model to a low order ( $n=5$ ) as defined in Eq. (1), so that the presentation of numerical results is manageable. Solving the algebraic eigenvalue problem produces the natural frequencies listed in Table 1.

Table 1 Natural Frequencies

Mode Number	Natural Frequency (rad/s)
1	0.0
2	1.13
3	3.17
4	6.54
5	11.86

For each of the numerical examples presented, the initial conditions are

$$\eta_1(0) = 0.51872 \quad (\text{rigid body displacement})$$

$$\eta_{2-5}(0) = 0$$

$$U_{\max} = 2$$

#### Control of Mode 1

We shall first investigate near minimum time maneuvers of the example problem with control of the rigid body mode being the only consideration. The true minimum time solution of the optimal control of a rigid body is well documented (Ref. 4) and establishes the lower bound for all

maneuvers. The time required to complete bang-bang maneuver of the spacecraft considered in the following examples is calculated to be  $t_f = 2.48$  sec. By adjusting the parameters ( $\alpha$  and  $\Delta\tau$ ) that govern the torque profile we can widely vary the configuration of the optimal control and consequently cause large variations in the maneuver time, and flexural energy.

In order to appreciate the degree to which the control can be manipulated, we shall examine rigid body maneuvers using control profiles obtained through relatively large variations of  $\alpha$  and  $\Delta\tau$ . In each case the maneuver time and residual structural energy are considered a measure of the success of each single axis maneuver, and each case will be quantitatively compared to the bang-bang maneuver which we found required 2.48 sec to complete with an energy spillover (as measured by the residual energy of the flexible modes) of  $E=2.3$  Nm. In each case a  $5^\circ$  maneuver is to be completed using a control saturation limit of 2 Nm.

Case 1  $\alpha = 0.999$   $\Delta\tau = 0.1$

For the first case, we shall attempt to approximate the bang-bang slew with a sharp rise time (10% of the total maneuver time) and an extremely sharp central switch. The control profile generated in the near minimum time problem for this example is shown in Fig. 3.

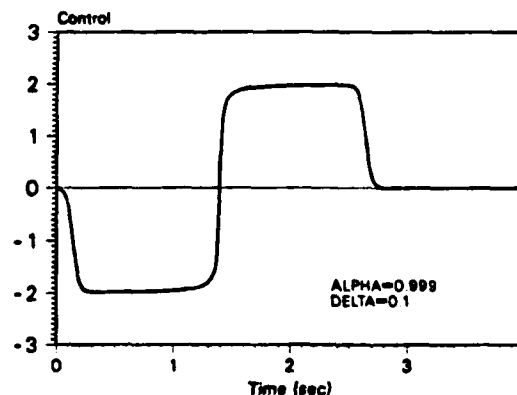


Figure 3 Control profile for Case 1

The time required for reorientation is  $t_f = 2.78$  sec and the residual energy is found to be  $E = 2.17$ . As we would expect the residual energy is diminished to some small degree since the control

for this example "rings" the structure less than the bang-bang control; however the cost is a 12% increase in the time required for completion of the rotation. Most of the residual energy is due to the excitation of the second mode, as shown in Fig. 4, and although this maneuver accomplishes the goal of controlling the rigid body mode, the flexural vibration would be too great for most practical applications.

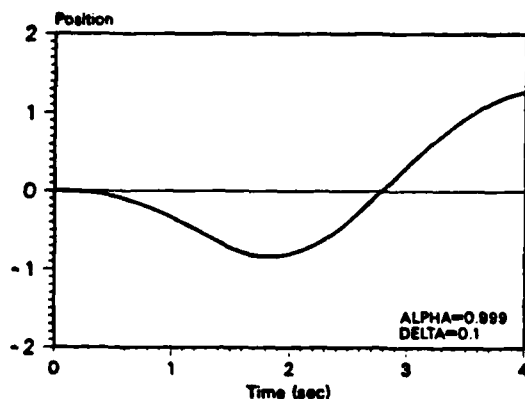


Figure 4 Residual Energy for Case 1

Case 2  $\alpha = 0.95$   $\Delta\tau = 0.1$

For the second case, we shall reduce the sharpness of the switch function while maintaining the same rise time. By far, the largest impulse applied to the structure is the sudden change in sign of the control moment. Therefore by reducing the control rate during the switch, a maneuver with less residual energy results. The control profile for this case is shown in Fig. 5, with a final maneuver time of  $t_f = 3.83$  sec and a total flexural energy of  $E = 0.78$ .

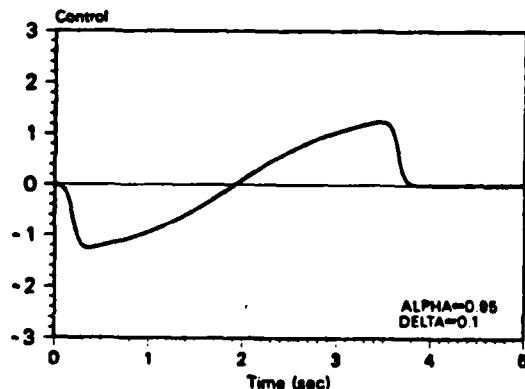


Figure 5 Control for Case 2

The residual energy is drastically lowered with respect to the bang-bang maneuver, a total reduction of 66%, with a subsequent increase of 54% in the time required for the reorientation. If flexural excitation were the primary consideration for a given application, this optimal control would prove most useful.

The range of the control parameters is quite extensive, and in fact, we can arbitrarily produce controls of extraordinarily different configurations. For example with  $\alpha = 0.999$  and  $\Delta\tau = 0.4$ , the control would appear as shown in Fig. 6, where the final time is  $t_f = 4.08$  sec and the flexural energy is 1.8471. Since the switch is sharp and the magnitude changes by  $2U_{max}$ , the energy is quite high. However as a consequence of the rise time requiring a full 40% of the total maneuver time, the minimum time is also quite large. Obviously, this particular control profile is of little practical use; however, the method that we have developed is sufficiently general in nature, that this form is available, should the need arise.

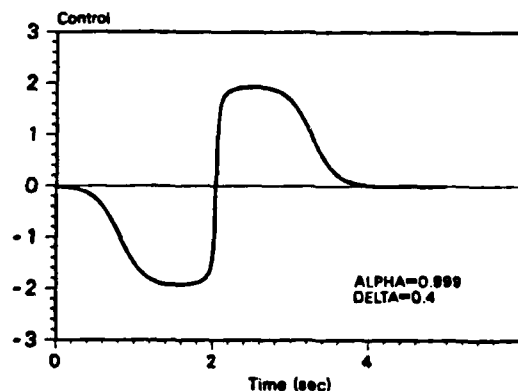


Figure 6 Control for  $\alpha = 0.999$  and  $\Delta\tau = 0.4$

The last extreme variation that we can make is to set  $\alpha = 0.95$  and  $\Delta\tau = 0.4$ , resulting in the control shape shown in Fig. 7. This maneuver is quite smooth with little flexural excitation (the final energy is 0.51), but the final time is 6.1 sec (a 145% increase over the bang-bang maneuver). This type of control resembles the results obtained (Ref. 4) from open loop formulations with penalties applied to the control rates and control accelerations.

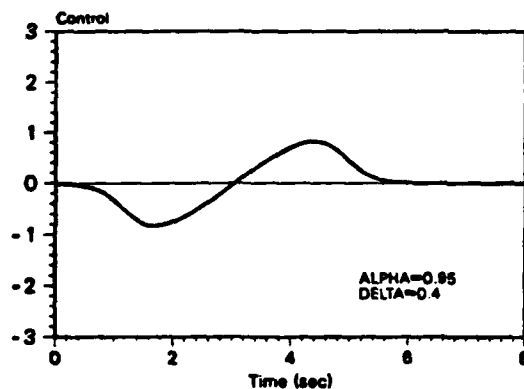


Figure 7 Control for  $\alpha = 0.95$  and  $\Delta t = 0.4$

#### Control of the Flexural Modes

Although the results presented in the preceding examples are rich in content with respect to optimizing the parameter selection for specific mission requirements (and our treatment of the subject has necessarily been brief), we shall now include the first flexural mode in the minimum time formulation. Furthermore, we shall consider only a variation in value of  $\alpha$ , keeping  $\Delta t$  fixed at 0.1 for simplicity

Case 3       $\alpha = 0.999$        $\Delta t = 0.1$

Setting  $\alpha = 0.999$ , the  $5^\circ$  rotation is accomplished in 4.98 sec with a total residual energy of 2.2 Nm. Notice that this energy level is higher than the final energy of Case 1. Yet when we examine the trajectories of the first and second modes shown in Figs. 8 and 9 respectively, the first two modes clearly contain no residual energy. The high energy content is a consequence of the combination of frequency content of the applied control (shown in Fig. 10) and the relatively closely spaced eigenvalues of this particular model. For example each natural frequency is very nearly twice the preceding modal frequency and nearly equal to the primary frequency of the control.

The optimal control switches three times during the course of the maneuver in order to control the first flexural mode. This indicates the high degree of flexibility of the spacecraft used in the numerical examples, and significantly different results have been obtained with other structural formulations.

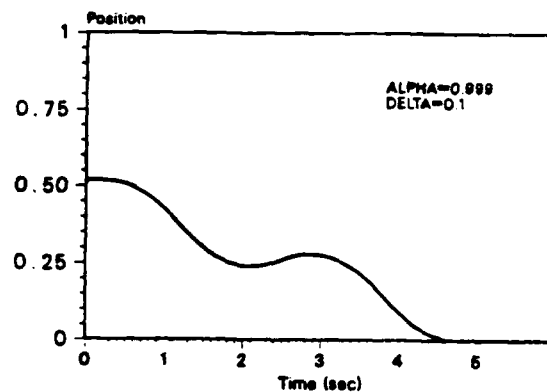


Figure 8 Trajectory of Mode 1

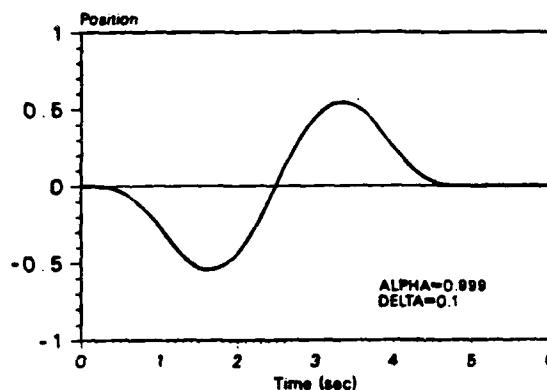


Figure 9 Trajectory of Mode 2

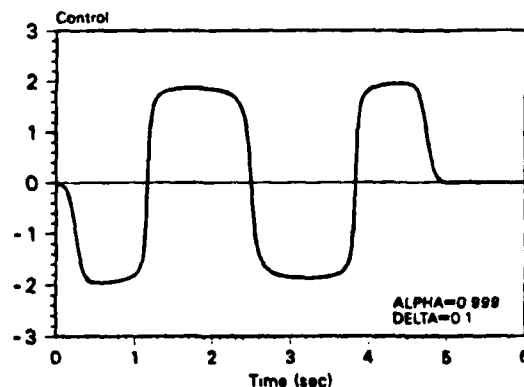


Figure 10 Control for Case 3

Case 4       $\alpha = 0.95$        $\Delta t = 0.1$

By reducing the control rate of the switch, we have demonstrated in Case 2 that the resulting energy levels were greatly reduced when controlling the rigid body mode when. Upon solving the near minimum time problem for  $\alpha = 0.95$  with control of the first flexural mode

included, the maneuver time is increased to 6.07 sec however the residual energy at the final time is 0.2 Nm. Clearly this is the better of the cases we have examined in terms of residual energy, at a high cost in the slewing time. The control profile, shown in Fig. 11, exhibits three switches as found in Case 3, but the magnitude of the change in the control is quite small by comparison, a direct cause of the low residual energy. In terms of final energy content, this is by far the most successful case presented however a toll is exacted in the form of increased maneuver time.

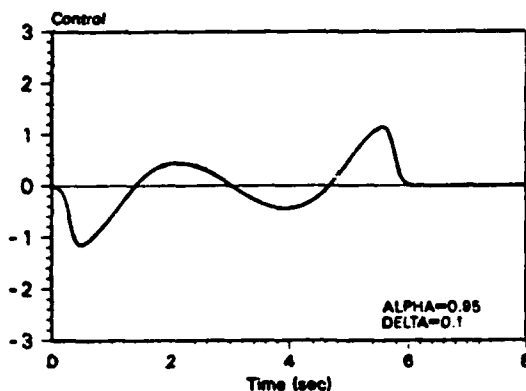


Figure 11 Control For Case 4

### Conclusions

We have presented a near minimum time, open loop optimal control formulation for flexible structures. The applied control is parameterized by two independent and arbitrary constants such that the control can be shaped to meet specific hardware constraints or mission requirements. Solution of the minimum time problem is usually rapid requiring four to six iterations for a low order system.

As a consequence of the ability to tune the controls, we have a means of evaluating specific tradeoffs with respect to maneuver time and residual energy as a "function" of the degree of control smoothness. For a series of solutions using the minimum time formulation with various values of the control parameters, surface plots can be produced giving excellent estimates of both the maneuver time and residual energy as a function of the independent variables. Taking this concept one step further, it is quite

possible that we may be able to fully parameterize the near minimum time optimal control problem, eliminating the need to solve nonlinear ODE's for each case (a topic of current and future research). The near minimum time formulation presents a practical and realistic approach to solving open loop, minimum time slewing maneuvers.

### References

1. Roberts, Sanford M. and Shipman, Jerome S., Two-Point Boundary Value Problems: Shooting Methods, American Elsevier Publishing Co., Inc., New York, NY, 1972.
2. Meile, A., "Method of Particular Solutions for Linear, Two-Point Boundary Value Problems," Journal of Optimization Theory and Applications, Vol. 2, No. 4, 1968.
3. Vadali, S.R., "Solution of the Two-Point Boundary Value Problems of Optimal Spacecraft Rotational Maneuvers," Ph.D. Dissertation, Virginia Polytechnic Institute and State University, 1982.
4. Junkins, J.L. and Turner, J.D., Optimal Spacecraft Rotational Maneuvers, Elsevier Science Publishers B.V., Amsterdam, Netherlands, 1986.
5. Kirk, Donald E., Optimal Control Theory: An Introduction, Prentice-Hall Inc., Englewood Cliffs, NJ, 1970.
6. Bryson, Arthur E. Jr. and Ho, Yu-Chi, Applied Optimal Control, Hemisphere Publishing Corp., Washington, D.C., 1975.
7. Subrahmanyam, M.B., "Computation of Optimal Controls by Newton's Method Using a Discretized Jacobian," Journal of Guidance, Control, and Dynamics, Vol. 9, No. 3, May-June, 1986.
8. Vander Velde, W.E., and He, J., "Design of Space Structure Control Systems Using On-Off Thrusters," Journal of Guidance, Control and Dynamics, Vol. 6, No. 1, Jan-Feb, 1983.
9. Meirovitch, L., Computational Methods in Structural Dynamics, Sijthoff & Noordhoff, Rockville, MD, 1980.

## **ATTACHMENT 2**

# **Feedback Control Design for Smooth Near-Minimum Time Rotational Maneuvers of Flexible Spacecraft**

## Near-Minimum Time, Closed Loop Slewing of Flexible Spacecraft

by

R. M. Byers,<sup>†</sup> S. R. Vadali<sup>‡</sup> and J. L. Junkins<sup>§</sup>  
Texas A&M University, College Station, Texas 77843

### Abstract

The near-minimum time single axis slewing of a flexible spacecraft with simultaneous suppression of vibration of elastic modes is considered. The hyperbolic tangent ( $\tanh$ ) function is used as a smooth approximation to the discontinuous  $\text{sgn}$  function occurring in the rigid body "bang-bang" control. Variable structure control concepts are used to identify the necessary characteristics of the control switching line. Simulations of the rest-to-rest and tracking maneuvers indicate that the elastic energy can be reduced by several orders of magnitude with only a modest increase in the maneuver time.

### Introduction

Many future large space structures, due to mass constraints, will be flexible. For the purpose of analysis these systems can be modelled with a large number of modes of vibration. For certain applications, it will be desirable that such a spacecraft be able to slew as rapidly as possible, within the operating limits of the control actuators. The problem of control design for rotational maneuver and vibration suppression of flexible spacecraft has been addressed extensively.<sup>1-10</sup> Optimal control theory can be applied to enforce quiescent terminal conditions on the flexible modes, usually by applying a quadratic cost function which weights the control rates and the states. The order of the system model grows rapidly as the number of flexible modes to be controlled is increased, making it impractical to attempt to control more than a few flexible modes.

---

<sup>†</sup> Graduate Student, Student Member AIAA

<sup>‡</sup> Assistant Professor, Member, AIAA

<sup>§</sup> TEES Chair Professor, Fellow, AIAA



Furthermore, there is no rigorous means by which control magnitude constraints may be enforced. Although a feedback method such as the Linear Quadratic Regulator (LQR) with terminal constraints<sup>9-11</sup> is attractive because it can enforce quiescent conditions on the elastic modes, its computational complexity is burdensome.

The optimal control solution to the minimum time, single axis, rotational maneuver problem for a rigid body gives a control scheme characterized by saturation of the control throughout the maneuver with at most one control switch which is instantaneous ("bang-bang"). Although not exactly achievable in physical systems, and even though the trajectories are extremely sensitive to variations in spacecraft parameters, this control law has wide application for rigid systems using on-off thrusters. When rigorously applied to flexible systems, however, the result is typically multiple control switches and excessive excitation of the flexible modes of vibration. Previous investigations of the near-time optimal maneuver for flexible systems<sup>7,8</sup> are open-loop designs requiring extensive computational effort. An alternative is to compute the required parameters for a number of initial conditions off-line and use table look-up and interpolation for a particular maneuver. This may involve excessive storage. We start with the assumption that the minimum time solution for a rigid spacecraft can serve as an initial approximation to the near-minimum time solution for a flexible structure. In other words we expect that near-minimum times can be achieved by limiting the number of control switches to one and vibration suppression can be achieved by torque smoothing. Singh, et al.<sup>8</sup> observe quantitatively that the difference between the minimum time for a rigid body and the actual time required for a flexible spacecraft is small for large angle maneuvers of systems of low flexibility and small available control torques.

To avoid exciting the flexible modes of vibration the discontinuous  $\text{sgn}$  function associated with the minimum time solution for a rigid body is approximated by the hyperbolic tangent ( $\tanh$ ) function. The parabolic switching function associated with the rigid body control is replaced by one which, also using the hyperbolic tangent function,

exploits the symmetry of the rigid body state trajectory.

The resulting control logic is a computationally simple, feedback design which causes the flexible system to come very close to the desired orientation (coarse maneuver) and corrects any residual error in a fine pointing mode using very small control inputs. A major feature of this control design is that only the rigid body components of the state vector must be considered by the control. This approach has been adapted for a multiple body/multiple actuator system.

### System Model and Equations of Motion

A generic flexible spacecraft is used for analysis (Fig. 1(a)). It consists of a rigid hub with four cantilevered flexible appendages. Continuous control torque is assumed to be provided by a single momentum exchange actuator in the central hub. Internal actuator dynamics are ignored. Only small anti-symmetric deformations (Fig. 1(b)) in the plane normal to the axis of rotation are assumed. Damping is assumed to be negligible and is ignored.

The dynamics of such a system may be modelled by the second order matrix equation:

$$M\ddot{\underline{q}} - K\underline{q} = \underline{V}u \quad (1)$$

where  $\underline{q}$  is the  $(n \times 1)$  vector of the generalized displacements of the configuration,  $M$  is the  $(n \times n)$  mass matrix,  $K$  is the  $(n \times n)$  stiffness matrix and  $\underline{V}$  is the  $(n \times 1)$  control influence matrix.

Unfortunately, these  $n$  equations are coupled and not in a convenient form for analysis. They can be decoupled by transforming from generalized coordinates to modal coordinates using the transformation:

$$\underline{q} = \Phi\underline{\eta} \quad (2)$$

where  $\Phi$  is the  $n \times n$  matrix of normalized eigenvectors. This yields the equations of motion:

$$\ddot{\underline{\eta}} + \Lambda\underline{\eta} = \underline{V}'u \quad (3)$$

where  $\Lambda$  is the diagonal matrix of the system's eigenvalues and  $V' = \Phi^T V$ . Since  $\lambda_1 = 0$ ,  $\eta_1 = \theta$ , where  $\theta$  is the spacecraft's rigid body mode coordinate in physical space.

These equations may be further reduced to a set of  $2n$  first order differential equations. By defining the  $(2n)$  vector:

$$\underline{\dot{z}} = \begin{pmatrix} \underline{\dot{\eta}} \\ \underline{\eta} \end{pmatrix} \quad (4)$$

the state space formulation can be expressed as:

$$\underline{\dot{z}} = A\underline{z} - B u; \quad \text{where: } A = \begin{pmatrix} 0 & I \\ -\Lambda & 0 \end{pmatrix} \quad B = \begin{pmatrix} 0 \\ V' \end{pmatrix} \quad (5)$$

Numerical integration by 4th order Runge-Kutta method was used on this system to analyze the first seven modes of the generic spacecraft.

#### Rigid Body Minimum Time Optimal Control Solution

Consider a system with only a rigid body mode with bounded control such that:

$$I\ddot{\theta} = u; \quad |u| \leq u_0 \quad (6)$$

$$\begin{aligned} \theta(0) &= \theta_0 & \dot{\theta}(0) &= \dot{\theta}_0 \\ \theta(t_f) &= 0 & \dot{\theta}(t_f) &= 0 \end{aligned}$$

where  $I$  is the moment of inertia,  $\theta(t)$  is the angular displacement, and  $u$  is the magnitude of the control. The closed loop solution to the rotational maneuver problem is well known:<sup>11,12</sup>

$$u = -u_0 \operatorname{sgn}(s) \quad (7)$$

$$s = \begin{cases} \theta(t) + I\dot{\theta}(t)\dot{\theta}(t)/2u_0, & 0 \leq t \leq t_1; \quad t_1 = \text{switch time} \\ \dot{\theta}(t), & t_1 < t \leq t_f \end{cases} \quad (8)$$

It is clear that the origin of the state space can be reached from any initial condition with a maximum of one control switch at some time  $t = t_1$  by initially applying  $\pm u_0$  as appropriate to intercept the switching function Eq. (8) then instantaneously switching to  $u = \mp u_0$ .

The time required to complete the maneuver may be found by integrating the state equations along the optimal path to yield:

$$t_f = \frac{I\dot{\theta}_0}{u_0} \text{sgn}(s_0) - 2\sqrt{\frac{I}{u_0} \theta_0 \text{sgn}(s_0) + \frac{1}{2} \left( \frac{I}{u_0} \dot{\theta}_0 \right)^2} \quad (9)$$

Setting  $\dot{\theta}_0 = 0$  gives the result for the "rest-to-rest" case:

$$t_f = 2\sqrt{\frac{I}{u_0} \theta_0} \quad (10)$$

The value of  $t_f$  found in Eq. (9) or (10) may be used as a starting point for any near-minimum time control law for a flexible structure. The degree to which the near-minimum time goal is achieved can be estimated by comparing the actual maneuver time with the idealized rigid body time computed above. However, this "bang-bang" control cannot be applied directly to a highly flexible system since the discontinuous nature of the control tends to excite the elastic modes.

#### Control Smoothing and Synthesis of the Feedback Control

The primary cause of excessive elastic mode excitation in flexible spacecraft comes from abrupt control changes. If we assume that initially the flexible modes are quiescent, logically a control which excites them very little throughout the maneuver will enhance our ability to suppress them at the final time. While the LQR control is nearly ideal in satisfying quiescent boundary conditions of controlled modes, it is less attractive for achieving near-minimum maneuver times. The final time must be specified and there is no rigorous means by which the control magnitude constraints may be enforced. In addition, it requires real-time, perfect knowledge of modal coordinates whereas in practice only a limited set of these may be estimated based on measurement of physical coordinates. To achieve acceptable smoothness,  $u$  and  $\dot{u}$  must be modelled as states with  $\ddot{u}$  becoming the control.<sup>10</sup> Finally, Bryson's method<sup>11</sup> to enforce the terminal boundary conditions is computationally demanding, requiring the solution of  $2n^2 + n$  differential equations

for  $n$  modelled modes, thereby making modelling more than a very few flexible modes impractical.

We seek a feedback system which, while providing the essential smooth controls, approximates the characteristics of the minimum time control and is not computationally intensive. In any continuous momentum exchange system, actuator dynamics provide control smoothing to a certain degree, but this alone is insufficient for vibration suppression.

### Smoothing Functions

Consider the approximation of the *sgn* function:<sup>13</sup>

$$\text{sgn}(s) \approx \tanh\left(\frac{s}{1-\alpha}\right) \quad (11)$$

where  $0 \leq \alpha < 1$  is a smoothing function. Figure 2(a) illustrates the function for several values of  $\alpha$ . As  $\alpha \rightarrow 1$  the approximation of the *sgn* function becomes arbitrarily good. Also note that, unlike the *sgn* function, which is undefined at  $s = 0$  the *tanh* function is continuous at all values of  $s$ . Alternatively, the *arctangent* function shows similar smoothing characteristics.<sup>7,14</sup> The *tanh* function is preferred here because it is easily represented in terms of exponential functions or series.

If we replace the *sgn* function in Eq. (7) with the *tanh* function in Eq. (11) we can realize any degree of smoothness desired for the control switch at  $t = t_1$  and all subsequent interior switches. However, the initial jump discontinuity at  $t = 0$  remains. This can be remedied by employing a multiplier function which ensures zero initial control magnitudes and control rates. Such a multiplier function is given by:<sup>15</sup>

$$m(t) = \tau^2(3 - 2\tau); \quad \tau = \begin{cases} t/T_1 & \text{for } t \leq T_1; \\ 1 & \text{for } t > T_1 \end{cases} \quad (12)$$

where  $T_1$  is "rise time" which can be selected to achieve whatever degree of control smoothness is desired. The profile of  $m(t)$  is shown in Fig. 2(b).

With these smoothing functions the control becomes:

$$u = -u_0 \left\{ \tanh\left(\frac{s}{1-\alpha}\right) \right\} m(t) \quad (13)$$

The use of these smoothing functions, however, is not compatible with the switching function prescribed for the minimum time control in Eq. (8), which itself is discontinuous at the control switch. In addition, the smoothed control cannot follow the optimal trajectory because of the inherent lag in the control switch. We observe for the rigid body rest-to-rest maneuver,  $t_1 = t_f/2$  from which it follows that the state space trajectory is symmetric about the  $\theta(t) = \theta_0/2$  line.

### Variable Structure Control Systems

Variable Structure Control Systems<sup>16-21</sup> change control laws along a switching line in order to drive the state space trajectory to the phase plane origin. Each control may, by itself, be unstable and generally the control is discontinuous at the switching line. Under certain conditions, once the state space trajectory intercepts the switching line, the control switches at high frequency to cause it to chatter along the switching line to the origin.

The minimum time control system is a variable structure system where the control is discontinuously switched at the switching line  $s = 0$  defined in Eq. (8). Now suppose that the parabolic switching line is replaced by a linear switching line of the form:

$$s = \dot{\theta} + k\theta = 0 \quad (14)$$

Under certain ideal circumstances, the state space trajectory will move along this switching line. The necessary conditions are:

$$\begin{aligned} \lim_{s \rightarrow 0^-} \dot{s} &> 0 \\ \lim_{s \rightarrow 0^+} \dot{s} &< 0 \end{aligned} \quad (15)$$

The effect of Eqs. (15) is that, as the trajectory crosses the  $s = 0$  line, the control changes sign and immediately forces it back toward the switching line. Ideally, control switching is instantaneous and the trajectory "slides" on the switching line to the origin. Hence this is called the "sliding regime". In real systems however, such infinite frequency switching is impossible and instead, switching will occur at some high frequency determined by the

limitation of the control mechanism. Slotine et al.<sup>20,21</sup> seek to avoid chattering via a multiplier function. The  $\tanh$  function serves the same purpose with increased smoothness. When the conditions of Eq. (15) are applied to Eqs. (6), (7) and (14) the following inequality results:<sup>18</sup>

$$I \dot{\theta} k = u_0 = k \cdot \frac{u_0}{I \dot{\theta}} \quad (16)$$

That is, if  $k = u_0 / I \dot{\theta}$ , regular switching occurs on or very near the switching line. Now define:

$$k_{max} = \frac{u_0}{I \dot{\theta}} \quad (17)$$

Replacing  $k$  with  $k_{max}$  in Eq. (14) gives:

$$\theta - \frac{I}{u_0} \dot{\theta} \ddot{\theta} = 0 \quad (18)$$

Thus, regular switching or sliding may be induced anywhere on the phase plane by selecting a switching function with the appropriate slope  $k$  at the point where switching is desired. To achieve near-minimum times for a maneuver it is desirable that regular switching occur at  $\theta_{switch} = \theta_0/2$ , the control saturates and the number of control switches is minimized. However, as the trajectory nears the origin, only small control inputs are necessary to correct any residual error.

The  $\tanh$  function again proves to be useful; consider the switching line described by:

$$s = \theta(t) - \frac{|\theta_{switch}|}{2} \left[ \tanh \left( \frac{\dot{\theta}(t) + \varphi}{1 - \beta} \right) + \tanh \left( \frac{\dot{\theta}(t) - \varphi}{1 - \beta} \right) \right] \quad (19)$$

where  $\beta$  is a smoothing factor and  $\varphi$  is a "deadband". Thus the switching function in the state space, is bounded by  $\pm |\theta_{switch}|$  and passes through the origin. Note that it satisfies the two requirements that were placed on the desired switching line. The slope of the function in the state space is infinite at  $\theta_{switch}$ , guaranteeing a regular switch as the trajectory crosses the  $s = 0$  line. Near the origin, however, by selection of the appropriate values of  $\beta$  and  $\varphi$ , the slope can be made sufficiently small so that the state trajectory will track the switching line.

### Smooth Control Law

At this point the smooth rest-to-rest maneuver can be assembled:

$$u = -u_0 \left\{ \tanh \left( \frac{s}{1-\alpha} \right) \right\} m(t) \quad (20)$$

$$s = \theta(t) - \frac{\theta_{switch}}{2} \left[ \tanh \left( \frac{\dot{\theta}(t) - \dot{\varphi}}{1-\beta} \right) - \tanh \left( \frac{\dot{\theta}(t) - \dot{\varphi}}{1-\beta} \right) \right] \quad (21)$$

$$\theta_{switch} = \frac{\theta_0}{2} \quad (22)$$

### Example Maneuvers

The parameters  $\alpha, \beta, \varphi$ , and  $T_1$  provide an infinite variety of "user control" over the sharpness of control switches, while still preserving saturation constraints and the feedback nature of the control law. Figures 3 and 4 illustrate two possibilities for selection of values for these parameters. Figure 3 shows that a close approximation of the minimum time control is possible by choosing  $\alpha$  and  $\beta$  close to one, and  $T_1$  small. The "bang-bang" control applied to a rigid spacecraft of equal moment of inertia is shown by the dashed line for comparison. Figure 4 compares the performance of the smooth control with relaxed values of  $\alpha, \beta$  and  $T_1$  to that of a terminally constrained LQR control in which only the rigid body mode and the first flexible mode of the spacecraft are measured and modelled. The maneuver time for the LQR was selected by trial such that the control just saturates.

Although symmetry of the state space trajectory is not guaranteed, the feedback control law developed above brings the rigid body mode near the origin with final time unspecified. The control may reach, but not exceed, the saturation limit and the energy of the flexible modes is dissipated via tracking a near-linear switching line at the end of the maneuver.

Especially noteworthy in this approach is the latitude which the designer has in choosing the degree of smoothness desired.  $T_1, \alpha, \beta$ , and  $\varphi$  are all discretionary parameters.  $T_1$  is the "rise time" parameter which determines the smoothness of the initial control input.



The value of  $\alpha$  primarily affects the smoothness of the mid-maneuver control switch, while  $\beta$  is the factor which controls the smoothness of the control near the origin. As  $\beta \rightarrow 1$ , the control transition will be rapid but tracking along the switching line will be slow. As  $\beta$  decreases, the control transition will be smooth and tracking of the switching line will be more rapid. However if  $\beta$  is made too small, the trajectory may "overshoot" the origin. The deadband in the switching line, determined by  $\varphi$  may be used to increase the slope of the switching line very near the origin to speed correction of residual error, while still allowing the value of  $\beta$  to stay relatively large. Although it is possible to have a similar deadband in the control itself, in general, little benefit has been found in such unless the system has a velocity constraint imposed. Since this is an undamped oscillatory system, the trajectory misses the target state by a small amount and must correct the error by tracking the switching line with very small control magnitudes. This is a shortcoming of this control law; it does not actively suppress flexible mode vibration until the end of the maneuver. Rather, it uses control smoothing to avoid exciting them. It is possible to use velocity feedback<sup>22</sup> to damp the critical flexible modes but this increases the rigid body mode maneuver time. This notwithstanding, this control does slew the spacecraft rapidly with low excitation of elastic mode energy. Robustness can be inferred; extensive structural identification is unnecessary; only direct measurement of the rigid body modes are considered. Moreover, although the smoothing parameters in the control law are affected by spacecraft parameters, e.g. moments of inertia, satisfactory values may be selected without accurate knowledge of the spacecraft structural data.

### Target Tracking

The rest-to-rest maneuver, although important, is fairly restrictive. In many scenarios the target is moving with respect to the spacecraft and it will be necessary not only to intercept its trajectory but to subsequently track it. While examining the target tracking problem, it is convenient to adjust our notation to reflect the fact that the desired final

state may not be stationary. Therefore we define the relative error coordinate system:

$$\epsilon = \theta - \theta_{target} \quad (23)$$

where  $\theta_{target}$  is the rigid body orientation of the target with respect to inertial frame whose origin is at the center of the spacecraft and  $\epsilon$  is the relative "error" between the spacecraft rigid body component and the the target states.

From Eq. (23) it follows:

$$\dot{\epsilon} = \dot{\theta} - \dot{\theta}_{target} \quad (24)$$

$$\ddot{\epsilon} = \ddot{\theta} - \ddot{\theta}_{target} \quad (25)$$

Which leads to the equations of motion for the rigid body system:

$$I\ddot{\epsilon} = u - I\ddot{\theta}_{target} \quad (26)$$

Equation (26) suggests that it is possible to express the target acceleration as an equivalent control magnitude.

If maximum control effort is applied to a rigid body, its state space trajectory describes a parabola. Along any given parabolic trajectory the relationship between  $\epsilon(t)$  and  $\dot{\epsilon}(t)$  remains constant; thus:

$$\epsilon(t) = \epsilon_0 - \frac{I}{2u} (\dot{\epsilon}_0^2 - \dot{\epsilon}(t)^2) \quad (27)$$

where  $u = \pm u_0$  as in Eq. (7). It is clear that it is possible to convert any "motion-to-rest" problem to an equivalent "rest-to-rest" problem by determining the value of  $\epsilon(t)$  where the state space trajectory intercepts the  $\dot{\epsilon} = 0$  axis of the phase plane. Setting  $\dot{\epsilon}(t) = 0$  in Eq. (27) and continuing the assumption that  $u = \pm u_0$  gives:

$$\dot{\epsilon}_0 = \epsilon_0 - \frac{I}{2u} \dot{\epsilon}_0^2 \quad (28)$$

with the regular switching angle defined:

$$\epsilon_{switch} = \frac{\dot{\epsilon}_0}{2} \quad (29)$$

The control law for the flexible spacecraft relies on the spacecraft approximately following these same trajectories. During  $0 \leq t \leq T_1$  however the flexible system does not exactly follow the ideal parabolic trajectory due to the presence of the multiplier function  $m(t)$  given in Eq. (12) and the flexible characteristics of the spacecraft. If we assume that the initial state is sufficiently far from the would-be switching line so that the control would saturate if not constrained by  $m(t)$  then the equation of motion (for a rigid system) for  $0 \leq t \leq T_1$  is:

$$I\ddot{c}(t)dt = \frac{t^2}{T_1^2} \left( 3 - 2\frac{t}{T_1} \right) u dt \quad (30)$$

On integrating twice, we obtain gives:

$$\dot{c}(T_1) = \dot{c}_0 - \frac{uT_1}{2I} \quad (31)$$

$$c(T_1) = c_0 - \dot{c}_0 T_1 - \frac{3uT_1^2}{20I} \quad (32)$$

After  $t > T_1$  we assume that the control has saturated and the trajectory is approximating the parabolic path. Therefore we can revise our estimate of  $\dot{c}_0$  by replacing  $c_0$  and  $\dot{c}_0$  in Eq. (31) with  $c(T_1)$  and  $\dot{c}(T_1)$  to give:

$$\begin{aligned} \dot{c}_0 &= \dot{c}(T_1) - \frac{I}{2u} \dot{c}(T_1)^2 \\ &= \dot{c}_0 - \frac{I}{2u} \dot{c}_0^2 - \frac{T_1 \dot{c}_0}{2} - \frac{u}{40I} T_1^2. \end{aligned} \quad (33)$$

### Target with Constant Angular Acceleration

We now consider the class of maneuvers in which a constant relative acceleration exists between the target state and the spacecraft. The "motion-to-rest" case, where a constant velocity difference initially exists is a special case of this problem; relative acceleration between the target state and the spacecraft is zero. In Eq. (26) it was observed that, for the rigid body system, the target acceleration could be expressed in terms an equivalent control input by multiplying the target acceleration by the spacecraft axial moment of

inertia. This allows us to reduce the problem to an equivalent "motion-to-rest" problem in which the control bounds are asymmetric about  $u = 0$ . That is:

$$\begin{aligned} u_{min} &\leq u \leq u_{max} \\ u_{min} &= -u_0 - I\ddot{\theta}_{target} \\ u_{max} &= -u_0 - I\ddot{\theta}_{target} \end{aligned}$$

Although  $\ddot{\theta}_{target}$  is not directly measurable, it can be deduced from Eq. (25) and will hereinafter be expressed as  $\ddot{\theta}_{target} = (\ddot{\theta} - \ddot{\epsilon})$ .

Figure 5 portrays a representative maneuver for the rigid body system in which the target and spacecraft states have a relative angular acceleration. Notice that the parabolic trajectories are not symmetric about the desired value of  $\epsilon_{switch}$ .

The equation for the equivalent "rest-to-rest" initial angle is expressed in terms of  $u = \pm u_0$  the sign of which, ironically, is dependent on the initial conditions. We cannot determine the value of  $s$  upon which the switching logic depends until  $\dot{\epsilon}_0$  and  $\epsilon_{switch}$  are calculated. But these cannot be calculated without knowing  $\text{sgn}(s)$ . A sign convention is established by recalling the parabolic switching function in Eq. (8) which can now be written:

$$s_p = \epsilon(t) + \frac{I}{2|u|} \dot{\epsilon}(t) \cdot \dot{\epsilon}(t) = 0. \quad (34)$$

This curve represents the optimal switchless trajectories to the origin and is constant regardless of initial conditions. All that is needed is the value of  $s_p(t=0) \equiv s_{p0}$ . Thus:

$$s_{p0} = \epsilon_0 + \frac{I}{2|u|} \dot{\epsilon}_0 \dot{\epsilon}_0. \quad (35)$$

Replacing  $u$  with the appropriate control magnitude gives:

$$s_{p0} = \epsilon_0 + \frac{I\dot{\epsilon}_0|\dot{\epsilon}_0|}{2[u_0 - I(\ddot{\theta} - \ddot{\epsilon})\text{sgn}(\dot{\epsilon}_0)]} \quad (36)$$

Recalling Eq. (33) and assuming that  $T_1 < t_1$  (where  $t_1$  is the time to the control switch):

$$\dot{\epsilon}_0 = \epsilon_0 - \frac{T_1}{2} \dot{\epsilon}_0 - \frac{I\dot{\epsilon}_0^2}{2[u_0\text{sgn}(s_{p0}) + I(\ddot{\theta} - \ddot{\epsilon})]} - \frac{[u_0\text{sgn}(s_{p0}) + I(\ddot{\theta} - \ddot{\epsilon})]T_1^2}{40I} \quad (37)$$

Now the asymmetric control bounds may be defined as:

$$u(t) = \begin{cases} u_1, & 0 \leq t \leq t_1 \\ u_2, & t_1 \leq t \leq t_f \end{cases} \quad (38)$$

where:

$$\begin{aligned} u_1 &= -u_0 \operatorname{sgn}(s_{p0}) - I(\ddot{\theta} - \ddot{c}) \\ u_2 &= u_0 \operatorname{sgn}(s_{p0}) - I(\ddot{\theta} - \ddot{c}) \end{aligned} \quad (39)$$

Thus, the trajectory for  $0 \leq t \leq t_1$  may be described by:

$$\epsilon(t) = \dot{\epsilon}_0 - \frac{I}{2u_1} \dot{\epsilon}(t)^2 \quad (40)$$

and the trajectory for  $t_1 \leq t \leq t_f$  is:

$$\epsilon(t) = \frac{I}{2u_2} \dot{\epsilon}(t)^2 \quad (41)$$

Equating Eqs. (40) and (41) gives:

$$\dot{\epsilon}_{switch}^2 = \frac{2\dot{\epsilon}_0}{I} \left( \frac{u_1 u_2}{u_1 - u_2} \right) \quad (42)$$

Substituting Eq. (42) into Eq. (41) gives:

$$\begin{aligned} \epsilon_{switch} &= \dot{\epsilon}_0 \left( \frac{u_1}{u_1 - u_2} \right) \\ &= \frac{\dot{\epsilon}_0}{2} \left( \frac{u_0 \operatorname{sgn}(s_{p0}) + I(\ddot{\theta} - \ddot{c})}{u_0 \operatorname{sgn}(s_{p0})} \right) \\ &= \frac{\dot{\epsilon}_0}{2} \left( \frac{u_0 + I(\ddot{\theta} - \ddot{c}) \operatorname{sgn}(s_{p0})}{u_0} \right) \end{aligned} \quad (43)$$

The major characteristic which distinguishes the constant acceleration case from the previous cases is the fact that, although the relative states go to the origin as before, the control does not go to zero. Once the target state is intercepted, continued control effort,  $u = I(\ddot{\theta} - \ddot{c})$ , is necessary to keep the target and spacecraft states coincidental. Thus it is necessary to rewrite Eq. (20):

$$u = \{-u_0 - I(\ddot{\theta} - \ddot{c}) \operatorname{sgn}(s)\} \left\{ \tanh \left( \frac{s}{1 - \alpha} \right) \right\} m(t) - I(\ddot{\theta} - \ddot{c}) m(t) \quad (44)$$

Inspection of Eq. (44) reveals that when  $s$  is sufficiently large to saturate the control:  $u = u_0$ , and as  $s \rightarrow 0$  near the origin,  $u = I(\ddot{\theta} - \ddot{e})$ , which is the behavior we desire. Unfortunately with this control, the sign of  $u(t)$  does not change at  $c(t) = c_{switch}$  as desired. Instead, the control actually changes sign where:

$$\{u_0 - I(\ddot{\theta} - \ddot{e})\text{sgn}(s)\} \left\{ \tanh\left(\frac{s}{1-\alpha}\right) \right\} = I(\ddot{\theta} - \ddot{e}) \quad (45)$$

Solving for  $s$  we find that the control switches at:

$$s_{switch} = \left(\frac{1-\alpha}{2}\right) \ln \left[ \frac{u_0 - I(\ddot{\theta} - \ddot{e})(\text{sgn}(s) - 1)}{u_0 - I(\ddot{\theta} - \ddot{e})(\text{sgn}(s) + 1)} \right] \quad (46)$$

Thus, in order to have the control switch as desired:

$$c_{switch} = \frac{\dot{e}_0}{2} \left( \frac{u_0 - I(\ddot{\theta} - \ddot{e})\text{sign}(s_{p0})}{u_0} \right) - s_{switch} \left( \frac{u_0 - I(\ddot{\theta} - \ddot{e})\text{sgn}(s_{p0})}{u_0} \right) \quad (47)$$

Equations (21), (44), (46) and (47) give a complete set of equations for controlling the spacecraft to track a target state with constant angular acceleration. They are, in fact, compatible with all previous maneuvers considered.

A representative maneuver is shown in Fig. 6. As one might expect from a near-minimum time maneuver, except for the influence of control smoothing, the control is saturated, until target interception. Subsequently, the control becomes a tracking control. Although post-rendezvous energy appears high, it is manifest as potential strain energy as a result continued control input to sustain tracking. Modal kinetic energy is very small. In fact, if the control in Eq. (20) is substituted for that in Eq. (44) the control would still attempt to track the target state. However, a steady state error results. This steady state error is found to be:

$$e(\infty) = \frac{1-\alpha}{2} \ln \left( \frac{u_0 - I(\ddot{\theta} - \ddot{e})}{u_0 + I(\ddot{\theta} - \ddot{e})} \right), \quad \dot{e}(\infty) = 0 \quad (48)$$

The accelerating target case illustrates a major advantage of this control design over the alternate approaches to quiescent boundary conditions such as the LQR. With only a

minor modification of the control law, a target with an acceleration component can be intercepted with a control profile which possesses the characteristics of a minimum time control; the control saturates and there is only a single control switch until the time very near the interception. No additional constraints beyond the kinematic constraints,  $e(t_f) = \dot{e}(t_f) = 0$  need be included.

### Multi-Body/Multi-Actuator Configurations

The control technique thus far developed is not restricted to single actuator, single body systems. It can also be applied to multiple, interconnected bodies with multiple controls. As a general illustration of the techniques required, consider the generic two-body system in Fig 7. This is an approximate model of the Rapid Retargeting and Precision Pointing (R2P2) experiment being conducted by Martin Marietta Corp. The dynamical system consists of two bodies;  $A$  is rigid while  $B$  is flexible. The actual dimensions of the R2P2 model are proprietary, but it is significantly larger and the flexible body  $B$  is qualitatively more rigid than the system heretofore considered. Body  $A$  has a continuous momentum exchange type actuator. In addition, an active joint ("gimbalflex") actuator which generates the torque  $U_B$  and the  $F_y$  parallel to the  $y$ -axis is required to prevent large lateral displacements between the two rotating bodies.

In developing the control for the multi-body system, we will proceed as before; first evaluating the rigid body dynamics and then smoothing the control for application to the flexible system.

After linearization, the equations of motion for the system may be expressed in matrix form:<sup>23</sup>

$$\begin{Bmatrix} \ddot{\theta} \\ \ddot{O} \\ \ddot{Y} \end{Bmatrix} = \begin{bmatrix} \frac{R_B}{I_B} & 0 & \frac{-1}{I_B} \\ \left(\frac{R_B}{I_B} - \frac{R_A}{I_A}\right) & \frac{1}{I_A} & -\left(\frac{1}{I_A} + \frac{1}{I_B}\right) \\ \left(\frac{1}{m_A} + \frac{1}{m_B} - \frac{R_A^2}{I_A} - \frac{R_B^2}{I_B}\right) & \frac{-R_A}{I_A} & \left(\frac{R_A}{I_A} - \frac{R_B}{I_B}\right) \end{bmatrix} \begin{Bmatrix} F_y \\ U_A \\ U_B \end{Bmatrix} \quad (49)$$

where  $m_{A,B}$  are the body masses,  $R_{A,B}$  are the moment arms from the mass centers to the interface and  $I_{A,B}$  are the moments of inertia about the centroidal axis of each body

respectively. In Eq. (49), for simplicity, we ignore all flexible body effects. We have, in other developments, included flexible body effects (of body  $B$ ) and the simulated controlled responses discussed below include flexible body effects.

The net control torque on  $A$  and  $B$  is:

$$\begin{aligned} U_{A_{net}} &= U_A - U_B - R_A F_y \\ U_{B_{net}} &= U_B - R_B F_y \end{aligned} \quad (50)$$

Two scenarios are examined. In the first, it is desired to rotate the entire system in a synchronized manner, so that  $\phi$ , the angle between the two bodies is kept as small as possible. In the second scenario, it is desired to rotate only the flexible portion of the system, leaving the rigid body orientation undisturbed. In both cases, the major task is ascertaining the permissible control limits for each actuator.

It is clear that the permissible torque to ensure synchronization may not coincide with the actual physical limits of the actuators. Generally, the physical limits of one of the actuators will constrain the remainder to some less than maximum limit. In addition, it is possible that the system may have acceleration or velocity limits which do not permit the full exploitation of the actuators. Here, we allow  $U_A$  to saturate and find new control limits for  $U_B$  and  $F_y$  to satisfy the constraints.

Setting  $\ddot{\phi} = 0$  in Eq. (49) and substituting Eq. (50) gives:

$$\frac{U_{A_{net}}}{U_{B_{net}}} = \frac{I_A}{I_B} \quad (51)$$

This result is confirmed by equating the maneuver times for each body from Eq. (10). Now setting  $\ddot{y} = 0$  in Eq. (49) to ensure the displacement between  $A$  and  $B$  remains small and substituting with Eqs. (50) and (51) gives:

$$F_y = \frac{(R_A + R_B)m_A m_B}{I_A(m_A + m_B)} U_{A_{net}} \quad (52)$$

Let the saturation torque of  $U_A$  be  $U_{A_0}$ . From Eqs. (50) and (52):

$$U_{A_{net,0}} = \frac{U_{A_0} I_A (m_A + m_B)}{(I_A - I_B)(m_A + m_B) - (R_A - R_B)^2 m_A m_B} \quad (53)$$



$F_{y_0}$  is now found from Eq. (52) and:

$$\dot{U}_{B0} = \frac{I_B}{I_A} \dot{U}_{A_{act},0} - R_B F_{y_0} \quad (54)$$

In the second case under consideration, it is desired to rotate the flexible body as rapidly as possible while leaving the rigid body's orientation undisturbed. Setting  $\ddot{\theta} = \ddot{\alpha}$  in Eq. (49) leads to the logical outcome that  $\dot{U}_{A_{act}} = 0$ . Now the flexible body actuator is the limiting factor; the control torque necessary to prevent  $A$  from rotating will be small compared to the actuator limits. Setting  $\ddot{Y} = 0$  gives:

$$F_y = \frac{R_B m_A m_B \dot{U}_B}{I_B m_B - I_B m_A - R_B^2 m_A m_B} \quad (55)$$

and, from Eq. (50), with  $\dot{U}_{A_{act}} = 0$ :

$$\dot{U}_A = \dot{U}_B + R_A F_y \quad (56)$$

If an initial displacement  $Y(0) = Y_0 > 0$  exist,  $\ddot{Y} = 0$  will result in a linear displacement in time between the two bodies. To compensate for this a damping term is introduced via:

$$\ddot{Y} = -2\zeta\omega_n\dot{Y} - \omega_n^2 Y = d \quad (57)$$

where  $\omega_n$  is selected to be some cutoff frequency appropriate to the structure and  $\zeta = 1$ . Equations (52) and (55) are used to calculate control limit  $F_{y_0}$  after which  $d$  (which is expected to be very small) is added to time varying value of  $F_y$  from those equations.

It is clear that in both scenarios the saturation limits of the controls are related by constant ratios. Once the control limits for the particular maneuver are established, it is a simple matter to apply them to the smoothing functions found previously. The control histories of the three actuators differ only in magnitude. Figure 8 shows the control of the flexible portion (body B) of the two-body spacecraft for a synchronized maneuver, including the rotational/vibrational coupling effects which cause the high frequency effects evident in Fig. 8 (b),(c). The high frequency effects are much more pronounced for sharper control histories.

### Conclusions

The problem of slewing a flexible spacecraft in near-minimum time has been considered. A relatively simple control scheme was developed by approximating the minimum time "bang-bang" control for a rigid body. The control law was modified to accommodate accelerating targets by converting the problem to an equivalent rest-to-rest maneuver with asymmetric control bounds. It was shown that it can be applied to systems with multiple bodies and actuators. Simulations using models of both very flexible, and nearly rigid structures verify that this approach is workable for a wide range of space structures.

Sufficient control smoothing and symmetry of the state space trajectory about the control switch are the most important factors in ensuring that the flexible modes of vibration are quiescent in the least time for rest-to-rest maneuvers. Of lesser importance is the smoothness of the initial and terminal control.

This control design is simple and can be executed in real time; it is very robust and unaffected by spacecraft parameter estimation error. Final time is not specified and state estimation is not required.

### Acknowledgments

This research was made possible by funding provided by the U.S. Air Force Office of Scientific Research (contract no. F49620-86-K-00014DEF under Dr. Anthony Amos) and Martin Marietta (Denver) Aerospace (contract no. GH-180166, with technical monitor Dr. Gary Skidmore). We are grateful for their support. Furthermore, we wish to acknowledge the invaluable assistance we received from A. M. Browder and Dr. R. C. Thompson. We value their friendship and encouragement as much as their technical expertise.

### References

- <sup>1</sup> Junkins, J.L. and Turner, J.D. *Optimal Spacecraft Rotational Maneuvers*, First Edition. Elsevier Scientific Publishing Co., New York, 1985. .
- <sup>2</sup> Turner, J.D. and Junkins, J.L., "Optimal Large Angle Single Axis Rotational Maneuvers of Flexible Spacecraft." *Journal of Guidance and Control*, Vol. 4, No. 6, Nov-Dec 1980, pp. 578-585.
- <sup>3</sup> Turner, J.D. and Chun, H.M., "Optimal Distributed Control of a Flexible Spacecraft Using Control-Rate Penalties in the Controller Design." presented at the AIAA AAS Astrodynamics Conference, San Diego, CA. 9-12 Aug 1982.
- <sup>4</sup> Juang, J.N., "Frequency-Shaped Large-Angle Maneuvers". AIAA Paper no. 87-0174. presented at the AIAA/AAS Aerospace Sciences Meeting, Reno, NV, Jan. 1987.
- <sup>5</sup> Vander Velde, W. and Jun He, "Design of Space Structure Control Using On-Off Thrusters," *Journal of Guidance, Control and Dynamics*, Vol. 6, No. 1, Jan-Feb 1983, pp. 53-60.
- <sup>6</sup> Floyd M.A., Doctor of Science Thesis, "Single Step Optimal Control of Large Space Structures," Massachusetts Institute of Technology, Cambridge, MA, 1984.
- <sup>7</sup> Singh, G., Kabamba, P.T. and McClamroch, N.H., "Planar Time Optimal, Rest to Rest, Slewing Maneuvers of Flexible Spacecraft," *Journal of Guidance, Control and Dynamics*, submitted for publication, June 1987.
- <sup>8</sup> Thompson, R.C., Junkins, J.L. and Vadali, S.R., "Near Minimum Time Open Loop Control of Dynamic Systems," presented at the AIAA Dynamics Specialists Conference, Monterey, CA, April 9-10, 1987.
- <sup>9</sup> Breakwell, J.A., "Optimal Feedback Slewing of Flexible Spacecraft," *Journal of Guidance and Control*, Vol. 4, No. 5, Sep-Oct 1981, pp. 472-479.
- <sup>10</sup> Junkins, J.L., "Comment on 'Optimal Feedback Slewing of Flexible Spacecraft'," *Journal of Guidance and Control*, Vol. 5, No. 3, May-June 1982, pp. 318.
- <sup>11</sup> Bryson, A.E. Jr., and Ho, Yu-chi, *Applied Optimal Control*, Revised Printing, Hemisphere Publishing Corp., Washington D.C., 1975, pp. 158-167.
- <sup>12</sup> Ryan, E.P., *Optimal Relay and Saturating Control System Synthesis*, First Edition, Peter Perigrinus Ltd., London, 1982. .
- <sup>13</sup> Wang, P.K.C., "Control of Distributed Parameter Systems." in *Advances in Control Systems*, Leondes, C.T., ED. New York: Academic Press, 1964, chap. . pp. 75-172.
- <sup>14</sup> Subrahmanyam, M.B., "Computation of Optimal Controls by Newton's Method Using a Discretized Jacobian," *Journal of Guidance, Control and Dynamics*, Vol. 9, No. 3, May-June 1986, pp. .

<sup>15</sup> Vadali, S. R. and Junkins, J.L., "Optimal Open-Loop and Stable Feedback Control of Rigid Spacecraft Attitude Maneuvers." *Journal of Astronautical Sciences*, Vol. 32, No. 2, Apr-Jun 1984, pp. 105-122.

<sup>16</sup> Itkis, U., *Control Systems of Variable Structure*, First Edition, Wiley, New York, 1976, .

<sup>17</sup> Öz H. and Özünger, Ü., "Variable Structure System Control for Flexible Spacecraft," presented at the AIAA/AAS Astrodynamics Conference, Seattle, WA, Aug 20-22, 1984.

<sup>18</sup> Vadali, S.R., "Variable Structure Control of Spacecraft Large Angle Maneuvers," *Journal of Guidance, Control and Dynamics*, Vol. 9, No. 2, Mar-Apr 1986, pp. 235-239.

<sup>19</sup> Mostafa, O. and Öz H., "Maneuvering of Flexible Spacecraft Via VSC," presented at the AIAA, AAS Guidance, Navigation and Control Conference, Williamsburg, VA, August 18-20, 1986.

<sup>20</sup> Slotine, J.J. and Sastry, S.S., "Tracking Control of Non-Linear Systems Using Sliding Surfaces with Applications to Robot Manipulators," *International Journal of Control*, Vol. 38, No. 2, 1983, pp. 465-492.

<sup>21</sup> Slotine, J.J., "Sliding Controller Design for Non-linear Systems," *International Journal of Control*, Vol. 40, No. 2, 1984, pp. 421-434.

<sup>22</sup> Balas, M.J., "Direct Velocity Feedback Control of Large Space Structures," *Journal of Guidance and Control*, Vol. 2, No. 3, May-Jun 1979, pp. 252-253.

<sup>23</sup> Browder, A.M. et al, "Control Methodologies for Spaced Based Laser Rapid Retargeting and Precision Pointing," Final Report under contract GH6-180166, for Martin Marietta Denver Aerospace, Texas A&M University, College Station, TX, Jan 1988.

<sup>24</sup> Byers, R.M., Master of Science Thesis, "Feedback Control Design for Smooth, Near Minimum Time Rotational Maneuvers of Flexible Spacecraft," Texas A&M University, College Station, TX, Aug 1987.

## LIST OF FIGURES

Figure 1. Flexible Spacecraft Model

- (a) Undeformed State
- (b) Anti-symmetric Deformations

Figure 2. Smoothing Functions

- (a) Hyperbolic Tangent Function
- (b) Multiplier Function

Figure 3. 15° Rest-to-Rest Maneuver

$$T_1 = .35 \text{ sec}, \alpha = .93, \beta = .97$$

- (a) Torque History
- (b) Elastic Mode Energy
- (c) State-Space Trajectory

Figure 4. 15° Rest-to-Rest Maneuver

$$T_1 = 1.0 \text{ sec}, \alpha = \beta = .92$$

- (a) Torque History
- (b) Elastic Mode Energy
- (c) State-Space Trajectory

Figure 5. Intercept of an Accelerating Target

Figure 6. Accelerating Target Intercept Maneuver

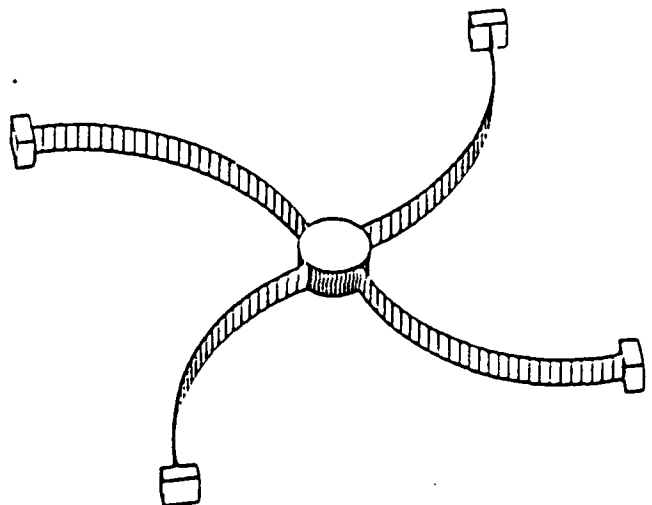
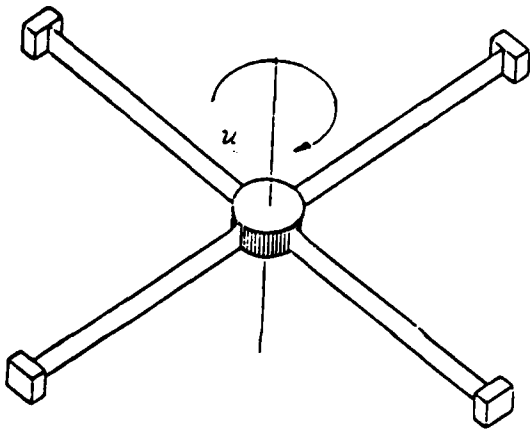
$$e_0 = -57.3^\circ, \dot{e}_0 = 2^\circ/\text{sec}, \ddot{\theta}_{\text{target}} = 5^\circ/\text{sec}^2$$

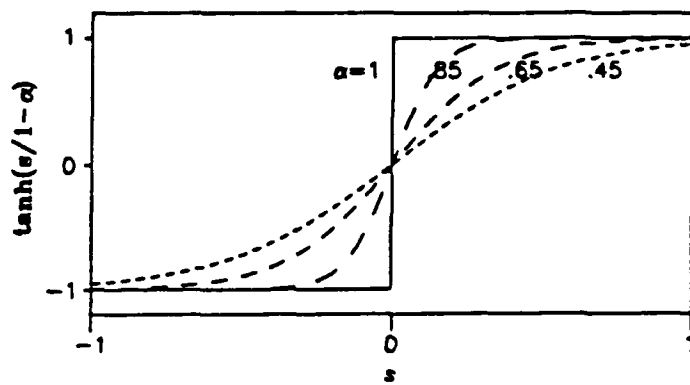
- (a) Torque History
- (b) Elastic Mode Energy
- (c) State-Space Trajectory

Figure 7. Multiple Body/Actuator System

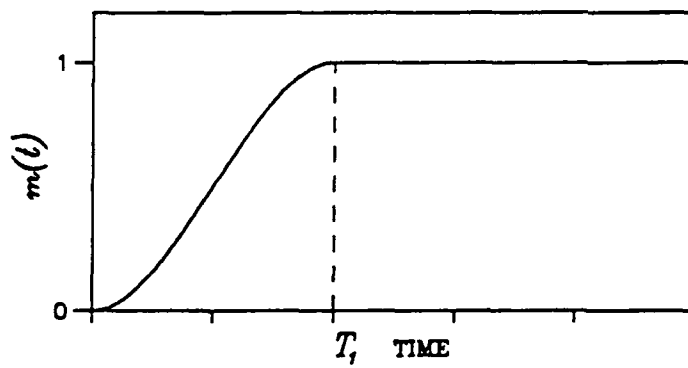
Figure 8. 10° Rest-to-Rest Maneuver

Fig. 1, 2, 3, 4, 5

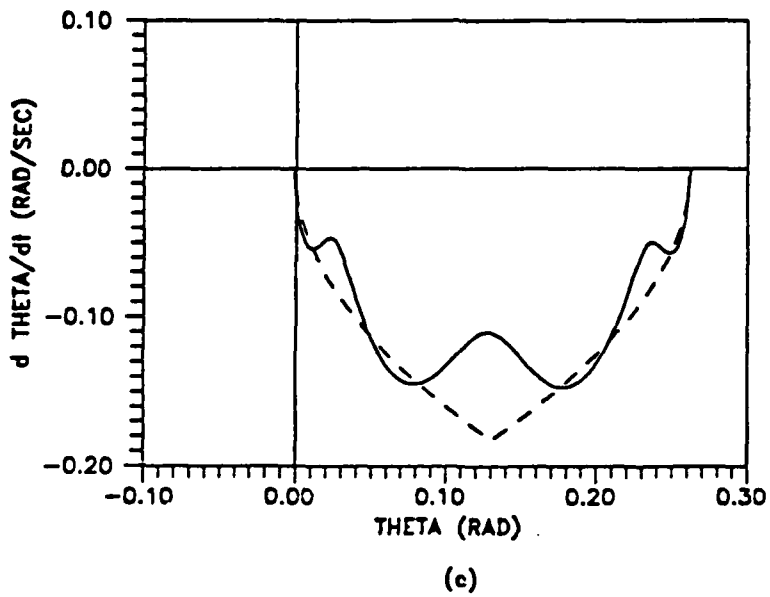
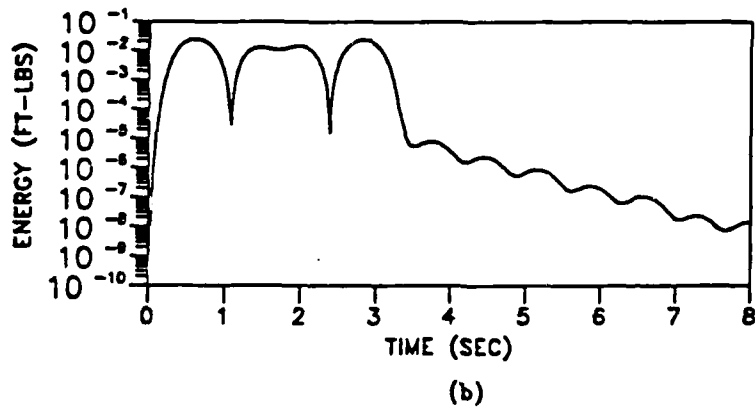
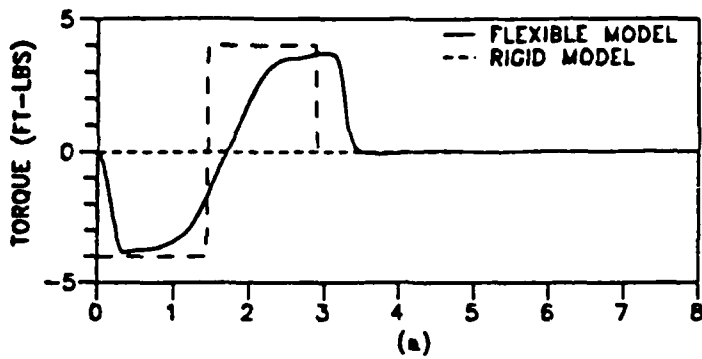




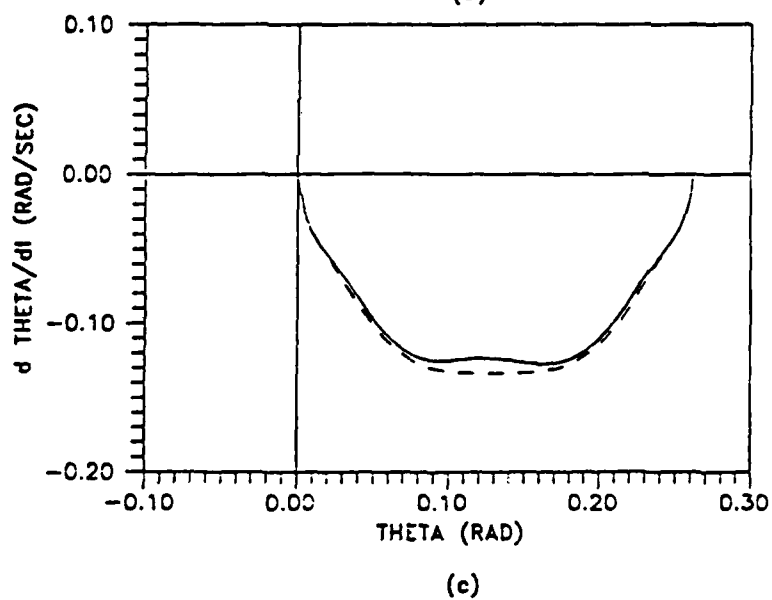
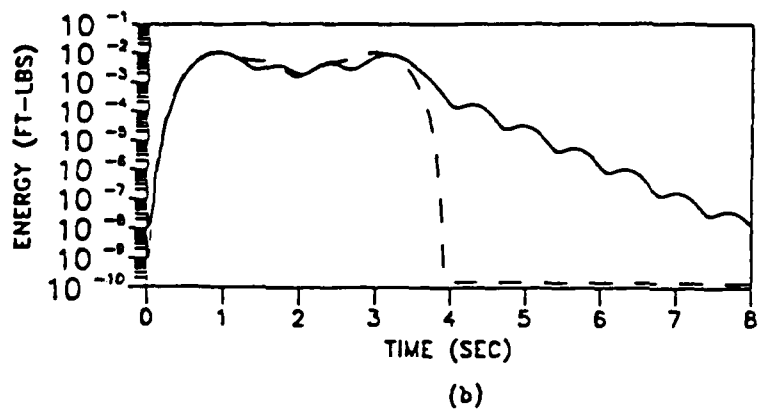
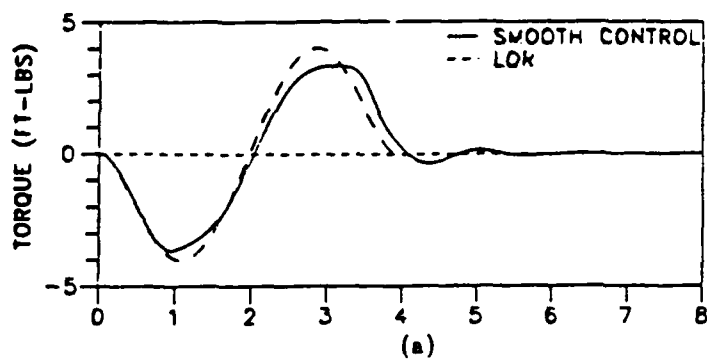
(a) Hyperbolic Tangent Function

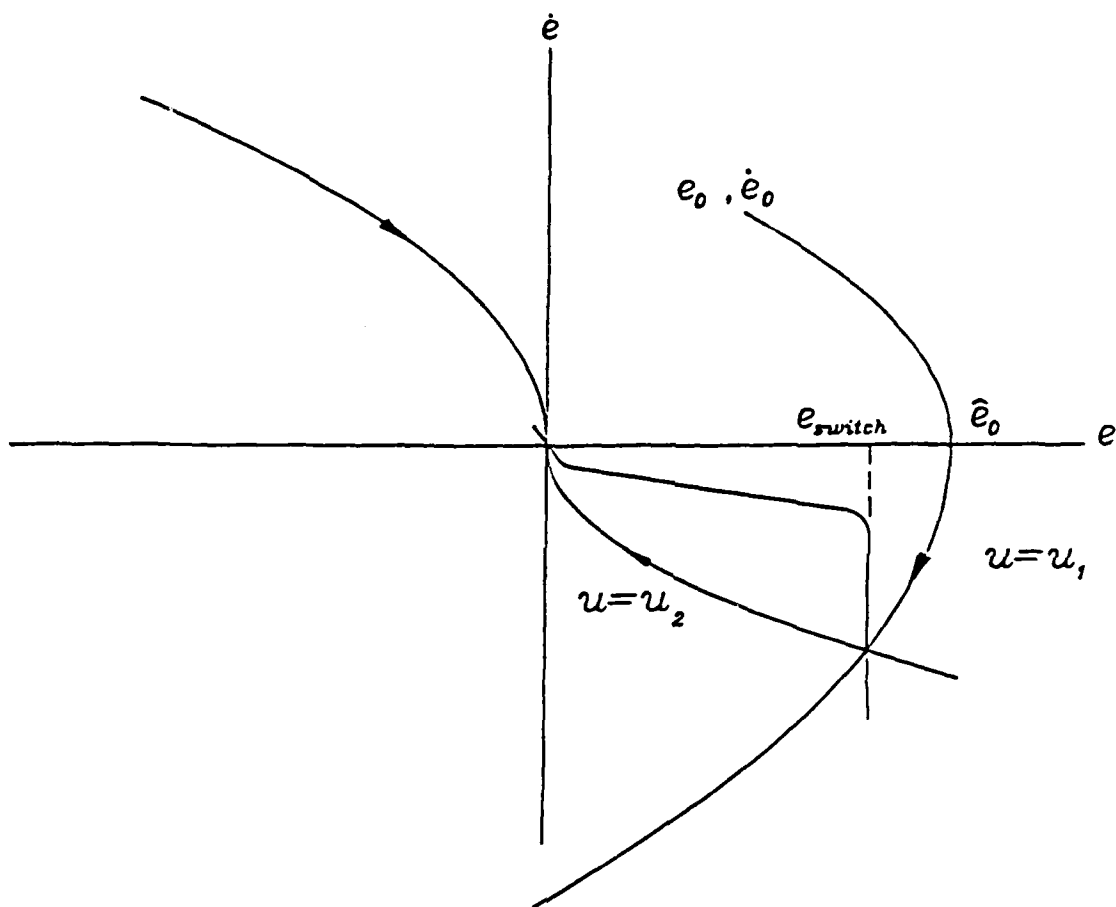


(b) Multiplier Function

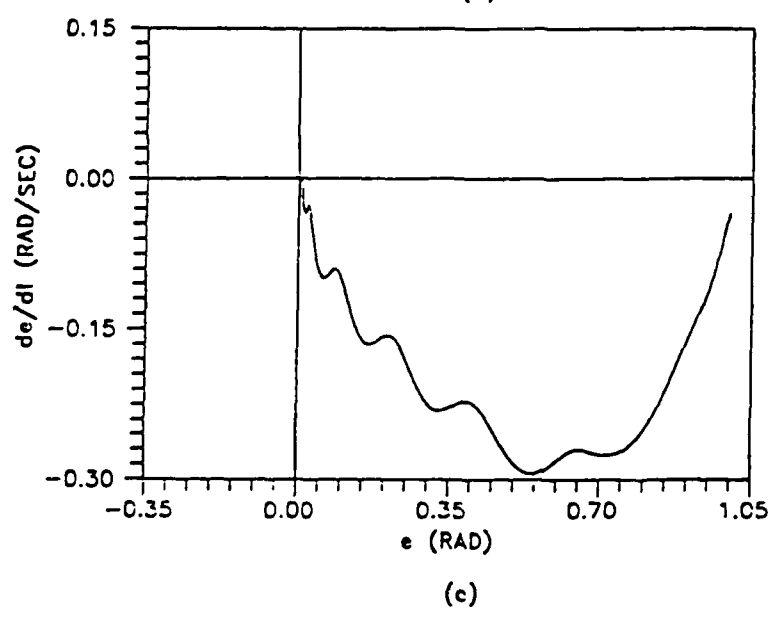
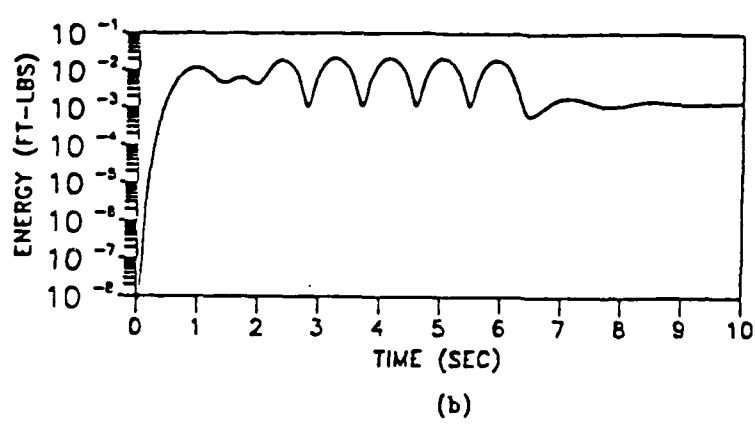
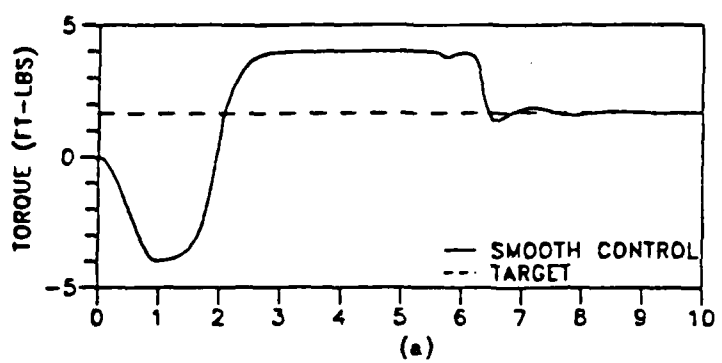




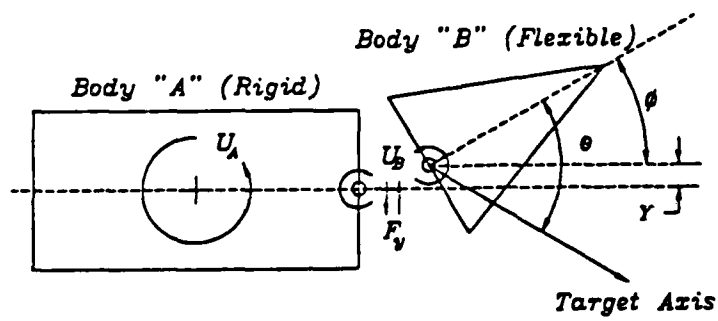




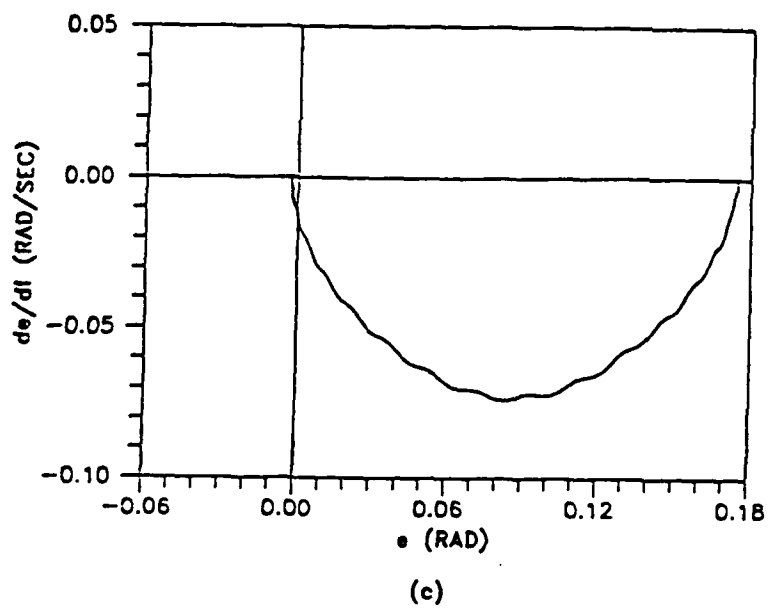
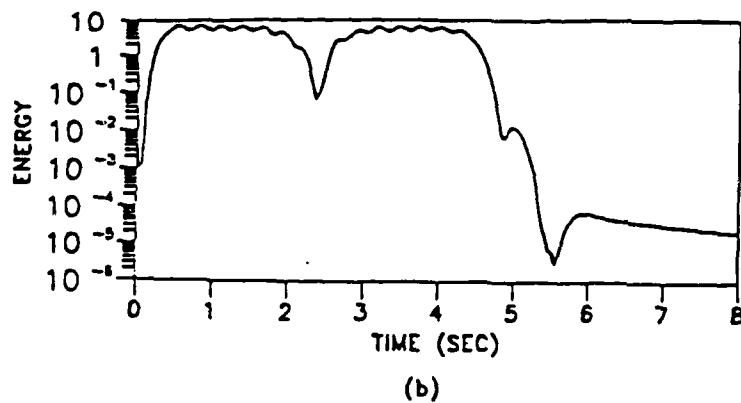
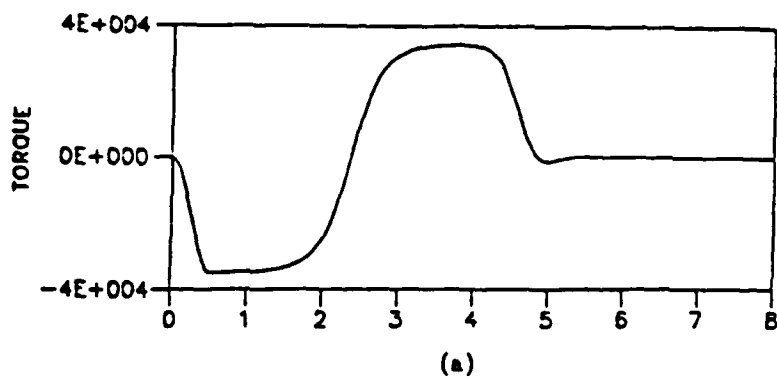
File 6



54 F. 11  
F. 11.2



$\Delta N = 4.5$   
 FIG 8 (a) (b) (c)



## **ATTACHMENT 3**

# **Feedback Control and Steering Laws for Spacecraft Using Single Gimbal Control Moment Gyros**

**FEEDBACK CONTROL AND STEERING LAWS FOR SPACECRAFT  
USING SINGLE GIMBAL CONTROL MOMENT GYROS**

**A Thesis  
by  
HWA-SUK OH**

**Submitted to the Graduate College of  
Texas A&M University  
in partial fulfillment of the requirement for the degree of  
MASTER OF SCIENCE**

**December 1988**

**Major Subject: Aerospace Engineering**

## ABSTRACT

Feedback Control and Steering Laws for Spacecraft  
using Single Gimbal Control Moment Gyros. (Dec. 1988)  
Hwa-Suk Oh, B.S., Hankuk Aviation College  
Chairman of Advisory Committee: Srinivas R. Vadali

The complete dynamic equations for large angle rotational maneuvers of spacecraft using single gimbal control momentum gyros are derived by Newton-Euler as well as Lagrangian approaches. Feedback control laws are developed by using Liapunov stability theory. Gimbal rate steering laws are derived by neglecting gimbal and wheel transverse inertia terms. A gimbal acceleration steering law is also developed by including all the CMG inertia terms.

With these control and steering laws, several rotational maneuvers are simulated numerically by a Runge-Kutta method. The feedback control laws in combination with either velocity or acceleration steering laws are shown to work well. Especially, a varying gain feedback control law is shown to be effective in alleviating the gimbal lock problem. It is found that the velocity steering law is adequate for simulations, but the acceleration steering law provides more reliable and useful data regarding gimbal torques. It is also observed that for a given maneuver, there exists a preferred set of gimbal angles which can aid in avoiding singularities.



## ACKNOWLEDGMENT

The author wishes to express his sincere appreciation to his advisor, Dr. S. R. Vadali, whose thoughtful guidance and patient understanding has helped him adjust to the rigors of graduate study. Thanks also to Dr. J. L. Junkins and Dr. G. M. Huang for their help and support and for serving on the graduate committee. The author is indebted to numerous colleagues for helpful discussion. Partial financial support was provided by AFOSR/AFAL contract F49620-86-K-0014DEF monitored by Dr. Alok Das and Dr. Anthony K. Amos. The support of TEES Engineering Excellence Fund as well as the Texas Advanced Technology Grant are also acknowledged.

The author is also most grateful to his parents for their unyielding support. Finally, the author thanks Yun-hi for her consistent encouragement and patience.

## TABLE OF CONTENTS

Chapter	Page
ABSTRACT .....	iii
ACKNOWLEDGMENTS .....	iv
TABLE OF CONTENTS .....	v
LIST OF TABLES .....	vii
LIST OF FIGURES .....	viii
I. INTRODUCTION .....	1
II. SYSTEM DYNAMICS .....	5
1. System Configuration .....	5
2. Kinematic Equations .....	7
3. Dynamic Equations .....	7
III. FEEDBACK CONTROL LAWS .....	14
IV. STEERING LAWS .....	19
1. Moore-Penrose Steering Law .....	19
2. Singularity Robustness Steering Law .....	21
3. Acceleration Steering Law .....	23
V. SIMULATIONS .....	25
1. Constant Gain Feedback with S-R Steering .....	28
2. Varying Gain Feedback with S-R Steering .....	30
3. Constant Gain Feedback with Acceleration Steering .....	30
4. Varying Gain Feedback with Acceleration Steering .....	31
5. Another Example Maneuver .....	32
VI. CONCLUSION AND RECOMMENDATIONS .....	33
REFERENCES .....	34

APPENDIX .....	63
VITA .....	66

## LIST OF TABLES

Table	Page
I. Simulation Model Characteristic Data . . . . .	36
II. System States for Simulation 1, 4, and 5 . . . . .	37
III. System States for Simulation 2, 3, and 6 . . . . .	37
IV. System States for Simulation 7 . . . . .	38

## LIST OF FIGURES

Figure	Page
1. System with the $i$ th SGCMG . . . . .	39
2. The $i$ th CMG related Frames and Vectors . . . . .	40
3. Pyramid Type CMG Configuration . . . . .	41
4. Results of Simulation 1 . . . . .	42
5. Results of Simulation 2 . . . . .	45
6. Results of Simulation 3 . . . . .	47
7. Results of Simulation 4 . . . . .	50
8. Results of Simulation 5 . . . . .	54
9. Results of Simulation 6 . . . . .	55
10. Results of Simulation 7 . . . . .	59

## CHAPTER I

### INTRODUCTION

Spacecraft attitude control systems use either external torques or internal torques. On-off thrusters are of the external type and employed for fast/coarse attitude control, but they are not suitable for precise attitude acquisition due to their discontinuous mode of operation. Reaction wheels and control moment gyros (CMGs) are internal torque devices; their operation is based on momentum exchange. Reaction wheel systems can achieve and maintain precise attitude due to their smooth operating modes. However, they are unsuitable for fast attitude maneuvers and their varying wheel speeds can cause structural dynamic excitations.

A control moment gyro is composed of two parts, a fixed speed rotating wheel and the gimbal(s). The axis of the wheel can rotate about the gimbal axis, and the gimbal is either free to rotate or fixed to the supporting structure of the spacecraft. When input torque is applied about the gimbal axis, output torque is exerted on the supporting structure about an axis normal to the gimbal axis as well as the spin axis. A CMG can be classified by the number of gimbals, i.e., single gimbal CMG (SGCMG) or double gimbal CMG (DGCMG). For the DGCMG, the output torque is transferred to the spacecraft by balancing it with the outer gimbal motor torque. Thus the problems of torque balancing and hardware complexity are disadvantages of DGCMG.

The SGCMG has simpler mechanical structure than DGCMG. It transfers the output torque directly to the structure, thus it does not need any balancing torque. Despite these advantages of SGCMG, serious analytical difficulties exist in the development of gimbal steering laws. These difficulties are due to "singularities"

---

Journal model is *AIAA Journal of Aircraft*.

which are intrinsic to the SGCMG.

Much work has been done to solve this singularity problem and several methods are shown effective in particular cases. Margulies and Aubrun<sup>1</sup> built the theoretical foundation and identified the different types of singularities. Cornick<sup>2</sup> developed singularity avoidance steering laws, and suggested a simple way to avoid singularities using null motion( gimbal motion for which no torque is produced ). Kurokawa *et al.*<sup>3</sup> proposed a steering law based on off-line calculation of all singularity locations in the gimbal angle space. As a particular singularity is approached, appropriate null motion is added. The storage required is about 250K bytes. Many other authors developed similar techniques to avoid singularities. However, Bauer<sup>4</sup> has shown that there is no general steering law to avoid all singularities.

Nakamura and Hanafusa<sup>5</sup> developed the so-called singularity robustness steering law (S-R steering law) for solving robot manipulator steering problem. Bedrossian<sup>6</sup> has shown that this law can be used for SGCMG systems and a large class of internal singularities can be avoided as there exist non-zero solutions at these singular points. At some singular points, the gimbal rates are infinitesimal, which causes the " gimbal lock " phenomenon. Nevertheless, this S-R steering law is very attractive due to the existence of solutions at many singular points, albeit approximate.

All the above authors developed steering laws by assuming the required torque to be of simple open loop forms and they also did not consider the effect of spacecraft dynamics on the performance of the steering laws. They also simplified the problem by neglecting the inertia of gimbals and the transverse inertia of rotating wheels.

For feedback control, control laws which define the required torque as a function of the states of the system have to be developed. Usually, control laws have

been derived from linearized system equations for small angle rotational maneuvers (attitude control). For feedback control of linear systems, Kalman and Bertram<sup>7</sup> first suggested an approach based on Liapunov's Second method. Vadali and Junkins<sup>8</sup> developed feedback control laws for reaction wheel systems using this approach. Wie and Barba<sup>9</sup> also suggested a similar technique for developing feedback control laws and suggested a means of using on-off thrusters for producing the desired torque. Before developing the control law, the dynamic equations should be derived first. The complexity of dynamic equations including the gyro inertia terms lead many authors to neglect them. For DGCMG, Ross and Melton<sup>10</sup> derived the dynamic equations including some of the inertia terms. They also used quaternions to describe the attitude of the spacecraft as well as the gimbal positions.

In this thesis, large angle rotational maneuvers of rigid spacecraft with SGCMGs are considered. In chapter 2, the complete dynamic equations including the gyro inertia terms are derived by Newton-Euler approach. They are derived from angular momentum analysis based on typical frame conventions<sup>11</sup>.

In chapter 3, feedback control laws are developed by using Liapunov's second theorem. The feedback control laws are quite general and can be used for slewing, motion-to-rest, rest-to-rest, as well as tracking maneuvers.

In chapter 4, two existing velocity steering laws are reviewed and different types of singularities are analyzed. The varying gain method is suggested for escaping from some internal singularities. An acceleration steering law is developed by including gimbal and wheel transverse moments of inertia.

In chapter 5, with these control and steering laws, several rotational maneuvers are simulated numerically by a Runge-Kutta method. The results of numerical simulations using different steering laws are compared.



Chapter 6 presents a summary and conclusion of the work contained in this thesis along with recommendations for further study in this area.

## CHAPTER II

### SYSTEM DYNAMICS

To derive the rotational equations of motion, there are two approaches, i.e. Lagrangian and Newton-Euler approach. Here, the Newton-Euler approach based on angular momentum of system is used. Euler parameters and angular velocities are used as vehicle states, and the gimbal angles and rates are used as CMG states.

At first, the system configuration is briefly described, and the relative location of each component is defined by several coordinate systems ( frames ), vectors, and matrices. Based on these definitions, kinematic and dynamic equations are derived.

#### 1. System Configuration

Consider an arbitrary asymmetric spacecraft equipped with  $n$  SGCMGs. The spacecraft system is divided into  $n + 1$  parts, i.e. a vehicle body and  $n$  SGCMGs. The vehicle body is assumed rigid. The system mass center  $C$  and the location of the  $i$ th CMG, are shown in Fig. 1.

Spacecraft attitude can be represented by relative rotation of vehicle body frame  $\{\hat{V}\}$  with respect to inertial frame  $\{\hat{N}\}$  through a direction cosine matrix  $C_V$  as

$$\{\hat{V}\} = C_V(\beta)\{\hat{N}\}, \quad (2-1)$$

where  $C_V(\beta)$  is parameterized as a function of Euler parameters as

$$C_V(\beta) = \begin{bmatrix} \beta_0^2 + \beta_1^2 - \beta_2^2 - \beta_3^2 & 2(\beta_1\beta_2 + \beta_0\beta_3) & 2(\beta_1\beta_3 - \beta_0\beta_2) \\ 2(\beta_1\beta_2 - \beta_0\beta_3) & \beta_0^2 - \beta_1^2 + \beta_2^2 - \beta_3^2 & 2(\beta_2\beta_3 + \beta_0\beta_1) \\ 2(\beta_1\beta_3 + \beta_0\beta_2) & 2(\beta_2\beta_3 - \beta_0\beta_1) & \beta_0^2 - \beta_1^2 - \beta_2^2 + \beta_3^2 \end{bmatrix}.$$

The center of the  $i$ th CMG is located at a distance  $r_i$  from the mass center of system. The  $i$ th gyro reference frame  $\{\hat{R}_i\}$  is embedded in the suspension structure, and the suspension structure is fixed in the vehicle body. Hence rotation of gyro

reference frame with respect to  $\{\underline{\hat{V}}\}$  can be described by a direction cosine matrix  $C_{Ri}$  as

$$\{\underline{\hat{R}}_i\} = C_{Ri}(\theta_i)\{\underline{\hat{V}}\}, \quad (2-2)$$

where  $\theta_i$  is a fixed configuration angle. Inside the suspension structure of each gyro, a gimbal is controlled to rotate. The gimbal frame  $\{\underline{\hat{G}}_i\}$  is embedded in each gimbal as shown in Fig. 2(a). The gimbal's rotation with respect to suspension structure can be represented by the location of gimbal frame with respect to gyro reference frame. Thus each gimbal frame is projected onto the gyro reference frame by a direction cosine matrix  $C_{Gi}$  as

$$\{\underline{\hat{G}}_i\} = C_{Gi}(\sigma_i)\{\underline{\hat{R}}_i\}, \quad (2-3)$$

where  $\sigma_i$  is the  $i$ th gimbal rotational angle with respect to  $\{\underline{\hat{R}}_i\}$ . When we consider the gimbal rotation axis as  $z$  axis of gimbal frame,  $C_{Gi}$  can be represented as

$$C_{Gi}(\sigma_i) = \begin{bmatrix} \cos \sigma_i & \sin \sigma_i & 0 \\ -\sin \sigma_i & \cos \sigma_i & 0 \\ 0 & 0 & 1 \end{bmatrix}.$$

From Eqs.(2-2) and (2-3), we can relate the gimbal frame with the vehicle frame as

$$\begin{aligned} \{\underline{\hat{G}}_i\} &= C_{Gi}(\sigma_i)C_{Ri}(\theta_i)\{\underline{\hat{V}}\} \\ &= C_i\{\underline{\hat{V}}\}, \end{aligned} \quad (2-4)$$

where  $C_i$  is a direction cosine matrix orienting the  $i$ th gimbal frame with respect to the vehicle frame, and it depends on the gyro cluster arrangement and the gimbal angles.

All the equations are derived using matrices and vectors for simplicity. Each vector is based in the proper frame. For example, the angular velocity  $\underline{\omega}$  of

vehicle is generally expressed in the vehicle frame, and it can be written as  $\underline{\omega} = [\omega_x \ \omega_y \ \omega_z]^T$ . Each gimbal can only rotate around  $z$  axis of each gimbal frame as shown in Fig. 2(a), so the angular velocity  $\dot{\phi}_i$  of the  $i$ th gimbal is expressed as  $\dot{\phi}_i = [0 \ 0 \ \dot{\phi}_i]^T$  in the gimbal frame. The rotational velocity of gyro wheel is expressed as  $\underline{\Omega} = [0 \ \Omega \ 0]^T$  in gimbal frame because the wheel can rotate only about  $y$  axis of gimbal frame. For any vector  $\underline{x} = [x_1 \ x_2 \ x_3]^T$  in this thesis,  $\tilde{x}$  represents the skew symmetric cross product matrix as

$$\tilde{x} = \begin{bmatrix} 0 & -x_3 & x_2 \\ x_3 & 0 & -x_1 \\ -x_2 & x_1 & 0 \end{bmatrix}.$$

## 2. Kinematic Equations

Spacecraft attitude can be represented by Euler parameters as shown in Eq.(2-1). The kinematic differential equation relating the time derivatives of the Euler parameters to the angular velocity vector  $\underline{\omega}$  of the vehicle, is expressed as follows<sup>8,11</sup>:

$$\dot{\underline{\beta}} = \frac{1}{2} G(\underline{\beta}) \underline{\omega}, \quad (2-5)$$

where

$$\underline{\beta} = \begin{bmatrix} \beta_0 \\ \beta_1 \\ \beta_2 \\ \beta_3 \end{bmatrix} \quad \text{and} \quad G(\underline{\beta}) = \begin{bmatrix} -\beta_1 & -\beta_2 & -\beta_3 \\ \beta_0 & -\beta_3 & \beta_2 \\ \beta_3 & \beta_0 & -\beta_1 \\ -\beta_2 & \beta_1 & \beta_0 \end{bmatrix}.$$

## 3. Dynamic Equations

To derive the dynamic equation of motion, either Newton-Euler approach or Lagrangian approach can be used. In this section, Newton-Euler approach is used and its results are compared with those of Lagrangian approach as shown in the Appendix.

The total angular momentum  $\underline{H}^{S/C}$  of system about the system mass center  $C$  is composed of the angular momenta of the vehicle and the  $n$  CMGs':

$$\underline{H}^{S/C} = \underline{H}^{V/C} + \sum_{i=1}^n \underline{H}_i^{G/C}. \quad (2-6)$$

Each angular momentum vector can be expressed in vehicle frame  $\{\underline{\hat{V}}\}$  as

$$\underline{H}^{V/C} = I^{V/C} \underline{\omega}, \quad (2-7)$$

$$\begin{aligned} \underline{H}_i^{G/C} &= m_i \underline{\tilde{r}}_i \dot{\underline{\tilde{r}}}_i + \underline{H}_i^{G/CG} \\ &= M_i \underline{\omega} + \underline{H}_i^{G/CG}, \end{aligned} \quad (2-8)$$

where  $I^{V/C}$  is the vehicle inertia matrix( does not contain gyro contribution),

$m_i$  is the mass of  $i$ th CMG,

$M_i$  is the contribution of the  $i$ th CMG mass

to the moment of inertia matrix about  $C$ , and

$\underline{H}_i^{G/CG}$  is the  $i$ th CMG angular momentum.

When we define the system inertia matrix  $I^S \equiv I^{V/C} + \sum_{i=1}^n M_i$ , the system total angular momentum can be written as

$$\underline{H}^{S/C} = I^S \underline{\omega} + \sum_{i=1}^n \underline{H}_i^{G/CG}. \quad (2-9)$$

The location of center of mass is fixed, and the value of  $I^S$  remains constant unless the payload is changed. In this thesis, the payload is assumed fixed.

The angular momentum  $\underline{H}_i^{G/CG}$  of each CMG can be derived in gimbal frame as

$$\begin{aligned} \underline{H}_i^{G/CG} &= (J^G C_i \underline{\omega} + J^G \dot{\underline{\alpha}}_i) + (J^W C_i \underline{\omega} + J^W \dot{\underline{\alpha}}_i + J^W \underline{\Omega}) \\ &= (J^G + J^W) C_i \underline{\omega} + (J^G + J^W) \dot{\underline{\alpha}}_i + J^W \underline{\Omega}, \end{aligned} \quad (2-10)$$

where  $J^G$  and  $J^W$  are the inertia matrices of the gimbal and gyro wheel respectively, expressed in gimbal frame. When we define the CMG inertia matrix as  $J \equiv J^G + J^W$  and axial angular momentum of wheel as  $\underline{h} \equiv J^W \underline{\Omega}$ , the above equation can be written as

$$\underline{H}_i^{G/CG} = J C_i \underline{\omega} + J \dot{\underline{c}}_i + \underline{h}. \quad (2-11)$$

To combine  $\underline{H}_i^{G/CG}$  with the vehicle's angular momentum, we rewrite the above equation in vehicle frame as

$$\underline{H}_i^{G/CG} = C_i^T J C_i \underline{\omega} + C_i^T J \dot{\underline{c}}_i + C_i^T \underline{h}. \quad (2-12)$$

Hence the total angular momentum  $\underline{H}^{S/C}$  of the system in vehicle frame can be expressed as

$$\underline{H}^{S/C} = I^S \underline{\omega} + \sum_{i=1}^n (C_i^T J C_i \underline{\omega} + C_i^T J \dot{\underline{c}}_i + C_i^T \underline{h}). \quad (2-13)$$

From Newton-Euler principle, the time derivatives of the total angular momentum of the system with respect to the inertial frame  $\{\hat{N}\}$  is equal to the external torque  $\underline{L}_c$  exerted on the system about the mass center  $C$  as follows:

$$\begin{aligned} \underline{L}_c &= \frac{d}{dt} (\underline{H}^{S/C})_N \\ &= I^S \dot{\underline{\omega}} + \tilde{\omega} I^S \underline{\omega} + \sum_{i=1}^n \frac{d}{dt} (\underline{H}_i^{G/CG})_N. \end{aligned} \quad (2-14)$$

$\frac{d}{dt} (\underline{H}_i^{G/CG})_N$  represents the torque  $\underline{L}_{Gi}$  exerted on the  $i$ th CMG, and  $-\underline{L}_{Gi}$  is the internal torque due to the  $i$ th CMG. The system equation of motion can then be written as

$$-\underline{L}_I + \underline{L}_c = I^S \dot{\underline{\omega}} + \tilde{\omega} I^S \underline{\omega}, \quad (2-15)$$

$$\text{where } \underline{L}_I = \sum_{i=1}^n \underline{L}_{Gi}.$$

In order to express  $\underline{L}_{Gi}$  explicitly in terms of system states, we have to differentiate  $\underline{H}_i^{G/CG}$ . As seen from Eqs.(2-11) and (2-12), it is better to differentiate  $\underline{H}_i^{G/CG}$  as follows:

$$\frac{d}{dt}(\underline{H}_i^{G/CG})_N = \frac{d}{dt}(\underline{H}_i^{G/CG})_{Gi} + {}^N\tilde{\omega}^G(\underline{H}_i^{G/CG}), \quad (2-16)$$

where  ${}^N\tilde{\omega}^G$  is the cross product matrix.

The first term on the right-hand side of the above equation can be written in gimbal frame as

$$\frac{d}{dt}(\underline{H}_i^{G/CG})_{Gi} = J\dot{C}_i\omega + JC_i\dot{\omega} + J\ddot{\sigma}_i + \dot{h}. \quad (2-17)$$

Since the gyro wheel angular velocity  $\Omega$  is constant,  $\dot{h} = 0$ . The time derivative of direction cosine matrix  $C_i$  is given by the following kinematic differential equation.

$$\dot{C}_i = -\tilde{\sigma}_i C_i. \quad (2-18)$$

Thus Eq.(2-17) can be rewritten as

$$\frac{d}{dt}(\underline{H}_i^{G/CG})_{Gi} = -J\tilde{\sigma}_i C_i\omega + JC_i\dot{\omega} + J\ddot{\sigma}_i. \quad (2-19)$$

The second term of Eq.(2-16) can be divided into two parts as

$${}^N\tilde{\omega}^G(\underline{H}_i^{G/CG}) = {}^N\tilde{\omega}^V(\underline{H}_i^{G/CG}) + {}^V\tilde{\omega}^G(\underline{H}_i^{G/CG}) \quad (2-20)$$

where each part can be expressed in gimbal frame as follows:

$${}^N\tilde{\omega}^V(\underline{H}_i^{G/CG}) = C_i\tilde{\omega}C_i^T(JC_i\omega + J\dot{\sigma}_i + \dot{h}), \quad (2-21)$$

$$\begin{aligned} {}^V\tilde{\omega}^G(\underline{H}_i^{G/CG}) &= \tilde{\sigma}_i(JC_i\omega + J\dot{\sigma}_i + \dot{h}) \\ &= \tilde{\sigma}_i(JC_i\omega + \dot{h}), \end{aligned} \quad (2-22)$$

as  $\ddot{\sigma}_i J \dot{\underline{\sigma}}_i = \underline{0}$ . Thus Eq.(2-20) can be rewritten as

$${}^N \tilde{\omega}^G (\underline{H}_i^{G/CG}) = C_i \tilde{\omega} C_i^T (J C_i \underline{\omega} + J \dot{\underline{\sigma}}_i + \underline{h}) + \ddot{\sigma}_i (J C_i \underline{\omega} + \underline{h}). \quad (2-23)$$

Therefore, from Eqs.(2-19) and (2-23), the time derivative of gyro angular momentum can be written in gimbal frame as

$$\begin{aligned} \frac{d}{dt} (\underline{H}_i^{G/CG})_N = & -J \ddot{\sigma}_i C_i \underline{\omega} + J C_i \dot{\underline{\omega}} + J \ddot{\underline{\sigma}}_i \\ & + C_i \tilde{\omega} C_i^T J C_i \underline{\omega} + C_i \tilde{\omega} C_i^T J \dot{\underline{\sigma}}_i + C_i \tilde{\omega} C_i^T \underline{h} \\ & + \ddot{\sigma}_i J C_i \underline{\omega} + \ddot{\sigma}_i \underline{h}. \end{aligned} \quad (2-24)$$

From this equation, we see that each CMG torque  $\underline{L}_{Gi}$  has three components,  $\underline{L}_{Gi} = [L_{G1} \ L_{G2} \ L_{G3}]^T$ . From Fig. 2(a), we see that the  $x$  axis component of  $\underline{L}_{Gi}$  represents the reaction torque due to directional change of wheel and gimbal angular momenta. The  $y$  axis component represents the reaction torque due to the motion of the gimbal frame. The  $z$  axis component represents the control motor torque  $u_i$  which can be expressed as

$$u_i = P_I \underline{L}_{Gi} \quad (2-25)$$

where  $P_I = [0 \ 0 \ 1]$ .

To combine  $\frac{d}{dt} (\underline{H}_i^{G/CG})_N$  with the time derivative of vehicle angular momentum, we rewrite Eq.(2-24) in vehicle frame as

$$\begin{aligned} \frac{d}{dt} (\underline{H}_i^{G/CG})_N = & -C_i^T J \ddot{\sigma}_i C_i \underline{\omega} + C_i^T J C_i \dot{\underline{\omega}} + C_i^T J \ddot{\underline{\sigma}}_i \\ & + \tilde{\omega} C_i^T J C_i \underline{\omega} + \tilde{\omega} C_i^T J \dot{\underline{\sigma}}_i + \tilde{\omega} C_i^T \underline{h} \\ & + C_i^T \ddot{\sigma}_i J C_i \underline{\omega} + C_i^T \ddot{\sigma}_i \underline{h}. \end{aligned} \quad (2-26)$$

Substitution of this expression for  $\frac{d}{dt} (\underline{H}_i^{G/CG})_N$  in Eq.(2-14) leads to



$$\begin{aligned}
(I^S + \sum_{i=1}^n C_i^T J C_i) \dot{\underline{\omega}} = & -\bar{\omega} I^S \underline{\omega} + \underline{L}_c \\
& - \sum_{i=1}^n (-C_i^T J \ddot{\sigma}_i C_i \underline{\omega} + C_i^T J \ddot{\sigma}_i \\
& + \bar{\omega} C_i^T J C_i \underline{\omega} + \bar{\omega} C_i^T J \dot{\sigma}_i + \bar{\omega} C_i^T \underline{h} \\
& + C_i^T \ddot{\sigma}_i J C_i \underline{\omega} + C_i^T \ddot{\sigma}_i \underline{h}). \quad (2-27)
\end{aligned}$$

To simplify the equation, define

$$\begin{aligned}
I & \equiv I^S + \sum_{i=1}^n C_i^T J C_i \\
D_3 \dot{\underline{\sigma}} & \equiv \sum_{i=1}^n (C_i^T \ddot{\sigma}_i J C_i \underline{\omega} - C_i^T J \ddot{\sigma}_i C_i \underline{\omega}) \\
D_2 \dot{\underline{\sigma}} & \equiv \sum_{i=1}^n \bar{\omega} C_i^T J \dot{\sigma}_i \\
D_1 \dot{\underline{\sigma}} & \equiv \sum_{i=1}^n C_i^T \ddot{\sigma}_i \underline{h} \\
B \ddot{\underline{\sigma}} & \equiv \sum_{i=1}^n C_i^T J \ddot{\sigma}_i, \quad (2-28)
\end{aligned}$$

where  $\dot{\underline{\sigma}} = [\dot{\sigma}_1 \ \dot{\sigma}_2 \ \dots \ \dot{\sigma}_n]^T$  and  $\ddot{\underline{\sigma}} = [\ddot{\sigma}_1 \ \ddot{\sigma}_2 \ \dots \ \ddot{\sigma}_n]^T$  represent respectively,  $n$  dimensional angular velocity vector and angular acceleration vector of the gimbals. Then the system dynamic equation can be represented as follows

$$\dot{\underline{\omega}} = -I^{-1} [\bar{\omega} I^S \underline{\omega} - \underline{L}_c + B \ddot{\underline{\sigma}} + (D_1 + D_2 + D_3) \dot{\underline{\sigma}} + \sum_{i=1}^n \bar{\omega} C_i^T (J C_i \underline{\omega} + \underline{h})]. \quad (2-29)$$

This equation can also be derived by Lagrangian approach as shown in the Appendix.

Since this dynamic equation obtained by including the CMG inertia terms is complicated, many studies neglect  $J$  in comparison to the vehicle inertia. For this special case, we need consider the angular momentum of the CMG again.

$$\underline{H}_i^{G/CG} = JC_i\omega + J\dot{\sigma}_i + \underline{h}. \quad (2-11)$$

The first term  $JC_i\omega$  is due to the rotation of spacecraft,  $J\dot{\sigma}_i$  is due to the rotation of the gimbal and  $\underline{h}$  is the axial momentum of the wheel. Gyro wheel usually rotates at much higher speed than  $\omega$  or  $\dot{\sigma}$ , so the magnitude of  $\underline{h}$  is much greater than that of  $(JC_i\omega + J\dot{\sigma}_i)$ . Thus we can often neglect the first two terms in Eq.(2-11). Then the angular momentum of CMG can be expressed as

$$\underline{H}_i^{G/CG} = \underline{h}. \quad (2-30)$$

That is, we can assume that the angular momentum of each CMG is a rotating vector. With this simplified notion, the dynamic equation can be reduced to the following:

$$\dot{\omega} = -(I^S)^{-1} [\tilde{\omega} I^S \omega - \underline{L}_c + D_1 \dot{\sigma} + \sum_{i=1}^n \tilde{\omega} C_i^T \underline{h}]. \quad (2-31)$$

Depending on whether  $J$  terms are included or not, either Eq.(2-29) or Eq.(2-31) can be used as a dynamic equation of system besides the kinematic equation. The gimbal motor torque equation is given by Eqs.(2-24) and (2-25).

## CHAPTER III

### FEEDBACK CONTROL LAWS

If the present state is known and it is desired to maneuver the spacecraft to a target state, we need a feedback control law which defines the required torque as a function of the current and target states. In many situations, linearized equations of motion can be used in developing feedback control laws applicable for small angle rotational maneuvers. For large angle rotational maneuvers, the system equations are nonlinear. For that case, one of the powerful methods for control design is Liapunov's second method. In this chapter, using the Liapunov approach, general feedback control laws for large angle rotational maneuvers of spacecraft with SGCMGs are derived for a wide class of maneuvers including slewing and tracking maneuvers.

Assume that present state of the system  $\underline{\omega}$ ,  $\underline{\beta}$ , and  $\underline{\sigma}$  can be measured in real time and we wish to maneuver the spacecraft to a desired target state  $\underline{\omega}_f$  and  $\underline{\beta}_f$  with the final  $\underline{\sigma}$  free. The error vectors  $\underline{\epsilon}_1$  and  $\underline{\epsilon}_2$  which represent the departure of the instantaneous states from target states can be written as

$$\underline{\epsilon}_1 = \underline{\beta} - \underline{\beta}_f \quad (3-1)$$

$$\underline{\epsilon}_2 = \underline{\omega} - \underline{\omega}_f. \quad (3-2)$$

Let  $V(\epsilon)$  be a trial Liapunov function defined as

$$\begin{aligned} V(\epsilon) &= V_1 + V_2 \\ &= k \underline{\epsilon}_1^T \underline{\epsilon}_1 + \frac{1}{2} \underline{\epsilon}_2^T I \underline{\epsilon}_2, \end{aligned} \quad (3-3)$$

where  $k$  is a positive constant, and  $I$  is the inertia matrix shown in Eq.(2-28). The time derivative of  $V_1$  can be derived as

$$\begin{aligned}
\dot{V}_1(e) &= 2k \underline{e}_1^T \dot{\underline{e}}_1 \\
&= 2k(\underline{\beta}_f^T - \underline{\beta}^T)(\dot{\underline{\beta}}_f - \dot{\underline{\beta}}) \\
&= -2k(\underline{\beta}^T \dot{\underline{\beta}}_f + \underline{\beta}_f^T \dot{\underline{\beta}}),
\end{aligned} \tag{3-4}$$

where  $\underline{\beta}_f^T \dot{\underline{\beta}}_f = 0$ , and  $\underline{\beta}^T \dot{\underline{\beta}} = 0$  due to the Euler parameter constraint  $\underline{\beta}^T \underline{\beta} = 1$ . From Eq.(2-5),  $\dot{\underline{\beta}}$  and  $\dot{\underline{\beta}}_f$  can be written as

$$\dot{\underline{\beta}} = \frac{1}{2} G(\underline{\beta}) \underline{\omega} \tag{3-5}$$

$$\dot{\underline{\beta}}_f = \frac{1}{2} G(\underline{\beta}_f) \underline{\omega}_f. \tag{3-6}$$

Hence each item in Eq.(3-4) can be expressed as

$$\underline{\beta}^T \dot{\underline{\beta}}_f = \frac{1}{2} \underline{\omega}_f^T G^T(\underline{\beta}_f) \underline{\beta}, \tag{3-7}$$

$$\underline{\beta}_f^T \dot{\underline{\beta}} = \frac{1}{2} \underline{\omega}^T G^T(\underline{\beta}) \underline{\beta}_f. \tag{3-8}$$

However,  $G^T(\underline{\beta}_f) \underline{\beta} = -G^T(\underline{\beta}) \underline{\beta}_f$ ; thus  $\dot{V}_1$  can be represented as

$$\dot{V}_1 = -k(\underline{\omega}^T - \underline{\omega}_f^T) G^T(\underline{\beta}) \underline{\beta}_f. \tag{3-9}$$

The time derivative of  $V_2$  can be derived as

$$\begin{aligned}
\dot{V}_2 &= \underline{e}_2^T I \dot{\underline{e}}_2 + \frac{1}{2} \underline{e}_2^T \dot{I} \underline{e}_2 \\
&= (\underline{\omega}^T - \underline{\omega}_f^T)(I \underline{\dot{\omega}} - I \underline{\dot{\omega}}_f) + (\underline{\omega}^T - \underline{\omega}_f^T) \frac{1}{2} \dot{I}(\underline{\omega} - \underline{\omega}_f).
\end{aligned} \tag{3-10}$$

From the definition in Eq.(2-28),  $\frac{1}{2} \dot{I}(\underline{\omega} - \underline{\omega}_f)$  can be derived as

$$\begin{aligned}
\frac{1}{2}\dot{I}(\underline{\omega} - \underline{\omega}_f) &= \frac{1}{2} \sum_{i=1}^n (C_i^T \ddot{\sigma}_i J C_i - C_i^T J \ddot{\sigma}_i C_i) (\underline{\omega} - \underline{\omega}_f) \\
&= -\left[ \frac{1}{2} \sum_{i=1}^n (C_i^T \ddot{\sigma}_i J C_i - C_i^T J \ddot{\sigma}_i C_i) \underline{\omega}_f \right. \\
&\quad \left. - \frac{1}{2} \sum_{i=1}^n (C_i^T \ddot{\sigma}_i J C_i - C_i^T J \ddot{\sigma}_i C_i) \underline{\omega} \right] \\
&= -\left[ \frac{1}{2} D_4 \underline{\dot{\sigma}} - \frac{1}{2} D_3 \underline{\dot{\sigma}} \right], \tag{3-11}
\end{aligned}$$

where  $D_4 \underline{\dot{\sigma}} \equiv \sum_{i=1}^n (C_i^T \ddot{\sigma}_i J C_i - C_i^T J \ddot{\sigma}_i C_i) \underline{\omega}_f$ . Equation (3-10) can then be written as

$$\begin{aligned}
\dot{V}_2 &= -(\underline{\omega}^T - \underline{\omega}_f^T) [I \underline{\dot{\omega}}_f + \tilde{\omega} I^S \underline{\omega} - \underline{L}_c \\
&\quad + B \underline{\ddot{\sigma}} + D \underline{\dot{\sigma}} + \sum_{i=1}^n \tilde{\omega} C_i^T (J C_i \underline{\omega} + \underline{h})], \tag{3-12}
\end{aligned}$$

where  $D \equiv D_1 + D_2 + \frac{1}{2}(D_3 + D_4)$ .

Therefore, the total time derivative  $\dot{V}$  can be written as

$$\begin{aligned}
\dot{V} &= -(\underline{\omega}^T - \underline{\omega}_f^T) [k G^T(\beta) \underline{\beta}_f + I \underline{\dot{\omega}}_f + \tilde{\omega} I^S \underline{\omega} - \underline{L}_c \\
&\quad + B \underline{\ddot{\sigma}} + D \underline{\dot{\sigma}} + \sum_{i=1}^n \tilde{\omega} C_i^T (J C_i \underline{\omega} + \underline{h})]. \tag{3-13}
\end{aligned}$$

For  $\dot{V}$  to be negative, it is sufficient that

$$\begin{aligned}
&[k G^T(\beta) \underline{\beta}_f + I \underline{\dot{\omega}}_f + \tilde{\omega} I^S \underline{\omega} - \underline{L}_c + B \underline{\ddot{\sigma}} + D \underline{\dot{\sigma}} + \sum_{i=1}^n \tilde{\omega} C_i^T (J C_i \underline{\omega} + \underline{h})] \\
&= K(\underline{\omega} - \underline{\omega}_f), \tag{3-14}
\end{aligned}$$

where  $K$  is a positive definite gain matrix defined as

$$K = \begin{bmatrix} K_{11} & K_{12} & K_{13} \\ K_{21} & K_{22} & K_{23} \\ K_{31} & K_{32} & K_{33} \end{bmatrix}.$$

We can rewrite Eq.(3-14) as follows:

$$B\ddot{\underline{\theta}} + D\dot{\underline{\theta}} = K(\underline{\omega} - \underline{\omega}_f) - kG^T(\beta)\underline{\beta}_f - I\dot{\underline{\omega}}_f - \tilde{\omega}I^S\underline{\omega} + \underline{L}_c - \sum_{i=1}^n \tilde{\omega}C_i^T(JC_i\underline{\omega} + \underline{h}). \quad (3-15)$$

The right-hand side of the above equation is defined as

$$\underline{L}_r \equiv K(\underline{\omega} - \underline{\omega}_f) - kG^T(\beta)\underline{\beta}_f - I\dot{\underline{\omega}}_f - \tilde{\omega}I^S\underline{\omega} + \underline{L}_c - \sum_{i=1}^n \tilde{\omega}C_i^T(JC_i\underline{\omega} + \underline{h}), \quad (3-16)$$

which is called the feedback control law. Then Eq.(3-15) can be written as

$$B\ddot{\underline{\theta}} + D\dot{\underline{\theta}} = \underline{L}_r, \quad (3-17)$$

which is called the steering equation. From Eqs.(3-16) and (3-17), we can see that  $\underline{L}_r$  or  $(B\ddot{\underline{\theta}} + D\dot{\underline{\theta}})$  is torque; hereafter  $\underline{L}_r$  is referred to as "required torque", and  $(B\ddot{\underline{\theta}} + D\dot{\underline{\theta}})$  as "output torque  $\underline{L}_o$ ." It is anticipated that during finite intervals, the required and output torques may not be equal to each other.

As we can see in Eq.(3-16),  $\underline{L}_r$  can be adjusted by changing the gain  $K$ . The easiest way to assign  $K$  is to make it a constant diagonal matrix as

$$K = \begin{bmatrix} K_1 & 0 & 0 \\ 0 & K_2 & 0 \\ 0 & 0 & K_3 \end{bmatrix}. \quad (3-18)$$

For critical damping in the linear range, it is assigned<sup>8</sup> as

$$K_i = \sqrt{2I_i k}. \quad (3-19)$$

Varying gains can also be used in Eq.(3-16). As discussed in the next chapter, this is desirable for perturbing the required torque direction.

When we neglect the inertia terms  $J$ , the steering equation Eq.(3-17) can be reduced to

$$D_1 \dot{\underline{\sigma}} = \underline{L}_r, \quad (3-20)$$

where

$$\begin{aligned} \underline{L}_r \equiv & K(\underline{\omega} - \underline{\omega}_f) - kG^T(\beta)\underline{\beta}_f - I^S \dot{\underline{\omega}}_f - \tilde{\omega} I^S \underline{\omega} + \underline{L}_c \\ & - \sum_{i=1}^n \tilde{\omega} C_i^T \underline{h}. \end{aligned} \quad (3-21)$$

That is, the output torque is reduced to  $D_1 \dot{\underline{\sigma}}$ , and we only need match  $D_1 \dot{\underline{\sigma}}$  with  $\underline{L}_r$  by steering the gimbals. From the definition of the  $i$ th CMG torque in Eq.(2-26) and  $D_1$  in Eq.(2-28), the  $i$ th column of  $D_1$  represents the  $x$ -axis reaction torque(output torque) of the  $i$ th CMG due to directional change of the wheel angular momentum. Thus the output torque  $D_1 \dot{\underline{\sigma}}$  represents the linear combination of output torques of each CMG torque. Therefore, when CMG inertia terms are neglected, we need a proper combination of each CMG output torque which should result in  $\underline{L}_r$ . Comparing Eq.(3-17) with Eq.(3-20), we see that a different steering logic should be used depending on whether the inertia terms are included or not.

## CHAPTER IV

### STEERING LAWS

When the feedback control law for the required torque is given, the next step is to develop a steering law which is defined as the kinematic relationships between gimbal rates and the required torque. That is, the gimbals should be properly steered to produce the required torque. Depending on whether inertia terms are included or not, steering equations are given by Eqs.(3-17) or (3-20), and a different steering law has to be developed for each case. When the inertia terms are neglected,  $\dot{\underline{\sigma}}$  steering or velocity steering of gimbals is used and when the inertia terms are included,  $\ddot{\underline{\sigma}}$  steering or acceleration steering is used. At first, we consider the simple steering equation

$$D_1 \dot{\underline{\sigma}} = \underline{L}_r. \quad (3-20)$$

#### 1. Moore-Penrose Steering Law

Matrix  $D_1$  in Eq.(3-20) is a function of  $\underline{\sigma}$ , i.e. its elements change as gimbals rotate. For three-axis maneuvers, usually more than three CMGs are used and  $D_1$  becomes a  $3 \times n$  dimensional rectangular matrix. Hence, determination of the gimbal rates becomes an under-determined problem. Thus there are many solutions for  $\dot{\underline{\sigma}}$  which satisfy Eq.(3-20). Naturally, it is appropriate to choose a minimum norm solution for  $\dot{\underline{\sigma}}$  by using the Moore-Penrose inverse. We can derive the solution by minimizing  $\frac{1}{2} \dot{\underline{\sigma}}^T \dot{\underline{\sigma}}$  subject to Eq.(3-20). The solution is

$$\dot{\underline{\sigma}} = D_1^T (D_1 D_1^T)^{-1} \underline{L}_r. \quad (4-1)$$

This is a velocity steering law. Unfortunately, this law cannot exist when  $\text{rank}(D_1)$  is less than three; the gimbal angles for which this happens are called singular gimbal



angles and the event is called a "singularity." Moreover, near singular points, the magnitude of  $\dot{\alpha}$  becomes excessive, violating the gimbal rate constraint. Hence, this steering law is of limited use unless augmented by some logic which accomodates the singularities.

Before discussing other steering laws, we need to discuss the singularity problem in depth. Each column of  $D_1$  represents the output torque vector of each CMG as shown in the previous chapter.  $D_1 \dot{\alpha}$  is the linear combination of each column of  $D_1$ . When  $\text{rank}(D_1)$  equals two, the column space of  $D_1$  becomes planar. That is, at a singularity, each output torque vector lies on the same plane. Then there exists a direction to which all the output torque vectors are perpendicular and an output torque can not be produced in that direction. In other words, at any singular point, there exists a unit vector  $\underline{a}$  which satisfies  $D_1^T \underline{a} = \underline{0}$ . The direction of this vector is called the "singular direction." Whenever the desired torque direction lies in the nullspace of  $D_1$ , no torque can be generated in that direction.

At any instance, each CMG angular momentum vector is perpendicular to the each output torque vector as shown in Fig. 2(a). Thus at a singularity, each CMG angular momentum vector is extremely (minimally or maximally) projected along the singular direction. When the projections are maximal, the singularity is directional "saturation" or "the external singularity." When some angular momentum vectors are minimally projected and the others are maximally projected, then the singularity is called "internal singularity."

If the required torque  $\underline{L}_r$  lies in the column space at a singularity, there obviously exists a minimum norm solution for  $D_1 \dot{\alpha} = \underline{L}_r$ . Unfortunately, this solution can not be obtained by M-P steering law. Either when the required torque is parallel to the singular direction or when it lies on the column space of  $D_1$ , we

can not use M-P steering law at singularities.

The best way to circumvent this problem is to avoid the singularity. Several avoidance techniques have been proposed and proven effective in particular cases. However, application of these avoidance techniques for maneuvering spacecraft reveals several defects. These techniques consider only the steering law without including the vehicle movement. When the vehicle movement is considered, these techniques fail to predict "future singular points" so that they can be avoided. Null motion avoidance law is one of these techniques. It uses a null solution of Eq.(3-20) to re-position the momentum vectors:

$$\dot{\underline{x}}_N = \gamma [\mathbf{I} - D_1^T (D_1 D_1^T)^{-1} D_1] \underline{l}, \quad (4-2)$$

where  $\gamma$  is a scalar and  $\underline{l}$  a  $n$  dimensional vector. If the number of CMGs is limited to 4 and  $rank(D_1)$  is three, null space of  $D_1$  is only one dimensional. Then there remains only one degree of freedom for  $\dot{\underline{x}}_N$ , thus this restricts the gimbal movement to one direction which is not sufficient to avoid all singularities. None of the singularity avoidance steering laws has been shown to be perfect in general. In this thesis, singularity avoidance laws will not be treated.

## 2. Singularity Robustness Steering Law

When the required torque is not exactly parallel to the singular direction, there exists a non-zero least-square solution of minimum norm for  $D_1 \dot{\underline{x}} = \underline{L}_r$  even at a singular point. If we can tolerate some deviations between the required torque  $\underline{L}_r$  and the output torque  $D_1 \dot{\underline{x}}$ , we may use this steering law. Nakamura and Hanafusa<sup>5</sup> invented the singularity robust steering law based on the least-square concept, for robot manipulator control. Bedrossian<sup>6</sup> applied this law and analyzed singularities for open loop torque generation without considering vehicle motion.

Before integrating the S-R steering law with feedback control law, further discussion of this law is necessary. S-R steering law is derived by minimizing with respect to  $\dot{\underline{\theta}}$

$$\frac{1}{2}\alpha\dot{\underline{\theta}}^T\dot{\underline{\theta}} + \frac{1}{2}(D_1\dot{\underline{\theta}} - \underline{L}_r)^T(D_1\dot{\underline{\theta}} - \underline{L}_r),$$

where  $\alpha$  is a weighting factor. After some matrix manipulation, the steering law is given by

$$\dot{\underline{\theta}} = D_1^T(D_1D_1^T + \alpha\mathbf{I})^{-1}\underline{L}_r. \quad (4-3)$$

When  $\alpha$  is zero, S-R steering law is the same as M-P steering law. Except near the vicinity of singular points, M-P steering law is acceptable. Thus it is better that  $\alpha$  remain zero normally, and increase as  $\det(D_1D_1^T)$  approaches zero. But at the switching point between two steering laws, there may exist an abrupt change in  $\dot{\underline{\theta}}$ . For a smooth maneuver, it is better to use S-R steering law for the entire maneuver. The selection procedure for  $\alpha$  will be treated in the next chapter.

In contrast to M-P steering law,  $\dot{\underline{\theta}}$  usually decreases in the vicinity of singular points and the output torque deviates from the required torque. It is a disadvantage of S-R steering law. But, at a singular point, there still exists a solution; existence of a reasonable solution at a singularity is the main advantage of this law. Thus, this law looks applicable at almost every situation if the torque deviation is tolerable occasionally.

However, when the required torque direction is parallel to the singular direction, i.e., when  $D_1^T\underline{L}_r = \underline{0}$ , the gimbal rates will be zero and there occurs the "gimbal lock" phenomenon. The gimbal lock problem is a defect of S-R steering law. To avoid the gimbal lock, we should prevent  $D_1^T\underline{L}_r$  from becoming  $\underline{0}$ . It would be better to divert our attention from steering law to the feedback control laws for the present.

By changing the feedback control law near a singularity, we can prevent the required torque from being parallel to the singular direction. It can be done by changing the gain matrix  $K$  in Eq.(3-16); however,  $K$  should still remain positive definite to guarantee a closed loop stable system. Hence, instead of a constant diagonal matrix  $K$  in Eq.(3-18), a perturbed gain matrix can be used in the vicinity of singular points as

$$K = \begin{bmatrix} K_1 & 0 & \delta K \\ \delta K & K_2 & 0 \\ 0 & \delta K & K_3 \end{bmatrix}, \quad (4-4)$$

where  $\delta K$  should be positive in order for  $K$  to remain positive definite. During normal operations,  $\delta K$  remains zero, but as  $D_1^T \underline{L}_r$  approaches 0,  $\delta K$  is increased such that the direction of  $\underline{L}_r$  moves away from the singular direction. It is better for the maximum value of  $\delta K$  to be small compared with  $K_i$  in order that the perturbation in the system response remains small. The selection of the maximum value of  $\delta K$  is based on trade-off between performance and controllability. Another perturbed gain matrix can be selected as

$$K = \begin{bmatrix} K_1 & -\delta K_3 & \delta K_2 \\ \delta K_3 & K_2 & -\delta K_1 \\ -\delta K_2 & \delta K_1 & K_3 \end{bmatrix}. \quad (4-5)$$

This matrix is still positive definite and moreover, it does not affect Liapunov rate as the perturbations  $\delta K_i$ , are organized in a skew symmetric form. The varying gain feedback control law can widen the usage of S-R inverse steering law.

### 3. Acceleration Steering Law

When the CMG inertia terms are included, the steering equation is given as

$$B\ddot{\underline{\sigma}} + D\dot{\underline{\sigma}} = \underline{L}_r. \quad (3-17)$$

It is convenient then to use  $\ddot{\underline{\sigma}}$  as a control. The effect of  $B\ddot{\underline{\sigma}}$  on the output torque is very small in comparison with the  $D\dot{\underline{\sigma}}$  term. As the entries of the matrix  $B$  are

quite small, if  $D\dot{\underline{\sigma}}$  is significantly different from  $\underline{L}_r$ , the gimbal accelerations will be high. Hence the direct solution of Eq.(3-17) is avoided. Instead, the alternate steering law of making  $D\dot{\underline{\sigma}}$  approach  $\underline{L}_r$  as closely as possible based on Liapunov's method, is one method to minimize  $\underline{\sigma}$  in an average sense.

Let  $V_\sigma$  be a trial Liapunov function defined as

$$V_\sigma = \frac{1}{2}(\dot{\underline{\sigma}}_f - \dot{\underline{\sigma}})^T(\dot{\underline{\sigma}}_f - \dot{\underline{\sigma}}), \quad (4-6)$$

where  $\dot{\underline{\sigma}}_f$  is the desired angular velocity of gimbals. Then the time derivative of  $V_\sigma$  becomes

$$\dot{V}_\sigma = (\dot{\underline{\sigma}}_f - \dot{\underline{\sigma}})^T(\ddot{\underline{\sigma}}_f - \ddot{\underline{\sigma}}). \quad (4-7)$$

For  $\dot{V}_\sigma$  to be negative, it is sufficient that the following condition must be satisfied:

$$(\ddot{\underline{\sigma}}_f - \ddot{\underline{\sigma}}) = -K_\sigma(\dot{\underline{\sigma}}_f - \dot{\underline{\sigma}}), \quad (4-8)$$

where  $K_\sigma$  is a positive definite gain matrix. Then  $\ddot{\underline{\sigma}}$  is given by

$$\ddot{\underline{\sigma}} = K_\sigma(\dot{\underline{\sigma}}_f - \dot{\underline{\sigma}}) + \ddot{\underline{\sigma}}_f. \quad (4-9)$$

As it is desirable that  $\dot{\underline{\sigma}}$  follows the S-R steering law, we can consider  $\dot{\underline{\sigma}}_f$  as obtained from the S-R steering law. If  $\ddot{\underline{\sigma}}_f$  is assumed small, then it can be neglected. Thus an acceleration steering law can be of the form

$$\ddot{\underline{\sigma}} = K_\sigma [D^T(DD^T + \alpha \mathbf{I})^{-1} \underline{L}_r - \dot{\underline{\sigma}}]. \quad (4-10)$$

The gain matrix  $K_\sigma$  depends on the allowable magnitude of  $\ddot{\underline{\sigma}}$ . As might be expected, the acceleration steering law is a little more complicated than the velocity steering law. Like S-R steering law without inertia terms, the gimbal lock phenomenon occurs when  $D^T \underline{L}_r = \underline{0}$ . However, the varying gain feedback control law can be used again to escape from such situations.

## CHAPTER V

### SIMULATIONS

So far the equations of motion, feedback control laws, and steering laws are derived. For a simulation without inertia terms, we need the following equations:

$$\dot{\underline{\beta}} = \frac{1}{2}G(\underline{\beta})\underline{\omega} \quad (2-5)$$

$$\dot{\underline{\omega}} = -(I^S)^{-1} [\tilde{\omega} I^S \underline{\omega} - \underline{L}_c + D_1 \dot{\underline{\sigma}} + \sum_{i=1}^n \tilde{\omega} C_i^T \underline{h}] \quad (2-31)$$

$$\dot{\underline{\sigma}} = D_1^T (D_1 D_1^T + \alpha \mathbf{I})^{-1} \underline{L}_r \quad (4-2)$$

$$\begin{aligned} \underline{L}_r \equiv & K(\underline{\omega} - \underline{\omega}_f) - kG^T(\underline{\beta})\underline{\beta}_f - I^S \dot{\underline{\omega}}_f - \tilde{\omega} I^S \underline{\omega} + \underline{L}_c \\ & - \sum_{i=1}^n \tilde{\omega} C_i^T \underline{h}. \end{aligned} \quad (3-21)$$

For a simulation with inertia terms, we need the following equations:

$$\dot{\underline{\beta}} = \frac{1}{2}G(\underline{\beta})\underline{\omega} \quad (2-5)$$

$$\dot{\underline{\omega}} = -I^{-1} [\tilde{\omega} I^S \underline{\omega} - \underline{L}_c + B \ddot{\underline{\sigma}} + (D_1 + D_2 + D_3) \dot{\underline{\sigma}} + \sum_{i=1}^n \tilde{\omega} C_i^T (J C_i \underline{\omega} + \underline{h})] \quad (2-29)$$

$$\ddot{\underline{\sigma}} = K_\sigma [D^T (D D^T + \alpha \mathbf{I})^{-1} \underline{L}_r - \dot{\underline{\sigma}}] \quad (4-10)$$

$$\begin{aligned} \underline{L}_r \equiv & K(\underline{\omega} - \underline{\omega}_f) - kG^T(\underline{\beta})\underline{\beta}_f - I \dot{\underline{\omega}}_f - \tilde{\omega} I^S \underline{\omega} + \underline{L}_c \\ & - \sum_{i=1}^n \tilde{\omega} C_i^T (J C_i \underline{\omega} + \underline{h}). \end{aligned} \quad (3-16)$$

Neglecting the CMG inertia terms would be better for simple analysis and simulation, but the more complicated acceleration steering law provides better understanding of the system. The primary advantage of including gimbal inertia terms

is that the magnitude of the gimbal motor torque can be obtained and the torque amplification property of the SGCMG can be examined. Other differences between the two steering laws are expected to be minimal and will be investigated by simulations. Simulations are done by using IMSL Library routine DIVPRK, which is a combination of fifth and sixth order Runge-Kutta methods.

Before simulations, we need to select the values of the several parameters which are used in simulations. In order to have a smooth maneuver,  $\alpha$  in Eqs.(4-2) and (4-9) is chosen to increase linearly as  $\det(DD^T)$  approaches zero as follows:

$$\alpha = \alpha_o \left(1 - \frac{\det(DD^T)}{d}\right), \quad (5-1)$$

where  $\alpha_o$  is a maximum value of  $\alpha$  and  $d$  is a normalizing scale factor for the determinant.

In order to monitor the margin of CMG capability, we need to monitor how close the CMGs come to saturation. By using a saturation index defined below, we can see the margin of CMG capability and distinguish the external singularity from the internal singularity in simulations.

**Definition :** Saturation index  $S$  is a measure which indicates the amount by which gyro angular momentum vectors are projected toward the required torque direction. For the  $i$ th CMG, it is defined as

$$S_i = \frac{1}{\pi} \cos^{-1} \left( \frac{-L_2}{\sqrt{L_1^2 + L_2^2}} \right), \quad \text{when } L_1^2 + L_2^2 \neq 0 \quad (5-2)$$

$$S_i = 1.0, \quad \text{when } L_1 = 0 \text{ and } L_2 = 0, \quad (5-3)$$

where  $L_j$  is the  $j$ th component of  $\underline{L}_r$  in the  $i$ th gimbal frame. Then the gyro cluster saturation index  $S$  is defined as

$$S = \frac{1}{n} \sum_{i=1}^r S_i. \quad (5-4)$$

This definition is motivated by the following reasoning: the angular momentum vector  $\underline{h}$  is fixed along  $y$  axis of each gimbal frame and the required torque vector  $\underline{L}_r$  moves around the center of the gimbal frame as shown in Fig. 2(b). When  $\underline{L}_r$  lies in the  $y$ - $z$  plane along the positive  $y$  direction,  $\underline{h}$  is maximally projected to  $\underline{L}_r$  and the index value is one. When  $\underline{L}_r$  lies with opposite direction,  $\underline{h}$  is minimally projected and the index value is zero. If  $\underline{L}_r$  lies between two extremal positions, the index value can be expressed with angle  $\epsilon$  between  $\underline{h}$  and the projection vector ( $L_1, L_2$ ) of  $\underline{L}_r$  on the  $x$ - $y$  plane. This relationship can be expressed as Eq.(5-2). When  $\underline{L}_r$  coincides with  $z$  axis,  $S_i$  is defined as one as Eq.(5-3). The gyro cluster saturation index  $S$  is a mean value of all saturation indices and its maximum value is one.

When the inertia terms are included,  $S$  can not be used as a rigorous measure for saturation because it only considers the gyro axial momentum and the transverse momentum and gimbal momentum are neglected. However, this index can be still used as a rough measure when the inertia terms are included.

For the varying gain feedback control law, the gain matrix  $K$  is chosen as given by Eq. (4-4). The value of  $\delta K$  is chosen to change along with another index which is called the orthogonality index  $O$ .

**Definition :** Orthogonality index is a measure of how close the required torque is orthogonal to the column space of  $D$  and is defined as

$$O = \frac{\underline{L}_r^T D D^T \underline{L}_r}{\|\underline{L}_r\|}, \quad (5-5)$$

where  $D = D_1$  when the inertia terms are neglected. The minimum value of  $O$  is zero which indicates exact orthogonality.



$\delta K$  increases as  $O$  approaches zero as

$$\delta K = \delta K_o \frac{(O_o - O)}{O_o}, \quad \text{when } O < O_o \quad (5-6)$$

$$\delta K = 0 \quad \text{when } O \geq O_o. \quad (5-7)$$

where  $\delta K_o$  is the maximum value of  $\delta K$ , and  $O_o$  is the reference value of  $O$ .

As we can see from Eqs.(4-3) and (4-10),  $\dot{\underline{\sigma}}$  and  $\ddot{\underline{\sigma}}$  will change abruptly at the initial time because  $\underline{L}_r$  is large and the gimbals are stationary. For a smooth initial maneuver, a multiplier function is designed such that, when multiplied with the feedback control law, smooth torques with zero initial magnitudes and moderate slopes result<sup>8</sup>. The multiplier function  $m(t)$  is given by

$$m(t) = \tau^2(3 - 2\tau), \quad \tau = \frac{t}{T_1} \quad \text{when } t \leq T_1 \quad (5-8)$$

$$m(t) = 1 \quad \text{when } t > T_1 \quad (5-9)$$

This multiplier function is used for simulation 5.

The simulation model is a rigid spacecraft with 4 pyramid-configured SGCMGs as shown in Fig. 3. The centroid of the bottom surface of pyramid is located at the mass center of system. The vehicle frame  $\{\underline{\hat{V}}\}$  is chosen so as to coincide with the principal axes of the system. The model characteristic data and several parameter values which are used in simulations are given in Table 1. The values for  $\alpha_o$ ,  $\delta K_o$ , and  $O_o$  were selected on the basis of a few trial simulations. The selection methods of optimum values are not addressed here.

### 1. Constant Gain Feedback with S-R steering

To begin with the discussion of simulations, consider two maneuvers using constant gain feedback control and the S-R steering law, neglecting the inertia terms. The main purpose of these simulations is to establish baselines showing how

the S-R steering law works in conjunction with a constant gain feedback control law.

### Simulation 1 : Motion-to-Rest Three-Axis Maneuver

The initial states and the target states are given in Table 2. Target states are fixed with respect to the inertial frame  $\{\hat{N}\}$ . As can be seen in Fig. 4, the maneuver is satisfactorily completed. In practice, the gimbal rates are typically limited to 1 or 2 rad/sec. Figure 4(d) shows that this limit is never active during the maneuver. As we can see in Fig. 4(e), the Liapunov function rate remains negative during maneuver. Figure 4(f) shows the indices:  $\det(D_1 D_1^T)$ ,  $S$ , and  $O$ . From this figure, we can see that the steering law does meet internal singularities on two occasions during which  $\underline{L}_r$  is not orthogonal to the singular direction.

However, as we can see in Fig. 4(g) and (h), the decrease of  $\dot{\underline{q}}$  near singularities causes some deviation of output torque from the required torque, which results in the fluctuations in the output torque curve. This fluctuation may not be desirable, especially for a flexible spacecraft. The deviation and fluctuation of torque is one of defects of S-R steering law although the law is much better than M-P steering law.

### Simulation 2: Rest-to-Rest Uni-directional Maneuver

To deliberately create a situation of "gimbal lock", the maneuver starts from the singular initial states where  $D_1^T \underline{L}_r = \underline{0}$  as shown in Table 3. The required torque is uni-directional but time varying. As expected, the gimbals remain "locked" at the initial states as shown in Fig. 5(c), and angular velocity does not change at all as shown in Fig. 5(a). That is due to  $D_1^T \underline{L}_r = \underline{0}$  at the initial time as evident from Fig. 5(f). From this simulation, we can see that even though we use S-R steering law, there still exists a singularity which can not be escaped with this law.

## 2. Varying Gain Feedback with S-R Steering

As a cure of the gimbal lock problem, the varying gain feedback control law is suggested in the previous chapter. To compare the results of the varying gain feedback control law with those of constant gain, the maneuver of simulation 2 is repeated with varying gain feedback control law.

### Simulation 3: Rest-to-Rest Uni-directional Maneuver

The initial conditions are same as for simulation 2. As shown in Fig. 6, it is possible to escape from the singularity at the initial time, and the maneuver is completed satisfactorily. Due to the varying gain which perturbs the required torque command, the maneuver is not purely uni-directional as shown in Figs. 6(a), (b), (g), and (h).

The spacecraft coasts in an output torque free mode during a finite time. This is because we meet another singularity, i.e. saturation which can be identified from Figs. 6(c) and (f). During this time, then gimbals are almost locked. During this "near saturation singularity", the output torque shows a large deviation from the required torque, as seen in Figs. 6(g) and (h). We can see that very near a saturation singularity, even the varying gain feedback control law is not effective to escape that singularity. That is due to the fact that CMG torque capability in the desired direction is limited.

Comparing simulation 3 with simulation 2, we conclude that the varying gain control law allows for escape from any singularity except for the exact saturation singularity.

## 3. Constant Gain Feedback with Acceleration Steering

When the inertia terms are included for a detailed analysis, Eqs.(2-5), (2-29),

and (4-9) are needed for simulation. At first, the constant gain feedback control is used. To compare the results with those of the velocity steering law, the initial conditions are selected as in simulation 1.

**Simulation 4: Motion-to-Rest Three-Axis Maneuver.**

As shown in Fig. 7, the results are very similar with those of simulation 1, but we see more realistic pictures now. Gimbal accelerations are shown in Fig. 7(d). As expected,  $\ddot{\theta}$  is very small during most of the maneuver. Unlike the required torque in Fig. 7(g), output torque has zero magnitude initially. This big difference causes the high acceleration of the gimbals at the initial time. Figures 7(i) and (j) show the torque amplification phenomenon clearly. By including the inertia terms, the gimbal motor torque  $u_i$  becomes meaningful and it can be used for other studies, *e.g.* power consumption analysis.

**Simulation 5: Motion-to-Rest Three-Axis Maneuver.**

To avoid high acceleration of the gimbals, the multiplier function discussed before is used. Simulation 4 is repeated with the multiplier function. Figures 8(a) and (b) show that the torque rise profile is smooth. We can see that the multiplier function is highly effective for smooth initial maneuvering.

#### 4. Varying Gain Feedback with Acceleration Steering

As long as we use the constant gain feedback control law, we can not escape from the singularities where  $D_1^T \underline{L}_r = \underline{0}$ . Hence a varying gain feedback control law is utilized in conjunction with an acceleration steering law in the next simulation.

**Simulation 6: Rest-to-Rest Uni-directional Maneuver**

The initial conditons are the same as those of simulation 3. Fig. 9 shows that initial singular states are successfully escaped, and maneuver is completed

satisfactorily. However, comparing Fig. 6(c) with Fig. 9(c), the final gimbal angles are much different. Thus, we can see that neglecting the CMG inertia terms in simulation may not produce realistic results.

Conclusively, we can see that the varying gain feedback control law provides an exit from any internal singularity, and it works well in conjunction with either velocity steering law or acceleration steering law.

### 5. Another Example Maneuver

So far several feedback control and steering laws have been simulated and compared. All the simulations have been started from the zero initial gimbal angles where  $\sum_{i=1}^n C_i^T \underline{h} = \underline{0}$ , i.e. zero initial total CMG angular momentum. In the next simulation, a different set of initial gimbal angles are used in order to see their effects on the maneuver.

#### Simulation 7: Motion-to-Rest Three-Axis Maneuver.

The initial gimbal angles corresponding to zero CMG momentum are selected as in Table 4. Figures 10(d) and (e) show that gimbal rates and accelerations are smoother and smaller compared with simulation 4. We meet a singularity only once as seen from Fig. 10(f). Figures 10(g) and (h) show that the torque deviation is smaller and the fluctuation is much less than before.

From this simulation, we can see that with some initial gimbal angles, the maneuver may be improved. When the gimbals are initially in unsuitable positions, a null motion based control can be used to move them to desirable positions. To find these desirable positions, optimal control theory ( or nonlinear programming ) can be used. A systematic means for obtaining preferred angles is worthy of future study.

## CHAPTER VI

### CONCLUSION AND RECOMMENDATIONS

A complete set of equations of motion including all the inertia terms has been derived in simple forms by using matrices and vector notations. Based on these equations of motion, feedback control laws have been developed by using Liapunov stability theory. The acceleration steering law based on the existing S-R steering law has also been developed.

The feedback control laws have been shown to work well in conjunction with either S-R steering law or acceleration steering law. It has been shown that there exist some singularities which cause gimbal lock when the constant gain feedback control law is used with these steering laws. The varying gain feedback control law has been shown to provide an exit from any internal singularity. S-R steering law has been proved to provide a workable steering law even at singularities. The acceleration steering law has shown similar characteristics with S-R steering law. It has been shown that the acceleration steering law provides more useful information about torques than velocity steering law. Many of the singularity problems encountered in the simulations can be eliminated by using higher CMG momentum or more CMGs. However, the choice of the CMG angular momentum was deliberate—to induce these singular effects.

The torque deviation problem in the above two steering laws still needs a further study. It has been suggested that a judicious choice of initial gimbal angles can help alleviate this problem. Further research is needed to establish a systematic method of finding suitable initial gimbal angles. The control and steering laws need better integration to solve the singularity problem completely.

## REFERENCES

- <sup>1</sup> Margulies, G. and Aubrun, J.N., "Geometric Theory of Single Gimbal Control Moment Gyro Systems," *Journal of Astronautical Sciences*, Vol. XXVI, No.2, Apr.-Jun. 1978, pp. 159-191.
- <sup>2</sup> Cornick, D.E., "Singularity Avoidance Control Laws for Single Gimbal Control Moment Gyros," AIAA paper 79-1698, AIAA Guidance and Control Conference, Boulder, Colorado, Aug 6-8, 1979.
- <sup>3</sup> Kurokawa, H., Yajima, N., and Usui, S., "A New Steering Law of a Single Gimbal CMG System of Pyramid Configuration," *Proceeding of the Xth IFAC Symposium on Automatic Control in Space*, Toulouse, France, June 25-28, 1985, P.249.
- <sup>4</sup> Bauer, S.R., "Single Gimbal CMG Steering Laws," Charles Stark Draper Laboratory, Inc., SGNM 10E-87-06, May 1987.
- <sup>5</sup> Nakamura, Y. and Hanafusa, H., "Inverse Kinematic Solutions with Singularity Robustness for Robot Manipulator Control," *Journal of Dynamic Systems, Measurement, and Control*, Vol.108, Sep. 1986, pp.163-171.
- <sup>6</sup> Bedrossian, N.S., "Steering Law Design for Redundant Single Gimbal Control Moment Gyro Systems," M.S. Thesis, Mechanical Engineering, Massachusetts Institute of Technology, Aug. 1987.
- <sup>7</sup> Kalman, R.E. and Bertram, J.E., "Control System Analysis and Design by the Second Method of Lyapunov," *Journal of Basic Engineering*, Vol.82, No.2, June 1960, pp.371-400.
- <sup>8</sup> Vadali, S.R. and Junkins, J.L., "Optimal Open-loop and Stable Feedback Control of Rigid Spacecraft Attitude Maneuvers," *Journal of Astronautical Sciences*, Vol.32, No.2, Apr.-Jun. 1984, pp.105-122.

- <sup>9</sup> Wie, B. and Barba, P.M., "Quaternion Feedback for Spacecraft Large Angle Maneuvers," *Journal of Guidance, Control, and Dynamics*, Vol.8, No.3, May-June, 1985, pp. 360-365.
- <sup>10</sup> Ross, I.M. and Melton, R.G., "Quaternion Formulation of Rotational Dynamics for a Double Gimbaled Momentum Wheel Control System," AAS paper 87-510, AAS/AIAA Astodynamics Specialist Conference, Kalispell, Montana, Aug.10-12, 1987.
- <sup>11</sup> Junkins, J.L. and Turner, J.D., *Optimal Spacecraft Rotational Maneuvers, Studies in Astronautics 3*, Elsevier Scientific Publishing Company, New York, 1985.
- <sup>12</sup> Vadali, S.R. and Junkins, J.L., "Spacecraft Large Angle Rotational Maneuvers with Optimal Momentum Transfer", AIAA-82-1469, AIAA/AAS Astodynamics Conference, San Diego, California, Aug. 9-11, 1982.
- <sup>13</sup> Vadali, S.R., "On The Euler Parameter Constraints", AIAA-88-0670, AIAA 26th Aerospace Sciences Meeting, Reno, Nevada, Jan. 11-14, 1988.
- <sup>14</sup> Greenwood, D.T., *Classical Dynamics*, Prentice-Hall Inc., Englewood Cliffs, N.J., 1977.
- <sup>15</sup> Meirovitch, L., *Methods of Analytical Dynamics*, McGraw-Hill Book Company, New York, N.Y., 1970.



Table 1. Simulation Model Characteristic Data

Item	Value	Units
$h$	1.8	Kg-m <sup>2</sup> /sec
$I_x$	86.215	Kg-m <sup>2</sup>
$I_y$	85.070	Kg-m <sup>2</sup>
$I_z$	113.565	Kg-m <sup>2</sup>
$J_x$	0.04	Kg-m <sup>2</sup>
$J_y$	0.05	Kg-m <sup>2</sup>
$J_z$	0.03	Kg-m <sup>2</sup>
$k$	1.0	N-m
$K_1$	13.13	N-m-sec
$K_2$	13.04	N-m-sec
$K_3$	15.08	N-m-sec
$K_o$	I	sec <sup>-1</sup>
$\delta K_o$	0.1	
$d$	100	
$O_o$	0.01	
$T_1$	10.0	sec
$\alpha_o$	0.1	
$\theta$	54.74	degree

**Table 2. System States for Simulation 1, 4, and 5**

States		Value	Units
Initial	$\underline{\omega}$	[ 0.01 0.05 0.001 ]	rad/sec
	$\underline{\beta}$	[ 0.707 0.707 0.0 0.0 ]	
	$\underline{\sigma}$	[ 0. 0. 0. 0. ]	degree
	$\underline{\dot{\sigma}}$	[ 0. 0. 0. 0. ]	rad/sec #
Target	$\underline{\omega}_f$	[ 0. 0. 0. ]	rad/sec
	$\underline{\beta}_f$	[ 1.0 0.0 0.0 0.0 ]	

**Table 3. System States for Simulation 2,3, and 6**

States		Value	Units
Initial	$\underline{\omega}$	[ 0.01 0.0 0.0 ]	rad/sec
	$\underline{\beta}$	[ 0.707 0.707 0.0 0.0 ]	
	$\underline{\sigma}$	[ -90. 0. 90. 0. ]	degree
	$\underline{\dot{\sigma}}$	[ 0. 0. 0. 0. ]	rad/sec #
Target	$\underline{\omega}_f$	[ 0. 0. 0. ]	rad/sec
	$\underline{\beta}_f$	[ 1.0 0.0 0.0 0.0 ]	

# ; only for acceleration steering

Table 4. System States for Simulation 7

States		Value	Units
Initial	$\underline{\omega}$	[ 0.01 0.05 0.001 ]	rad/sec
	$\underline{\beta}$	[ 0.707 0.707 0.0 0.0 ]	
	$\underline{\sigma}$	[ 45. -45. 45. -45. ]	degree
	$\underline{\dot{\sigma}}$	[ 0. 0. 0. 0. ]	rad/sec
Target	$\underline{\omega}_f$	[ 0. 0. 0. ]	rad/sec
	$\underline{\beta}_f$	[ 0. 0. 0. 0. ]	

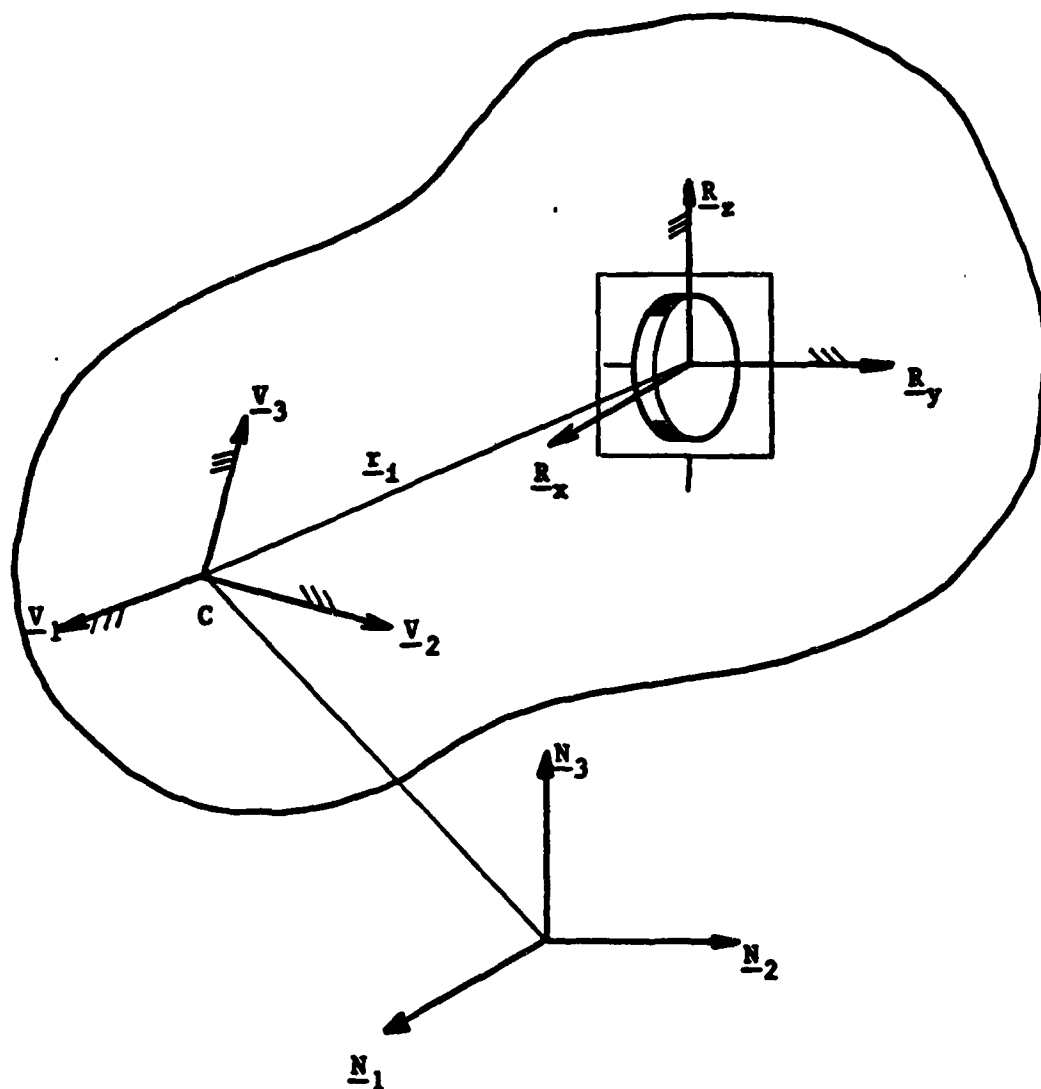


Fig. 1. System with the  $i$ th SGCMG.

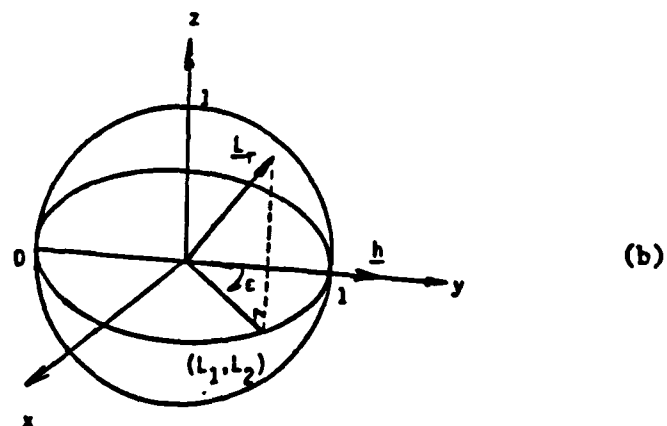
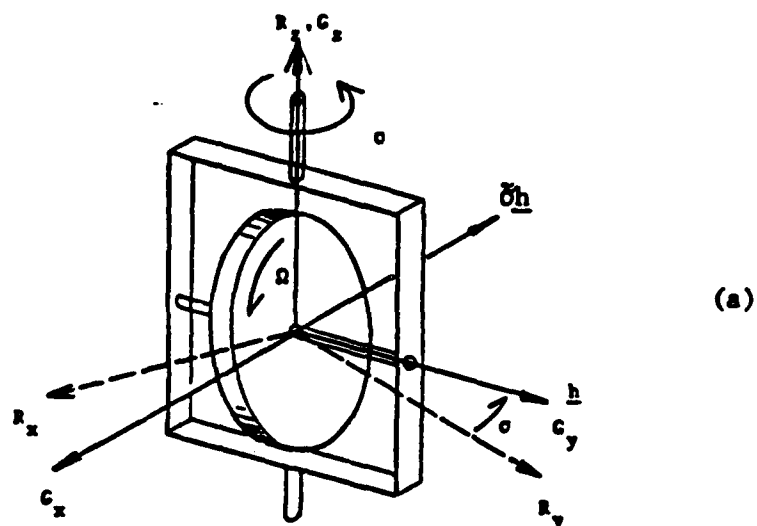
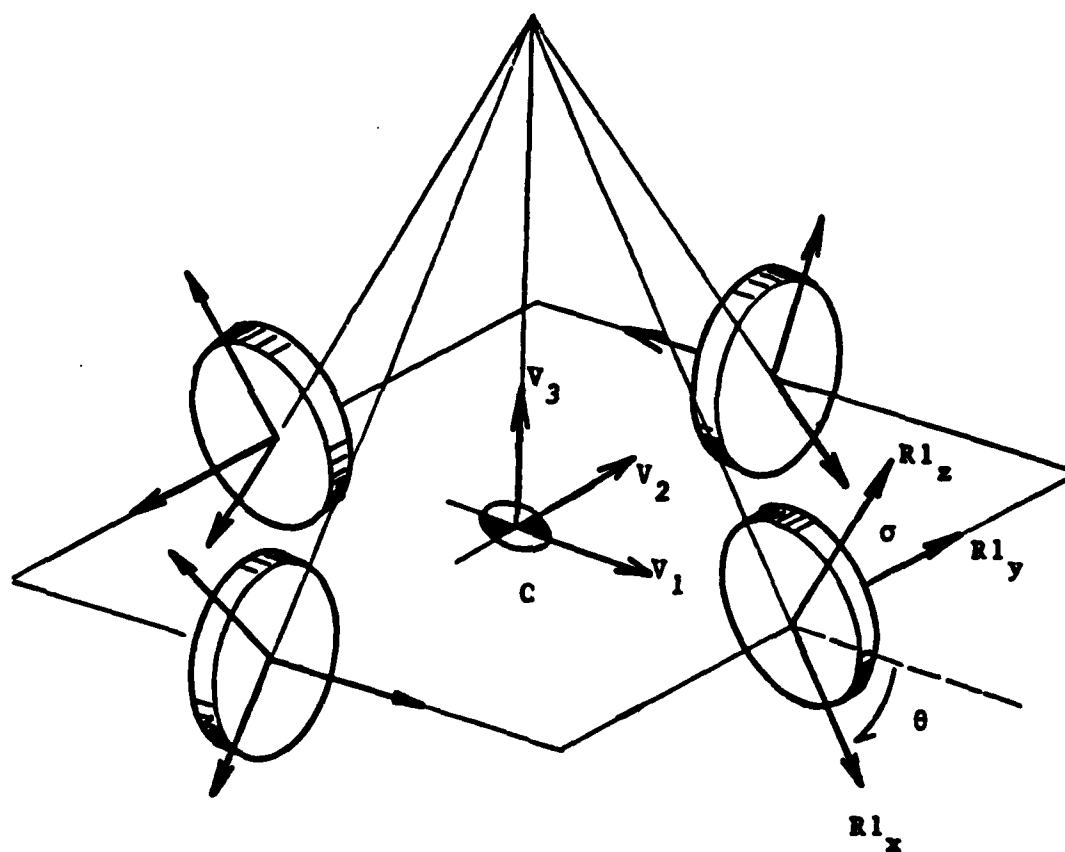
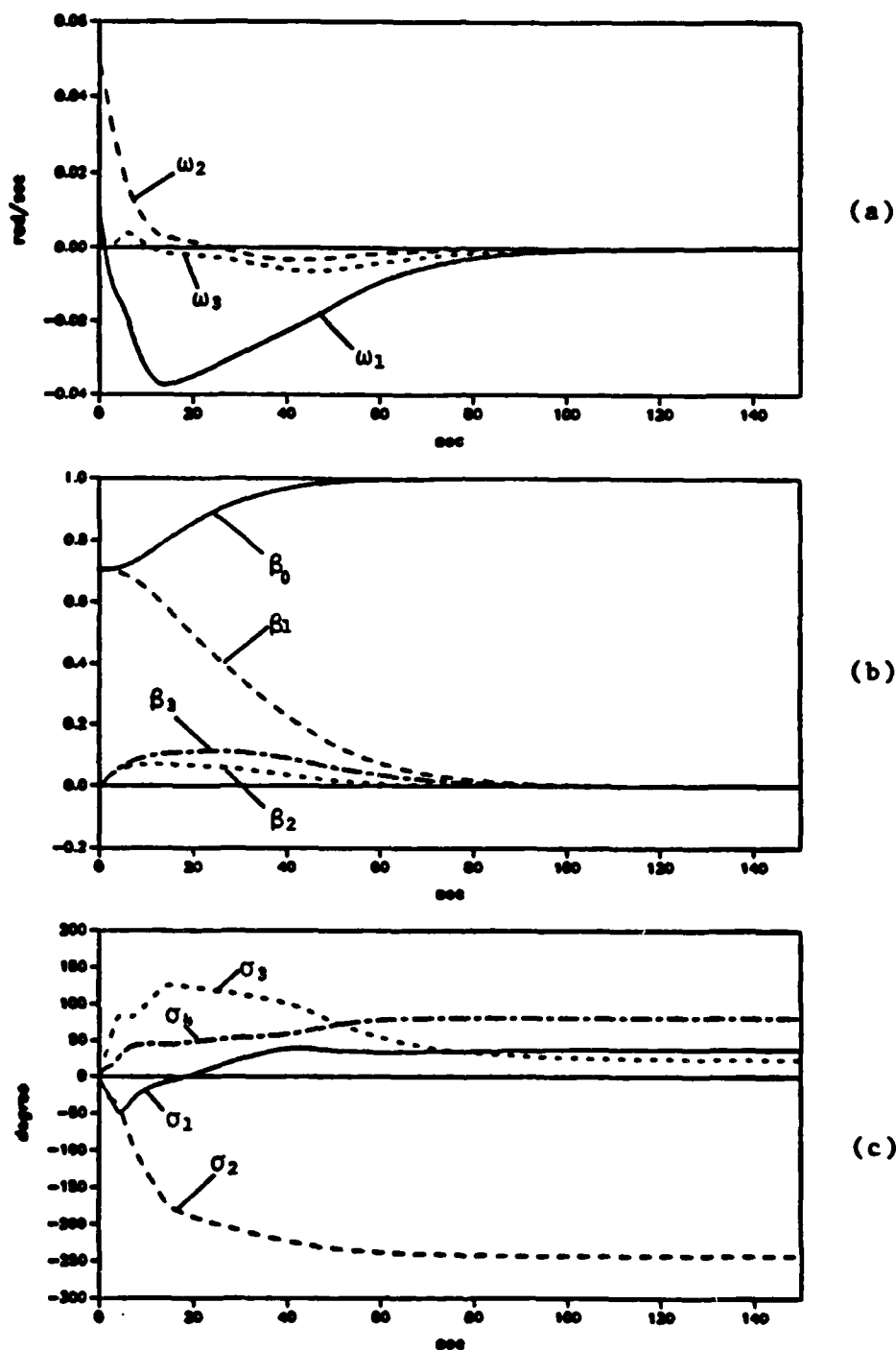


Fig. 2. The  $i$ th CMG related Frames and Vectors.



**Fig. 3. Pyramid Type CMG Configuration.**



**Fig. 4. Results of Simulation 1.**  
 (a) Spacecraft Angular Velocity  
 (b) Spacecraft Attitude( Euler parameters )  
 (c) CMG gimbal angles

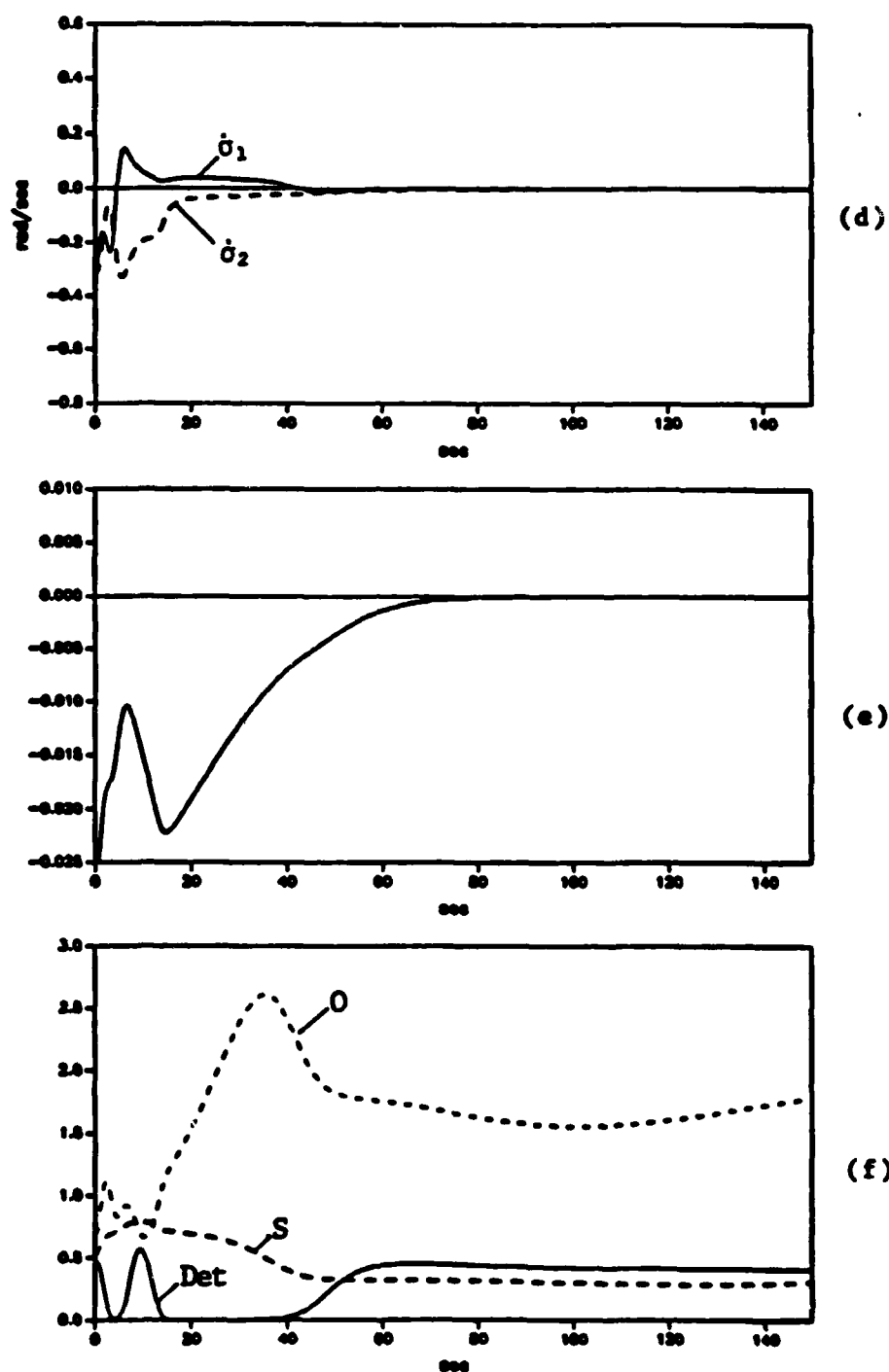


Fig. 4. Results of Simulation 1. (continued)

(d) Gimbal Rates of 1st and 2nd CMG

(e) Liapunov Function Rate

(f) Singularity Indices



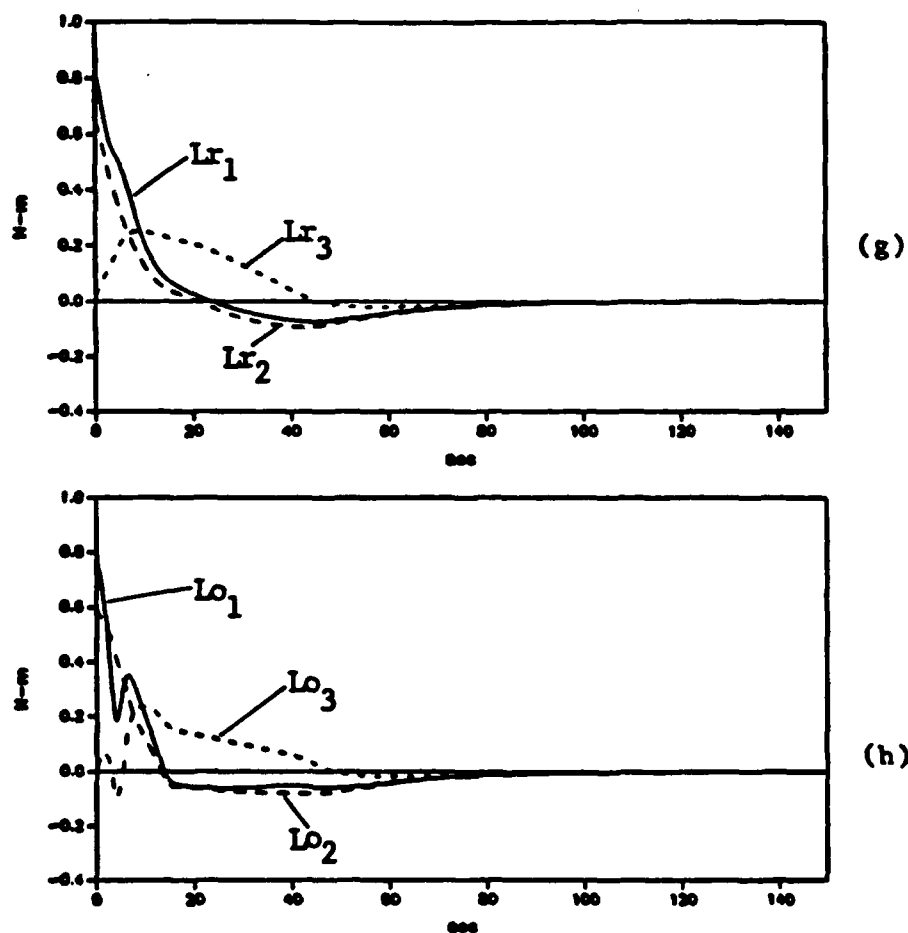
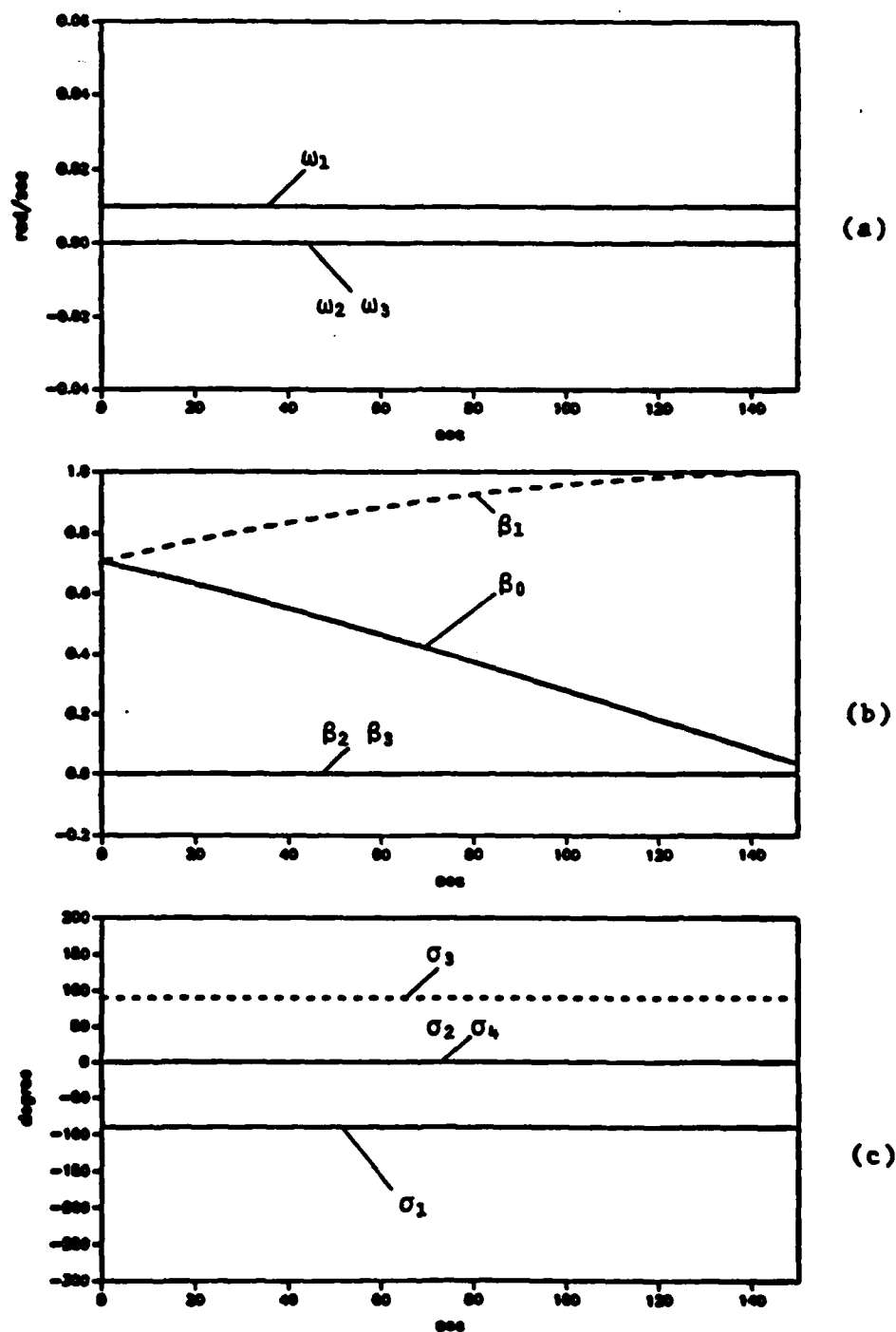


Fig. 4. Results of Simulation 1. (continued)

(g) Required Torque

(h) Output Torque



**Fig. 5. Results of Simulation 2.**  
 (a) Spacecraft Angular Velocity  
 (b) Spacecraft Attitude( Euler parameters )  
 (c) CMG gimbal angles

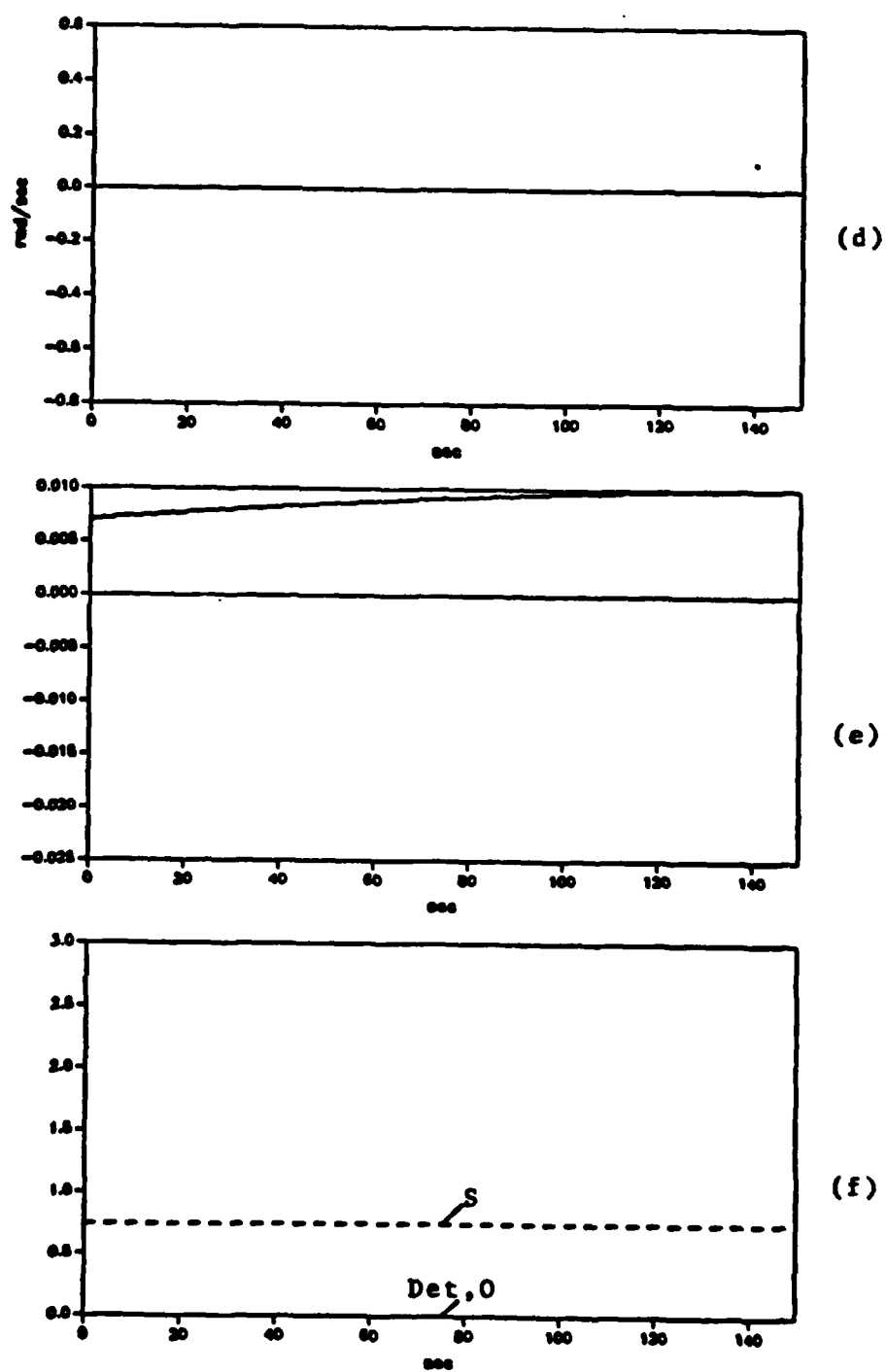
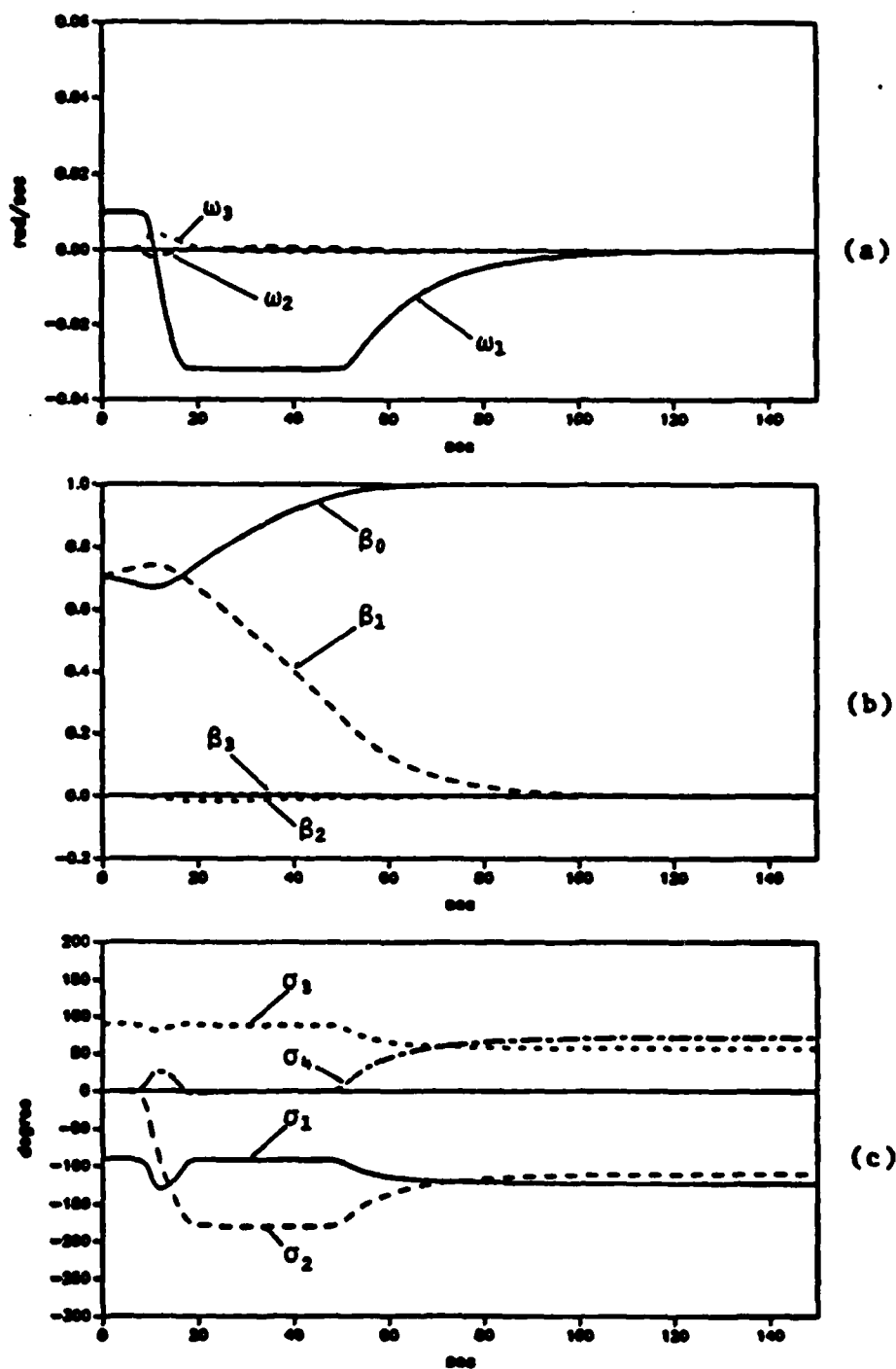


Fig. 5. Results of Simulation 2. (continued)

(d) Gimbal Rates of 1st and 2nd CMG

(e) Liapunov Function Rate

(f) Singularity Indices



**Fig. 6. Results of Simulation 3.**

(a) Spacecraft Angular Velocity

(b) Spacecraft Attitude( Euler parameters )

(c) CMG gimbal angles

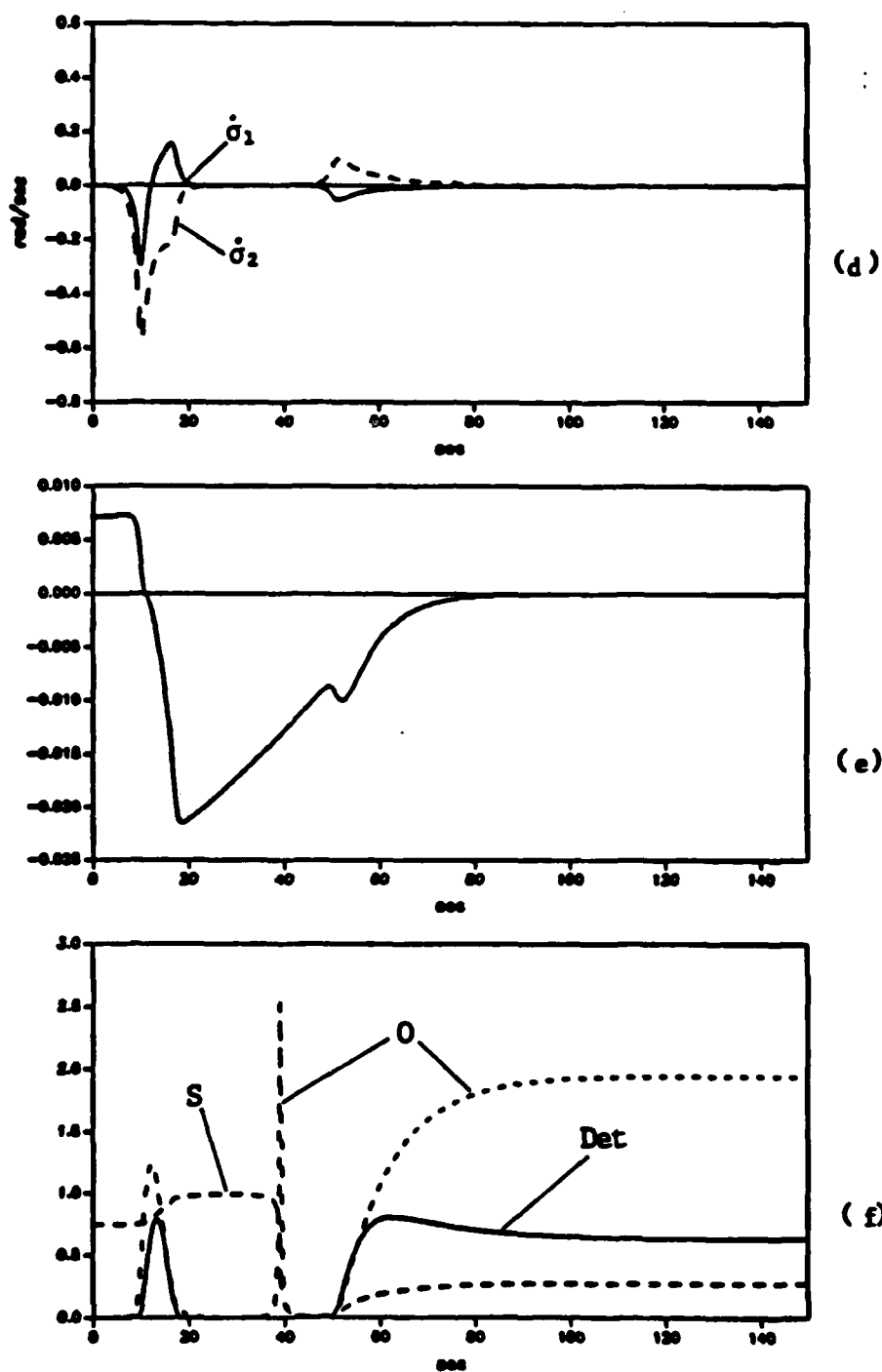


Fig. 6. Results of Simulation 3. (continued)

(d) Gimbal Rates of 1st and 2nd CMG

(e) Liapunov Function Rate

(f) Singularity Indices

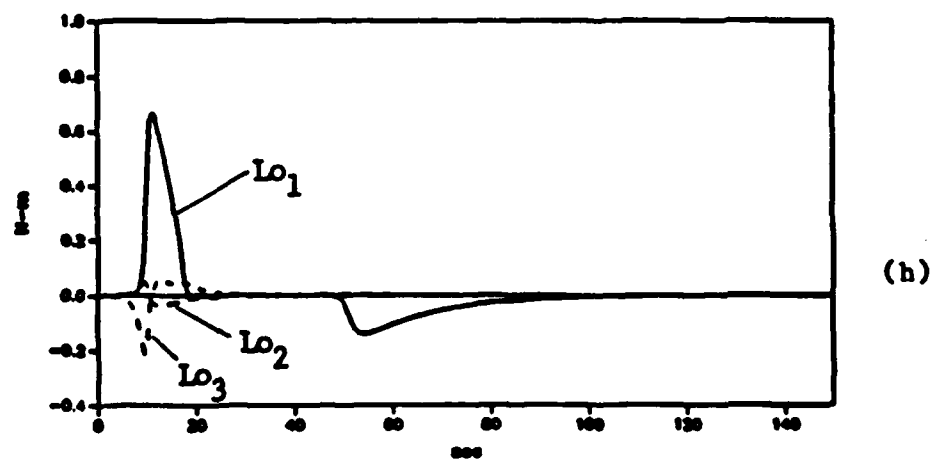
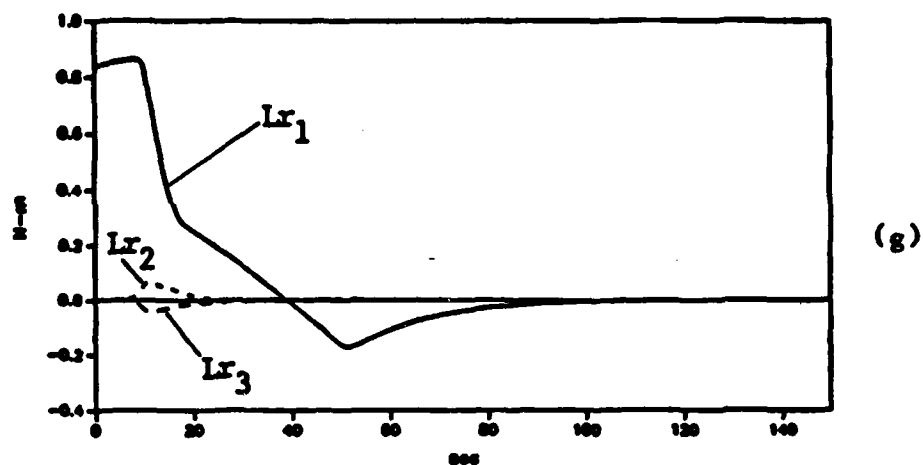
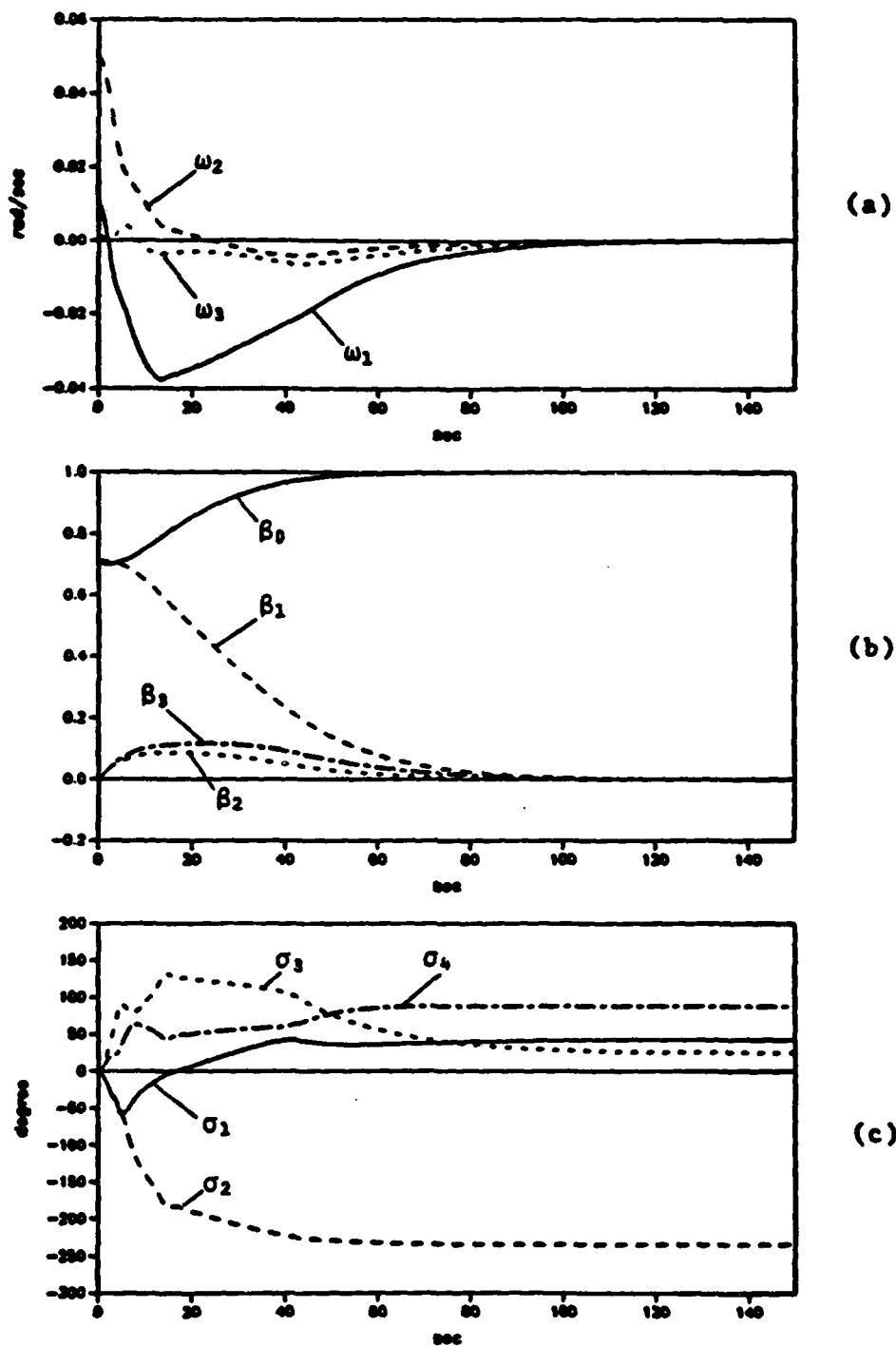


Fig. 6. Results of Simulation 3. (continued)

(g) Required Torque

(h) Output Torque



**Fig. 7. Results of Simulation 4.**

(a) Spacecraft Angular Velocity

(b) Spacecraft Attitude( Euler parameters )

(c) CMG gimbal angles

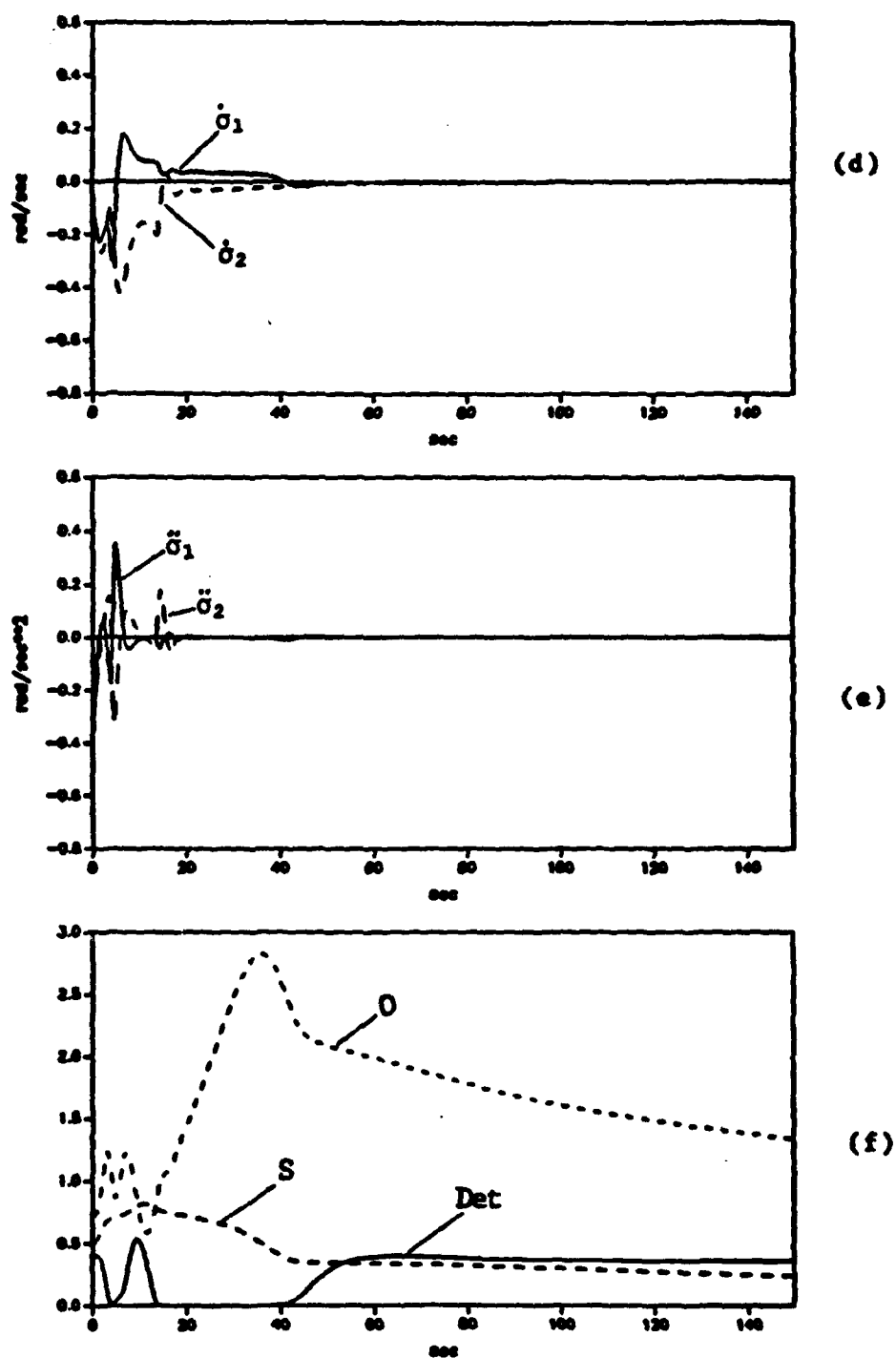


Fig. 7. Results of Simulation 4. (continued)

(d) Gimbal Rates of 1st and 2nd CMG

(e) Gimbal accelerations of 1st and 2nd CMG

(f) Singularity Indices



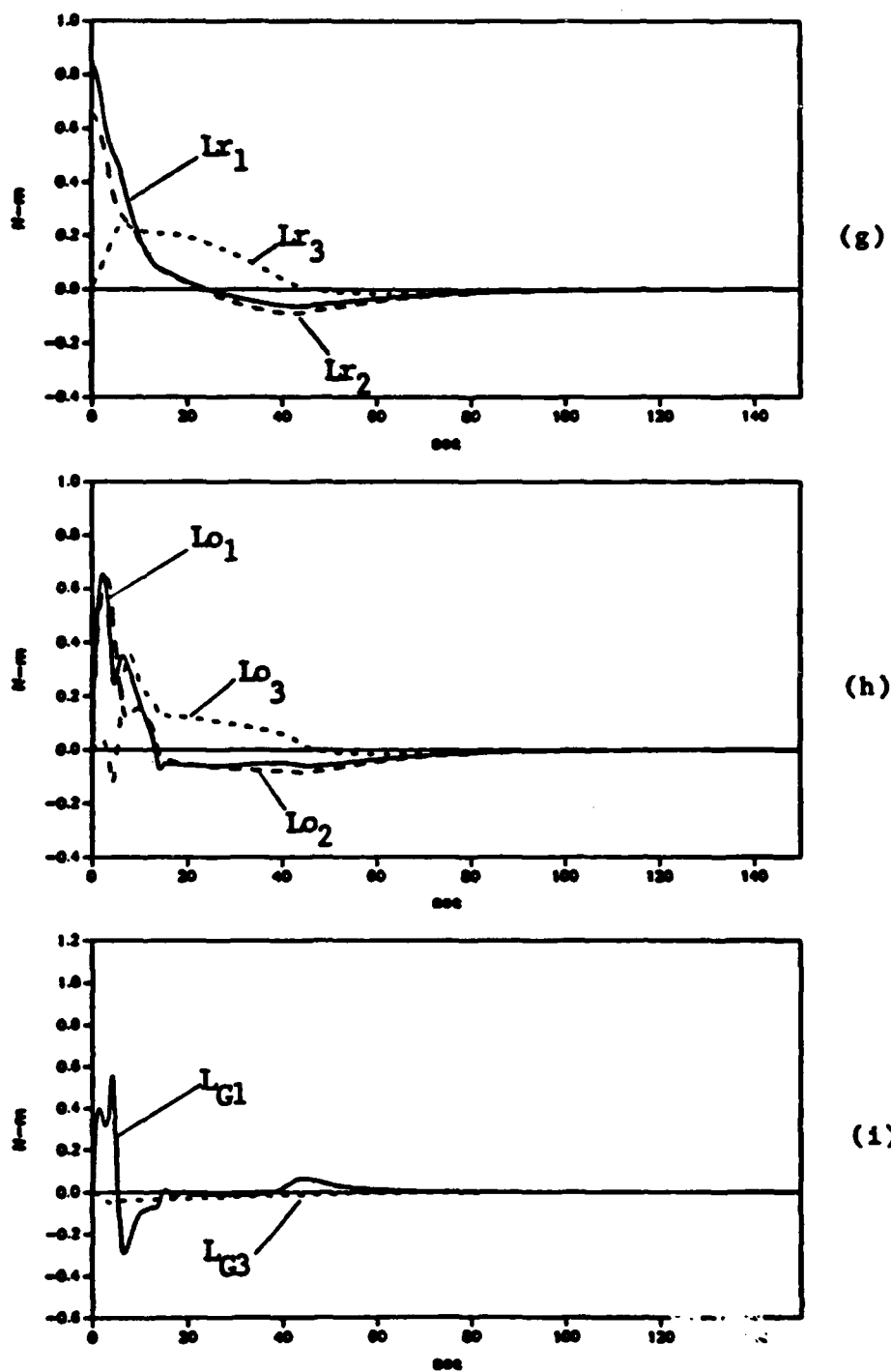


Fig. 7. Results of Simulation 4. (continued)

(g) Required Torque

(h) Output Torque

(i) 1st CMG torque

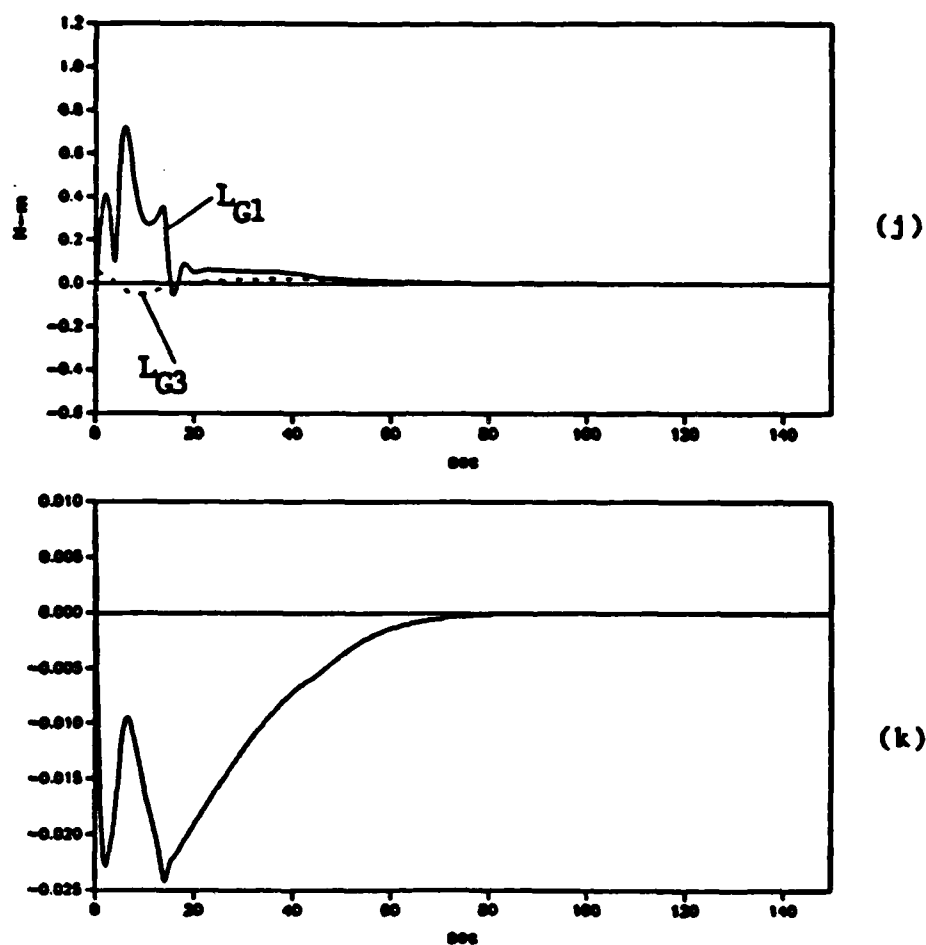


Fig. 7. Results of Simulation 4. (continued)

(j) 2nd CMG Torque

(k) Liapunov Function Rate

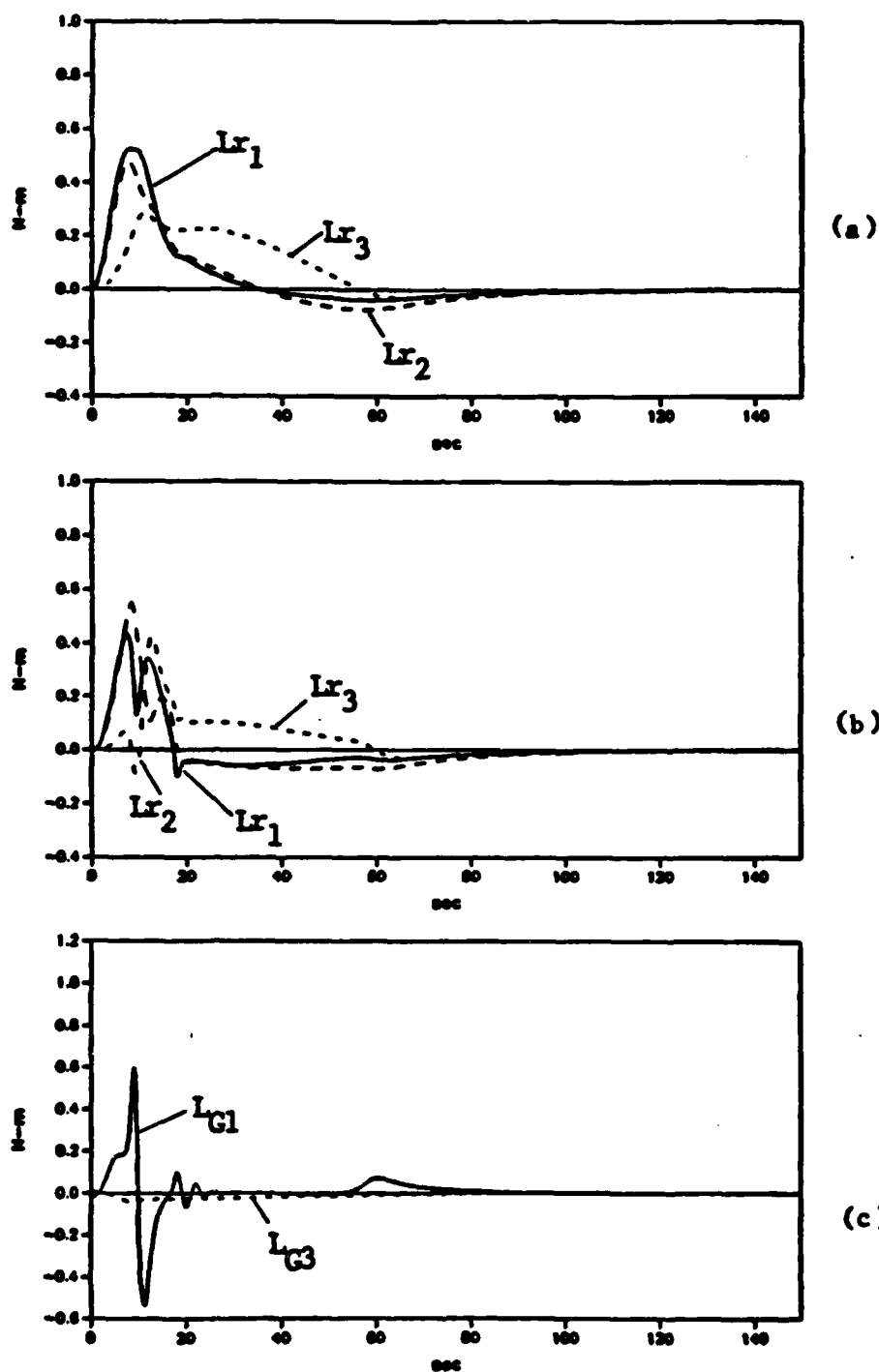
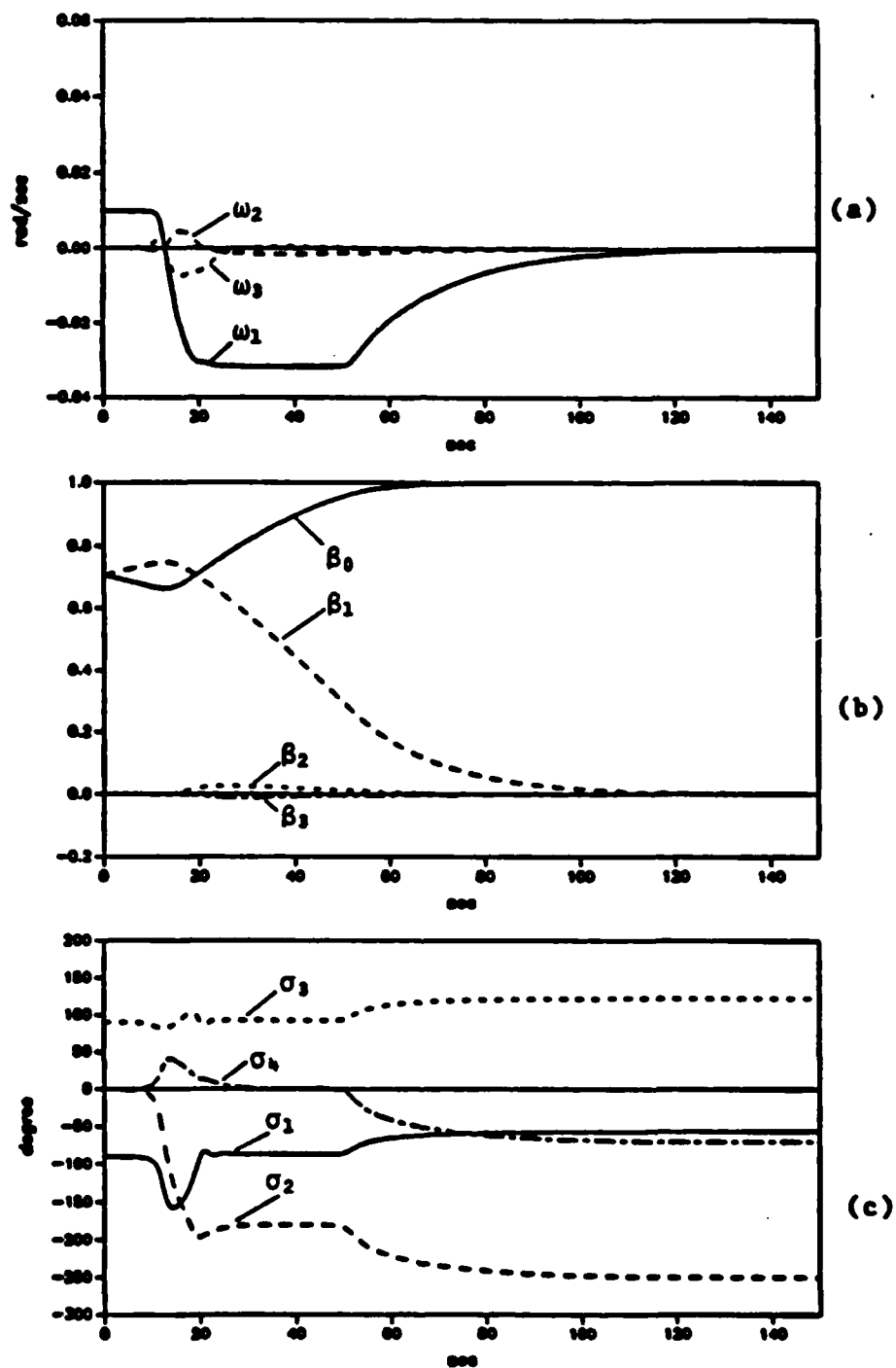


Fig. 8. Results of Simulation 5.

- (a) Required Torque
- (b) Output Torque
- (c) 1st CMG torque



**Fig. 9. Results of Simulation 6.**

- (a) Spacecraft Angular Velocity
- (b) Spacecraft Attitude( Euler parameters )
- (c) CMG gimbal angles

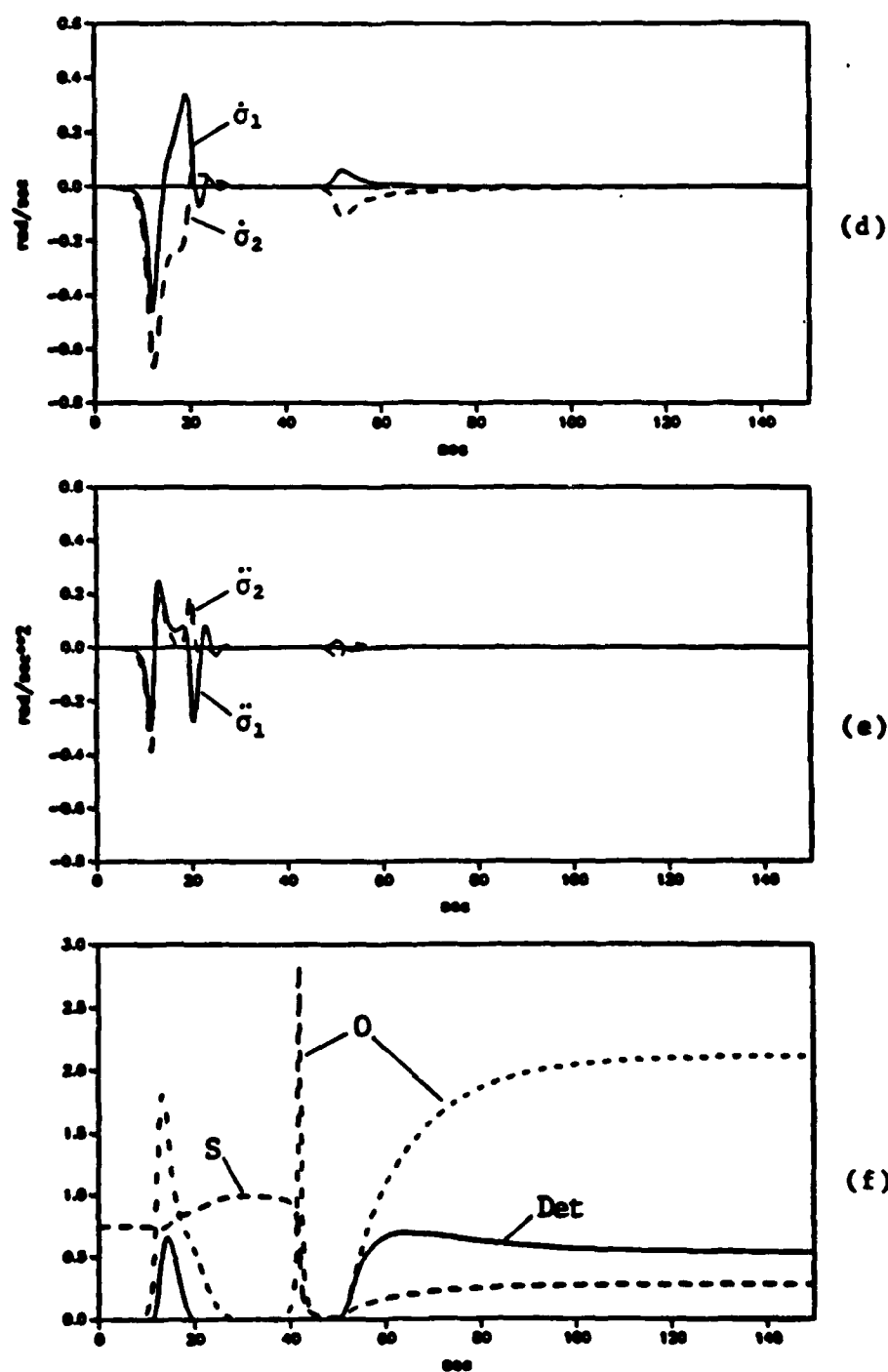


**Fig. 9. Results of Simulation 6. (continued)**  
 (d) Gimbal Rates of 1st and 2nd CMG  
 (e) Gimbal accelerations of 1st and 2nd CMG  
 (f) Singularity Indices

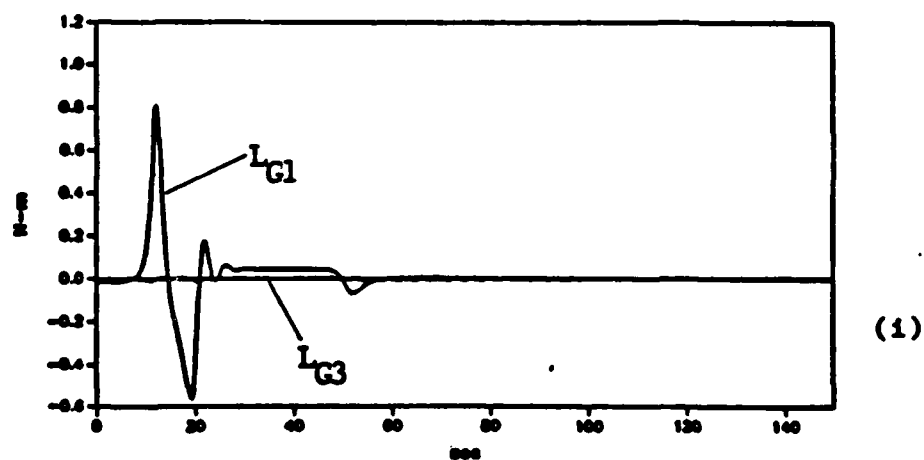
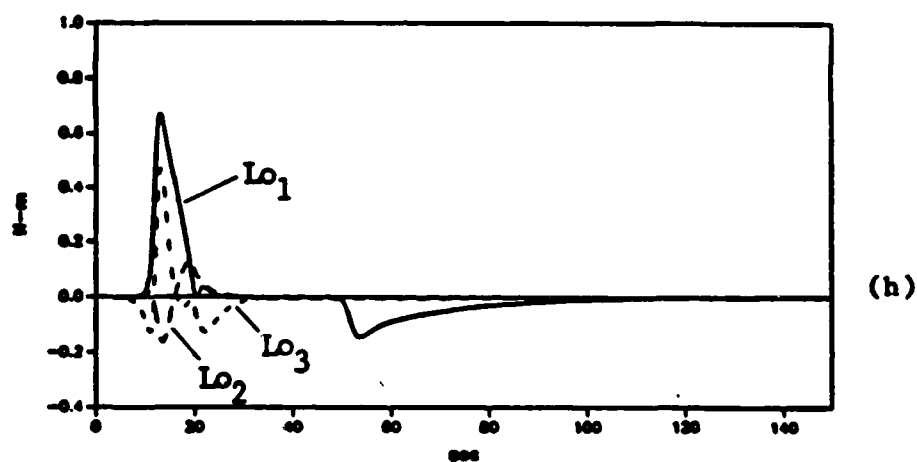
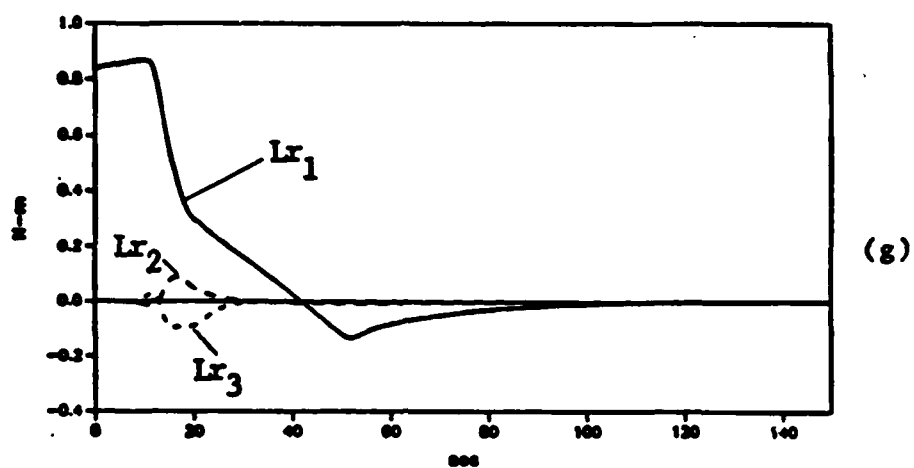


**Fig. 9. Results of Simulation 6. (continued)**

(g) Required Torque

(h) Output Torque

(i) 1st CMG torque

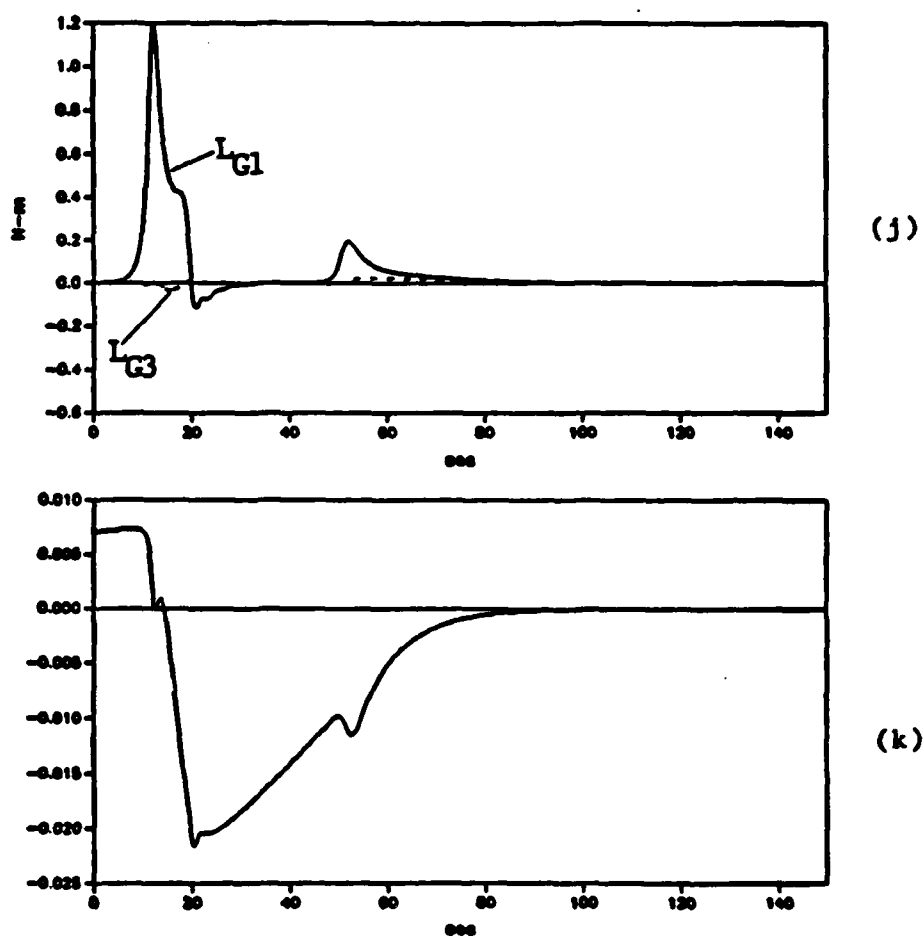
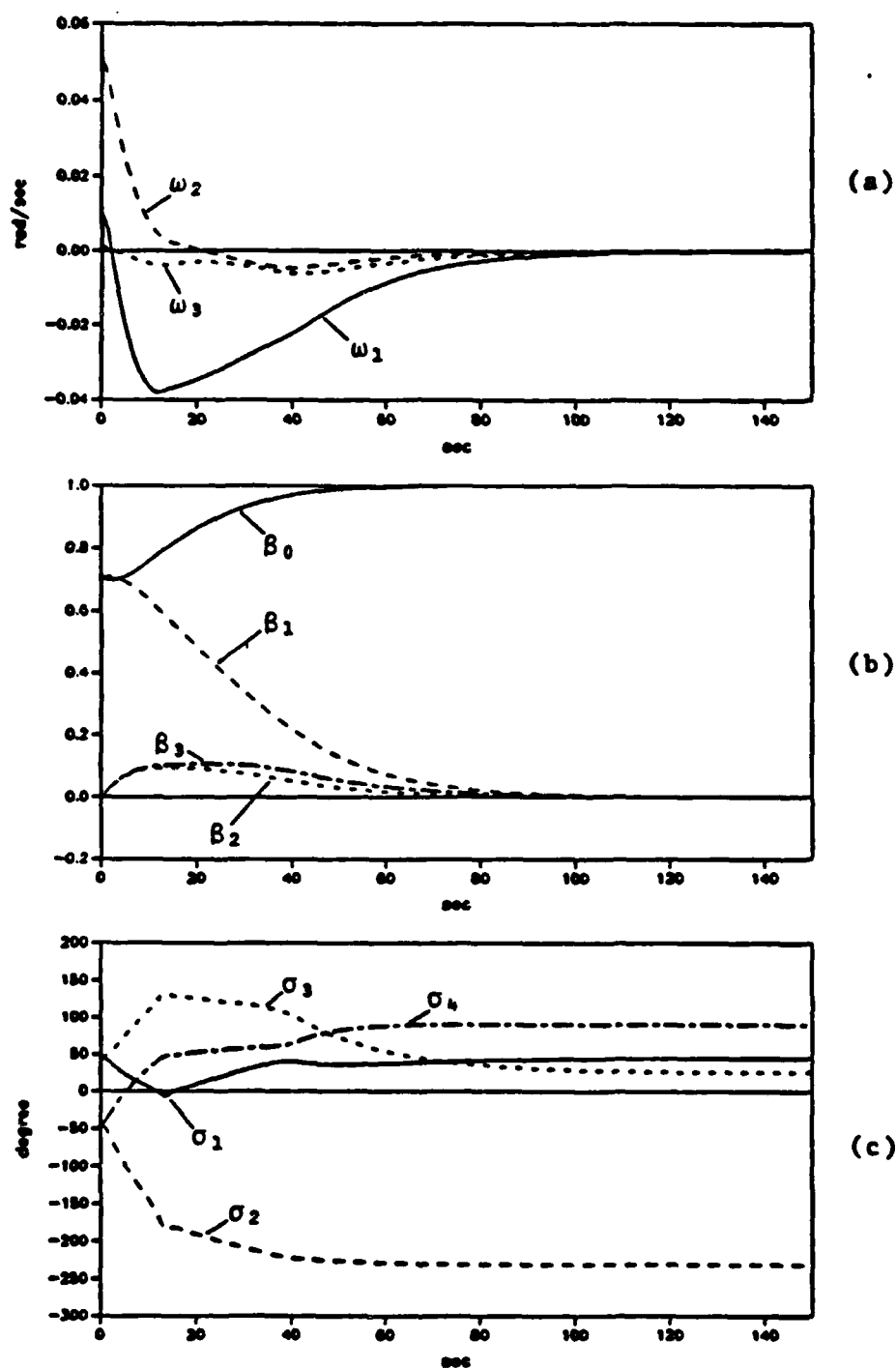


Fig. 9. Results of Simulation 6. (continued)

(j) 2nd CMG Torque

(k) Liapunov Function Rate



**Fig. 10. Results of Simulation 7.**

(a) Spacecraft Angular Velocity

(b) Spacecraft Attitude( Euler parameters )

(c) CMG gimbal angles



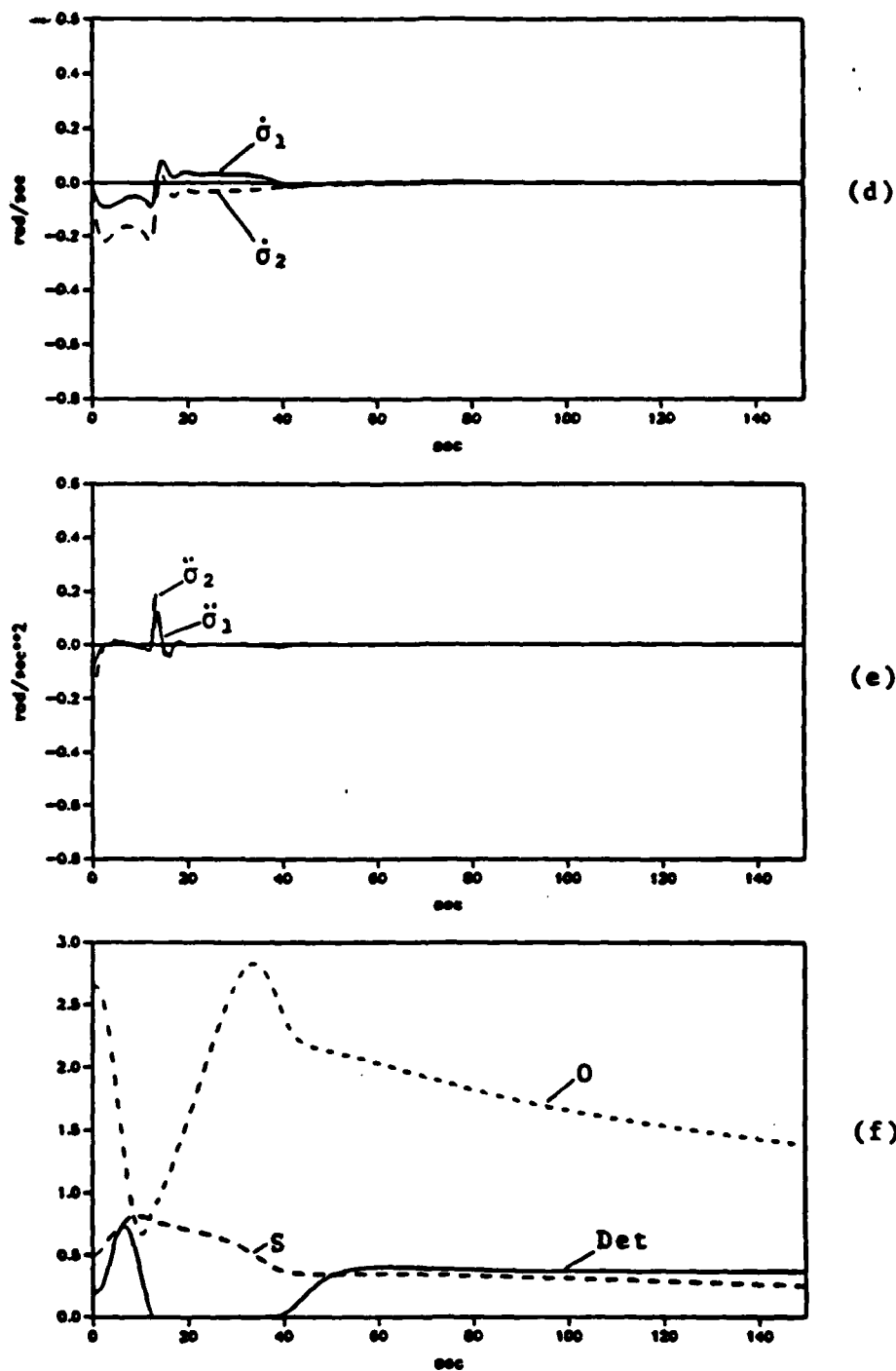


**Fig. 10. Results of Simulation 7. (continued)**  
 (d) Gimbal Rates of 1st and 2nd CMG  
 (e) Gimbal accelerations of 1st and 2nd CMG  
 (f) Singularity Indices

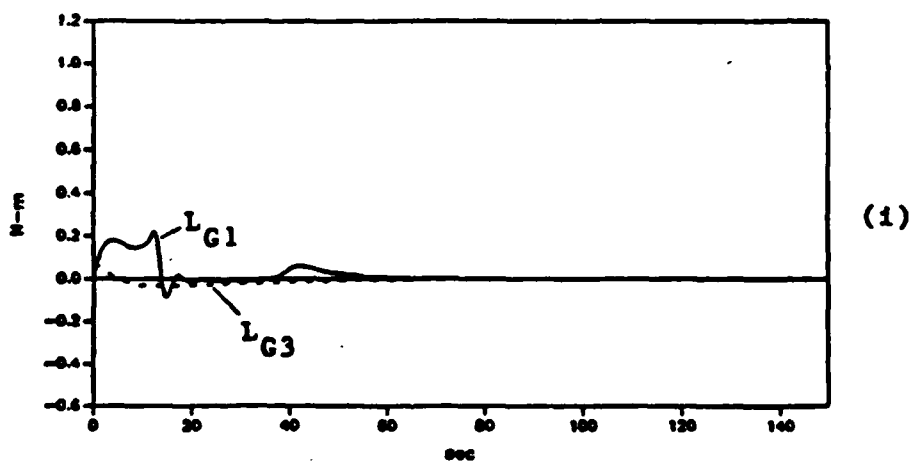
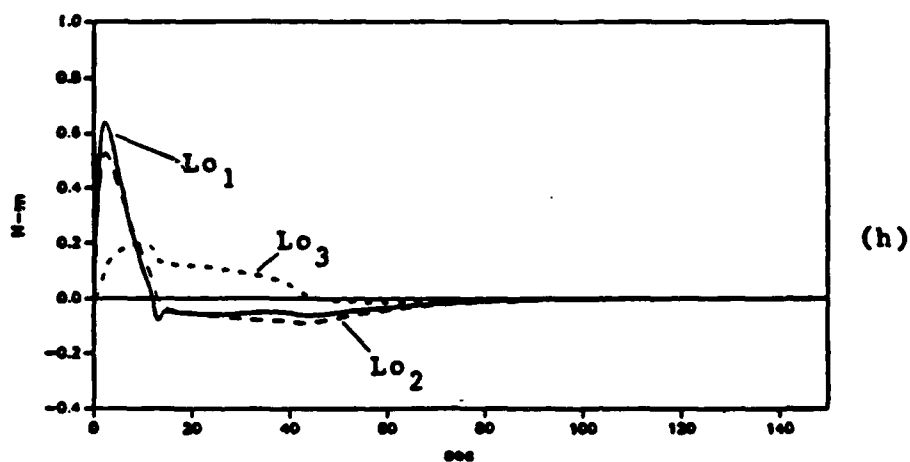
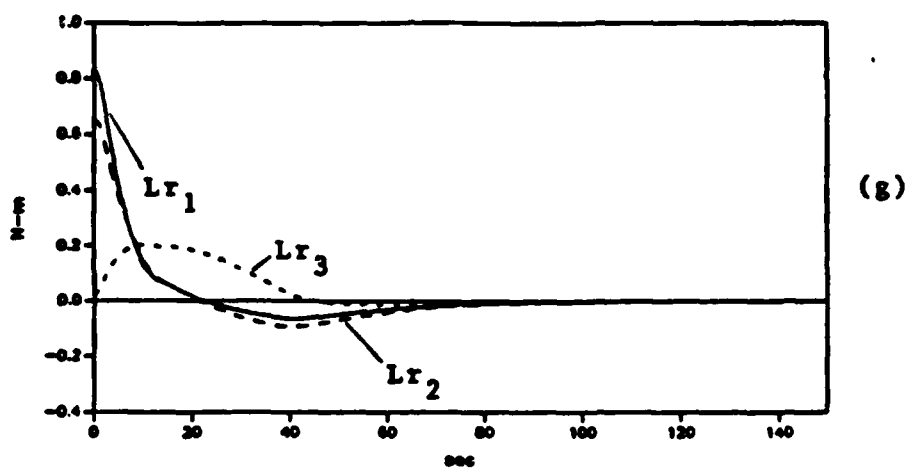


Fig. 10. Results of Simulation 7. (continued)

(g) Required Torque

(h) Output Torque

(i) 1st CMG torque

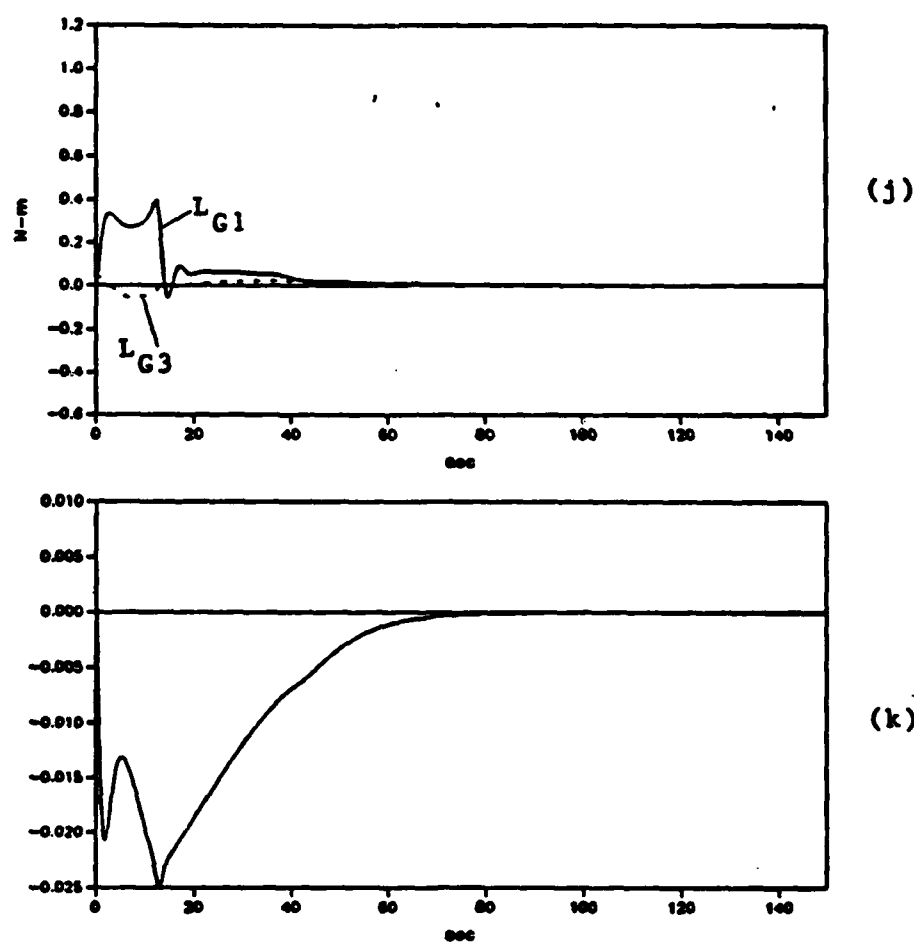


Fig. 10. Results of Simulation 7. (continued)  
(j) 2nd CMG Torque  
(k) Liapunov Function Rate

## APPENDIX

# DYNAMIC EQUATIONS DERIVED FROM LAGRANGE EQUATIONS

Lagrangian approach to deriving dynamic equation is well known<sup>13-15</sup>. First, we need to express kinetic energy of system in terms of generalized coordinates and their derivatives.

## 1. Kinetic Energy of System

The system kinetic energy  $T_r$  including one CMG can be written as

$$T_r = \frac{1}{2} N_{\omega}^V \cdot I^V \cdot N_{\omega}^V + \frac{1}{2} N_{\omega}^V \cdot \underline{M}_{G.C} \cdot N_{\omega}^V + \frac{1}{2} N_{\omega}^G \cdot \underline{J}_G \cdot N_{\omega}^G + \frac{1}{2} N_{\omega}^W \cdot \underline{J}_W \cdot N_{\omega}^W. \quad (A-1)$$

$N_{\omega}^W$  can be expressed as  $N_{\omega}^W = N_{\omega}^G + G_{\omega}^W$ . Substituting this for  $N_{\omega}^W$  in Eq.(A-1) and defining  $(I^V + \underline{M}_{G.C}) \equiv I^S$ , we obtain

$$T_r = \frac{1}{2} N_{\omega}^V \cdot I^S \cdot N_{\omega}^V + \frac{1}{2} N_{\omega}^G \cdot \underline{J}_G \cdot N_{\omega}^G + \frac{1}{2} N_{\omega}^G \cdot \underline{J}_W \cdot N_{\omega}^W + G_{\omega}^W \cdot \underline{J}_W \cdot N_{\omega}^G + \frac{1}{2} G_{\omega}^W \cdot \underline{J}_W \cdot G_{\omega}^W. \quad (A-2)$$

Using the definition  $(\underline{J}_G + \underline{J}_W) \equiv \underline{J}$ , the above equation can be written as

$$T_r = \frac{1}{2} N_{\omega}^V \cdot I^S \cdot N_{\omega}^V + \frac{1}{2} N_{\omega}^G \cdot \underline{J} \cdot N_{\omega}^G + G_{\omega}^W \cdot \underline{J}_W \cdot N_{\omega}^G + \frac{1}{2} G_{\omega}^W \cdot \underline{J}_W \cdot G_{\omega}^W. \quad (A-3)$$

Therefore, the system rotational kinetic energy  $T_r$  can be represented using the matrices and vectors as

$$T_r = \frac{1}{2} \underline{\omega}^T I^S \underline{\omega} + \frac{1}{2} (C_i \underline{\omega} + \dot{\underline{c}}_i)^T \underline{J} (C_i \underline{\omega} + \dot{\underline{c}}_i) + (C_i \underline{\omega} + \dot{\underline{c}}_i)^T \underline{J}_W \underline{\Omega} + \frac{1}{2} \underline{\Omega}^T \underline{J}_W \underline{\Omega}. \quad (A-4)$$

## 2. Dynamic Equation of System

The kinematic equation is represented by Euler parameters. Vadali<sup>13</sup> derived the dynamic equations using Euler parameters as generalized coordinates. In this thesis, other generalized coordinates are chosen. Imagine  $\phi_1, \phi_2$ , and  $\phi_3$  as generalized coordinates (not Euler angles) whose time derivatives are assumed to be  $\omega_x, \omega_y$ , and  $\omega_z$ , respectively. The Lagrangian function  $L = T$ , and it is composed of generalized coordinates  $\underline{\sigma}$  and generalized velocities  $\omega_x, \omega_y, \omega_z, \dot{\underline{\sigma}}$ , and  $\underline{\Omega}$ .

For the vehicle coordinates, the dynamic equations are derived as follows:

$$\frac{\partial L^T}{\partial \phi_i} = 0, \quad (\text{A-5})$$

$$\frac{\partial L^T}{\partial \underline{\omega}} = I^S \underline{\omega} + C_i^T J(C_i \underline{\omega} + \dot{\underline{\sigma}}_i) + C_i^T J_W \underline{\Omega}, \quad (\text{A-6})$$

$$\begin{aligned} \text{and} \quad \frac{d}{dt} \left( \frac{\partial L^T}{\partial \underline{\omega}} \right)_N &= I^S \dot{\underline{\omega}} + \tilde{\omega} I^S \underline{\omega} \\ &+ \frac{d}{dt} (C_i^T J C_i \underline{\omega})_V + \tilde{\omega} (C_i^T J C_i \underline{\omega}) \\ &+ \frac{d}{dt} (C_i^T J \dot{\underline{\sigma}}_i)_V + \tilde{\omega} (C_i^T J \dot{\underline{\sigma}}_i) \\ &+ \frac{d}{dt} (C_i^T J_W \underline{\Omega})_V + \tilde{\omega} (C_i^T J_W \underline{\Omega}), \end{aligned} \quad (\text{A-7})$$

where each time derivative with respect to vehicle frame can be derived as

$$\frac{d}{dt} (C_i^T J C_i \underline{\omega})_V = C_i^T \dot{\tilde{\sigma}}_i J C_i \underline{\omega} - C_i^T J \tilde{\sigma}_i C_i \underline{\omega} + C_i^T J C_i \dot{\underline{\omega}} \quad (\text{A-8})$$

$$\frac{d}{dt} (C_i^T J \dot{\underline{\sigma}}_i)_V = C_i^T \dot{\tilde{\sigma}}_i J \dot{\underline{\sigma}}_i + C_i^T J \ddot{\underline{\sigma}}_i \quad (\text{A-9})$$

$$\frac{d}{dt} (C_i^T J_W \underline{\Omega})_V = C_i^T \dot{\tilde{\sigma}}_i J_W \underline{\Omega} + C_i^T J_W \dot{\underline{\Omega}} \quad (\text{A-10})$$

Then Eq. (A-7) can be written as

$$\begin{aligned}
\frac{d}{dt} \left( \frac{\partial L^T}{\partial \underline{\omega}} \right)_N &= I^S \underline{\dot{\omega}} + \bar{\omega} I^S \underline{\omega} \\
&+ C_i^T \bar{\sigma}_i J C_i \underline{\omega} - C_i^T J \bar{\sigma}_i C_i \underline{\omega} + C_i^T J C_i \underline{\dot{\omega}} + \bar{\omega} (C_i^T J C_i \underline{\omega}) \\
&+ C_i^T \bar{\sigma}_i J \underline{\dot{\sigma}}_i + C_i^T J \underline{\dot{\sigma}}_i + \bar{\omega} (C_i^T J \underline{\dot{\sigma}}_i) \\
&+ C_i^T \bar{\sigma}_i J_W \underline{\Omega} + C_i^T J_W \underline{\dot{\Omega}} + \bar{\omega} (C_i^T J_W \underline{\Omega}). \tag{A-11}
\end{aligned}$$

The generalized force corresponding to  $\phi$  is external torque  $\underline{L}_c$ , and the system dynamic equation is written as

$$\underline{L}_c = \frac{d}{dt} \left( \frac{\partial L^T}{\partial \underline{\omega}} \right)_N. \tag{A-12}$$

Combining  $\underline{\dot{\omega}}$  terms in Eq.(A-11) and using  $I \equiv (I^S + C_i^T J C_i)$ ,  $\underline{\dot{\Omega}} = \underline{\Omega}$ , and  $\underline{h} \equiv J_W \underline{\Omega}$ , the system dynamic equation can be written as

$$\begin{aligned}
\underline{L}_c &= I \underline{\dot{\omega}} + \bar{\omega} I^S \underline{\omega} \\
&+ C_i^T \bar{\sigma}_i J C_i \underline{\omega} - C_i^T J \bar{\sigma}_i C_i \underline{\omega} + \bar{\omega} (C_i^T J C_i \underline{\omega}) \\
&+ C_i^T J \underline{\dot{\sigma}}_i + \bar{\omega} (C_i^T J \underline{\dot{\sigma}}_i) \\
&+ C_i^T \bar{\sigma}_i \underline{h} + \bar{\omega} (C_i^T \underline{h}). \tag{A-13}
\end{aligned}$$

When we consider all  $n$  CMGs, the system equation of motion can be expressed as

$$\begin{aligned}
\underline{\dot{\omega}} &= -I^{-1} [\bar{\omega} I^S \underline{\omega} - \underline{L}_c + \sum_{i=1}^n \bar{\omega} C_i^T J C_i \underline{\omega} \\
&+ \sum_{i=1}^n \{ C_i^T \bar{\sigma}_i J C_i \underline{\omega} - C_i^T J \bar{\sigma}_i C_i \underline{\omega} \\
&+ \bar{\omega} C_i^T J \underline{\dot{\sigma}}_i + C_i^T \bar{\sigma}_i \underline{h} \\
&+ C_i^T J \underline{\dot{\sigma}}_i + \bar{\omega} C_i^T \underline{h} \} ]. \tag{A-14}
\end{aligned}$$

## **ATTACHMENT 4**

# **Robust Eigenstructure Assignment by a Projection Method: Applications Using Multiple Optimization Criteria**

**Robust Eigenstructure Assignment by a Projection Method:  
Applications Using Multiple Optimization Criteria**

***D. W. Rew and J. L. Junkins***  
***Texas A&M University***  
***College Station, Texas 77843***

***and***

***J. N. Juang***  
***NASA Langley Research Center***  
***Hampton, Virginia, 23665***

***presented to***

***AAS/AIAA Astrodynamics Conference***  
***Kalispell, Montana, August 10-13, 1987***



ROBUST EIGENSTRUCTURE ASSIGNMENT BY A PROJECTION METHOD:  
APPLICATIONS USING MULTIPLE OPTIMIZATION CRITERIA

D.W. Rew<sup>\*</sup> and J.L. Junkins<sup>\*\*</sup>  
Texas A&M University  
College Station, Texas 77843

and

J-N. Juang<sup>+</sup>  
Structural Dynamics Branch  
NASA Langley Research Center, MS/230  
Hampton, Virginia 23665

ABSTRACT

A methodology for robust eigenstructure assignment for multivariable feedback systems is presented. The algorithm is based upon a pole placement technique utilizing projections onto subspaces of admissible eigenvectors. We introduce new ideas to generate target (desired) sets of unitary eigenvectors and determine optimal feasible eigenvectors in a least square sense. We also establish useful connections between the pole placement by independent modal space control and the method introduced in this paper.

A multi-criterion optimization algorithm is also presented, which takes efficient advantage of the present eigenstructure assignment method. These developments show significant improvement over an earlier version of this algorithm in both computational cost and accuracy. This optimization process appears to be numerically robust and suitable for high dimensional multi-criterion optimizations; it is especially attractive for computer aided design of control systems.

---

\* Research Associate, Dept. of Aerospace Engineering; Member AIAA.  
\*\* TEES Chair Professor, Dept. of Aerospace Engineering; Fellow AIAA.  
+ Senior Research Scientist, NASA; Associate Fellow AIAA.

## I. INTRODUCTION

Eigenstructure assignment has been shown to be a useful tool for state and output feedback system designs. This approach allows the designer to directly choose eigenvalues and to explore the arbitrariness of admissible eigenvectors. These ideas were introduced by Brogan in Ref. [1]. Subsequent authors utilize formulations based upon either Sylvester equation [2,3] or projections to a subspace of admissible eigenvectors [4,5]. These formulations are conceptually equivalent [1-5], in the sense that they share the same parameterization scheme for eigenvectors. Differences arise among the several algorithms because of choices on criteria which generate the closed-loop eigenvectors, as well as implementation details.

The success of these approaches [1-5] depends mainly upon the selection of criteria or parameters sets which determine the closed-loop eigenvectors. It is well known that near orthogonality is very desirable to minimize sensitivity of eigenvalue placement to model errors. Arbitrary selection of feasible eigenvectors may cause the eigenvector modal matrix to be ill-conditioned. If this is the case, the associated gain matrix may not be accurately calculated and further, the closed-loop system may be a highly sensitive design. Therefore, generation of well-conditioned eigenvectors is a key issue for this family of pole placement algorithms with regards to both insensitive feedback system design and numerical stability. This consideration motivated the present study.

In this paper, we introduce a new scheme to generate unitary basis for the desired eigenvectors and determine admissible eigenvectors close to them in a least square sense. A similar approach can be found in Ref. [7], which employs an orthogonal projection scheme to iteratively improve conditioning of eigenvectors. As mentioned in Ref. [7], the convergence of their iteration is

not assured. The algorithm developed herein utilizes a noniterative scheme in conjunction with an orthogonal projection concept. As suggested in Ref. [8], and motivated by Ref. [9], open-loop eigenvectors are also considered as one choice for the desired eigenvectors and the results are compared with those obtained by the new algorithm. For special cases with the same number of controls as number of controlled modes, the performance of pole placement techniques by the present approach and by the independent modal space control (IMSC) method [9] is examined and useful insights on design strategies regarding eigenstructure assignments are provided.

A robust eigenstructure obtained by the proposed algorithm (to satisfy conditions specified in the space of closed-loop eigenvalues and eigenvectors) can be further tuned and constrained to satisfy other design conditions, imposed for instance, upon average state error energy and average control energy, as in Ref. [10]. The parameterization scheme based upon subspaces of eigenvectors, as developed herein, is employed for multiple objective optimizations. This approach enables us to improve the computational efficiency over Ref. [10] since the iterative solution of the eigenvalue problem is avoided. These savings are most significant, especially for high-dimensional applications.

Section II presents the formulation of the proposed eigenstructure assignment algorithm. Section III summarizes the multiple objective optimization ideas for average state error energy and average control energy, and presents the stability robustness measure which we consider an attractive design criterion. In Section IV, we present computational results obtained for an illustrative sixth order mass-spring system, and a more significant 24th reduced order model of a flexible space structure. Finally, Section V offers concluding remarks.

## II. ROBUST EIGENSTRUCTURE ASSIGNMENT ALGORITHM

In this section, a pole placement algorithm based on defining subspaces of admissible eigenvectors is described. The formulation of appropriate least square problems for a prescribed set of eigenvalues offers the choice of determining eigenvectors as close as possible to i) a prescribed set of unitary basis vectors, ii) the open-loop eigenvectors. The first choice is explored by utilizing singular value decomposition (SVD) of a matrix to establish admissible basis vectors for all modes. The second choice suggested in Ref. [8], is compared with the independent modal space control (IMSC) method for structural systems with same number of controllers as number of controlled modes.

A specialized algorithm for mechanical vibrating systems is also provided. This method takes special advantage of the structure of the eigenvectors to define a more efficient eigenstructure assignment method for second order systems.

### Preliminaries

Consider the linear dynamical system in the state-space form

$$\dot{x} = Ax + Bu, \quad x(0) = x_0 \quad ; \quad (\dot{\phantom{x}}) = \frac{d}{dt}(\phantom{x}) \quad (1)$$

with the linear feedback control

$$u = -Gx \quad (2)$$

where  $A$  is the  $N \times N$  plant matrix,  $B$  is the  $N \times m$  control input matrix

and  $G$  is the  $m \times N$  gain matrix. We assume, for initial simplicity, that the full state is measurable and the pair  $(A, B)$  is completely controllable. Also, we assume that  $\text{rank}(B) = m$ .

From Eqs. (1) and (2), we form the closed-loop system

$$\dot{x} = (A - BG)x$$

and corresponding eigenvalue problems

$$(A - BG) \phi_i = \lambda_i \phi_i$$

$$(A - BG)^T \psi_i = \lambda_i \psi_i \quad i = 1, 2, \dots, N$$

NOTE TO  
TYPESETTER - THE  
GREEK SYMBOLS WITH  
(3)  
UNDERLINES SHOULD  
BE BOLDFACE TYPE  
MY WORD PROCESSOR  
COULD NOT MAKE THEM  
BOLDFACE.

(4a)

(4b)

*John  
Gurke*

where  $\phi_i$  and  $\psi_i$  are the right and left eigenvectors, respectively, corresponding to the eigenvalue  $\lambda_i$ . We adopt the usual normalization for the eigenvectors by scaling them such that

$$\phi_i^* \phi_i = 1 \quad \psi_i^T \phi_j = \delta_{ij} \quad (5)$$

where  $\phi_i^*$  is the conjugate transpose of  $\phi_i$ , and  $\psi_i^T$  is the transpose of  $\psi_i$ . Then, the central constraint in the eigenvalue assignment problem is to determine the gain matrix  $G$  which results in a prescribed set of eigenvalues. Noting that  $G$  is an  $m \times N$  dimensional matrix, it is evident that the problem is underdetermined. We can choose  $N \times (m-1)$  parameters arbitrarily for  $N$  prescribed eigenvalues.

### Sylvester's Equation

The pole placement algorithm of Ref. [3] utilizes the parameter vector  $h_i$  defined by

$$h_i = G\phi_i \quad (6)$$

Rewrite Eq. (4) with this as "Sylvester's equation":

$$(A - \lambda_i I)\phi_i = Bh_i \quad (7)$$

or in matrix form

$$A\Phi - \Phi\Lambda = BH \quad (8)$$

where  $\Phi = [\phi_1, \phi_2, \dots, \phi_N]$

$\Lambda = \text{diag}[\lambda_1, \lambda_2, \dots, \lambda_N]$

and  $H = [h_1, h_2, \dots, h_N] = G\Phi$

The pole placement scheme based on Sylvester's equation (Eq. (7) or (8)) can be summarized as follows:

For given set of A, B matrices, and for prescribed  $\Lambda$  matrix, we can choose an arbitrary H matrix and solve for  $\Phi$  from Eq. (8). Then, provided the  $\Phi$  matrix is well-conditioned, we can solve for G from the linear system:

$$G\Phi = H \quad (9)$$

Notice, from inversion of Eq. (7) that

$$\phi_i = (A - \lambda_i I)^{-1} Bh_i \quad (10)$$

So, if  $\lambda_i$ 's are distinct from their open-loop positions, the columns of  $H$  directly generate the corresponding closed-loop eigenvectors.

### Projection Method

An arbitrary choice of  $h_i$  in Eq. (10) may produce poorly-conditioned eigenvectors and thus result in an inaccurate calculation of the corresponding gain matrix. If this is the case, the resulting closed-loop eigenvalues may be different from the prescribed set and more importantly, their placement is likely to be highly sensitive with respect to perturbation of plant parameters or control gain themselves. This is because of the well-known truth [11] that the condition number of the closed-loop modal matrix of eigenvectors is a measure of eigensolution sensitivity. To eliminate this problem, we develop a systematic scheme designed to determine  $h_i$  vectors which generate well-conditioned eigenvectors. In what follows, we formulate an optimization problem and describe an algorithm to generate unitary basis for desired eigenvectors.

From Eq. (10), we observe that the admissible eigenvectors are also determined by unitary basis vectors which span the column space of  $(A - \lambda_i I)^{-1}B$ . Identifying such basis as the columns of the  $N \times m$  matrix,  $U_i$ , we rewrite Eq. (10) through an appropriate choice of  $h_i$  as

$$\underline{x}_i = U_i h_i \quad (11)$$

There are several ways [7,8] to compute the basis matrix  $U_i$ ; i) by decomposing  $(A - \lambda_i I)^{-1}B$  using the singular-value-decomposition (SVD) or QR algorithms, ii) by computing the complement  $B^\perp$  of the column space of  $B$

(i.e.,  $B^T B = 0$ ) and the complement of the column space of  $B^T(A - \lambda_1 I)$ , or iii) by generating the complement of the column space of  $[A - \lambda_1 I \ B]$ . For the calculation of  $U_1$ , we adopt the second approach, since it does not require inverse of  $(A - \lambda_1 I)$ . It should be noted that when  $B$  is a full-rank square matrix, the orthogonal complement does not exist. If this is the case, the equation (10) can be replaced by  $B^{-1}(A - \lambda_1 I)\underline{x}_1 = h_1$ , which means that for any given vector  $\underline{x}_1$ , there exists a unique vector  $h_1$ .

Assuming that the desired eigenvector,  $\hat{\underline{x}}_1$  is given, we formulate the least-square problem

$$\hat{\underline{x}}_1 = U_1 h_1 + \underline{\Delta}_1 \quad (12)$$

The admissible eigenvector  $\underline{x}_1$  and the corresponding minimized residual error vector  $\underline{\Delta}_1$  are then obtained, using the orthogonal projection

$$\underline{x}_1 = U_1 U_1^* \hat{\underline{x}}_1 \quad (13)$$

and

$$\underline{\Delta}_1 = \hat{\underline{x}}_1 - \underline{x}_1 = (I - U_1 U_1^*) \hat{\underline{x}}_1 \quad (14)$$

Now, we need to select the target (desired) basis vectors  $\hat{\underline{x}}_1$  such that the resulting modal matrix is well conditioned. With Eq. (14), analogous to developments in [8], we define an optimization problem as

$$\begin{aligned} &\text{minimize} & J = & \sum_{i=1}^N \underline{\Delta}_i^* \underline{\Delta}_i \\ &\hat{\underline{x}}_k, k=1,2,\dots,N \end{aligned} \quad (15)$$

$$\text{subject to } \hat{\underline{x}}_i^* \hat{\underline{x}}_j = \delta_{ij}, \quad i, j = 1, 2, \dots, N \quad (16)$$



This problem can be solved by using available nonlinear programming algorithms. The parameterization of the unitary basis may, however, be tedious and lead to a highly nonlinear optimization problem. A more direct and less rigorous approach is then to choose some judicious unitary basis and solve the unconstrained optimization problem of Eq. (15). Thus, we develop an algorithm to generate unitary basis from the subspace matrices,  $U_i$ ,  $i=1,2,\dots,N$  for admissible eigenvectors.

Define the global matrix  $S$  as

$$S = [U_1, U_2, \dots, U_N] \quad (17)$$

and take SVD of  $S$  to get

$$S = \hat{U} \Sigma V^* \quad (18)$$

where  $\Sigma$  is the diagonal singular value matrix, and  $\hat{U}$ ,  $V$  are the left and right singular vectors, respectively. We hypothesize that since  $\hat{U}$  is a unitary matrix spanning the space of all admissible eigenvectors, it will prove an attractive set of target eigenvectors. Now, it remains to determine which unitary basis vectors should be assigned to each of the  $N$  least square problems of Eq. (12) corresponding to each particular assigned eigenvalue, such that the performance index  $J$  of Eq. (15) is minimized. Based upon this approach, we summarize the main steps of the proposed algorithm as follows:

Step 1: For  $i=1,2,\dots,N$ , compute the unitary basis matrix  $U_i$  of the column space of the  $(A-\lambda_i I)^{-1}B$  matrix.

Step 2: Find the left singular vectors  $\hat{U} = [\hat{u}_1, \hat{u}_2, \dots, \hat{u}_N]$  of the matrix  $S$  defined by Eq. (17) and set  $\hat{\phi}_1 = \hat{u}_1$  for  $i=1, 2, \dots, N$ .

Step 3: For  $i=1, 2, \dots, N$ , determine the index  $k$  for  $k$ th desired eigenvector  $\hat{\phi}_k$  which minimizes  $\|\hat{\Delta}_1\| = \|(I - U_1 U_1^*) \hat{\phi}_k\|$ . Store this index in the array,  $q(i)=k$ , and remove  $\hat{\phi}_k$  from the set of desired basis.

Step 4: Calculate admissible eigenvectors and parameter vectors

$$\phi_i = U_1 U_1^* \hat{\phi}_k, \quad k = q(i)$$

Step 5: Determine the gain matrix  $G$  by solving

$$G\phi = B^+(A\phi - \phi\lambda),$$

where the  $m \times N$  matrix  $B^+$  is the pseudo inverse [15] of the  $B$  matrix.

The above process is easily modified to accommodate two other attractive sets of target sectors. When the open-loop eigenvectors are considered as the desired closed-loop eigenvectors, Step 2 should be replaced by computation of the right eigenvectors of the open-loop system matrix. Reference [8] offers a third alternative choice for the target vectors, namely the columns of the unitary matrix which lies nearest (least square sense) to the open loop eigenvectors.

#### Specialization for Mechanical Second Order Systems

When we deal with the  $n$  second order differential equations of mechanical vibrating systems, it is not necessary to determine  $2n \times 2n$  eigenvector matrix

for the corresponding  $2n$  first order state space equations. In fact, we can reduce dimensionality in half and consider the  $n \times n$  modal matrix. Suppose that a mechanical system is defined by the  $n$  second order equations of motion

$$M\ddot{y} + C\dot{y} + Ky = Du \quad (19)$$

where  $y$  and  $u$  are the configuration and control vectors, respectively,

$M$  is an  $n \times n$  positive definite mass matrix,  $K$  and  $C$  are  $n \times n$  positive semi-definite stiffness and damping matrices, respectively, and  $D$  is an  $n \times m$  control influence matrix (assumed to be of maximum rank  $m$ ).

For this system, we introduce the feedback control in the form

$$u = G_1 y + G_2 \dot{y} \quad (20)$$

Substituting Eq. (20) into Eq. (19), we obtain the closed-loop system

$$M\ddot{y} + C\dot{y} + Ky = D [G_1 \ G_2] \text{col}(y, \dot{y}) \quad (21)$$

and the corresponding eigenvalue problem

$$(\lambda_1^2 M + \lambda_1 C + K) \underline{a}_1 = D [G_1 \ G_2] \text{col}(\underline{a}_1, \lambda_1 \underline{a}_1) \quad (22)$$

Similar to Eq. (6), we define the parameter vector  $h_1$  as

$$h_1 = [G_1 \ G_2] \text{col}(\underline{a}_1, \lambda_1 \underline{a}_1) \quad (23)$$

Assuming that the inverse of the coefficient matrix of the left-hand side of

Eq. (22) exists, we can write the modal sub-vector,  $\underline{a}_i$  with Eq. (23) as

$$\underline{a}_i = (\lambda_i^2 M + \lambda_i C + K)^{-1} D h_i \quad (24)$$

Obviously, as before, existence of the inverse in Eq. (24) depends upon assigning the eigenvalue  $\lambda_i$  to positions other than the open-loop eigenvalue position. It should be noted that the modal vector for the velocity vector  $\dot{y}$  is simply  $\lambda_i \underline{a}_i$ . Also, note that if the vectors  $\underline{a}_i$ ,  $i=1,2,\dots,n$ , are a unitary set, then so are the eigenvectors  $\text{col}(\underline{a}_i, \lambda_i \underline{a}_i)$ ,  $i=1,2,\dots,n$  for the corresponding closed-loop system in the state-space form. Therefore, we conclude that the same procedure developed in the previous section can be used for the system of Eq. (19) with the formulation of Eq. (24). That is, after completing the calculation of admissible modal vectors  $\underline{a}_i$ ,  $i=1, 2, \dots, n$ , we form  $2n \times 2n$  eigenvector matrix such that

$$\Phi = \begin{bmatrix} \alpha & \bar{\alpha} \\ \alpha \Lambda & \bar{\alpha} \Lambda \end{bmatrix} \quad (25)$$

where  $\Lambda$  is the diagonal eigenvalue matrix and  $\alpha$  is the  $n \times n$  modal matrix for the displacement vector  $y$  and  $(\bar{\phantom{x}})$  denotes the complex conjugate.

With this, we compute the gain matrix  $[G_1 \ G_2]$  by solving the linear system

$$[G_1 \ G_2] \Phi = H \quad (26)$$

where  $H$  is an  $m \times 2n$  matrix defined by

$$H = [h_1 \ h_2 \ \dots \ h_n \ \bar{h}_1 \ \bar{h}_2 \ \dots \ \bar{h}_n] \quad (27)$$

Eq. (24) provides useful insight on the independent modal space control (IMSC) algorithm of Ref. [9] for the case when  $D=I$  and  $C=0$ . In what follows, we review the pole placement technique by the IMSC method.

### Eigenstructure Assignment by IMSC method

A key feature of in the IMSC method is the determination of feedback control which preserves the open-loop modal matrix, so that the closed-loop system becomes totally decoupled. For the system of Eq. (19) with  $C=0$  and  $D=I$ , we introduce the modal coordinate  $\underline{\eta}$  defined by

$$\underline{y} = \underline{\alpha} \underline{\eta} \quad (28)$$

where  $\underline{\alpha}$  is the modal matrix which satisfies

$$\underline{K} \underline{\alpha} = \underline{M} \underline{\alpha} \underline{\Omega} \quad (29)$$

with the diagonal natural frequency matrix  $\underline{\Omega}$  given by

$$\underline{\Omega} = \text{diag}[\omega_1^2, \omega_2^2, \dots, \omega_n^2] \quad (30)$$

Note that the modal vectors  $\underline{\alpha}_i$  are normalized by

$$\underline{\alpha}_i^T \underline{M} \underline{\alpha}_j = \delta_{ij} \cdot \underline{\alpha}_i^T \underline{K} \underline{\alpha}_j = \omega_i^2 \delta_{ij}. \quad (31)$$

Rewrite Eq. (19) in the modal-space form as

$$\ddot{\underline{y}} + \Omega \underline{y} = \underline{w} \quad (32)$$

by identifying the modal force  $\underline{w} = \underline{a}^T \underline{D} \underline{u}$ . If a feedback control with diagonal gain matrices is introduced in Eq. (32), then the uncoupled structure of independent modal space equations is maintained. Therefore, with a proper choice of diagonal gain matrices, we can place the closed-loop eigenvalues arbitrarily. For this case, we can write the eigenvectors for the open- and closed-loop systems in the state-space form as

$$\underline{\phi}_i^o = \text{col}(\underline{a}_i, j\omega \underline{a}_i), \quad \underline{\phi}_i^c = \text{col}(\underline{a}_i, \lambda_i \underline{a}_i); \quad j^2 = -1 \quad (33)$$

where the superscripts o and c represent open-loop and closed-loop, respectively.

For the case with  $\underline{D}=\underline{I}$ , we rewrite Eq. (24) as

$$\underline{a}_i = (\lambda_i^2 \underline{M} + \lambda_i \underline{C} + \underline{K})^{-1} \underline{h}_i \quad (34)$$

Observing that the columns of the coefficient matrix in the right-hand side span a complete  $n$ -dimensional space, we conclude that the closed-loop eigenvectors for the displacement  $\underline{y}$  can be arbitrarily assigned. In other words, Eq. (34) has exact solution for any  $\underline{a}_i$  vector. Therefore, the closed-loop modal vector obtained by projecting an open-loop one will be exactly same vector as obtained by IMSC method for each desired eigenvalue. If  $\underline{M}$  is the identity matrix, from Eq. (31), we notice that the modal matrix whose columns contain  $\underline{a}_i$  is a unitary matrix. For this special case, the projection methods based on unitary basis vectors and open-loop modal vectors, and IMSC method will generate equally well-conditioned closed-loop eigenvectors.

However, the projection algorithm based on unitary basis may not produce the same gain matrix since the unitary basis vectors selected for this algorithm generally do not coincide with the orthogonal open-loop modal vectors. It should be noted that it is, however, generally impossible to have a perfectly conditioned closed-loop eigenvectors for pairs of complex conjugate eigenvalues, since self-conjugate eigenvectors are not orthogonal.

### III. APPLICATIONS TO MULTI-CRITERION OPTIMIZATION PROBLEMS

As shown in the previous section, the closed-loop eigenvectors can be easily parameterized with a pre-defined eigenvector subspace for each eigenvalue assigned. Due to the underdetermined nature of the problem, the elements of the parameter matrix  $H$  of Eq. (9) or (24) obtained by using the projection technique can be further tuned to satisfy some other design specifications or performance index minimization. As in the previous version of multi-criterion design methodology of Ref. [10], we consider expected state error and control energy, and a stability robustness measure (condition number of eigenvectors) as design criteria.

In Ref [10], we demonstrated that a nonlinear optimization technique based upon minimum norm correction strategy with a homotopy technique [13,14] is suitable for multi-criterion approaches.

In this section, we first define the three objective functions and establish their derivatives with respect to the elements of the parameter vectors. Next, we define a multiple objective (MO) problem and briefly describe its solution process. Also, a procedure to generate multiple criterion trade-off surfaces is discussed.

## Objective Functions and Their Derivatives

### 1) State Error and Control Energy

For the closed-loop system described by Eq. (3), we define the state and control energy, respectively, as

$$J_s = \int_0^{\infty} x^T Q_s x \, dt \quad (35)$$

$$J_u = \int_0^{\infty} u^T Q_u u \, dt \quad (36)$$

$Q_s$  and  $Q_u$  are selected based upon physical considerations; these integrals (or their expected) values can be evaluated, as we show below, from the solution of a pair of Lyapunov equations. Assuming that  $\Phi$  is the closed loop eigenvector matrix, we introduce the coordinate transformation

$$x = \Phi z \quad (37)$$

Noting from Eqs. (2), (9) and (37) that  $u = -Hz$ , we rewrite Eqs. (35) and (36) as

$$J_s = \int_0^{\infty} z^* \Phi^* Q_s \Phi z \, dt \quad (38)$$

$$J_u = \int_0^{\infty} z^* H^* Q_u H z \, dt \quad (39)$$

Again, rewrite Eq. (3) in the modal space form as

$$\dot{z} = \Lambda z, \quad z(0) = \Phi^{-1} x_0 \quad (40)$$



where  $\Lambda$  is the prescribed diagonal matrix of eigenvalues. It is well known [12] that the integrals of Eqs. (38) and (39) can be evaluated by solving Lyapunov matrix equations

$$P_S \Lambda + \Lambda^* P_S + \Phi^* Q_S \Phi = 0 \quad (41)$$

$$P_U \Lambda + \Lambda^* P_U + H^* Q_U H = 0 \quad (42)$$

The solutions of these can be written in the indexed form as

$$P_{s1j} = - \Phi_1^* Q_S \Phi_j / (\lambda_1^* + \lambda_j) \quad (43)$$

$$P_{u1j} = - h_1^* Q_U h_j / (\lambda_1^* + \lambda_j) \quad (44)$$

Now, we write  $J_S$  and  $J_U$  in terms of  $P_S$ ,  $P_U$  and the initial state values as

$$J_S = \text{trace}(\tilde{P}_S X_0) \quad (45)$$

$$J_U = \text{trace}(\tilde{P}_U X_0) \quad (46)$$

where

$$\tilde{P}_S = (\Phi^*)^{-1} P_S \Phi^{-1}, \quad \tilde{P}_U = (H^*)^{-1} P_U H^{-1}, \quad X_0 = x_0 x_0^T$$

Next, we will derive the partial derivatives of the objective functions with respect to the parameter vector  $h_i$ . Denoting by  $\Delta_k$  the derivative with respect to the  $k$ th element of the parameter matrix  $H$ , we write the eigenvector derivatives as

$$\Delta_k \phi_i = U_i \Delta_k h_i \quad (47)$$

Also, the derivative of the inverse of the modal matrix can be written as

$$\Delta_k \phi^{-1} = -\phi^{-1} (\Delta_k \phi) \phi^{-1} \quad (48)$$

Therefore, the derivatives of  $J_s$  and  $J_u$  can be directly obtained by using Eqs. (43), (44), (47) and (48).

Given Eqs. (45) and (46), we can consider the initial conditions  $x_0$  to be random and it is easy to average (take expected value) of  $J_s$  and  $J_u$  over a distribution of initial conditions [12]. If we replace  $X_0 = x_0 x_0^T$  in Eqs. (45) and (46) by the initial condition covariance matrix, the Eqs. (45) and (46) are immediately interpreted as the expected state error and control energies, respectively (i.e., their average over a distribution of initial conditions).

#### 11) Stability Robustness Index

As a third performance measure, condition numbers of the closed-loop eigenvectors are utilized for the multiple objective optimizations. As shown in Ref. [11], conditioning of eigenvectors is directly related to the sensitivity of each eigenvalue to perturbations in the elements of the closed-loop system matrix. The condition number  $c_i$  for  $i$ th eigenvalue is defined [11] by

$$c_i = \|\underline{\psi}_i\| \geq 1 \quad (49)$$

where  $\underline{\psi}_i$  is the left eigenvector and normalized by Eq. (5). Note that  $c_i$ , for

all  $i$ , take the minimum value if and only if the closed-loop eigenvector matrix is normal. It is also shown in Ref. [11] that the condition numbers (or sensitivities) are bounded by

$$\max_j c_j \leq k(\phi) = \| \phi \| \cdot \| \phi^{-1} \| \quad (50)$$

where  $k(\cdot)$  denotes the condition number and  $\| \cdot \|$  represents the spectral norm of a matrix. We consider the condition number of Eq. (49) as a third performance function, i.e.,

$$J_e = k(\phi) \quad (51)$$

Similar to the previous cases, the derivatives of  $J_e$  with respect to the parameter vector,  $h_i$  can be obtained by using Eqs. (47) and (48).

It should be noted that the parameter vector  $h_i$  is complex for a complex eigenvalue so the  $h_i$  vector has  $2m$  parameters. Equivalent formulations in a real form can be developed for evaluations of objective functions and their derivatives.

As shown here, the evaluations of the objective functions and their derivatives involve only simple matrix algebra but include the necessity of taking a matrix inverse. Therefore, it is very important to use strategies which lead to well-conditioned matrices and select numerical algorithm carefully. In implementing the above robust eigenstructure algorithms, we find the gain matrix computation to be much more numerically stable, compared to previous version of the algorithm (see Ref.[10]), which requires solving Sylvester equations and Lyapunov equations. We used conventional Gaussian elimination to carry out the solution for the gain matrix in Eq. (26). The

optimization procedure described in the next part is based on a prescribed set of eigenvalues and the eigenvector subspace computed apriori, we used the simple parameterization of the eigenvectors given by Eq. (11), to find the  $h$  vectors which most nearly (least square sense) yield the target eigenvectors.

### Multiple Objective Optimizations

As described above, when a set of eigenvalues are prescribed, the objective functions can be written in terms of the parameters  $H$  as

$$J_i = J_i(H), i=s,u,e \quad (52)$$

We begin by designating one of the indices as "primary". For the present discussion, we adopt the robustness index  $J_e$  as primary. The set  $\Omega$  of admissible  $H$  matrices is, in the most general case,  $C^{m \times N}$  (all  $m \times N$  complex matrices). Due to the high dimensionality of this general optimization problem, some initial attention to judicious subproblems is appropriate. We first address minimizing globally a primary objective (say  $J_e$ , the robustness index), using any available nonlinear programming algorithm.

We denote the  $H$  matrix which solves the primary optimization problem

$$\begin{array}{ll} \text{minimize } J_e(H) \\ H \in \Omega \end{array} \quad (53)$$

as  $H_e^*$ .

At the minimum  $J_e$  solution point  $H_e^*$ , we evaluate the gradient vectors of the secondary performance indices (for simple notations, we treat the  $H$  matrix as a column vector)

$$\mathbf{v}_s \equiv \text{col} \left( \frac{\partial J_s}{\partial h_{11}}, \frac{\partial J_s}{\partial h_{21}}, \dots, \frac{\partial J_s}{\partial h_{mn}} \right) \Big|_{H = H_e^*} \quad (54)$$

$$\mathbf{v}_u \equiv \text{col} \left( \frac{\partial J_u}{\partial h_{11}}, \frac{\partial J_u}{\partial h_{21}}, \dots, \frac{\partial J_u}{\partial h_{mn}} \right) \Big|_{H = H_e^*} \quad (55)$$

To obtain the steepest descent directions, these are normalized steepest using their vector norm values as

$$\hat{\mathbf{v}}_s = -\mathbf{v}_s / \|\mathbf{v}_s\| \quad (56)$$

$$\hat{\mathbf{v}}_u = -\mathbf{v}_u / \|\mathbf{v}_u\| \quad (57)$$

We now consider the following parameterization of the H matrix over the space  $\mathbf{a}^*$ :

$$H(\alpha_s, \alpha_u) = \|H_e^*\| \left( H_e^* / \|H_e^*\| + \alpha_s \hat{\mathbf{v}}_s + \alpha_u \hat{\mathbf{v}}_u \right) \quad (58)$$

with the scalars  $(\alpha_s, \alpha_u)$  varied over a specified finite range of real values. Notice that sweeping  $\alpha_s$  and  $\alpha_u$  generates a very special two-parameter family of H-variations (and implicitly, gain variations), in the directions of the gradients of the secondary performance indices  $(J_s, J_u)$ , evaluated locally at the optimum  $J_e$  solution. While these gradients are locally evaluated, the  $\alpha$ -variations are finite, and thus the finite gain variational behavior of all three indices can be studied in  $\mathbf{a}^*$ .

Notice, the multiple objective optimization problem is near-trivial, if we restrict attention to the gains generated by the set  $\mathbf{a}^*$  of Eq. (58). Tradeoff surfaces  $J_e(\alpha_s, \alpha_u)$ ,  $J_s(\alpha_s, \alpha_u)$ ,  $J_u(\alpha_s, \alpha_u)$  and implicitly  $J_e(J_s, J_u)$  are determined by sweeping  $\alpha_s$  and  $\alpha_u$  to define a family of H matrices in Eq.

(58), then simply calculating the three indices on an  $(\alpha_s, \alpha_u)$  grid establishes the tradeoff. Obviously a more general multiple objective optimization problems results if we adopt a higher dimensional parameterization of  $H$ .

The general multiple objective optimization (MO) problem can be defined as

$$\underset{H \in \Omega}{\text{minimize}} \quad J = \text{col}(J_s, J_u, J_e) \quad (59)$$

This problem obviously involves attempting to minimize three performance indices; it can be approached by using a nonlinear programming method based upon minimum norm correction strategy in conjunction with a homotopy technique [13,14]. The essential feature of the algorithm is to solve a set of nonlinear equations

$$J_i^* - J_i(H) = 0, \quad i=s,u,e$$

where  $J_i^*$  is the  $i$ th desired goal. The  $J_i^*$  may be interpreted as "the best one could possibly hope for" values which one does not actually expect to achieve due to competition among the three indices. Instead of attempting to solve these equations directly (which typically do not have an exact feasible solution), the first step is to generate a homotopy family of problems with "portable" goal function values defined by the linear map:

$$J_i^p(\gamma) = \gamma J_i^* + (1-\gamma) J_i(H_{\text{start}}) \quad (61)$$

with a homotopy parameter  $\gamma$  satisfying  $0 \leq \gamma \leq 1$ . Then, sweeping  $\gamma$  from

zero to one, we solve Eq. (60) with one or more of the desired goals  $J_i^*$  replaced by  $J_i^D(\gamma)$ . Since Eq. (60) is usually an underdetermined system, we use a standard minimum norm correction technique. The minimum norm seeks a minimum modification of  $H$  on each iteration to satisfy the currently specified "portable" goals  $J_i^D(\gamma)$ . The advantage of this process is due to improved convergence, since each local iteration can be initiated with a close estimate of the solution at each homotopy step. Whenever  $\gamma$  can't be advanced further without encountering a convergence failure (due to competition among indices), then the process is terminated.

Utilizing the nonlinear programming technique described here, we solve a set of the problems of Eq. (61) with different combinations of objective values,  $(J_s^*, J_u^*, J_e^*)$ . The points in the objective function space generated by this scheme will be interpolated and plotted for trade-off surfaces. The overall procedure can be summarized as follows:

1. Select the robustness index  $J_e$  as the primary objective function and optimize it over a predefined domain of the  $(J_s, J_u)$  space (with  $J_s$  and  $J_u$  constrained only by upper and lower bounds).
2. Starting with the solution found in Step 1,
  - 2.1 specify values for  $J_s^*$  and  $J_u^*$  (from a grid of values near the Step 1 convergence).
  - 2.2 solve the equations
 
$$J_s^* - J_s(H) = 0$$

$$J_u^* - J_u(H) = 0$$
  - 2.3 optimize  $J_e$  subject to the above two equality constraints.
  - 2.4 save  $(J_s^*, J_u^*, J_e^*)$  and if the grid in  $(J_u^*, J_s^*)$  is complete, go to Step 3

2.5 select new objective values of  $J_s^*$  and  $J_u^*$ , and go to Step 2.2

3. Interpolate the data and plot trade-off surface.

The convergence achieved in Step 1 is typically, but not always, on the boundary of the  $J_s$ ,  $J_u$  feasible region. Also, due to nonlinearity, convergence to a local rather than the global extremum sometimes occurs. This first optimization is obviously critical, so some variation in starting conditions is recommended. In order to define the trade-off surface uniquely, the local optimizations of Step 2.3 should be done to a fairly sharp tolerance. All the points on the generated trade-off surface should be interpreted as maximally robust designs (minimum  $J_e$ ) for given expected state error and control energy. Each point on the surface corresponds to a set of feedback gains. Therefore, this surface offers an infinity of choices for feedback designs, designs for implementation can be selected with good visibility of the implicit compromises being made.

Occasionally, we have encountered regions of  $(J_s, J_u)$  space in which the optimization of  $J_e$  does not converge reliably. Some unresolved and difficult questions associated with these convergence failures are the following: Under what conditions on the plant matrices  $A$  and  $B$ , can we guarantee that the multi-criterion surfaces i) exist at least in some region of  $(J_s, J_u, J_e, H)$ , ii) are unique, and iii) satisfy the practical requirement of being simply connected over the region of interest. While these are difficult theoretical issues, it is not difficult to demonstrate that practical application of the idea is possible without rigorously resolving these issues [10].



#### IV. COMPUTATIONAL STUDIES

##### **Robust Eigenstructure Assignment**

The projection algorithm developed in Section II has been tested for several models in two classes; 1) sixth order mass-spring systems with three actuators, 11) a 24th reduced order model of a flexible space structure with six actuators.

The six actuators on the flexible structure are assumed to impart three orthogonal forces and three orthogonal moments to the structure at a single point. Conceptually, this is an idealized model of an active joint between a large rigid body and the flexible structure. The active joint has small passive spring and damping constants in the absence of an active command, thus the six "rigid body" modes frequencies are very small, but non zero for the open loop case (Table 2.1). The travel limits of the active joint must also be considered in practical applications. In all of the examples below, we consider the full state feedback case; we did not address sensing and estimation, but we have implicitly assumed that the six across the joint displacements and the first six modal amplitudes and their time derivatives were available from an estimation process.

The specifications of Model 1-3 with various mass matrices in the first class are given in Table 1.1. For the second class, we generated four models (Models 4-7) by varying the order (twice the number of controlled modes) of the flexible system from 12 to 24. The open-loop and desired closed-loop frequencies and damping factors for each model in this class are given in Table 2.1.

For the seven structural systems, we tested the projection method based upon unitary target basis vectors (Algorithm I) and the projection method based upon open-loop target eigenvectors (Algorithm II). For the three models

in the first class, we tested also the pole placement algorithm by IMSC method (Algorithm III). IMSC could not be tested for the flexible structure without introducing additional actuators above the adapted number ( $m=6$ ) which was held fixed. In Tables 1.2 and 2.2, we report condition numbers of the closed-loop eigenvectors (generally, not the open-loop modal matrix) and Frobenius norms of the gain matrices for each model.

As shown in Table 1.2, the same results were obtained by Algorithms II and III for all models. For models with the same number of controllers as the number of modes, Algorithm II is obviously equivalent to the IMSC method, since the open-loop modal matrix are preserved. For the case with the unitary open-loop modal matrix (Model 1), the condition number obtained by all three algorithms is exactly the same. For this case, Algorithm I, however, generates a different gain matrix, because the unitary basis employed in the projection step does not coincide with the unitary open-loop modal vectors. For Model 3, Algorithm I performs superior to Algorithms II and III. The reason is that the condition of open-loop modal matrices depend upon the mass and stiffness matrices. It is obvious that large mass variations in either  $M$  or  $K$  serve to nearly pin or release one or two of the three masses, and of course, the physical significance of this simple example is dubious. However, it is not uncommon that the effective "modal mass" or "modal stiffness" associated with various degrees of freedom (in more complicated many-degree-of-freedom examples) varies by orders of magnitude. In fact, the eigenvalue spectrum (of the free vibration eigenvalue problem) often displays several orders of magnitude variation and therefore presents analogous conditioning issues in practical applications. From these observations and other numerical studies, we conclude that the open-loop modal matrix is not generally the optimal choice of closed-loop modal matrix, vis-a-vis conditioning of the

closed loop eigenvalue problem, for systems with general mass and stiffness matrices.

Test results for Models 4,5,6, and 7 are interesting since these are more consistent with the models encountered in practical applications and also reveal the usefulness of our results for the few actuators, many modes case ( $m < n$ ). As an illustration, we seek to impose substantial damping ( $\zeta = .7$ ) in all modes. In practice, for flexible structure control, we would probably settle for much smaller stability margins on the seventh and higher modes (i.e., the controlled modes). As shown in Table 2.2, Algorithm I performs better than Algorithm II, in these examples, as regards conditioning (robustness) of closed-loop eigenvectors.

Table 1.1 Test Examples (Mass-Spring Systems)

MODEL* NO.	MASS MATRIX	DESIRED EIGENVALUE	
		Freq(rad/sec)	Damping Factor
1	$M = \text{diag}[1,1,1]$	$\omega_1 = 1.44$ $\omega_2 = 4.47$ $\omega_3 = 6.92$	$\zeta_1 = \zeta_2 = \zeta_3 = 0.5$
2	$M = \text{diag}[10^2,1,1]$	$\omega_1 = 0.89$ $\omega_2 = 2.33$ $\omega_3 = 6.76$	$\zeta_1 = \zeta_2 = \zeta_3 = 0.5$
3	$M = \text{diag}[10^3,10^2,1]$	$\omega_1 = 0.09$ $\omega_2 = 0.95$ $\omega_3 = 4.70$	$\zeta_1 = \zeta_2 = \zeta_3 = 0.5$

\* All the models have the same stiffness matrix:

$$K = \begin{bmatrix} 20 & -10 & 0 \\ -10 & 30 & -20 \\ 0 & -20 & 20 \end{bmatrix}$$

Table 1.2 Performance of Eigenstructure Assignment Algorithm

MODEL NO.	$k(\phi^o)^{**}$	Algorithm I*		Algorithm II*		Algorithm III*	
		$k(\phi^c)^{**}$	$IGI_f$	$k(\phi^c)$	$IGI_f$	$k(\phi^c)$	$IGI_f$
1	6.92	9.26	50.91	9.26	19.83	9.26	19.83
2	7.10	9.04	68.39	10.39	45.08	10.39	45.08
3	20.79	10.08	121.79	22.31	128.96	22.31	128.96

\* Algorithm I - Projection method using unitary vectors as targets

Algorithm II - Projection method using open-loop eigenvectors as targets

Algorithm III - IMSC method

\*\*The superscript o and c denote open-loop and closed-loop, respectively.

Table 2.1 Test Examples (Flexible Space Structure)

MODE NO.	OPEN-LOOP EIGENVALUE		DESIRED CLOSED-LOOP EIGENVALUE	
	Freq(rad/sec)	Damp Fac.	Freq(rad/sec)	Damp Fac.
1	$4.90 \times 10^{-4}$	.001	6.78	.70
2	$4.46 \times 10^{-4}$	.001	8.17	.70
3	$4.27 \times 10^{-4}$	.001	8.98	.70
4	$2.57 \times 10^{-4}$	.001	8.79	.70
5	$1.95 \times 10^{-4}$	.001	11.97	.70
6	$1.07 \times 10^{-4}$	.001	15.26	.70
7	22.36	.001	16.46	.70
8	20.49	.001	18.40	.70
9	20.86	.001	20.10	.70
10	42.28	.001	21.86	.70
11	42.28	.001	23.87	.70
12	61.95	.001	67.23	.70

Table 2.2 Performance of Eigenstructure Assignment Algorithm

Model No.	No. of States and No. of Controls n m		Algorithm I*		Algorithm II*	
			k(•)	$\ G\ _f$	k(•)	$\ G\ _f$
4	12	6	31.	234,000	32.	208,000
5	16	6	347.	786,749	461.	906,380
6	20	6	8,342.	1,904,002	14,753.	7,913,951
7	24	6	11,406.	5,920,422	25,495.	10,730,075

\*Algorithm I - Projection method using unitary vectors as targets

Algorithm II - Projection method using open-loop eigenvectors as targets

### Applications using multiple optimization criteria

We selected Model 4 of Tables 2.1 and 2.2 for the study of the variational behavior of the three performance indices. The robustness index  $J_e$  is considered as a primary objective and its optimal solution is obtained by the projection method. Two parameter ( $\alpha_s$  and  $\alpha_u$  of Eq. (58)) optimization in the direction of  $J_s$  and  $J_u$  gradients is employed for evaluation of the initial design and for study of behavior of each performance index in the region defined by the inequalities  $-10 \leq \alpha_s \leq 10$ ,  $-10 \leq \alpha_u \leq 10$ . The three-dimensional plots of each performance index versus  $(\alpha_s, \alpha_u)$  are given in Fig. 1-3. Notice from Eq. (58) that a positive value of  $\alpha_s$  (or  $\alpha_u$ ) represents decrease of the state energy (or control energy).

As can be seen in Fig. 1, the initial design ( $\alpha_s = \alpha_u = 0$ ) is obviously optimal for maximum robustness (minimum condition number). This three dimensional plot also provides information on the sensitivity of the robustness index  $J_e$  with respect to the parameter variations (implicitly, gain variations). The design points in the region defined by  $0 < \alpha_s < 2.5$  are attractive since the surface in this region is near-planar. Similar observations can be made from Figs. 2 and 3 for state energy and control energy, respectively. From these three performance surfaces, we conclude that the design points in the region of  $0 < \alpha_s < 2.5$  and  $-2.5 < \alpha_u < 0$  are attractive candidates for a feedback design, since they satisfy eigenvalue placement constraints and have low values of the three performance indices and low sensitivity to gain variations. It should be stressed, however, that these surfaces apply to gain variations which preserve the closed loop eigenvalue positions. In essence, these surfaces display the additional performance tradeoffs available after one has prescribed the position of the closed loop eigenvalues. Clearly a more general family of surfaces (with

larger performance variations) is obtained if we admit eigenvalue placement variations in the optimization process. In summary, from simultaneous study of these surfaces, we can immediately identify the region of low sensitivity and small performance indices.

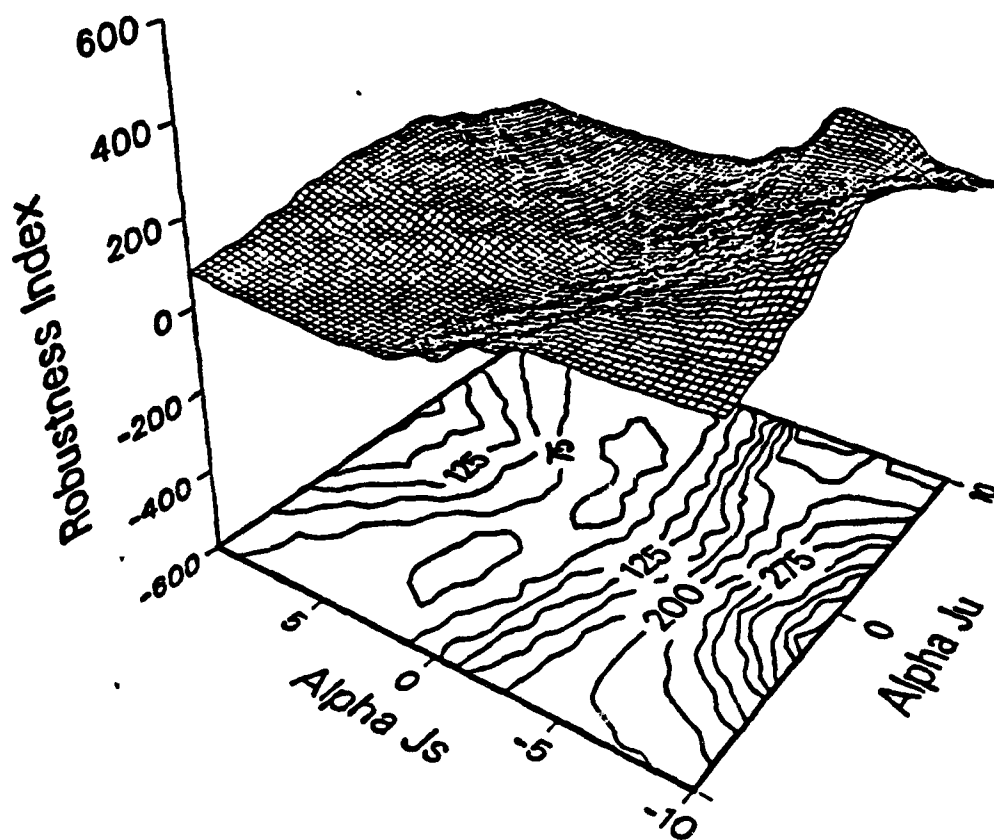


Figure 1. Behavior of Robustness Index in Vicinity of Optimal Robustness Design



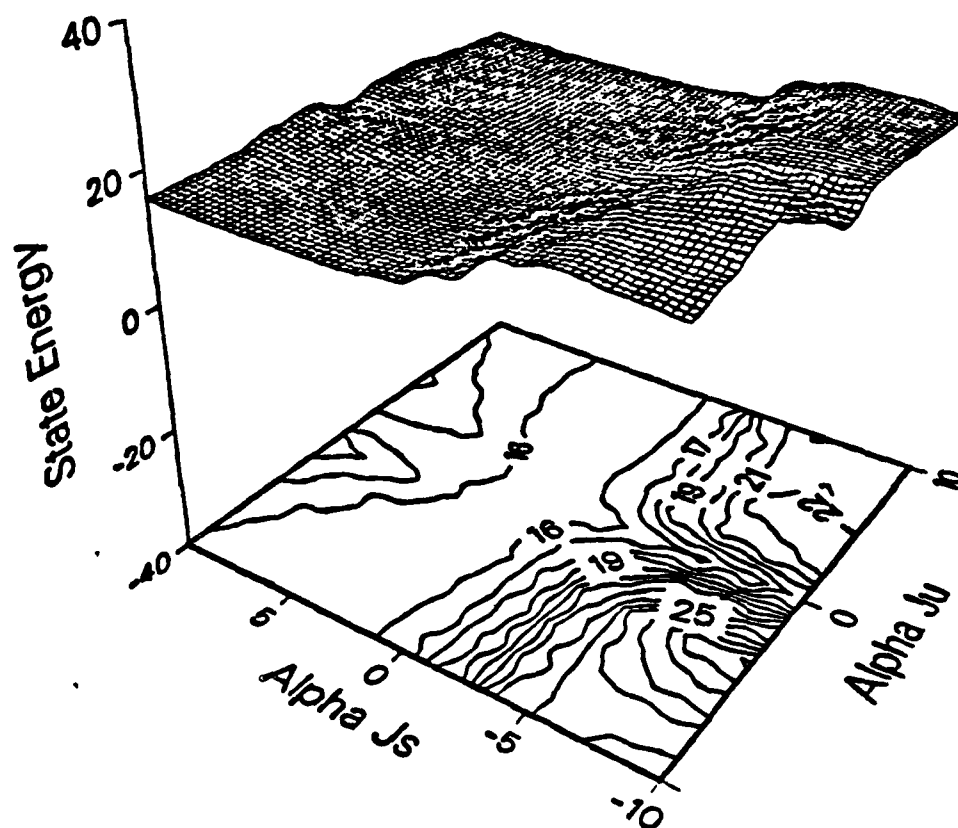


Figure 2. Behavior of State Error Energy in Vicinity of Optimal Robustness Design

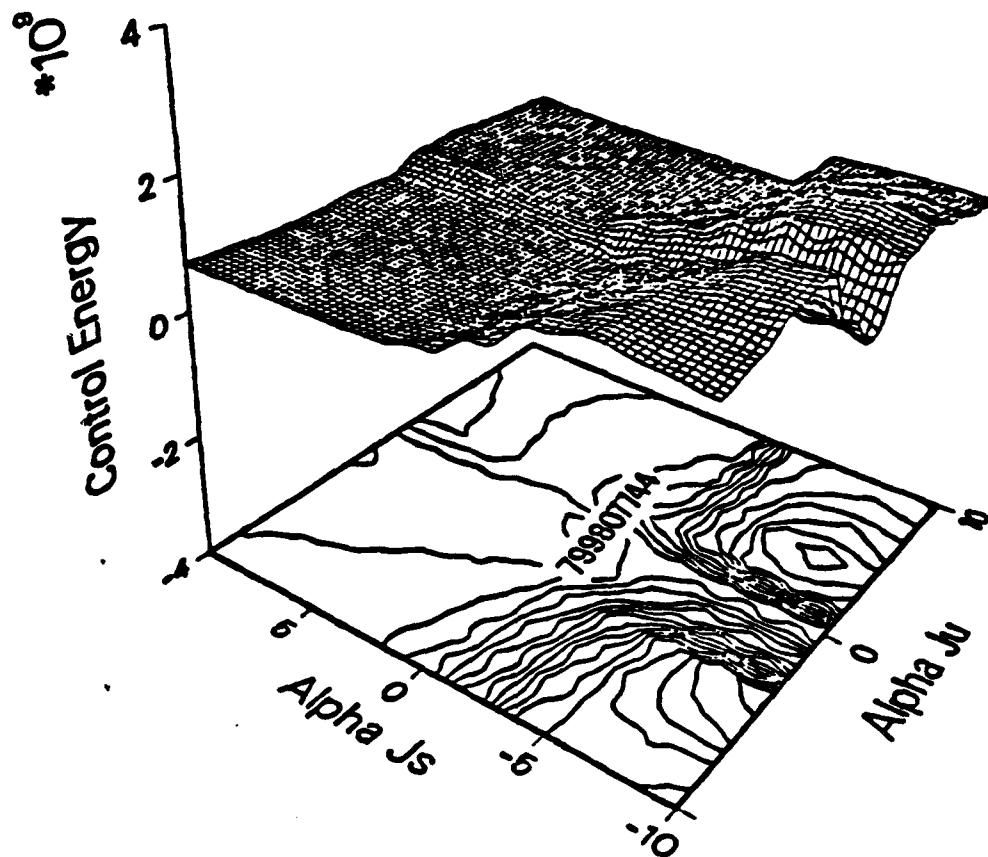


Figure 3. Behavior of Control Energy in Vicinity of Optimal Robustness Design

## V. CONCLUSIONS

In this paper, we develop a new methodology for robust eigenstructure assignment and multivariable feedback gain design. This algorithm is based upon a pole placement technique which employs projections onto subspaces of admissible eigenvectors. It utilizes a new scheme to generate desired target eigenvectors and determine the corresponding admissible eigenvectors in a least square sense. Numerical studies demonstrate that the proposed algorithm is applicable to systems of at least moderate dimensionality. We also establish some interesting special case ( $m=n$ ) connections to the independent modal space control approach. We show, via counter example, that using open-loop eigenvectors as the target closed-loop eigenvectors is generally not optimal vis-a-vis conditioning (robustness) of the closed-loop eigenvectors, even for the  $m=n$  case.

A new approach is presented for evaluating optimal control designs by introducing judicious gain variations in the gradient directions of secondary performance indices. This approach leads to multiple criterion performance tradeoff surfaces as a function of gain variations. Region of low sensitivity and small values of secondary indices can be immediately identified from simultaneous study of these surfaces. This approach is especially attractive for computer aided design of control systems.

## VI. REFERENCES

- [1] Brogan, W.L., Modern Control Theory, Quantum Publishers, Inc., New York, N.Y., 1974, pp. 311-315.
- [2] Bhattacharyya, S.P. and E. deSouza, "Pole Assignment via Sylvester's Equation," Syst. and Contr. Letters, Vol. 1, No. 4, Jan. 1982, pp. 261-263.

- [3] Cavin III, R.K. and S.P. Bhattacharyya, "Robust and Well-Conditioned Eigenstructure Assignment via Sylvester's Equation," J. of Optimal Contr. Appl. and Method., Vol. 4, 1983, pp. 205-212.
- [4] Porter, B. and J.J. D'Azzo, "Algorithm for Closed-Loop Eigenstructure Assignment by State Feedback in Multivariable Linear Systems," Int. J. of Control, Vol. 27, No. 6, 1978, pp. 943-947.
- [5] Moore, B.C., "On the Flexibility Offered by State Feedback in Multivariable Systems Beyond Closed-Loop Eigenvalue Assignments," IEEE Tr. on AC, Vol. AC-21, 1976, pp. 689-692.
- [6] Wonham, W.M., "On Pole Assignment in Multi-input, Controllable Linear Systems," IEEE Tr. on AC, Vol. AC-12, 1967, pp. 660-665.
- [7] Kautsky, J., N.K. Nichols and P. Van Dooren, "Robust Pole Assignment in Linear State Feedback," Int. J. of Control, Vol. 41, No. 5, 1985, pp. 1129-1155.
- [8] Juang, J-N., K.B. Lim and J.L. Junkins, "Robust Eigensystem Assignment," preprint of a paper submitted to 1987 AIAA Guidance and Control Conference, Dec. 1986.
- [9] Oz, H. and Meirovitch, L., "Optimal Modal-Space Control of Flexible Gyroscopic Systems," J. of Guidance and Control, Vol. 3, Nov.-Dec. 1980, pp. 220-229.
- [10] Rew, D.W. and J.L. Junkins, "Multi-criterion Approaches to Optimization of Linear Regulators," to appear the J. of Astronautical Sciences, Sept. 1986, AIAA paper 86-2198-CP.
- [11] Wilkinson, J.H., The Algebraic Eigenvalue Problems, Oxford Univ. Press, Oxford, 1965.
- [12] Fleming, P.J., "An Application of Nonlinear Programming to the Design of Regulators Using a Linear-Quadratic Formulation," Int. J. of Control, 1983.
- [13] Junkins, J.L. and J.P. Dunyak, "Continuation Methods for Enhancement of Optimization Algorithms," Presented to 19th Annual Meeting, Society of Engineering Science, University of Missouri, Rolla, Oct. 1982.
- [14] Junkins, J.L., "Equivalence of the Minimum Norm and Gradient Projection Constrained Optimization Techniques," AIAA Journal, Vol. 10, No. 7, pp. 927-929, July 1972.
- [15] Golub, G.H. and W. Kahan, "Calculating the Singular Values and Psuedo-inverse of a Matrix," SIAM Numerical Analysis, Vol. 2, 1965, pp. 202-224.

## **ATTACHMENT 5**

# **Robust Eigensystem Assignment for Flexible Structures**

**ROBUST EIGENSYSTEM ASSIGNMENT FOR FLEXIBLE STRUCTURES**

**Jer-Nan Juang<sup>\*</sup> and Kyong B. Lim<sup>#</sup>**  
Structural Dynamics Branch  
NASA Langley Research Center, MS/230  
Hampton, Virginia, 23665

**and**

**John L. Junkins<sup>+</sup>**  
Texas A&M University  
College Station, Texas, 77843

**Paper No. 87-2252-CP**

**Presented at the AIAA Guidance, Navigation and Control Conference**

**Doubletree Hotel, Monterey, California**

**August 17-19, 1987**

**Accepted for publication in the Journal of Guidance, Control and Dynamics**

---

<sup>\*</sup>Senior Research Scientist, NASA; Associate Fellow AIAA

<sup>#</sup>Engineering Specialist, PRC Kentron Inc.; Member AIAA

<sup>+</sup>TEES Professor, Department of Aerospace Engineering; Fellow AIAA

# ROBUST EIGENSYSTEM ASSIGNMENT FOR FLEXIBLE STRUCTURES

Jer-Nan Juang<sup>\*</sup> and Kyong B. Lim<sup>#</sup>  
Structural Dynamics Branch  
NASA Langley Research Center, MS/230  
Hampton, Virginia, 23665

and

John L. Junkins<sup>+</sup>  
Texas A&M University  
College Station, Texas, 77843

## ABSTRACT

An improved method is developed for eigenvalues and eigenvectors placement of a closed-loop control system using either state or output feedback. The method basically consists of three steps. First, the singular value or QR decomposition is used to generate an orthonormal basis that spans admissible eigenvector space corresponding to each assigned eigenvalue. Secondly, given a unitary matrix, the eigenvector set which best approximates the given matrix in the least-square sense and still satisfy eigenvalue constraints is determined. Thirdly, a unitary matrix is sought to minimize the error between the unitary matrix and the assignable eigenvector matrix. For use as the desired eigenvector set, two matrices, namely, the open-loop eigenvector matrix and its closest unitary matrix are proposed. The latter matrix generally encourages both minimum conditioning and control gains. In addition, the algorithm is formulated in real arithmetic for efficient implementation. To illustrate the basic concepts, numerical examples are included.

## NOMENCLATURE

- A open-loop state matrix ( $2n \times 2n$ )
- B control input matrix ( $2n \times m$ )
- $c_k$  real coefficients corresponding to  $k$ -th assignable eigenvector ( $v_k \times 1$ )
- $c_2( )$  condition number of ( ) in matrix 2-norm
- $\hat{c}_k$  optimal real coefficients corresponding to  $k$ -th assignable eigenvector ( $v_k \times 1$ )
- G feedback gain matrix ( $m \times \gamma$ )
- H measurement matrix ( $\gamma \times 2n$ )
- m number of inputs
- p number of pairs of conjugate eigenvalues assigned
- Q desired set of orthogonal eigenvectors ( $2n \times 2p$ )
- $V_{ok}$  orthogonal basis for null space of  $\Gamma_k$

$V_{OK}$  orthogonal complement to the null space of  $\Gamma_K$   
 $w_K$  weighting factor corresponding to least-square error of  $K$ -th eigenvector  
 $\gamma$  number of outputs  
 $\lambda_{rK}$  real component of  $K$ -th closed-loop eigenvalue  
 $\lambda_{iK}$  imaginary component of  $K$ -th closed-loop eigenvalue  
 $v_{rK}$  real component of  $K$ -th closed-loop eigenvector  
 $v_{iK}$  imaginary component of  $K$ -th closed-loop eigenvector  
 $\Gamma_K$  an expanded matrix characterizing the closed-loop system ( $4n \times (4n + 2m)$ )  
 $v_K$  dimension of the null space of  $\Gamma_K$   
 $\phi_{rK}$  real component of assigned eigenvector corresponding to  $c_K$   
 $\phi_{iK}$  imaginary component of assigned eigenvector corresponding to  $c_K$   
 $\sigma$  singular values  
 $\| \cdot \|_F$  Frobenius norm

## 1. INTRODUCTION

It is known that eigensystem assignment using linear, constant state or output feedback for multi-input multi-output (MIMO) systems plays a key role in shaping transient response. Wonham<sup>1</sup> first related controllability and eigenvalue assignability for state feedback of MIMO systems. Issues arising from the non-uniqueness of control gains (or eigenvectors) for placing eigenvalues were investigated by many researchers after Moore<sup>2</sup> characterized the class of all closed-loop eigenvector sets attainable for a given set of eigenvalues. Along the similar line, many coinciding results and extensions, such as multiple eigenvalues assignment for the output feedback, have been published as exemplified by.<sup>3-5</sup>

The problem of developing reliable algorithms for designing controllers that are robust in addition to satisfying eigenvalue placement constraints has recently been an area of active research. Robustness herein refers to the property whereby the closed-loop eigenvalues are insensitive to the system uncertainties and/or perturbations. The class of perturbations considered here includes parameter perturbations in the plant or gain matrices for constant, linear, time invariant dynamical system. A recent review of robustness theory and analysis considered here is given in Ref. 6. Among the many published works that are related to robustness theory and optimization, there appears to be at least four methods that address the problem of robustness or sensitivity optimization subject to eigenvalue placement constraints. The first class of methods<sup>7-8</sup>, involves the selection of eigenvector sets that satisfy modal insensitivity and eigenvalue placement constraint equations simultaneously. A major drawback to this approach is the difficulty in satisfying modal insensitivity and eigenvalue placement



constraint equations simultaneously. Special cases are proposed that somehow ease the difficulty. An important distinct feature in the first method is the need for evaluating derivatives of system matrices with respect to suspected uncertain parameters. The second class of methods<sup>9-10</sup>, involve a direct optimization of a scalar index which is related to the condition number while subject to eigenvalue placement constraints in the form of Sylvester's equations. Similar to the above approach, the third class of methods<sup>6</sup> consider the direct minimization of robustness measures, including a norm of eigenvalue sensitivity and various other robustness measures, subject to explicitly stated equality and inequality constraints on eigenvalues. The second and third methods involve iterative algorithms, which require computation of various sensitivities and may be computationally expensive for large systems. However, the use of sequential linear programming and Homotopy methods<sup>6,11</sup> in the latter approach, makes the algorithm numerically robust, easy to implement, and perhaps most importantly, informative when no solution exists for the stated problem. A fourth method<sup>12</sup> uses the concept of orthogonal projection into linear subspaces of eigenvectors to iteratively improve various equivalent measures of conditioning. This method utilizes an orthonormal basis that spans the subspaces which satisfy eigenvalue placement constraints. This method is based on QR and SVD algorithms and is consequently numerically stable in addition to being efficient since no derivative calculations are required as in the previous methods.

In this paper, a design algorithm is introduced which amounts to an extension of the fourth method in at least three ways, namely, (1) non-iterative, (2) extension to output feedback, and (3) use of design freedom to encourage minimum gain configuration when the number of eigenvalues to be placed is less than the number assignable. Furthermore, several insights pertaining to the robust eigensystem assignment problem is presented. First, a closed form expression for the set of eigenvectors which are closest, in a least-squares sense, to an apriori specified matrix and still assign desired eigenvalues is obtained. The remaining freedom on the choice of apriori matrix is discussed in detail. In particular, the unitary matrix closest to the open-loop eigenvector matrix is recommended. The above choice is believed to produce both well conditioning and minimum control effort. In addition, this paper addresses the important case where a fewer number of eigenvalues are specified than is possible. It is shown that the gain matrix satisfies an underdetermined set of linear equations which naturally leads to a unique minimum norm gain. Furthermore, the need for minimum gain controllers motivates us to introduce a correlation criteria. It is based on orthogonal projections<sup>13</sup>, for identifying the best desired eigenvector corresponding to each subspace of admissible eigenvectors. The correlation problem is clearly more evident in the direct output feedback case. The correlation procedure also takes into consideration the weighting of eigenvectors due to observability in addition to projection magnitudes. Finally, it should be mentioned that all formulations involve real arithmetic.

## 2. STATE FEEDBACK FORMULATION

In the analysis and design of the dynamics and vibration control of flexible structures, a set of second order linear, constant coefficient, ordinary differential equations are frequently used. This leads to an even dimensioned state space. Although not restricted to even dimensions, let  $A$  be the state matrix of order  $2n$  and  $B$  the  $2n \times m$  influence matrix of the  $m$  control inputs for a linear, time-invariant, constant gain feedback system. Assume that full state feedback is used to design the controller with gain matrix  $G$  of dimension  $m \times 2n$ . For computational efficiency, the eigensolution of the closed-loop system  $[A + BG]$  can then be written as

$$[A + BG]\Psi_k = \Psi_k \Lambda_k; k = 1, \dots, n \quad (1)$$

where  $\Psi_k = [\Psi_{rk}, \Psi_{ik}]$  is the  $2n \times 2$  real eigenvector matrix corresponding to the

$2 \times 2$  real block eigenvalue matrix  $\Lambda_k = \begin{bmatrix} \lambda_{rk} & \lambda_{ik} \\ -\lambda_{ik} & \lambda_{rk} \end{bmatrix}$ . The above subscripts "r" and "i" refer to the real and imaginary parts of the assumed self conjugate set of eigenvectors whereas subscript "k" refers to the mode number. Expanding Eq.(1) yields the following two equations

$$[A + BG] \Psi_{rk} = \lambda_{rk} \Psi_{rk} - \lambda_{ik} \Psi_{ik} \quad (2)$$

$$[A + BG] \Psi_{ik} = \lambda_{ik} \Psi_{rk} + \lambda_{rk} \Psi_{ik} \quad (3)$$

Rearranging Eqs.(2) and (3) in a compact matrix form produces

$$\begin{bmatrix} A - \lambda_{rk}I & \lambda_{ik}I & B & 0 \\ -\lambda_{ik}I & A - \lambda_{rk}I & 0 & B \end{bmatrix} \begin{bmatrix} \Psi_{rk} \\ \Psi_{ik} \\ G\Psi_{rk} \\ G\Psi_{ik} \end{bmatrix} = \Gamma_k \Phi_k = 0 \quad (4)$$

Note that Eq. (4) also holds for the case of repeated complex conjugate pairs of eigenvalues. For the case of real, repeated eigenvalues,  $\Gamma_k$  and  $\Phi_k^T$  in Eq. (4) reduces to  $[A - \lambda I \mid B]$  and  $[\Psi_k^T, (G\Psi_k)^T]$  respectively. The only assumption required in the above formulation is that the system be nondefective, i.e., a full set of eigenvectors corresponding to the eigenvalues to be assigned exists. Since the above generalizations are straightforward, only the case where complex conjugate pairs of eigenvalues are assigned will be presented, which is most common in the vibration control of flexible structures.

### 2.1 Eigenvalue Assignment

To obtain the nontrivial solution space of the homogeneous equation (4), the singular value decomposition (SVD) is applied to the matrix  $\Gamma_k$  yielding

$$\Gamma_K = U_K \Sigma_K V_K^T = U_K \begin{bmatrix} \sigma_K & 0 \\ 0 & 0 \end{bmatrix} \begin{bmatrix} V_{OK}^T \\ V_{OK}^T \end{bmatrix} \quad (5)$$

It follows that the matrix  $V_{OK}$ , represents a set of orthogonal basis vectors spanning the null space of the matrix  $\Gamma_K$  so that<sup>13</sup>

$$\Gamma_K \phi_K = \Gamma_K V_{OK} c_K = 0. \quad (6)$$

Note that if  $\Gamma_K$  is not close to a matrix of lesser (or higher) rank (which is easily found from the singular values; hence the advantage of using SVD), the above basis for null space,  $V_{OK}$ , can be computed more efficiently by taking the QR decomposition of  $\Gamma_K^T$ .

To obtain an expression for gain matrix, choose a particular set of vectors,  $\phi_K$  ( $K=1, \dots, p$ ) satisfying Eq. (6), corresponding to some choice  $c_K$ , and partition the vector  $\phi_K$  into four components such that

$$\Gamma_K \phi_K \triangleq \Gamma_K \begin{bmatrix} \phi_{rk} \\ \phi_{ik} \\ \hat{\phi}_{rk} \\ \hat{\phi}_{ik} \end{bmatrix} = \Gamma_K \begin{bmatrix} v_{ork} \\ v_{oik} \\ \hat{v}_{ork} \\ \hat{v}_{oik} \end{bmatrix} c_K = 0 ; \quad K=1, \dots, p \quad (7)$$

Observation of Eqs. (4) and (7) indicates that

$$G [\phi_{rk} \phi_{ik}] = [\hat{\phi}_{rk} \hat{\phi}_{ik}] ; \quad K=1, \dots, p \quad (8)$$

Form the matrix equation

$$G \Phi \triangleq G[\phi_{r1}, \phi_{i1}, \phi_{r2}, \phi_{i2}, \dots, \phi_{rp}, \phi_{ip}] \\ = [\hat{\phi}_{r1}, \hat{\phi}_{i1}, \hat{\phi}_{r2}, \hat{\phi}_{i2}, \dots, \hat{\phi}_{rp}, \hat{\phi}_{ip}] = \hat{\Phi} \quad (9)$$

A matrix inversion is required in the computation of the gain matrix  $G$ . However, if the number of eigenvalues to be assigned,  $p$ , is less than the number assignable,  $n$ , Eq. (9) becomes underdetermined which leads naturally to a minimum gain solution. In order to assure that the above matrix is well conditioned for inversion, the condition number of the matrix,  $\Phi$ , should be the smallest possible. Interestingly, the above numerical requirement for well conditioning of the matrix inversion problem corresponds exactly to the eigenvalue conditioning problem since  $\Phi$  consists of eigenvectors. In general, the set of eigenvectors in the matrix  $\Phi$  generated by some choice of  $c_K$  (see Eq. (6)),

$$[v_{or1}, v_{oi1}, \dots, v_{orp}, v_{oip}] \text{diag}[c_1, c_1, \dots, c_p, c_p] \\ \triangleq v_o c = \hat{\Phi} = [\phi_{r1}, \phi_{i1}, \dots, \phi_{rp}, \phi_{ip}], \quad (10)$$

will not be perfectly conditioned, i.e., orthogonal.

## 2.2 Optimal Eigenvalue Conditioning

From Eq. (10), the achievable (or admissible) eigenvectors corresponding to a set of eigenvalues can be re-written as

$$\tilde{v}_{ok} c_k = \tilde{q}_k \quad ; \quad k=1, \dots, p \quad (11)$$

where  $\tilde{v}_{ok} \triangleq \begin{bmatrix} v_{ork} \\ v_{oik} \end{bmatrix}$ ,  $\tilde{q}_k \triangleq \begin{bmatrix} q_{rk} \\ q_{ik} \end{bmatrix}$  and  $c_k$  is a coefficient vector of dimension

$$v_k = 4n + 2m - \text{rank}(\Gamma_k) \quad (12)$$

Except for a small class of degenerate cases,  $\Gamma_k$  will usually be a full rank matrix so that the following relation holds:

$$v_k = 2m \leq 4n \quad (13)$$

It is clear then that Eq. (11) represents a set of overdetermined equations. Thus eigenvectors cannot be arbitrarily assigned due to the insufficient number of independent control inputs. The number of control inputs consequently affects the degree of orthogonality or robustness achievable for the closed-loop system. The matrix  $\Phi$  must therefore be constructed with some choices of  $c_k$  such that  $\Phi$  is the best least-square approximation to a perfectly conditioned matrix.

Based on the above observations, suppose that a unitary matrix  $Q$  where

$$Q = [q_{r1}, q_{i1}, \dots, q_{rp}, q_{ip}]$$

is given. The weighted sum error in the approximation of the unitary matrix by the achievable closed-loop eigenvector matrix is

$$J(Q, c_k) = \sum_{k=1}^p |\tilde{q}_k - \tilde{v}_{ok} c_k|_F^2 w_k; \quad \tilde{q}_k = [q_{rk}, q_{ik}] \quad (14)$$

where  $w_k$  represents the weighting factor associated with the error in approximating the  $k$ -th desired vector  $\tilde{q}_k$ . Assuming that  $Q$  is fixed in Eq. (14), the least-squares solution for each mode which best approximates the unitary matrix  $Q$  yields

$$\begin{aligned} \hat{c}_k &= (\tilde{v}_{ok}^T \tilde{v}_{ok})^{-1} \tilde{v}_{ok}^T \tilde{q}_k; \quad k=1, \dots, p \\ &= [v_{ork}^T v_{ork} + v_{oik}^T v_{oik}]^{-1} [v_{ork}^T q_{rk} + v_{oik}^T q_{ik}] \end{aligned} \quad (15)$$

To explore the possibility of improving the degree of orthogonality further, substitute Eq. (15) into Eq. (14) to obtain the following problem:

$$\text{Minimize } J(Q) \quad (16)$$

$$\text{Subject to } Q^T Q = I$$

where

$$J(Q) = \sum_{k=1}^p |[I - \tilde{v}_{ok} (\tilde{v}_{ok}^T \tilde{v}_{ok})^{-1} \tilde{v}_{ok}^T] \tilde{q}_k|_F^2 w_k$$

Equation (16) shows that the error cost function depends on the apriori chosen unitary matrix  $Q$ . There must exist an optimal unitary matrix which minimizes this

error. There are several ways to solve this equation numerically. However, a closed form, perhaps approximate, solution is currently being sought.

In order to obtain a reasonably good solution, the unitary matrix closest to the open-loop eigenvector matrix is proposed, as the desired set. Denoting the open-loop eigenvector matrix by  $\Psi_0$ , the unitary matrix,  $Q$ , closest to the matrix

$\Psi_0$  can be defined as<sup>13</sup>

$$\text{Minimize } \|\Psi_0 - Q\|_F \quad (17)$$

$$\text{Subject to } Q^T Q = I.$$

The closest unitary matrix  $Q$  is then

$$Q = UV^T \quad (18)$$

where

$$\Psi_0 = U\Sigma V^T.$$

The reason for this particular choice is twofold. First, it is intuitively obvious that the control gains will be close to zero if the desired eigenvector is similar to the open-loop eigenvector when the desired eigenvalues are close to the open-loop eigenvalues. Secondly, the open-loop eigenvector may not be unitary, i.e. not perfectly conditioned, so that the closest unitary neighbor would encourage the selection of a well-conditioned achievable set.

### 2.3 Discussion

A comparison with results due to Kautsky, Nichols and Van Dooren<sup>12</sup> is made. They pose the same basic problem, namely, find an orthonormal set of vectors that minimizes (maximizes) some weighted measure of subspace angles between the orthogonal set and the corresponding achievable (complementary to achievable) space. They propose an iterative algorithm involving plane rotations, to preserve orthogonality of a starting set, until acceptable values for various measures of conditioning are achieved. The difference between the method in Ref. 12 and the method presented in this paper is in the definition of the cost function for measuring nearness to orthogonality and the order of computations.

The choice of open-loop eigenvector and its closest unitary matrix, as proposed, is believed to be suitable for the purpose of generating well-conditioned eigensystem with small control gains. The implication is that the element of iterative search (as suggested in Ref. 12) for the "optimal" unitary (or orthogonal) matrix appears unnecessary in practice for many test problems as indicated in Ref. 16.

## 3. DIRECT OUTPUT FEEDBACK FORMULATION

It is generally agreed that full states are not usually available in practice without estimators or observers. In this section, the previous derivations for

state feedback are generalized to design output feedback. The main characteristics of output feedback is its simplicity in generating control commands directly by a linear combination of the available outputs.

The eigenvalue problem can be written as

$$[A + BGH]\Psi_k = \Psi_k \Lambda_k; \quad k = 1, \dots, p \quad (19)$$

where  $A$ ,  $B$ ,  $\Psi_k$ , and  $\Lambda_k$  are as previously defined in Eq. (1). Matrices  $G$  and  $H$  represent the output feedback gain and the measurement matrices of dimensions  $m \times \gamma$  and  $\gamma \times 2n$  respectively. The corresponding eigenvalue equations in real form are

$$\Gamma_k \Phi_k = 0$$

where

$$\Phi_k = \begin{bmatrix} \Psi_{rk} \\ \Psi_{ik} \\ GH \Psi_{rk} \\ GH \Psi_{ik} \end{bmatrix}$$

and  $\Gamma_k$  is defined in Eq. (4). Since the  $\Gamma_k$  matrices are identical to the case for full state feedback, the corresponding admissible eigenvector spaces are identical. However, the procedures for computing the gain matrices differ. Note that the number of pairs of conjugate eigenvalues,  $p$ , that can be placed using output feedback is limited as shown in Ref. 4 by

$$2p \leq \max(m, \gamma) \quad (20)$$

The equation for computing the output feedback gain matrix for placing  $p$  pairs of conjugate modes can be written as

$$GH[\Phi_{r1}, \Phi_{i1}, \dots, \Phi_{rp}, \Phi_{ip}] = [\hat{\Phi}_{r1}, \hat{\Phi}_{i1}, \dots, \hat{\Phi}_{rp}, \hat{\Phi}_{ip}]$$

or

$$GH\Phi = \hat{\Phi} \quad (21)$$

From Eq. (21), observe that the uniqueness of gain matrix depends on the number of conjugate pairs of eigenvalues to be placed, i.e.,

$$2p < \gamma \quad \text{underdetermined} \quad (22a)$$

$$2p = \gamma \quad \text{unique} \quad (22b)$$

$$2p > \gamma \quad \text{overdetermined} \quad (22c)$$

The previous conditions assume that the eigenvectors selected,  $\Phi$ , are completely observable. Equation (22a) is the most practical case where the number of eigenvalue pairs to be placed is expected to be less than the number of independent measurements. The least-squares, minimum norm solution or the unique inverse solution can be expressed in terms of the Moore-Penrose pseudo-inverse<sup>13</sup>,

$$G = \hat{\Phi}(H\Phi)^+ \quad (23)$$

where

$$(H\Phi)^+ = V \Sigma^+ U^T$$

$$H\Phi = [U_0 | U_0] \begin{bmatrix} \sigma_1 & & & \\ & . & & 0 \\ & & \sigma_k & \\ 0 & & & 0 \end{bmatrix} \begin{bmatrix} |v_\sigma^T| \\ |v_0^T| \end{bmatrix}$$

$$\Sigma_0^+ = \text{diag } (1/\sigma_1, \dots, 1/\sigma_k)$$

The use of SVD provides reliable numerical results for the Moore-Penrose pseudo-inverse in Eq. (23)<sup>14</sup>. For the typical underdetermined case, Eq. (23) represents the minimum gain solution, which is highly desirable in practice. Indeed, the motivation for the work reported herein is to develop reliable algorithms for designing well-conditioned controllers with minimum gains.

Finally, for the case where the number of actuators exceeds the number of measurements (which is uncommon in practice), the same analysis as described previously leads to similar equations by simply taking the transpose of Eq. (19) and it will not be elaborated.

#### 4. MAXIMUM PROJECTION CORRELATION CRITERION

The freedom in selecting a particular unitary matrix to generate a corresponding set of admissible eigenvectors is further investigated in this section. In addition to robustness in the eigenvalue conditioning sense, physical limitations on controller magnitudes suggest, if possible, a minimum feedback gain configuration.

For a given set of orthogonal column vectors, the resulting condition number and the norm of gain matrix depend on the choice of the vector to be used for each mode. For problems with closely spaced modes, as is common in flexible space structures<sup>15</sup>, the correlation between open-loop modes and subspaces of admissible eigenvectors may not be obvious. This is also evident for unitary matrices which do not have direct physical meaning. The approach taken here to resolve the above correlation problem is to search for the mode with the maximum orthogonal projection among the given set of desired eigenvectors into each admissible eigenvector subspace. Let

$$\rho_{rj}^k = H V_{ork} V_{ork}^T q_{rj}, \quad \rho_{ij}^k = H V_{oik} V_{oik}^T q_{ij}$$

and  $Q \triangleq [q_{r1}, q_{i1}, \dots, q_{rn}, q_{in}]$ . Now compute

$$\rho_f(k) = \text{Maximum}_j |\rho_{rj}^k| + |\rho_{ij}^k|;$$

for  $j=1, \dots, n$ ,  $j \neq f(\gamma)$  and  $\gamma=1, \dots, k-1$

(24)

The integer  $f(k)$  ( $k=1, \dots, p$ ) is the desired eigenvector number having the maximum projection onto  $k$ -th subspace of admissible eigenvectors and  $\rho_f(k)$  represents the maximum projection sum of real and imaginary components. The observability plays

an important role in determining the correlation of desired eigenvectors with the subspaces of admissible closed-loop eigenvectors. Maximum projection is meaningless if the eigenvector is unobservable!

## 5. NUMERICAL EXAMPLES

### Example 1: Full state feedback

To demonstrate the method, consider a simple linear dynamical system consisting of three lumped mass-spring-dashpot, connected in series and fixed at one end (see Figure 1). The equation of motion can be written as

$$M\ddot{\xi} + C\dot{\xi} + K\xi = Du$$

$$u = Gx; \quad x^T = [\xi^T, \dot{\xi}^T]$$

The mass, damping, stiffness and force distribution matrices are respectively chosen as

$$M = \text{diag}(1, 1, 1)$$

$$C = \begin{bmatrix} c_1 + c_2 & -c_2 & 0 \\ \text{Sym} & c_2 + c_3 & -c_3 \\ & & c_3 \end{bmatrix}$$

$$K = \begin{bmatrix} 10 & -5 & 0 \\ \text{Sym} & 25 & -20 \\ & & 20 \end{bmatrix}$$

$$D = \begin{bmatrix} 1 & 0 \\ 0 & 0 \\ 0 & 1 \end{bmatrix}$$

The above matrices represent a system with two actuators located at degrees of freedom one and three.

### Example 1.1: Full state feedback with no damping

The undamped system has  $c_1=c_2=c_3=0$ . The frequency and damping ratios are given in Table 1 as follows,

Table 1 Frequency and Damping Ratio for the Mass-Spring Example

Mode #	OPEN-LOOP		CLOSED-LOOP	
	$\omega^o$	$\zeta^o$	$\omega$	$\zeta$
1	1.0344	0	1.0482	.5765
2	3.2934	0	3.2891	.2959
3	6.5638	0	6.4857	.0651



where the eigenvalue,  $\lambda_i = -\zeta_i \omega_i \pm j \omega_i (1-\zeta_i^2)^{1/2}$ . The condition number of the corresponding undamped open-loop modal matrix is unity since the eigenvectors are orthogonal. The norm of gains and condition numbers corresponding to four sets of desired eigenvectors are as follows,

Table 2 Condition Number and Norm of Gain

Case	Q	Maximum Projection Correlation	$\ G\ _F$	$c_2(\Psi)$
1	I	No	38.23	11.24
2	I	Yes	21.81	9.05
3	$\Psi_0$	No	2.85	3.17
4	$\Psi_0$	Yes	2.85	3.17
5	(Direct Velocity Feedback)		2.82	6.96

Case 5 in Table 2 represents the directly collocated velocity feedback configuration of the form

$$u_1 = -2 \dot{x}_1 \text{ and } u_3 = -2 \dot{x}_3$$

From Table 2, it is seen that the use of open-loop eigenvectors as desired closed-loop eigenvectors gives the smallest condition numbers and small gains. The correlation of a desired set of eigenvectors with respect to the assignable eigenvector subspaces improved the gain norm and condition number for the identity matrix. However, for the open-loop eigenvector case, the average correlation using eigenvalue magnitudes is sufficiently good (.9488 out of a perfect correlation of 1) such that the eigenvector correlation is not needed.

The gain matrices for cases 3 and 4 are as follows,

$$G = \begin{bmatrix} -.0057 & -.1199 & .1124 & -1.8815 & .1687 & .0299 \\ -.1985 & .1200 & -.0126 & .1340 & -.1001 & -2.1185 \end{bmatrix}$$

The above gain matrix is close to the "physically robust" directly collocated velocity feedback configuration as mentioned earlier. It is interesting to note that the open-loop eigenvector case gives more robust (in the eigenvalue conditioning sense) closed-loop configuration than the collocated velocity feedback configuration for this example. Of course, the eigenvalue/eigenvector assignment algorithm is an "inverse" design algorithm while the direct velocity feedback case is obtained by a "forward" design process where eigenvalues cannot be assigned conveniently.

#### Example 1.2: Full state feedback with damping

The damping coefficient used were  $c_1=2$ ,  $c_2=.5$ , and  $c_3=2$ . The frequency and damping ratios are given in Table 3. It is seen that the open-loop eigenvalues and closed-loop eigenvalues are not well correlated.

**Table 3** Frequency and Damping Ratio for the Mass-Spring-Dashpot Example

OPEN-LOOP			CLOSED-LOOP	
Mode #	$\omega^0$	$\zeta^0$	$\omega$	$\zeta$
1	1.0481	.1442	3.1622	.3162
2	3.2517	.3647	3.8078	.3939
3	6.5606	.3296	4.4384	.3830

The condition number of the open-loop modal matrix is 6.5249 and not unity since the eigenvectors are not orthogonal. The norm of gains and condition numbers corresponding to various sets of desired eigenvectors are shown in Table 4.

**Table 4** Condition Number and Norm of Gain

Case	Q	Maximum Projection Correlation	$\ G\ _F$	$c_2(\Psi)$
1	I	No	29.76	28.72
2	I	Yes	27.62	22.97
3	$\Psi_0$	No	26.96	26.20
4	$\Psi_0$	Yes	26.77	22.41
5	$UV^T$	No	26.88	23.11
6	$UV^T$	Yes	26.81	21.72

From the norm of gain matrices, it is seen that the choice of closed-loop eigenvectors closest to identity matrix (case 1) requires a large control effort with the worst conditioning. With projection correlation, the gains and condition number are improved (case 2). The use of open-loop eigenvectors as desired closed-loop eigenvectors without (case 3) and with (case 4) projection correlation gives improved results over the case of identity matrices. With the use of the closest unitary matrix to the open-loop eigenvector matrix (cases 5 and 6), a slight further improvement results. The closest unitary matrix, as expected, gives smaller condition number than the corresponding non-orthogonal open-loop eigenvector matrix.

Although no theoretical basis exists at present, numerical results reported in Ref. 16 showed that, among a large set of test unitary matrices generated at random, the case closest to the open-loop eigenvector matrix produced norm of gain matrix and condition number close to the optimum values of this set. Further work is needed to find the global optimum non-iteratively if possible for Eq. (16).

## Example 2: Direct Output Feedback

The system investigated is a reduced order finite element model of the MAST truss beam structure as shown in Figure 2 (see Refs. 17 and 18 for detailed description). The model includes the deployer retractor assembly, Shuttle inertia properties, and rigid platforms for sensors and actuators allocation. There are three secondary actuator locations distributed along the beam and one primary at the tip. Each of the secondary actuator stations contains two actuators acting in the same plane. The primary station has four actuators to impart torques as well as in-plane forces. Also included are displacement and velocity sensors collocated with the actuators for a total of 20 measurements.

The reduced order model consists of 92 first order equations and it includes actuator/sensor dynamics and six rigid body degrees of freedom in addition to elastic deformation. A total of ten actuators using twenty output measurements (out of which 19 was found to be linearly independent) are used to increase the damping ratio of a selected set of elastic modes to 5%. Although nineteen eigenvalues are assignable, only nine pairs of complex eigenvalues (corresponding to elastic modes) are assigned. The corresponding frequencies and damping values are shown in Table 5:

Table 5 Frequency and Damping Ratio for MAST Structure

Mode #	OPEN-LOOP		CLOSED-LOOP	
	$\omega^0$ (Hz)	$\zeta^0$	$\omega$ (Hz)	$\zeta$
1	.1833	.0044	.1833	.0500
2	.2411	.0049	.2411	.0500
3	1.3308	.0232	1.3308	.0500
4	1.3876	.0223	1.3876	.0500
5	1.5541	.0211	1.5541	.0500
6	3.7919	.0063	3.7919	.0500
7	3.9698	.0061	3.9698	.0500
8	5.3483	.0051	5.3483	.0500
9	6.6509	.0054	6.6509	.0500

Since not all eigenvalues can be assigned, due to the limitation of the number of measurements or the actuator, the remaining eigenvalues are not guaranteed to remain stable. For this example, two residual modes became unstable. Further research is needed to alleviate the stability problem for direct output feedback.

## 6. Concluding Remarks

In this paper, a novel algorithm using real arithmetic is presented for eigenvalue placement using Singular Value Decomposition (SVD) for state or output feedback. By using the orthogonal basis generated by SVD, to span the subspace of eigenvectors satisfying desired eigenvalue, the optimal set of eigenvectors can be

written down easily provided the optimum unitary matrix is known apriori. For cases where the number of eigenvalues to be assigned is less than the order of the system, low eigenvalue sensitivity and small control gains can be obtained by carefully selecting the desired eigenvector set via the orthogonal projection correlation criteria. Numerical examples provide some indication of the simplicity and usefulness of the approach and in particular, the advantage of using the open-loop eigenvector matrix or its closest unitary matrix as the desired eigenvector matrix. However, it is clear that the results outlined here is by no means complete and in particular, further work is needed to address the stability problem related to the unassigned eigenvalues for the direct output feedback.

#### Acknowledgments

The authors would like to thank Mr. Lucas G. Horta of NASA Langley Research Center for providing the MAST example problem. The comparisons in example 1.1 has been suggested by Professor B. Wie of the University of Texas at Austin and is appreciated.

#### References

- <sup>1</sup>Wonham, W.M., "On Pole Assignment in Multiinput, Controllable Linear Systems," IEEE Transactions on AC, Vol. AC-12, 1967, pp. 660-665.
- <sup>2</sup>Moore, B.C., "On the Flexibility Offered by State Feedback in Multivariable Systems Beyond Closed-Loop Eigenvalue Assignments," IEEE Transactions on AC, Vol. AC-21, 1976, pp.689-692.
- <sup>3</sup>Klien, G. and Moore, B.C., "Eigenvalue-Generalized Eigenvector Assignment with State Feedback," IEEE Transactions on AC, Vol. AC-22, 1977, pp. 140-141.
- <sup>4</sup>Srinathkumar, S., "Eigenvalue/Eigenvector Assignment Using Output Feedback," IEEE Transactions on AC, Vol. AC-23, No. 1, 1978, pp. 79-81.
- <sup>5</sup>Porter, B. and D'Azzo, J.J., "Algorithm for Closed-Loop Eigenstructure Assignment by State Feedback in Multivariable Linear Systems," International Journal of Control, 1978, Vol. 27, No. 6, pp.943-947.
- <sup>6</sup>Lim, K.B., "A Unified Approach to Structure and Controller Design Optimizations," Ph.D Dissertation, Virginia Polytechnic Institute & State University, Blacksburg, VA, August 1986.
- <sup>7</sup>Raman, K.V., "Modal Insensitivity with Optimality," Ph.D Dissertation, Drexel University, Philadelphia, PA, June 1984.
- <sup>8</sup>Howze, J.W. and Cavin, R.K. III, "Regulator Design with Modal Insensitivity," IEEE Transactions on AC, Vol. AC-24, No. 3, June 1979, pp. 466-469.
- <sup>9</sup>Bhattacharyya, S.P. and DeSouza, E., "Pole Assignment via Sylvester's Equations," Systems and Controls Letters, Vol. 1, No. 4, 1982, pp. 261-263.

- <sup>10</sup>Cavin, R.K. III and Bhattacharyya, S.P., "Robust and Well-Conditioned Eigenstructure Assignment via Sylvester's Equations," Optimal Control Applications and Methods, Vol. 4, 1983, pp. 205-212.
- <sup>11</sup>Horta, L.G., Juang, J-N., and Junkins, J.L., "A Sequential Linear Optimization Approach for Controller Design," Journal of Guidance, Control and Dynamics, Vol. 9, No. 6, Nov-Dec 1986, pp.699-703.
- <sup>12</sup>Kautsky, J., Nichols, N.K. and Van Dooren, P., "Robust Pole Assignment in Linear State Feedback," International Journal of Control, 1985, Vol. 41, No. 5, pp. 1129-1155.
- <sup>13</sup>Golub, G.H. and Van Loan, C.F., Matrix Computations, John Hopkins University Press, Baltimore, MD, 1983.
- <sup>14</sup>Klema, V.C. and Laub, A.J., "The Singular Value Decomposition: Its Computation and Some Applications," IEEE Transactions on AC, Vol. AC-25, No. 2, April 1980, pp. 164-176.
- <sup>15</sup>Juang, J-N, and Pappa, R.S., "An Eigensystem Realization Algorithm for Modal Parameter Identification and Modal Reduction," Journal of Guidance, Control and Dynamics, Vol. 8, No. 5, September-October, 1985, pp. 620-627.
- <sup>16</sup>Lim, K.B., Kim, Z-C., and Juang, J-N., "Normality Measure as a Conditioning Index in Robust Eigensystem Assignment," NASA TM-89095, June, 1987.
- <sup>17</sup>Horta, L.G., et.al., "Analysis and Simulation of the MAST (COFS-I Flight Hardware)," First NASA/DOD CSI Technology Conference, Norfolk, VA, November 18-21, 1986, pp. 515-532.
- <sup>18</sup>Talcott, R. C., and Shipley, J. W., "Description of the Mast Flight System," First NASA/DOD CSI Technology Conference, Norfolk, VA, November 18-21, 1986, pp.253-263.

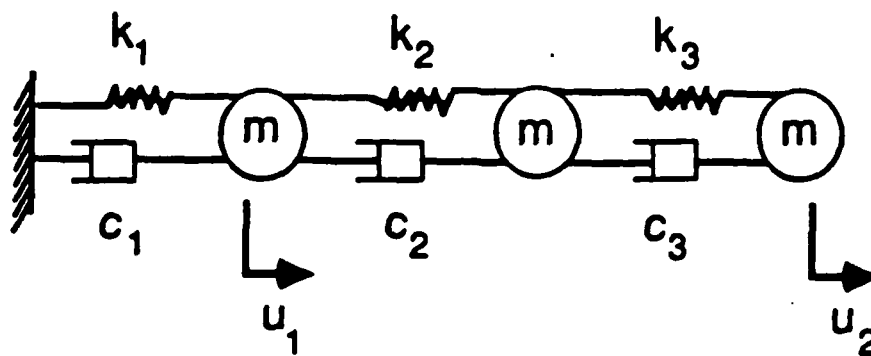


Fig. 1 Three-Spring-dashpot System



Fig. 2 The Mast truss beam structure

## **ATTACHMENT 6**

# **Re-Examination of Eigenvector Derivatives**

# **Re-examination of Eigenvector Derivatives**

**K.B. Lim, J.L. Junkins, B.P. Wang**

Reprinted from



## **Journal of Guidance, Control, and Dynamics**

Volume 10, Number 6, November-December 1987, Pages 581-587  
AMERICAN INSTITUTE OF AERONAUTICS AND ASTRONAUTICS, INC.  
370 L'ENFANT PROMENADE, SW • WASHINGTON, DC 20024



# Re-examination of Eigenvector Derivatives

K. B. Lim\* and J. L. Junkins†

Texas A & M University, College Station, Texas

and

B. P. Wang‡

University of Texas, Arlington, Texas

Copy available to DTIC does not  
permit fully legible reproduction

Analytical expressions for eigenvector derivatives for general non-self-adjoint systems using a modal expansion approach have not been correctly derived in several papers and books that address this problem. A common mistake in several developments on deriving eigenvector derivatives (or its perturbation forms) has been to ignore the eigenvector in question, in the expansion of its derivative, although the remaining eigenvectors forming the basis are generally non-orthogonal. This assumption is based upon explicit or implicit heuristic arguments that only directional changes contribute to eigenvector sensitivity. It is shown in this paper that the above assumption and the resulting equations are incorrect, except for the classical and most commonly encountered case of a self-adjoint problem having orthogonal eigenvectors. For the non-self-adjoint case, certain basis coefficients in the eigenvector derivative expansion have not been resolved correctly in the literature. A careful re-examination of the eigenvalue problem reveals that the two independent sets of normalizations (required for uniquely specifying the right and left eigenvectors) can be used to uniquely determine the basis coefficients. The solution derived herein for the eigenvector derivatives is shown to have generally nonzero projections onto all eigenvectors. It is also shown that basis coefficients for left and right eigenvector derivatives are related by a simple expression. A numerical example is included to demonstrate the present formulation for eigenvector derivatives with respect to a scalar parameter. We also extend Nelson's algebraic approach (for self-adjoint eigenvalue problems) to the general non-self-adjoint problem and the modal truncation approach to approximate eigenvector derivatives for the non-self-adjoint case.

## Introduction

THE usefulness of modal sensitivities for analysis and design of engineering systems is well known. Some specific applications include identification of dynamical systems,<sup>1,2</sup> redesign of vibratory systems,<sup>3,4</sup> and design of control systems by pole placement.<sup>5-7</sup> In the above algorithms, eigenvalue and eigenvector derivatives with respect to design parameters are often required. We present here a brief literature survey on the development of derivative formulations using modal expansion or algebraic approaches. Wilkinson<sup>8</sup> and Meirovitch<sup>9</sup> present clear derivations of first-order perturbation equations for a general real matrix. Wittrick<sup>10</sup> derived the first derivatives of eigenvalues, while Fox and Kapoor<sup>11</sup> extended these results to include the first derivatives of eigenvectors for real symmetric systems. Although the first general expressions for eigenvalue and eigenvector derivatives for non-self-adjoint systems via modal expansion appears to be given by Plaut and Huseyin,<sup>12</sup> it is clear that the work by Rogers<sup>13</sup> precedes the former work. In particular, it appears that Rogers was the first to recognize the need for two sets of normalization conditions for nonsymmetric eigensystems; this truth has been largely ignored in subsequent work, leading to some confusion in the literature on eigenvector derivatives. In fairness to these authors,<sup>13,14</sup> their formulations are correct but incomplete. In essence, the present paper provides the

completion of their developments. Additionally, we present a new relationship between left and right eigenvector derivatives.

The above-mentioned methods all utilize the modal approach for computing eigenvector derivatives. For extremely large systems, these approaches may not be very desirable. During the last decade, several "algebraic" methods<sup>15,16</sup> have emerged for computing eigenvector derivatives; these require only the knowledge of the eigenvector being differentiated. However, these algebraic methods require the solution of auxiliary sets of linear equations that may be ill-conditioned, thus requiring careful attention from the user. An improved modal method<sup>17</sup> has also been developed for the self-adjoint generalized eigenproblem in structural dynamics. Several methods of computing eigenvector derivatives have also been reported recently by Sutters et al.<sup>18</sup> They conclude that the improved modal method<sup>17</sup> is competitive with Nelson's algebraic method<sup>15</sup> vis-a-vis efficiency for many applications. A recent paper by Adelman and Haftka<sup>19</sup> discusses additional literature on eigenvector derivatives.

## Numerical Example

We demonstrate here, using a (5 × 5) real matrix, the calculation of right and left eigenvector derivatives with respect to a single parameter. The randomly chosen matrix is

$$A(\rho) = \begin{bmatrix} 1.7 & 3.2 & 4. & 2. & -1. \\ 3.6 & 2 & (2+\rho) & -9 & .1 \\ 1.7 & 0 & -3.5 & 9.4 & 2.9 \\ -6 & 2. & 5. & 0 & -3 \\ 0 & -3.9 & 1.2 & -4.5 & 1.1 \end{bmatrix}$$

where  $\rho$  is the scalar parameter appearing linearly only in location (2,3) of matrix  $A$ . The nominal matrix was chosen as the above matrix  $A$  when  $\rho = 0$ . It follows that the partial derivative of  $A$  with respect to  $\rho$  is zero except at location (2,3) where it equals unity.

Received May 12, 1986; revision received Feb. 20, 1987. Copyright © 1987 by John L. Junkins. Published by the American Institute of Aeronautics and Astronautics, Inc. with permission.

\*Research Associate, Department of Aerospace Engineering (currently Engineering Specialist, PRC Kentron Inc., Hampton, VA). Member AIAA.

†TEES Chair Professor, Department of Aerospace Engineering, Fellow AIAA.

‡Associate Professor, Department of Mechanical Engineering, Member AIAA.

The nominal right and left eigenvalue problems of Eqs. (1) and (2) were solved and the eigenvectors normalized by Eqs. (12) and (13) to unity. By using the above normalized nominal eigenvectors, the right eigenvector derivatives were computed using Eqs. (16-18) and the left eigenvector derivatives using Eqs. (19), (20), and (22). Furthermore, the right and left eigenvector derivatives were computed for two cases, namely, "with" ( $\alpha_{ii} \neq 0, \gamma_{ii} \neq 0, i = 1, \dots, 5$ ) and "without" ( $\alpha_{ii} = 0, \gamma_{ii} = 0, i = 1, \dots, 5$ ) the diagonal terms in the eigenvector expansion equations (16) and (19).

To provide a basis for comparison, the above-computed eigenvector derivatives are compared to each other and to eigenvector derivatives computed using finite differences. The  $i$ th finite-difference eigenvector derivatives are computed as

$$\frac{\partial x_i}{\partial \rho}(\rho_0, \Delta \rho) \approx \frac{x_i(\rho) - x_i(\rho_0)}{\Delta \rho}$$

where  $\Delta \rho = \rho - \rho_0$ .

Since the accuracy of the above approximation depends on the choice of the finite step size  $\Delta \rho$ , a graph of normalized error ( $10^{-7}$  corresponds approximately to  $n$ -digit accuracy) incurred in eigenvector derivatives computed by finite differencing was plotted with respect to step size as shown in Fig. 1. It can be seen from the figure that the "optimum" step size for computing the finite-difference derivative is about  $\Delta \rho = 0.3 \times 10^{-5}$  and the finite-difference derivative and the derivative computed by the formula "with" diagonal terms correlate to within six decimal places. The finite-difference derivatives can be calculated to five or better digits for  $\Delta \rho$  in the interval  $10^{-7} < \Delta \rho < 10^{-4}$ . From the other experiments, depending upon the local behavior of the eigenvectors and machine word length, we can usually use this experimental approach to find a  $\Delta \rho$  range giving five-to-six digit confirmation of Eqs. (16-22). Of course, the importance of the analytical partial derivatives lies in the fact that we do not require the finite-

difference approximation and its associated numerical pitfalls and experimentation.

Table 1 shows the right and left eigenvector derivatives computed in three different ways, namely, "without" diagonal terms, "with" diagonal terms, and by finite difference with step size  $0.3 \times 10^{-5}$ . It can be concluded that the eigenvector derivatives computed using the formula "with" diagonal terms shows very accurate agreement (identical, to within small errors in the sixth digit) with the optimized finite-difference approximations. The errors between the finite-difference results and the "without" results are essentially the missing diagonal terms; these frequently occur in the second and third digits. Furthermore, neglecting the diagonal terms in the eigenvector derivative calculation often leads to serious errors, as is evident in Table 1. In summary, the first-order change in

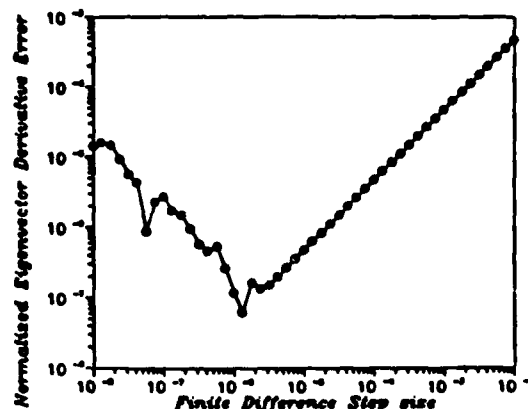


Fig. 1 Normalized error of finite-difference right eigenvector derivative for mode 1.

Table 1 Finite-difference eigenvector derivatives (step size =  $0.3 \times 10^{-5}$ )

With diagonal terms									
Right									
Re( $x_1$ )	Im( $x_1$ )	Re( $x_2$ )	Im( $x_2$ )	Re( $x_3$ )	Im( $x_3$ )	Re( $x_4$ )	Im( $x_4$ )	Re( $x_5$ )	Im( $x_5$ )
-0.0201	0.0000	0.0106	0.0000	-0.0221	0.0271	-0.0221	-0.0271	-0.0247	0.0000
0.0871	0.0000	-0.0206	0.0000	-0.0020	-0.0160	-0.0020	0.0160	0.0159	0.0000
0.0084	0.0000	0.0094	0.0000	-0.0002	0.0015	-0.0002	-0.0015	-0.0159	0.0000
-0.0184	0.0000	0.0042	0.0000	-0.0010	-0.0120	-0.0010	0.0120	-0.0075	0.0000
0.0255	0.0000	0.0039	0.0000	0.0102	0.0156	0.0102	-0.0156	-0.0051	0.0000
Left									
Re( $y_1$ )	Im( $y_1$ )	Re( $y_2$ )	Im( $y_2$ )	Re( $y_3$ )	Im( $y_3$ )	Re( $y_4$ )	Im( $y_4$ )	Re( $y_5$ )	Im( $y_5$ )
0.0072	0.0000	0.0020	0.0000	0.0089	0.2608	0.0089	-0.2608	0.0192	0.0000
0.0055	0.0000	0.0069	0.0000	-0.0028	-0.1874	-0.0028	0.1874	0.0042	0.0000
-0.0172	0.0000	-0.0639	0.0000	-0.0210	0.0142	-0.0210	-0.0142	0.0454	0.0000
0.0258	0.0000	-0.0539	0.0000	0.0534	0.0423	0.0534	-0.0423	0.0807	0.0000
0.0081	0.0000	-0.0238	0.0000	0.0153	0.1654	0.0153	-0.1654	0.0496	0.0000
Without diagonal terms									
Right									
Re( $x_1$ )	Im( $x_1$ )	Re( $x_2$ )	Im( $x_2$ )	Re( $x_3$ )	Im( $x_3$ )	Re( $x_4$ )	Im( $x_4$ )	Re( $x_5$ )	Im( $x_5$ )
-0.0143	0.0000	0.0015	0.0000	-0.0109	0.0144	-0.0109	-0.0144	-0.0434	0.0000
0.0907	0.0000	-0.0262	0.0000	-0.0527	-0.0221	-0.0527	0.0221	0.0010	0.0000
-0.0147	0.0000	0.0063	0.0000	0.0130	0.0043	0.0130	-0.0043	-0.0095	0.0000
-0.0067	0.0000	0.0006	0.0000	0.0191	0.0004	0.0191	-0.0004	-0.0056	0.0000
0.0341	0.0000	0.0102	0.0000	-0.0490	-0.0089	-0.0490	0.0089	0.0161	0.0000
Left									
Re( $y_1$ )	Im( $y_1$ )	Re( $y_2$ )	Im( $y_2$ )	Re( $y_3$ )	Im( $y_3$ )	Re( $y_4$ )	Im( $y_4$ )	Re( $y_5$ )	Im( $y_5$ )
0.0020	0.0000	0.0095	0.0000	0.0449	0.1439	0.0449	-0.1439	0.0121	0.0000
-0.0021	0.0000	0.0132	0.0000	0.0037	-0.0944	0.0037	0.0944	0.0129	0.0000
0.0031	0.0000	-0.0500	0.0000	-0.0162	0.0180	-0.0162	-0.0180	0.0138	0.0000
0.0000	0.0000	-0.0158	0.0000	0.0148	0.1128	0.0148	-0.1128	0.0363	0.0000
0.0016	0.0000	-0.0185	0.0000	0.0535	0.1205	0.0535	-0.1205	0.0205	0.0000

ANALYTICAL  
DERIVATIVE  
(Eqs 16-18)

AND

FINITE DIFFERENCE  
DERIVATIVE  
( $\Delta \rho = 0.3 \times 10^{-5}$ )

ANALYTICAL  
DERIVATIVE  
(Eqs 16-18)

WITH

$\alpha_{ii} = 0$

$\gamma_{ii} = 0$

an eigenvector has a nonzero projection onto the eigenvector, for non-self-adjoint systems.

The present paper is most concerned with the correction of an assumption made in several completed derivations of equations for the eigenvector derivatives (e.g., as found in Refs. 9, 10, and 20) and resolving an indeterminacy remaining in Ref. 13. A careful re-examination of the role played by the normalizations and biorthogonality conditions for a general non-self-adjoint eigenvalue problem leads to a unique generalization and correction of equations for eigenvector derivatives derived in the previous papers and books cited.

Additionally, Nelson's algebraic method<sup>15</sup> is extended for computing both the right and left eigenvector derivatives. Finally, the improved modal method<sup>17</sup> is extended to the general (non-self-adjoint) eigenvalue problem.

### The Eigenvalue Problem

We begin by reviewing familiar results for the non-self-adjoint eigenvalue problem. Let us write the right and left eigenvalue problems as

$$\text{Right: } Ax_j = \lambda_j x_j, \quad j = 1, \dots, n \quad (1)$$

$$\text{Left: } y_i^T A = \lambda_i y_i^T, \quad i = 1, \dots, n \quad (2)$$

where  $A$  is a nondefective  $n \times n$  real matrix,  $x_j$  and  $y_i$  the  $j$ th  $n \times 1$  complex-valued eigenvectors, and  $\lambda_j$  a generally complex eigenvalue of  $A$ .

Premultiplying Eq. (1) by  $y_i^T$  and postmultiplying Eq. (2) by  $x_j$ , we get

$$y_i^T A x_j = \lambda_j y_i^T x_j \quad (3)$$

$$y_i^T A x_j = \lambda_i y_i^T x_j \quad (4)$$

By subtracting Eq. (4) from Eq. (3), we get

$$0 = (\lambda_j - \lambda_i) y_i^T x_j \quad (5)$$

Restricting ourselves to the class of problems where the eigenvalues are distinct, Eq. (5) leads to the biorthogonality property

$$y_i^T x_j = 0, \quad i \neq j \quad (6)$$

For  $i = j$ , the left and right eigenvectors can be normalized such that

$$y_i^T x_i = s_i, \quad i = 1, \dots, n \quad (7)$$

where  $s_i$  represents chosen normalization constants, commonly set to unity. At this point, we note the fact that biorthogonality of Eq. (6) is a property of the eigensystem and is independent of whatever a priori normalizations (of  $x_j$  or  $y_i$ ) have been imposed, which are also arbitrary.

In matrix notation, Eqs. (4), (6), and (7) can be written as the pair of matrix equations

$$Y^T A X = S \Lambda \quad (8)$$

$$Y^T X = S \quad (9)$$

where  $S = \text{diag}(s_1, \dots, s_n)$ ,  $\Lambda = \text{diag}(\lambda_1, \dots, \lambda_n)$ , and  $X, Y$  are  $n \times n$  right and left modal matrices (containing  $x_j$  and  $y_i$ , respectively, as columns). Note that from Eq. (9), we could solve for  $X$  or  $Y$  since

$$Y = (X^{-1})^T S \quad (10)$$

$$X = (Y^{-1})^T S \quad (11)$$

From the above equations, it is apparent that after solving the right eigenvalue problem and imposing arbitrary normalizations on the columns  $x_j$  of  $X$ , we still need to choose  $S$  (i.e., the second set of  $n$  normalization constants) to solve for  $Y$  from Eq. (10) uniquely. [Incidentally, we note that Eq. (11) of Ref. 14, supposedly providing an expression for an incomplete set of left eigenvectors from a corresponding set of right eigenvectors, requires the inversion of a singular matrix! It is clear that the solution in Ref. 14, for the incomplete set case, is nonunique.] Similarly, if the left eigenvalue problem were solved instead, then  $X$  is computed from Eq. (11). In other words, the two sets of eigenvectors,  $X$  and  $Y$ , require two independent, arbitrary sets of normalizations for their unique representations. We stress here the fact that simply requiring that  $S = I$ , as is common practice, does not uniquely scale  $X$  and  $Y$  for non-self-adjoint systems. Henceforth, we let the two sets of normalizations be represented by

$$x_i^T x_i = f_i, \quad i = 1, \dots, n \quad (12)$$

$$y_i^T x_i = s_i, \quad i = 1, \dots, n \quad (13)$$

where  $f_i$  and  $s_i$ ,  $i = 1, \dots, n$ , are fixed normalization constants. We note above that Eq. (12) amounts to a generalization of the normalization approach of Ref. 14 where the element corresponding to a displacement coordinate with the largest modulus is set to unity.

### Eigenvalue Derivatives

For completeness, we rederive the eigenvalue derivatives with respect to a scalar parameter  $\rho$ . First, we take partial derivatives of Eq. (1) to get

$$\frac{\partial A}{\partial \rho} x_j + A \frac{\partial x_j}{\partial \rho} = \frac{\partial \lambda_j}{\partial \rho} x_j + \lambda_j \frac{\partial x_j}{\partial \rho} \quad (14)$$

We then premultiply the above equation by  $y_j^T$  to obtain

$$y_j^T \frac{\partial A}{\partial \rho} x_j + y_j^T (A - \lambda_j I) \frac{\partial x_j}{\partial \rho} = \frac{\partial \lambda_j}{\partial \rho} y_j^T x_j$$

so that by Eq. (2), the eigenvalue derivative expression takes the form

$$\frac{\partial \lambda_j}{\partial \rho} = \frac{1}{s_j} \left( y_j^T \frac{\partial A}{\partial \rho} x_j \right) \quad (15)$$

where  $s_j$  is the  $j$ th normalization constant chosen in Eq. (13).

### Eigenvector Derivatives

Here, we derive an expression for eigenvector derivatives along the lines of Ref. 13 by using  $(x_1, \dots, x_n)$  as basis vectors,

$$\frac{\partial x_i}{\partial \rho} = \sum_{j=1}^n a_{ij} x_j \quad (16)$$

Since the eigenvalues were assumed distinct, this always leads to a set of  $n$  eigenvectors that are linearly independent and that may be used as a set of basis vectors for spanning the complex  $n$ -dimensional space. To obtain expansion coefficients  $a_{ij}$ ,  $i, j = 1, \dots, n$ , we begin by substituting Eq. (16) into Eq. (14) and premultiply by  $y_i^T$  to get

$$y_i^T \frac{\partial A}{\partial \rho} x_i + \sum_{j=1}^n a_{ij} \lambda_j y_i^T x_j = \frac{\partial \lambda_i}{\partial \rho} y_i^T x_i + \lambda_i \sum_{j=1}^n a_{ij} y_i^T x_j$$

and by using biorthogonality conditions, we obtain

$$(\lambda_k - \lambda_i) a_{ik} y_i^T x_k = \frac{\partial \lambda_i}{\partial \rho} y_i^T x_k - y_i^T \frac{\partial A}{\partial \rho} x_k$$

Since  $A$  was assumed to have distinct eigenvalues, we can solve for  $a_{ik}$  as

$$a_{ik} = -\frac{1}{(\lambda_k - \lambda_i) s_k} \left( y_i^T \frac{\partial A}{\partial \rho} x_k \right), \quad k \neq i \quad (17)$$

We note that, for computational efficiency, the matrix-vector multiplication required in Eq. (15) could be stored for use in Eq. (17). For the case of  $i = k$ ,  $a_{ii}$  can be computed from the normalization condition of Eq. (12). By taking its partial derivatives and using Eq. (16), we find

$$\begin{aligned} \frac{\partial x_i^T}{\partial \rho} x_i &= 0 \\ a_{ii} x_i^T x_i + \sum_{j=1}^n a_{ij} x_j^T x_i &= 0 \end{aligned}$$

which leads to the expression

$$a_{ii} = -\frac{1}{f_i} \sum_{j=1}^n a_{ij} x_j^T x_i \quad (18)$$

where  $f_i$  is the  $i$ th normalization constant chosen in Eq. (12). It can be deduced from Eq. (18) that the diagonal terms  $a_{ii}$  become identically zero if: 1) matrix  $A$  has orthogonal eigenvectors (for example,  $A$  is real and symmetric) or 2) the  $i$ th eigenvector is insensitive with respect to a particular parameter except in the  $i$ th eigenvector direction. We also observe from Eqs. (17) and (18) that the off-diagonal and diagonal coefficients  $a_{ik}$  and  $a_{ii}$  depend on the normalization constants  $s_k$  and  $f_i$ , respectively.

To obtain left eigenvector derivatives, we similarly let

$$\frac{\partial y_i}{\partial \rho} = \sum_{j=1}^n \gamma_{ij} y_j \quad (19)$$

By taking partial derivatives of Eq. (2), substituting Eq. (19), and postmultiplying by  $x_k$ , we obtain

$$\sum_{j=1}^n \gamma_{ij} y_j^T A x_k + y_i^T \frac{\partial A}{\partial \rho} x_k = \frac{\partial \lambda_i}{\partial \rho} y_i^T x_k + \lambda_i \sum_{j=1}^n \gamma_{ij} y_j^T x_k$$

By using Eqs. (1) and (6), we get

$$\begin{aligned} \gamma_{ik} \lambda_k y_k^T x_k + y_i^T \frac{\partial A}{\partial \rho} x_k &= \frac{\partial \lambda_i}{\partial \rho} y_i^T x_k + \lambda_i \gamma_{ik} y_k^T x_k \\ (\lambda_k - \lambda_i) \gamma_{ik} y_k^T x_k &= \frac{\partial \lambda_i}{\partial \rho} y_i^T x_k - y_i^T \frac{\partial A}{\partial \rho} x_k \\ \gamma_{ik} &= -\frac{1}{(\lambda_k - \lambda_i) s_k} \left( y_i^T \frac{\partial A}{\partial \rho} x_k \right), \quad k \neq i \quad (20) \end{aligned}$$

By comparing Eqs. (17) and (20), we observe the antisymmetric property

$$\gamma_{ik} = -a_{ik}, \quad k \neq i \quad (21)$$

For  $k = i$ ,  $\gamma_{ii}$  and  $a_{ii}$  are related through the normalization relation of Eq. (13). Thus, by taking the partial derivative of

Eq. (13), we get

$$\frac{\partial y_i^T}{\partial \rho} x_i + y_i^T \frac{\partial x_i}{\partial \rho} = 0$$

and by using the expansions of Eqs. (16) and (19)

$$\begin{aligned} \sum_{j=1}^n \gamma_{ij} y_j^T x_i + y_i^T \sum_{j=1}^n a_{ij} x_j &= 0 \\ \gamma_{ii} y_i^T x_i + a_{ii} y_i^T x_i &= 0 \\ \gamma_{ii} &= -a_{ii} \quad (22) \end{aligned}$$

From Eqs. (21) and (22), we observe the nice relationship between the left and right eigenvector derivative expansion coefficients,

$$[\gamma] = -[a]^T \quad (23)$$

provided, of course, that the normalization constants  $s_k$  are chosen to have the same values. The significance of Eq. (23) is clear: the left and right eigenvector derivatives map into each other uniquely.

The above procedure can be extended to the generalized eigenvalue problem of the form

$$\begin{aligned} Ax_i &= \lambda_i Bx_i \\ A^T y_i &= \lambda_i B^T y_i, \quad i = 1, \dots, n \end{aligned}$$

with biorthogonality and normalizations

$$\begin{aligned} y_k^T Bx_i &= \delta_{ik}, \quad i, k = 1, \dots, n \\ x_i^T Bx_i &= 1, \quad i = 1, \dots, n \end{aligned}$$

After some algebra analogous to the above developments, it can be shown that the eigenvalue and eigenvector derivatives take the form

$$\begin{aligned} \frac{\partial \lambda_i}{\partial \rho} &= y_i^T \left( \frac{\partial A}{\partial \rho} - \lambda_i \frac{\partial B}{\partial \rho} \right) x_i \\ \frac{\partial x_i}{\partial \rho} &= \sum_{k=1}^n a_{ik} x_k, \quad \frac{\partial y_i}{\partial \rho} = \sum_{k=1}^n \gamma_{ik} y_k \end{aligned}$$

where

$$\begin{aligned} a_{ik} &= \frac{y_i^T \left( \frac{\partial A}{\partial \rho} - \frac{\partial \lambda_i}{\partial \rho} B - \lambda_i \frac{\partial B}{\partial \rho} \right) x_k}{(\lambda_k - \lambda_i)}, \quad i \neq k \\ &= -\frac{1}{2} \left[ x_i \frac{\partial B}{\partial \rho} x_i + \sum_{j=1}^n a_{ij} x_j^T (B + B^T) x_i \right], \quad i = k \quad (24) \\ \gamma_{ik} &= \frac{y_i^T \left( \frac{\partial A}{\partial \rho} - \frac{\partial \lambda_i}{\partial \rho} B - \lambda_i \frac{\partial B}{\partial \rho} \right) x_k}{(\lambda_i - \lambda_k)}, \quad i \neq k \\ &= -y_i^T \frac{\partial B}{\partial \rho} x_k - a_{ii}, \quad i = k \quad (25) \end{aligned}$$

It is interesting to note that for the special case where  $A$  and  $B$  are real and symmetric, the eigenvector derivative coefficients reduce, as a consequence of orthogonality, to the forms originally derived in Ref. 12. Furthermore, if  $B$  is in addition constant (with respect to  $\rho$ 's variation)—for exam-

ple, the standard symmetric eigenvalue problem where  $B = I$ —then the diagonal coefficients vanish and this conforms to the standard symmetric case found in Refs. 9 and 10. However, if  $A$  is nonsymmetric, the eigenvectors are not generally orthogonal and the diagonal coefficients from Eqs. (24) and (25) are clearly nonzero, even when  $B$  is a constant. This crucial result directly contradicts the reasoning in Ref. 20 where the diagonal coefficients are noted to be "arbitrary" and hence the "most convenient" choice is zero, which is clearly in error! This result is also interesting in the context of a first-order eigenvector perturbation analysis since it implies that, in the modal expansion of a particular eigenvector, the contribution of the change in the eigenvector in the same direction cannot be assumed zero in general for non-self-adjoint problems, as done commonly, for example in Ref. 10, but subsequently corrected in Ref. 22.

### An Improved Modal Method

Equation (16) for eigenvector derivatives requires the knowledge of all  $n$  eigenvectors. For large systems, only the lowest  $L$  pairs of eigensolutions may be computed accurately, where  $L \ll n$ . In this case, an improved modal method, analogous to the modal truncation method reported in Ref. 17, can be derived, provided matrix  $[A]$  is nonsingular.

Rewrite Eq. (16) as

$$\frac{\partial x_i}{\partial \rho} = a_{ii} x_i + z_i \quad (26)$$

where

$$z_i = \sum_{j=1}^n a_{ij} x_j \quad (27)$$

Using Eq. (24), Eq. (27) can be written as

$$z_i = \sum_{j=1}^n \frac{y_j^T F_i}{\lambda_i - \lambda_j} x_j$$

or

$$z_i = \sum_{j=1}^L \frac{y_j^T F_i}{\lambda_i - \lambda_j} x_j + \sum_{j=L+1}^n \frac{y_j^T F_i}{\lambda_i - \lambda_j} x_j \quad (28)$$

where

$$F_i = \left( \frac{\partial A}{\partial \rho} - \frac{\partial \lambda_i}{\partial \rho} B - \lambda_i \frac{\partial B}{\partial \rho} \right) x_i \quad (29)$$

and we have assumed that  $i \leq L$ . If the eigenvalues are numbered according to their magnitude in ascending order, then for the class of problems with a large frequency gap is

$$\lambda_j - \lambda_i = \lambda_j \quad \text{for } j > L$$

It is clear that the above approximation is very accurate for  $j \gg L$ . Thus, Eq. (28) can be written, letting  $z_i$  be approximated by  $\bar{z}_i$ , as

$$\bar{z}_i = \sum_{j=1}^L \frac{y_j^T F_i}{\lambda_i - \lambda_j} x_j + \sum_{j=L+1}^n \frac{y_j^T F_i}{-\lambda_j} x_j \quad (30)$$

which can be rewritten as

$$\bar{z}_i = \sum_{j=1}^L \frac{y_j^T F_i}{\lambda_i - \lambda_j} x_j + \sum_{j=1}^L \frac{y_j^T F_i}{-\lambda_j} x_j - \sum_{j=1}^L \frac{y_j^T F_i}{-\lambda_j} x_j \quad (31)$$

The biorthogonality conditions can be written in matrix form as

$$[Y]^T [A] [X] = [A] \quad (32)$$

or

$$[X]^{-1} [A]^{-1} ([Y]^T)^{-1} = [A]^{-1}$$

Thus,

$$[A]^{-1} = [X] [A]^{-1} [Y]^T \quad (33)$$

or

$$[A]^{-1} = \sum_{j=1}^n \frac{x_j y_j^T}{\lambda_j} \quad (34)$$

Using the spectral decomposition of Eq. (34), the second summation on the right-hand side of Eq. (31) becomes  $-A^{-1} F_i$ , and Eq. (31) can be written as

$$\bar{z}_i = \sum_{j=1}^L \frac{y_j^T F_i}{\lambda_i - \lambda_j} x_j - A^{-1} F_i + \sum_{j=1}^L \frac{y_j^T F_i}{\lambda_j} x_j \quad (35)$$

We note that the  $A^{-1} F_i$  term in Eq. (35) approximates the effect of higher-order modal components on eigenvector derivatives of lower-order modes. Presumably, for many cases, this approximation is more accurate than an initial expansion involving only the first  $L$  modes. Now the modal representation of eigenvector derivative can be approximated as

$$\frac{\partial x_i}{\partial \rho} = \bar{a}_{ii} x_i + \bar{z}_i \quad (36)$$

where  $\bar{a}_{ii}$  can be computed by requiring

$$\frac{\partial}{\partial \rho} (x_i^T B x_i) = 0$$

which leads to

$$\bar{a}_{ii} = -\frac{1}{2} \left( x_i^T \frac{\partial B}{\partial \rho} x_i + x_i^T B \bar{z}_i + \bar{z}_i^T B x_i \right) \quad (37)$$

For the class of problems that satisfy the previously mentioned frequency conditions, the modal approximation of Eq. (36) may represent a significant improvement over Eq. (16), vis-a-vis computation, and often provides acceptable precision. For problems without well-separated eigenvalues, similar approximations can be developed with the summation of Eq. (16) truncated after a few terms.

For self-adjoint eigenvalue problems in structural dynamics, this improved modal approximation approach has been demonstrated to be efficient and accurate.<sup>18</sup> Similarly, the derivatives of the left eigenvectors can be computed using the following improved modal approximation:

$$\frac{\partial y_i}{\partial \rho} = \bar{y}_{ii} y_i + \bar{w}_i \quad (38)$$

where

$$\bar{w}_i = \sum_{j=1}^L \gamma_{ij} y_j - A^{-1} G_i + \sum_{j=L+1}^n \frac{G_i^T x_j}{\lambda_j} y_j \quad (39)$$

$$G^T = y^T \left( \frac{\partial A}{\partial p} - \frac{\partial \lambda}{\partial p} B - \lambda \frac{\partial B}{\partial p} \right) \quad (40)$$

$$\bar{z}_r = -y^T \frac{\partial B}{\partial p} x - \bar{z}_r - \bar{v}_r^T Bx - y^T B \bar{v}_r \quad (41)$$

and  $\gamma_r$  is given by Eq. (25).

### Algebraic Method for Computing Eigenvector Derivatives

Nelson<sup>15</sup> has proposed an algebraic method for computing eigenvector derivatives. In this formulation, the only information needed is the eigenvector being differentiated. Following the approach used in Ref. 15, we summarize equations for computing  $\partial \lambda / \partial p$  and  $\partial y / \partial p$ .

Right eigenvector:

$$\frac{\partial x_r}{\partial p} = a_r x_r + V_r \quad (42)$$

where  $V_r$  is the solution of

$$\bar{Z} V_r = -\bar{F}_r \quad (43)$$

and where  $\bar{Z}$  is matrix  $Z$  with the  $r$ th column and  $r$ th row replaced by  $e_r$  and  $e_r^T$ , respectively;  $e_r$  is a vector containing one in element  $r$  and zeroes elsewhere,  $Z = A - \lambda_r B$ ,  $\bar{F}_r$  is vector  $F_r$  with the  $r$ th row replaced by 0,  $F_r$  is given by Eq. (29), and

$$a_r = -\frac{1}{2} \left( x_r^T \frac{\partial B}{\partial p} x_r + V_r^T B x_r + x_r^T B V_r \right) \quad (44)$$

Left eigenvector:

$$\frac{\partial y_r}{\partial p} = \gamma_r y_r + V_r \quad (45)$$

where  $V_r$  is the solution of

$$\bar{Z}^T V_r = -\bar{G}_r \quad (46)$$

$\bar{Z}^T$  = matrix  $Z^T$  with  $r$ th column and  $r$ th row replaced by  $e_r$  and  $e_r^T$ , respectively;  $\bar{G}_r = (\partial / \partial p)(Z^T y_r)$ ,  $\bar{G}_r$  is vector  $G_r$  with the  $r$ th row replaced by a row of zeros, and

$$\gamma_r = -y_r^T \frac{\partial B}{\partial p} x_r - a_r - V_r^T B x_r - y_r^T B V_r \quad (47)$$

In the above formulation, the value  $r$  is chosen to correspond to the maximum component of  $x_r$  (or  $y_r$ ) in order to achieve computational robustness.

Using the above formulations, the eigenvector derivatives can be computed using only the eigenvector of interest together with some algebraic manipulations. The success of this method hinges on the existence of a well-conditioned nonsingular  $\bar{Z}$ . A more general algebraic method, which eliminates this restriction, has been reported by Chen and Wei.<sup>16</sup> Their formulation is based upon the matrix decomposition and generalized inverse techniques.

The present approach can be extended to the case of repeated eigenvalues. This has already been done for self-adjoint systems by Ojalvo.<sup>21</sup> In the next section, we present a numerical example to demonstrate the errors incurred in neglecting the diagonal terms in the evaluation of eigenvector derivatives via modal expansion for a non-self-adjoint problem.

### Conclusions

We have highlighted the need for two independent sets of normalizations to uniquely define the right and left eigenvector sets. This is crucial in the complete formulation of eigenvector derivatives via modal expansion. In addition, a concise equation relating left and right eigenvector derivative expansion coefficients is given. We have also demonstrated beyond any doubt that the first-order change in an eigenvector has a generally nonzero projection onto the eigenvector, for non-self-adjoint systems.

For many non-self-adjoint systems (encountered commonly, for example, in linear control theory), the matrices are fully populated. The consequence is that algebraic methods that take advantage of the bandedness patterns of the matrices become less attractive than modal expansion methods, where solutions of auxiliary linear equations are not needed other than solution of the eigenvalue problem itself. Additionally, since no auxiliary linear equations need to be solved, the associated possibility of rank deficiency is avoided. On the other hand, the theoretical problem of requiring "all" eigenvectors in modal expansion methods may turn out in many applications not to pose a practical difficulty.

These latter issues cannot be resolved completely on the basis of analytical arguments. Their resolution requires numerical analysis in the context of particular applications.

### References

- Collins, J.D. et al., "Statistical Identification of Structures," *AIAA Journal*, Vol. 12, Feb. 1972, pp. 185-190.
- Berman, A. and Flannelly, W.G., "Theory of Incomplete Models of Dynamic Structures," *AIAA Journal*, Vol. 9, Aug. 1971, pp. 1461-1467.
- Haftka, R.T. et al., "Sensitivity of Optimized Control Systems to Minor Structural Modifications," *AIAA Paper 85-0807*, April 1985.
- Lim, K.B. and Junkins, J.L., "Optimal Redesign of Dynamic Structures via Sequential Linear Programming," *Proceedings of 4th International Modal Analysis Conference*, Union College, New York, Feb. 1986, pp. 1615-1620.
- Chou, Y.-F. and Chen, J.-S., "Structural Dynamics Modification via Sensitivity Analysis," *Proceedings of 3rd International Modal Analysis Conference*, Union College, New York, Jan. 1985, pp. 483-489.
- Bodden, D.S. and Junkins, J.L., "Eigenvalue Optimization Algorithms for Structural/Control Design Iterations," Paper presented at American Control Conference, San Diego, CA, June 1984.
- Junkins, J.L., Bodden, D.S., and Turner, J.D., "A Unified Approach to Structure and Control System Design Iterations," Paper presented at Fourth International Conference on Applied Numerical Modelling, Tainan, Taiwan, Dec. 1984.
- Lim, K.B. and Junkins, J.L., "Minimum Sensitivity Eigenvalue Placement Using Sequential Linear Programming," *Proceedings of the Mountain Lake Dynamics & Control Institute*, edited by J.L. Junkins, Virginia Polytechnic Institute, Blacksburg, June 1985, pp. 122-144.
- Wilkinson, J.H., *The Algebraic Eigenvalue Problem*, Oxford University Press, Oxford, England, 1965, p. 68.
- Meirovitch, L., *Computational Methods in Structural Dynamics*, Sijthoff & Noordhoff, Groningen, The Netherlands, 1980, p. 102.
- Wittrick, W.H., "Rates of Change of Eigenvalues with Reference to Buckling and Vibration Problems," *Journal of the Royal Aeronautical Society*, Vol. 66, No. 621, Sept. 1962, pp. 590-591.
- Fox, R.L. and Kapoor, M.P., "Rates of Change of Eigenvalues and Eigenvectors," *AIAA Journal*, Vol. 6, Dec. 1968, pp. 2426-2429.
- Plaut, R.H. and Huseyin, K., "Derivatives of Eigenvalues and Eigenvectors in Non-Self-Adjoint Systems," *AIAA Journal*, Vol. 11, Feb. 1973, pp. 250-251.
- Rogers, L.C., "Derivatives of Eigenvalues and Eigenvectors," *AIAA Journal*, Vol. 8, May 1970, pp. 943-944.
- Nelson, R.B., "Simplified Calculation of Eigenvector Derivatives," *AIAA Journal*, Vol. 14, Sept. 1976, pp. 1201-1205.
- Chen, S.Y. and Wei, F.S., "Systematic Approach for Eigensensitivity Analysis," *Proceedings of AIAA/ASME/ASCE/AHS 26th Structures, Structural Dynamics and Materials Conference*, Pt. 2, AIAA, New York, April 1985, pp. 178-183.
- Wang, B.P., "An Improved Approximate Method for Computing Eigenvector Derivatives," Paper presented in work-in-progress ses-

INSER THE NUMERICAL EXAMPLE PP 581-593

sions. AIAA/ASME/ASCE/AHS 26th Structures, Structural Dynamics and Materials Conference, Orlando, FL, April 1985.

<sup>19</sup>Sutter, T.R., Camarda, C.J., Walsh, J.L. and Adelman, H.M., "A Comparison of Several Methods for the Calculation of Vibration Mode Shape Derivatives." *Proceedings of AIAA/ASME/ASCE/AHS 27th Structures, Structural Dynamics and Materials Conference*, Pt. 2, AIAA, New York, May 1986, pp. 256-265.

<sup>20</sup>Adelman, H.M. and Haftka, R.T., "Sensitivity Analysis of Discrete Structural Systems." *AIAA Journal*, Vol. 24, May 1986, pp. 823-832.

<sup>21</sup>Porter, B. and Crossley, T.R., *Modal Control: Theory and Applications*, Taylor & Francis, London, 1972, p. 25.

<sup>22</sup>Ojalvo, I.U., "Efficient Computation of Mode-Shape Derivatives for Large Dynamic Systems." *Proceedings of AIAA/ASME/ASCE/AHS 27th Structures, Structural Dynamics and Materials Conference*, Pt. 2, AIAA, New York, May 1986, pp. 242-247.

<sup>23</sup>Meirovitch, L. and Ryland, G., "A Perturbation Technique for Gyroscopic Systems with Small Internal and External Damping." *Journal of Sound and Vibration*, Vol. 100, No. 3, 1985, pp. 393-408.

## **ATTACHMENT 7**

# **Probability of Stability: New Measures of Stability Robustness for Linear Dynamical Systems**



# Probability of Stability: New Measures of Stability Robustness for Linear Dynamical Systems

K. B. Lim<sup>1</sup> and J. L. Junkins<sup>2</sup>

## Abstract

The problem of quantifying stability robustness due to parameter perturbations is addressed. A judiciously weighted eigenvalue sensitivity index is proposed for use in stability robustness optimization problems. A new stochastic measure of stability robustness suitable for structured perturbations is proposed. As a special case of this new measure, a set of weights reflecting stability margins of individual modes and probability distributions of uncertain parameters are obtained. In addition, matrix theory is used to establish some connections between the eigenvalue sensitivity matrix, eigenvalue perturbations, and associated cost functions of the system sensitivity.

## Introduction

This paper is motivated by our desire to explore the significance of the eigenvalue sensitivity measures and their associated weights with respect to stability robustness under parameter perturbations. Robustness measures are important in many engineering design problems wherein an uncertain mathematical model is used and a design goal is to minimize the sensitivity of some a priori specified performance measure with respect to a selected set of uncertain parameters. In particular, we consider here the sensitivity and stability margins of closed loop eigenvalues which have been recognized as important elements in the design of a class of linear feedback control systems [1-3]. In this paper, the word "robustness" is used in the broad sense of susceptibility of a defined property of a mathematical model with respect to ignorance of the actual system represented by our model.

For the purpose of discussion in this paper, we define two types of uncertainties. "Structured" uncertainty includes those variations in a model of correct mathematical form which are a consequence of uncertainty of the numerical values assigned to the

<sup>1</sup>Engineering Specialist, PRC Kentron Inc., 303 Butter Farm Rd., Suite 100, Hampton, VA 23666.

<sup>2</sup>Professor, Department of Aerospace Engineering, Texas A&M University, College Station, TX 77843; Fellow AAS.

physical parameters (e.g., those specifying geometry, mass, stiffness, damping, etc.). Structured variations preserve many features of a mathematical model (e.g., sparsity patterns of system model matrices) and distribute a given parametric uncertainty consistent with the local sensitivity of the mathematical model to that uncertain parameter. "Unstructured" certainty, on the other hand, essentially discards the physical modeling process and adopts the elements of the differential equation or transfer function system's matrices as the fundamental mathematical model. This approach considers independent unconstrained variations of these matrix elements instead of the more fundamental and usually fewer parameters in a well conceived mathematical model. Because the unstructured uncertainty variations do not enforce physical modelling assumptions, this approach usually gives rise to heavily redundant and physically impossible variations. In the sense that the unstructured variations do not generally correspond to unique physical parameters for the plant, the variations may not be physically possible. On the other hand, if "the physics" are very poorly understood, the unstructured approach may prove appropriate. With the possible exception of errors incurred by finite word length of a digital computer, most perturbations that are of practical interest in the design of control systems for flexible structures are usually highly structured. As a consequence, the need for robustness measures specially tailored for structured perturbations is apparent. In this context, the present paper addresses the structured perturbation case by analyzing a weighted and normalized eigenvalue sensitivity matrix as a robustness index along with a physically meaningful set of weights.

Although both eigenvalues and eigenvectors determine the total transient response of linear systems, eigenvalue location completely determines the absolute and relative stability of a system. Hence, only eigenvalue sensitivity will be considered in the following discussions. However, the two are closely related because the eigenvector set collectively dictates eigenvalue sensitivity as clearly evident from [3].

The main result of this paper is the development of a new measure for stability robustness under structured perturbations. The structured perturbations are modelled from a probabilistic perspective and the condition of asymptotic stability is taken as a well defined event. This approach leads to a probabilistic measure of stability robustness ("probability of stability"), defined herein as the probability of all eigenvalues remaining on the left hand side of the imaginary axis in eigenspace. It is an obvious qualitative truth that we should seek designs which have a high "probability of stability" in the presence of structured plant variations. It is seen that under certain physically reasonable assumptions, the probability of stability expression reduces to a simple form. Interestingly, the idealized form is shown equivalent to a heuristically motivated quadratic measure of eigenvalue sensitivity and in addition, a particular set of weights results which physically reflects the uncertainty structure and the relative stability margins of individual modes.

The outline of this paper is as follows: The next section motivates and discusses the minimization of a direct measure of weighted eigenvalue sensitivity with respect to uncertain parameters. An intuitively attractive set of weights are suggested for use in eigenvalue sensitivity optimization applications. The most direct measure of a weighted sum square of eigenvalue sensitivity introduced in the earlier section is re-examined in the third section from the perspective of matrix operator norm theory.

wherein the sensitivity matrix is considered as a typical linear transformation matrix which maps a vector of parameter perturbations into eigenvalue perturbations. As a result, a matrix norm of a weighted eigenvalue sensitivity matrix is suggested for use as an index of overall sensitivity. The third section also provides some connection between the sensitivity measures introduced in the second and third sections. The main result of this paper is then presented in the fourth section. A new probabilistic definition of stability robustness is introduced and under reasonable assumptions the new robustness measure is shown to be closely related to the measure of eigenvalue sensitivity introduced earlier.

### Eigenvalue Sensitivity Optimization

For a general  $n$ th order linear time invariant system with  $\ell$  parameters considered uncertain, we assume that we have available a matrix of  $(n \times \ell)$  partial derivatives representing the sensitivities of every computed eigenvalue with respect to a set of  $\ell$  uncertain parameters [4]. For the present discussion, ignore model truncation issues wherein the higher frequency computed eigenvalues and eigenvectors are poor approximations of the physical system. Consider the minimization of a weighted norm of the eigenvalue sensitivity matrix with respect to a set of design variables. For the purpose of formulating a mathematical programming problem, a scalar index which captures the overall sensitivity is desirable. One such direct measure of eigenvalue sensitivity is

$$J(p) \triangleq \sum_{i=1}^n \sum_{j=1}^{\ell} \left| \frac{\partial \lambda_i}{\partial p_j} \right|^2 w_{ij} \quad (1)$$

where  $w_{ij}$  is a nonnegative weighting factor associated with the sensitivity of the  $i$ th eigenvalue,  $\lambda_i$ , with respect to the  $j$ th parameter,  $p_j$ . By definition, the minimum  $J$  could take is zero. For purposes of establishing algorithms for direct minimization, equation (1) can be linearized about a nominal design point,  $p^r$ , to obtain

$$J(p) = J(p^r) + 2 \sum_{j=1}^{\ell} S_j(p^r) \Delta p_j + O(\Delta p^2) \quad (2)$$

where the sensitivity is

$$S_j(p_r) = \sum_{i=1}^n \sum_{k=1}^{\ell} w_{ik} \left[ \operatorname{Re} \left\{ \left( \frac{\partial \lambda_i}{\partial p_k} \right)^* \left( \frac{\partial^2 \lambda_i}{\partial p_j \partial p_k} \right) \right\} - \frac{1}{\operatorname{Re}(\lambda_i)} \left| \frac{\partial \lambda_i}{\partial p_k} \right|^2 \operatorname{Re} \left\{ \frac{\partial \lambda_i}{\partial p_j} \right\} \right] \quad (3)$$

with  $p = p^r + \Delta p$  and "\*" represents complex conjugate. We recommend, as one good choice for weights, the following ratio:

$$w_{ik} = \sigma_{p_k}^2 / (-\operatorname{Re} \lambda_i)^2 \quad (4)$$

where  $\sigma_{p_k}^2$  is an estimate of the variance of  $p_k$ . This choice is implicit in equation (3). In an optimization setting we have the choice of using some nominal  $\lambda$ 's to compute constant weights, or allowing the  $w_{ik}$  to vary as the  $\lambda_i$  change. The latter (locally variable) weighting procedure is more general and is recommended. Notice this weight choice emphasizes sensitivity of the least stable eigenvalues with respect to the most uncertain parameters. In the next section, an alternative probabilistic justification for

equations (1) and (4) is given. Reference [5] demonstrates the feasibility of using the above linearized index of sensitivity to attain a local minimum sensitivity configuration while simultaneously placing eigenvalues, for a numerical example involving a significant dimension model (twentieth order with fifty-five design variables).

The measure of eigenvalue sensitivity as given in equation (1) is limited from both application and theoretical viewpoints. First, there is the possibility of uncertain parameters that differ vastly in terms of units or orders of magnitudes. This leads to some difficulty in the selection of weights to capture the overall sensitivity; hence the recommendation of a set of weights as given in equation (4). We note the nontrivial requirement for  $(n \times \ell)$  weights. Although a good knowledge of the relative weights for the eigenvalue set and the parameters set independently can be expected, their coupling effects are sometimes difficult to anticipate. A second possible limitation of equation (1) is the lack of a directly quantifiable interpretation of the numerical value of the cost function. This observation follows from the fact that the eigenvalue sensitivity matrix can be viewed as a typical linear transformation matrix whose properties include a limit on the size of the output corresponding to a bounded input, i.e., an operator norm of the eigenvalue sensitivity matrix. The next section exploits this idea to address the above mentioned limitations.

### Eigenvalue Perturbations and the Sensitivity Matrix

We examine closely the significance of a matrix of eigenvalue sensitivities using concepts from matrix operator norm theory. We begin by writing the linearly predicted changes in  $n$ -eigenvalues due to small changes in  $\ell$ -parameters as

$$\begin{Bmatrix} \Delta\lambda_1 \\ \vdots \\ \Delta\lambda_n \end{Bmatrix} = \begin{bmatrix} \frac{\partial\lambda_1}{\partial p_1} & \cdots & \frac{\partial\lambda_1}{\partial p_\ell} \\ \vdots & & \vdots \\ \frac{\partial\lambda_n}{\partial p_1} & \cdots & \frac{\partial\lambda_n}{\partial p_\ell} \end{bmatrix} \begin{Bmatrix} \Delta p_1 \\ \vdots \\ \Delta p_\ell \end{Bmatrix} \quad (5)$$

or

$$\Delta\lambda = G \Delta p \quad (6)$$

where  $G$  represents the  $(n \times \ell)$  matrix Jacobian of eigenvalue sensitivities. Reference [4] provides an excellent survey of various techniques to compute eigenvalue sensitivity. Let us next define a weighted vector norm of eigenvalue change as

$$\|\Delta\lambda\|^w \triangleq (\Delta\lambda^H W \Delta\lambda)^{1/2} \quad (7)$$

where the weight matrix  $W$  can be taken as a designer specified positive definite symmetric matrix which weighs the sensitivity of individual modes. As in the previous discussion, we would almost certainly penalize heavily the marginally stable eigenvalues. Here, superscript " $H$ " represents Hermitian transpose. A qualitatively reasonable set of matrix elements to reflect stability margins in equation (7) is

$$W_{ij} = \frac{1}{\text{Re}(\lambda_i) \text{Re}(\lambda_j)} \quad (i, j = 1, \dots, n) \quad (8)$$

We also choose to normalize (nondimensionalize or weight) our parameter changes by

$$\delta_i = \frac{\Delta p_i}{\sigma_{p_i}} \quad (i = 1, \dots, \ell) \quad (9)$$

where  $\sigma_{p_i}$  represents the assumed standard deviation of the  $i$ th uncertain parameter, or in general, some other appropriate nondimensionalization constant, and rewrite equation (9) as a linear transformation

$$\Delta p = \theta \delta \quad (10)$$

where

$$\theta \triangleq \text{diag}\{\sigma_{p_1}, \dots, \sigma_{p_\ell}\} \quad (11)$$

We note that  $\delta$  represents an  $\ell$ -vector of nondimensionalized (normalized) parameter change. It is clear from equation (9) that a more uncertain parameter corresponds to a larger standard deviation and this in turn admits a larger parameter perturbation, for  $\delta^T \delta = 1$ .

By using equations (10) and (6), we obtain from equation (7) the following:

$$\begin{aligned} (\|\Delta \lambda\|^n)^2 &= \Delta \lambda^H W \Delta \lambda \\ &= \delta^T Q \delta \end{aligned} \quad (12)$$

where

$$Q \triangleq \theta^T G^H W G \theta \quad (13)$$

Since  $W$  is assumed symmetric,  $Q$  is hermitian and by Rayleigh's principle [6], an upper bound for the weighted eigenvalue change from equation (12) is

$$(\|\Delta \lambda\|^n)^2 \leq \lambda_{\max}(Q) \delta^T \delta \quad (14)$$

By induction,  $\lambda_{\max}(Q)$  represents an upper bound on the square of weighted eigenvalue error norms,  $\|\Delta \lambda\|^n$ , for all normalized perturbations  $\delta$  satisfying

$$\delta^T \delta \leq 1 \quad (15)$$

Investigating further, we note that since  $W$  is a symmetric and positive definite matrix, it can be decomposed by Cholesky factorization [6] to

$$W = LL^T \quad (16)$$

where  $L$  is a lower triangular matrix. As a result of equation (16),  $Q$  of equation (12) can be rewritten as

$$Q = (L^T G \theta)^H (L^T G \theta) \geq 0 \quad (17)$$

so that

$$\lambda_{\max}(Q) = \bar{\sigma}(L^T G \theta) \quad (18)$$

where  $\bar{\sigma}$  represents the maximum singular value. In words, equation (18) represents a convenient scalar index for a weighted and normalized measure of eigenvalue sensitivity. For a typical application,  $L$  and  $\theta$  may be specified by the designer while the

elements of  $G$  may be iteratively adjusted to minimize the overall sensitivity measure in equation (18). Note the physical significance of the  $L$  and  $\theta$  terms.

For the special case where  $W$  and  $\theta$  are identity matrices, the above sensitivity measure reduces to the simple form

$$\lambda_{\max}(Q) = \overline{\sigma}(G) = \|G\|_2 \quad (19)$$

where  $\|\cdot\|_2$  denotes the matrix two-norm. It should be emphasized here that although both equations (1) and (18) represent sensitivity indices, only equation (18) is directly related to a linearly predicted bound on weighted and normalized eigenvalue perturbation. Note that the above derivations are analogous to the concept of matrix operator norms [6].

Next, we develop a relationship between the cost functions in equations (1) and (7). In the process a connection between the set of weights in equation (1) and equation (12) is established.

We begin by rewriting equation (6) in the form

$$\Delta\lambda = D \text{vec}(G) \quad (20)$$

where

$$\text{vec}(G) \triangleq \begin{Bmatrix} \left\{ \begin{matrix} \lambda_{1,1} \\ \vdots \\ \lambda_{1,t} \end{matrix} \right\} \\ \vdots \\ \left\{ \begin{matrix} \lambda_{n,1} \\ \vdots \\ \lambda_{n,t} \end{matrix} \right\} \end{Bmatrix} \quad (21)$$

$$D \triangleq \begin{bmatrix} \Delta p^T & & & \\ & \Delta p^T & & \\ & & \ddots & \\ & & & \Delta p^T \end{bmatrix} \quad (22)$$

$$(\quad)_{,i} \triangleq \frac{\partial(\quad)}{\partial p_i} \quad (23)$$

By substituting equation (20) into equation (7) we obtain

$$\begin{aligned} \Delta\lambda^H W \Delta\lambda &= \{\text{vec}(G)^H D^T W D \{\text{vec}(G)\} \\ &= \{\text{vec}(G)\}^H [W \otimes \{\Delta p\} \{\Delta p\}^T] \{\text{vec}(G)\} \end{aligned} \quad (24)$$

where the symbol " $\otimes$ " denotes a Kronecker product [7].

Since  $\Delta p = p - \bar{p}$  where  $\bar{p}$  represents nominal (expected) parameter vector and  $p$  can be considered a vector of random variables (assumed distributed about a mean of

$\bar{p}$ ), we can take the expectation of equation (24) to obtain the relation

$$E[\Delta\lambda^H W \Delta\lambda] = \{\text{vec}(G)\}^H [W \otimes \mu_{pp}] \{\text{vec}(G)\} \quad (25)$$

where  $\mu_{pp}$  denotes the covariance matrix of parameter errors [8], i.e.,

$$\mu_{pp} = E[\{\Delta p\} \{\Delta p\}^T] \quad (26)$$

In general,  $W \otimes \mu_{pp}$  is a fully populated matrix of dimension  $(n \times \ell)$  by  $(n \times \ell)$ . For the special case where the weight matrix,  $W$ , is diagonal (i.e. no penalty for products of eigenvalue perturbations), and the parameter errors are uncorrelated, it can be shown that equation (25) reduces to the form

$$E[\Delta\lambda^H \text{diag}\{w_1, \dots, w_n\} \Delta\lambda]$$

$$= \{\text{vec}(G)\}^H \begin{bmatrix} w_1 \sigma_{p1}^2 & & & & 0 \\ & \ddots & & & \\ & & w_1 \sigma_{p\ell}^2 & & \\ & & & \ddots & \\ & 0 & & & w_n \sigma_{p1}^2 \\ & & & & & \ddots \\ & & & & & & w_n \sigma_{p\ell}^2 \end{bmatrix} \{\text{vec}(G)\} \quad (27)$$

$$= \sum_{j=1}^{\ell} \sum_{i=1}^n |\lambda_{i,j}|^2 w_i \sigma_{pj}^2 \quad (28)$$

where  $\sigma_{pj}$  represents the standard deviation of the  $j$ th parameter error distribution. It is clear that the above special case of minimizing equation (25) is identical to minimizing the heuristic measure of equation (1). Since equation (27) is a special case of equation (7) and in addition, equation (18) is a bound on equation (7), it can be concluded that the general measure of equation (1) can be considered a special case of the measure given by equation (18), i.e. when the Kronecker product in equation (24) is diagonal, as in equation (27). In other words, equation (18) is a more general expression for eigenvalue sensitivity of a system than equation (1), a measure which includes a penalty on the coupling of eigenvalue sensitivities and permits correlated parameter errors.

### Probability of Stability

The earlier sections involved a deterministic approach to eigenvalue sensitivity in which two sets of weights were intuitively suggested to reflect the statistics of parameter uncertainties and stability margins of individual modes. Also in the last section, we developed a justification for the set of weights associated with parameter uncertainty. Although the statistics of eigenvalue sensitivity have been considered by taking the expectation of some a priori defined sensitivity measure, the statistics of stability and a probabilistic justification for the eigenvalue weights  $(1/\text{Re}\lambda_i)$  to reflect relative stability margins has not been discussed. In this section, we introduce a gen-

eral statistical measure of stability robustness due to parameter uncertainty. We then obtain as a special case, a more rigorous justification of the results in earlier sections.

### Definitions

We begin by assuming that the probability density function of eigenvalues about a nominal (or mean) point in eigenspace is available, either by an analytical or numerical mapping from (the system model) parameter space. Of course, generally, this mapping is nontrivial and may require approximate numerical methods. The "probability of stability,"  $P_s$ , is defined as

$$\begin{aligned} P_s &\triangleq P[\lambda_i \in \Phi; i \in N] \quad (N = \{1, \dots, n\}) \\ &= \int_{\Phi} p_{\lambda}(\lambda_1, \dots, \lambda_n) d\lambda_1 \dots d\lambda_n \end{aligned} \quad (29)$$

where  $p_{\lambda}$  represents the probability density function of eigenvalues,  $\lambda$ . The domain of integration,  $\Phi$ , in equation (29) consists of the entire left half of the hyperplane (corresponding to the space where all eigenvalues have negative real components) which has a dimension of order  $2n$ . The above probability distribution is geometrically clear for the case of a single complex random variable (single random eigenvalue in this case), unlike its generalization to a function of  $n$  complex random variables. The domain of integration can be simplified by rewriting the density function in terms of a new set of real nondimensionalized random variables defined here as

$$\xi_i \triangleq \frac{\text{Re}\{\Delta\lambda_i\}}{-\text{Re}\{\bar{\lambda}_i\}} \quad (i \in N) \quad (30)$$

$$\Delta\lambda_i = \lambda_i - E(\lambda_i) \quad (31)$$

where  $E(\lambda_i) = \bar{\lambda}_i$  denotes the expected (or mean) eigenvalues corresponding to the expected (or mean) values of those physical parameters which are considered random variables. We note from equation (30) that at  $\xi_i = 1$ , the perturbed  $i$ th eigenvalue will be on the imaginary axis. Clearly, a necessary and sufficient condition which guarantees the system will remain asymptotically stable is all normalized eigenvalue perturbation must satisfy

$$\xi_i < 1 \quad (i \in N) \quad (32)$$

More specifically, equation (32) can be used as the definition of the stability event. By using the condition of equation (32), we now rewrite the probability of stability, defined earlier in equation (29), in terms of the nondimensionalized real part of eigenvalue perturbation as

$$\begin{aligned} P_s &= P[\xi_i < 1; i \in N] \\ &= \int_{-\infty}^1 \dots \int_{-\infty}^1 p_{\xi}(\xi_1, \dots, \xi_n) d\xi_1 \dots d\xi_n \end{aligned} \quad (33)$$

We mention here that in applying equation (33) to real systems, the density function,  $p_{\xi}$ , will be negligible for  $\xi \ll -1$  if we restrict ourselves to problems where the physical parameter perturbations, along with the corresponding perturbation in the eigen-



values, are reasonably bounded about its nominal point. In other words, for virtually all systems of practical interest,  $p_i \rightarrow 0^+$  as  $\xi_i \rightarrow -\infty$  for all  $i$ ,  $i \in N$ . The above physical property motivates further simplifying assumptions in the sequel. We obtain a convenient lower bound for equation (33) provided a few reasonable conditions are met. It should also be pointed out that for eigenvalue placement problems, the remaining freedom in the gain matrix after imposing the desired closed loop eigenvalues,  $\{\bar{\lambda}\}$ , (see for example [3]) may be used to optimize the stability robustness measure in equation (33). It is clear that this optimization will necessarily involve a reconfiguration of the probability density function,  $p_i$ , such as to maximize the probability of stability functional of equation (33).

#### *Probability of Stability for Linearized, Gaussian System*

To obtain further insight into the nature of the above robustness measure, let us consider the linearized behavior of the eigenvalues as given in equation (6) and take the real part of the equation

$$\text{Re}\{\Delta\lambda\} \cong \text{Re}\{G\} \Delta p \quad (34)$$

By rewriting equation (30) in vector form, we get

$$\xi = V \text{Re}\{\Delta\lambda\} \quad (35)$$

where

$$V = \text{diag}\left(\frac{1}{-\text{Re}\{\bar{\lambda}_1\}}, \dots, \frac{1}{-\text{Re}\{\bar{\lambda}_n\}}\right) \quad (36)$$

In terms of parameter perturbations, the normalized eigenvalue perturbation can be approximated from equation (34) and (35) as

$$\xi \cong V \text{Re}\{G\} \Delta p \quad (37)$$

It follows that the covariance of the parameter uncertainty,  $\Lambda_{pp}$ , can be mapped linearly into the covariance of eigenvalue perturbations,  $\Lambda_{\xi\xi}$ , through (see for example, [8])

$$\begin{aligned} \Lambda_{\xi\xi} &= E[\xi\xi^T] \\ &= V \text{Re}\{G\} \Lambda_{pp} \text{Re}\{G\}^T V \end{aligned} \quad (38)$$

and if the random vector of parameter perturbations are assumed to have a joint Gaussian distribution, then the probability distribution of normalized eigenvalue perturbation will also be Gaussian. Thus, the probability density function of  $\xi$  can be written as

$$p_i = \frac{1}{(2\pi)^{n/2} |\Lambda_{\xi\xi}|^{1/2}} \exp\left(-\frac{1}{2} \xi^T \Lambda_{\xi\xi}^{-1} \xi\right) \quad (39)$$

#### *Bounds on Probability of Stability for Gaussian Systems*

To obtain a lower bound on the robustness measure given in equation (33), let us consider integrating over a unit volume of an  $n$ -dimensional hypersphere,  $B$ , as

shown in Fig. 1. We see that a sufficient condition for satisfying equation (32), i.e., asymptotic stability is

$$\Omega = \xi^T \xi < 1 \quad (40)$$

It follows that

$$\begin{aligned} P[\xi \in B] &= P[\Omega < 1] \\ &= \int_B p_\xi(\xi_1, \dots, \xi_n) d\xi_1 \dots d\xi_n \end{aligned} \quad (41)$$

The lower bound on the probability of stability as given by equation (41) can in turn be bounded by very simple expressions for Gaussian systems if we consider the probability functions in spherical coordinates in  $n$  dimensions. Through the above transformation of coordinates, it can be shown (see for example [8]) that the probability of  $\xi$  lying inside the quadratic hyperellipsoid,

$$\xi^T \Lambda_{\xi\xi}^{-1} \xi = R^2 \quad (42)$$

is given by

$$\begin{aligned} P[\xi^T \Lambda_{\xi\xi}^{-1} \xi < R^2] &= \int_{\Gamma} \frac{1}{(2\pi)^{n/2} |\Lambda_{\xi\xi}|^{1/2}} \exp\left(-\frac{1}{2} \xi^T \Lambda_{\xi\xi}^{-1} \xi\right) d\xi_1 \dots d\xi_n \\ &= \frac{1}{(2\pi)^{n/2}} \int_0^R \exp\left(-\frac{1}{2} r^2\right) f(r) dr \end{aligned} \quad (43)$$

where  $f(r)$  is the  $n$ -dimensional spherically symmetric volume element (eg:  $n = 1$ ,  $f(r) dr = 2 dr$ ;  $n = 2$ ,  $f(r) dr = 2\pi r dr$ ;  $n = 3$ ,  $f(r) dr = 4\pi r^2 dr$ ). We note that the domain of integration,  $\Gamma$ , is over the hyperellipsoid whose surface is defined by equation (42). This domain over the hyperellipsoid is obviously different from the domain enclosed by hypersphere,  $B$ , which is required in equation (41). From Fig. 2, it is clear that the required integral over the hypersphere,  $B$ , can be bounded by the integrals over two corresponding hyperellipsoids,  $\Gamma_1$ ,  $\Gamma_2$ , i.e.

$$P[\xi \in \Gamma_1] \leq P[\xi \in B] \leq P[\xi \in \Gamma_2] \quad (44)$$

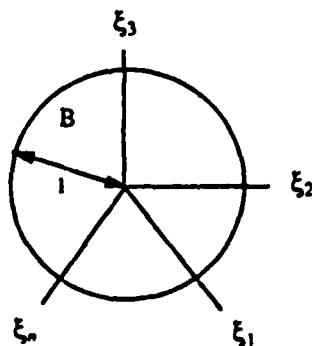


FIG. 1.  $n$ -dimensional Sphere.

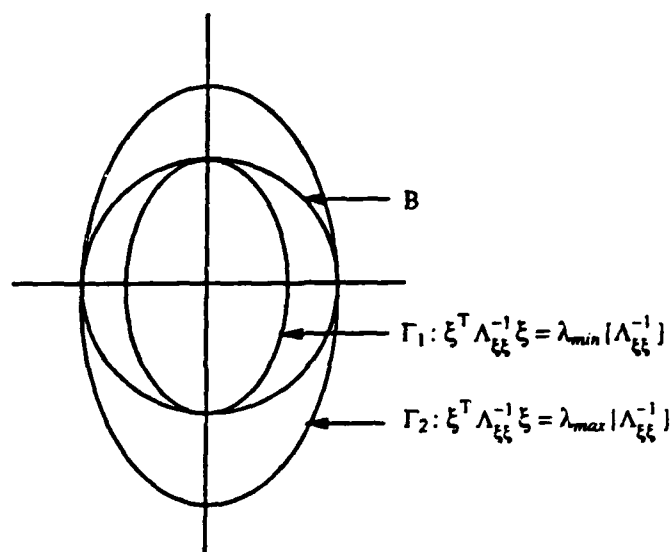


FIG. 2. Hyperellipsoid Bounds for the Unit Hypersphere.

where the two hyperellipsoids are given as

$$\Gamma_1: \xi^T \Lambda_{\xi\xi}^{-1} \xi \leq \lambda_{\min}[\Lambda_{\xi\xi}^{-1}] \quad (45)$$

$$\Gamma_2: \xi^T \Lambda_{\xi\xi}^{-1} \xi \leq \lambda_{\max}[\Lambda_{\xi\xi}^{-1}] \quad (46)$$

It follows that

$$\int_B p_\xi(\xi_1, \dots, \xi_n) d\xi_1 \dots d\xi_n \geq \frac{1}{(2\pi)^{n/2}} \int_0^{R_*} \exp\left(-\frac{1}{2}r^2\right) f(r) dr \quad (47)$$

where

$$R_* = \sqrt{\lambda_{\min}[\Lambda_{\xi\xi}^{-1}]} \quad (48)$$

The right hand side of equation (47) represents a convenient lower bound on the probability of stability within linearity assumptions for Gaussian parameter uncertainties. From a geometrical perspective (see Fig. 2), it is clear that the "tightness" of the above lower and upper bounds in equation (44) can be quantified by the ratio

$$\frac{\lambda_{\max}[\Lambda_{\xi\xi}^{-1}]}{\lambda_{\min}[\Lambda_{\xi\xi}^{-1}]} \geq 1 \quad (49)$$

with the ratio of unity corresponding to the equality condition in equation (47)

#### *Probability of Stability and Weights for Eigenvalue Sensitivity*

The integrand appearing in the right hand side of equation (47) is always positive and therefore its integral is a monotonically increasing function of the upper limit of integration,  $R_*$ . This means that (since the integrand has a fixed form)  $R_*$  must be directly related to a measure of probabilistic stability robustness to within linearity and Gaussian assumptions. For stability robustness optimization, the above observation

suggests the maximization of the scalar index,  $R$ , or

$$\begin{aligned} R^2 &= \lambda_{\min}[\Lambda_{\xi\xi}^{-1}] \\ &= \frac{1}{\lambda_{\max}[\Lambda_{\xi\xi}]} \end{aligned} \quad (50)$$

where the weighted covariance of eigenvalue perturbation matrix,  $\Lambda_{\xi\xi}$ , is given by equation (38). It is easily seen from equation (50) that the covariance of the normalized eigenvalue vector is inversely proportional to the above measure of robustness, which seems intuitively correct.

It is interesting to note that the scalar index in equation (50) is closely related to the scalar index suggested in equation (18). Firstly, we note that maximizing the robustness index in equation (50) is equivalent to minimizing its reciprocal  $\lambda_{\max}[\Lambda_{\xi\xi}]$ . Next, by rewriting the covariance matrix in equation (38) as

$$\Lambda_{\xi\xi} = SS^T \quad (51)$$

where

$$S = V \operatorname{Re}\{G\} \Lambda_{pp}^{1/2} \quad (52)$$

we see that

$$\lambda_{\max}[\Lambda_{\xi\xi}] = \bar{\sigma}[S] \quad (53)$$

By comparing equations (18) and (53), the following set of weights are suggested,

$$\theta = \Lambda_{pp}^{1/2} = (E[(p - \bar{p})(p - \bar{p})^T])^{1/2} \quad (54)$$

$$L = V = \operatorname{diag}\left(-\frac{1}{\operatorname{Re}(\bar{\lambda}_1)}, \dots, -\frac{1}{\operatorname{Re}(\bar{\lambda}_n)}\right) \quad (55)$$

The above relationships on the weights derived from a probabilistic standpoint provides an alternative justification for the heuristically motivated weights in equations (4) and (18).

### Example

In order to illustrate the physical significance of the probability of stability concept, let us consider the stability robustness of the familiar single degree of freedom oscillator

$$m\ddot{x} + c(p_1, p_2)\dot{x} + kx = 0 \quad (56)$$

The effective damping,  $c$ , is assumed to be a function of two random parameters,  $p_1$  and  $p_2$  having joint Gaussian distribution. The corresponding eigenvalues can be expressed as

$$\lambda_{1,2} = \frac{-c \pm \sqrt{c^2 - 4mk}}{2m} \quad (57)$$

For the underdamped case, which is typical for structural vibration problems,

$$\operatorname{Re}(\lambda_1) = \operatorname{Re}(\lambda_2) = \operatorname{Re}(\lambda) = -\frac{c}{2m} \quad (58)$$

Since the real components of the two eigenvalues are identical, we need to consider only one of the eigenvalues,  $\lambda$ , and its perturbation,  $\Delta\lambda$ . Assuming  $m$  and  $k$  fixed and the mean values of  $p_1$  and  $p_2$  given such that the system is nominally stable, i.e.,  $\text{Re}(\lambda) < 0$ , the likelihood of the stability event or probability of stability depends on the distribution of  $p_1$  and  $p_2$ . For illustration purposes we assume the ad hoc nonlinear dependence

$$c(p_1, p_2) = p_1(1 + p_2^3) \quad (59)$$

From equations (58) and (59), linearization leads to

$$\begin{aligned} \text{Re}(\Delta\lambda) &= -\frac{1}{2m} \left[ \frac{\partial c}{\partial p_1} \quad \frac{\partial c}{\partial p_2} \right] \begin{Bmatrix} \Delta p_1 \\ \Delta p_2 \end{Bmatrix} \\ &= \text{Re}(G) \Delta p \end{aligned} \quad (60)$$

where

$$\text{Re}(G) = \left[ -\frac{1}{2m} (1 + p_2^3) \quad -\frac{1}{2m} (3p_1 p_2^2) \right] \quad (61)$$

$$\Delta p = \begin{Bmatrix} \Delta p_1 \\ \Delta p_2 \end{Bmatrix} \quad (62)$$

The nondimensionalized real eigenvalue perturbation of equation (30) becomes

$$\xi \triangleq \frac{\text{Re}(\Delta\lambda)}{-\text{Re}(\lambda)} \quad (63)$$

or

$$\xi = V \text{Re}(G) \Delta p \quad (64)$$

where

$$V = \frac{1}{-\text{Re}(\lambda)} \quad (65)$$

The parameter covariance locally maps, using equation (38), to the eigenvalue covariance through

$$\Lambda_{\xi\xi} = V \text{Re}(G) \Lambda_{pp} \text{Re}(G)^T V \quad (66)$$

$$= \frac{1}{c^2} [1 + p_2^3 \quad 3p_1 p_2^2] \Lambda_{pp} \begin{bmatrix} 1 + p_2^3 \\ 3p_1 p_2^2 \end{bmatrix} \quad (67)$$

$$= \frac{1}{c^2} \{ (1 + p_2^3) \sigma_{11}^2 + (3p_1 p_2^2)^2 \sigma_{22}^2 + 2(1 + p_2^3) (3p_1 p_2^2) \mu_{12} \} \quad (68)$$

where

$$\Lambda_{pp} = \begin{bmatrix} \sigma_{11}^2 & \mu_{12} \\ \mu_{12} & \sigma_{22}^2 \end{bmatrix} > 0 \quad (69)$$

The probability of stability as given in equation (33) can be written as [9]

$$P_s = \int_{-\infty}^1 p_\xi d\xi \quad (70)$$

$$= \frac{1}{\sqrt{\Lambda_{\xi\xi}}\sqrt{2\pi}} \int_{-\infty}^1 \exp\left(-\frac{\xi^2}{2\Lambda_{\xi\xi}}\right) d\xi \quad (71)$$

$$= \frac{1}{2} \left[ 1 + \operatorname{erf}\left(\frac{1}{\sqrt{2\Lambda_{\xi\xi}}}\right) \right] \quad (72)$$

where

$$\operatorname{erf}(z) = \frac{2}{\sqrt{\pi}} \int_0^z e^{-t^2} dt \quad (73)$$

Observe that as  $\Lambda_{\eta\eta}$  approaches zero (i.e. parameters,  $p_1$  and  $p_2$  become increasingly more certain), the probability of stability  $P_s$  in equation (72) approaches unity as one would expect. A lower bound in equation (47) of the probability of stability given in equation (72) can be written as,

$$P[\xi \in \Gamma_1] = \frac{2}{\sqrt{2\pi}} \int_0^{R_*} e^{-r^2/2} dr = \frac{2}{\sqrt{\pi}} \int_0^{R_* \sqrt{2}} e^{-t^2} dt \quad (74)$$

where

$$R_* = \frac{1}{\sqrt{\Lambda_{\xi\xi}}} \quad (75)$$

so that

$$P[\xi \in \Gamma_1] = \operatorname{erf}\left(\frac{1}{\sqrt{2\Lambda_{\xi\xi}}}\right) \leq \frac{1}{2} + \frac{1}{2} \operatorname{erf}\left(\frac{1}{\sqrt{2\Lambda_{\xi\xi}}}\right) = P_s \quad (76)$$

The probability of stability and its lower bound for the SDOF example is illustrated in Fig. 3 by the shaded areas. Note that for this SDOF case, the lower and upper bounds given in equation (44) are the same.

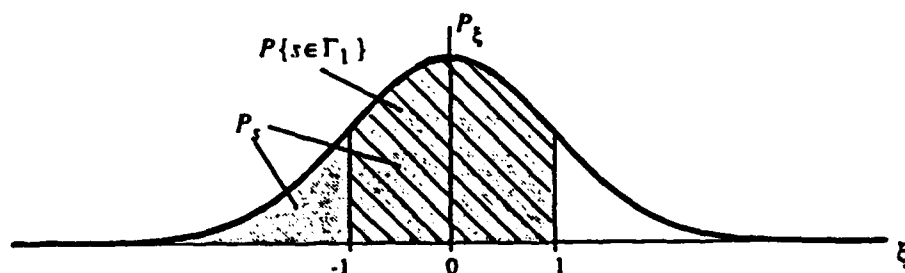


FIG. 3. Probability of Stability and its Lower Bound Eigenvalue Perturbation for the SDOF Example.

## Concluding Remarks

In summary, we have presented a new scalar index that is suitable for use as a cost function in the problem of eigenvalue sensitivity/stability robustness optimization. The significance of the eigenvalue sensitivity matrix is also established in a systematic manner. The cost function allows the user to easily input weights that specify the relative importance among a critical subset of modes and/or uncertain parameters independently. A locally variable weight matrix is introduced which penalizes least stable eigenvalues more heavily and emphasizes sensitivity with respect to poorly known parameters as compared to well known parameters. The numerical value of the cost function itself is directly related to a linearized upper bound on a weighted eigenvalue error measure due to a bounded set of normalized perturbations of uncertain parameters of unit magnitude. We have seen that the simplifying assumptions of eigenvalue linearizations and Gaussian statistics reduces the probability of stability expression to a simple form. Clearly, this is not possible in all cases, and in general, the probability density function for eigenvalues has to be generated numerically. Further research is therefore recommended to determine the applicability of the simplifying assumptions and the level of difficulty or the feasibility in generating the density function for the class of problems of interest.

Perhaps the main practical significance of the probability of stability approach is the justification of a set of weights for use in stability robustness analysis or optimizations. However, the above concept is intuitively attractive and holds promise for further extensions.

## References

- [1] HOWZE, J. W. and CAVIN, R. K., III "Regulator Design with Modal Insensitivity," *IEEE Transactions on Automatic Control*, Vol. AC-24, No. 3, June, 1979, pp. 466-469.
- [2] QIU, H. and GOURISHANKAR, V. G. "Design of Optimal Feedback Controllers for Minimum Eigenvalue Sensitivity," *Optimal Control Applications & Methods*, Vol. 5, pp. 309-317, 1984.
- [3] JUANG, J.-N., LIM, K. B., and JUNKINS, J. L. "Robust Eigensystem Assignment for Flexible Structures," AIAA Paper No. 87-2252-CP.
- [4] ADELMAN, H. M. and HAFTKA, R. T. "Sensitivity Analysis of Discrete Structural Systems," *AIAA Journal*, Vol. 24, No. 5, May 1986, pp. 823-832.
- [5] LIM, K. B. "A Unified Approach to Structure and Controller Design Optimizations," Ph.D. Dissertation, VPI&SU, August 1986.
- [6] STEWART, G. W. *Introduction to Matrix Computations*, New York: Academic Press, 1973.
- [7] BELLMAN, R. *Introduction to Matrix Analysis*, New York: McGraw-Hill, 1960, Chapter 20.
- [8] JUNKINS, J. L. *Introduction to Optimal Estimation of Dynamical Systems*, Sijthoff-Noordhoff International Publishers, Alphen Ann den Rijn, Netherlands, 1978.
- [9] ABRAMOWITZ, M. and STEGUN, I. A. (editors) *Handbook of Mathematical Functions*, Dover Publications, Inc., New York, 1972, p. 297.

## **ATTACHMENT 8**

# **Unified Optimization of Structures and Controllers**



# **Unified Optimization of Structures and Controllers**

J. L. Junkins and D. W. Rew  
Texas A&M University

March 1987

*a preprint to appear in*

***Large Space Structures: Dynamics and Control***

S. N. Atluri and A. K. Amos, editors

Springer-Verlag Berlin Heidelberg New York Tokyo  
to appear 1987

# Unified Optimization of Structures and Controllers

J. L. Junkins and D. W. Rew  
Texas A&M University

## Introduction

Given a differential equation *model* for a dynamical system, representing for example, a flexible structure, associated sensors and actuators, and a nominally stabilizing (optimal in some sense) feedback control law, a fundamental question is the following: will the feedback control law stabilize and near-optimally control the *actual* system? Of course, there are many interesting and significant issues raised by this question. The modeling process is always imperfect, among the several important sources of error are the following: (i) ignorance of the actual mass, stiffness, and energy dissipation properties, as well as boundary conditions and geometric parameters, (ii) discretization and truncation errors associated with representing a continuous system in terms of a finite number of degrees of freedom, (iii) neglect of nonlinearities, (iv) ignorance of external disturbances, and (v) poorly modeled sensors and actuators.

Indeed, even if one restricts the discussion to systems adequately modeled by a finite set of linear ordinary differential equations, the effects of uncertain parameters and disturbances results in analytical and practical implementation difficulties. The additional issues raised by the possibility that the structure can be re-designed to enhance controlled performance increase the dimensionality and difficulty of dealing comprehensively with the above issues. Improved methodology for solving the high dimensioned structural control problem is of central importance for the coming generation of large flexible space structures. In the present discussion, we emphasize development of robust eigenstructure assignment methods, and summarize some optimization methods in which both the controller and selected structural parameters are re-designed to improve robustness. A multi-criterion approach is presented by which one can study the tradeoff between robustness and competing performance measures (such as average control energy, average state errors, sensitivity measures, and structural mass).

## Preliminaries

Consider a finite order discrete model of a linear structure of the form

$$M\dot{z} + C\dot{z} + Kz = Du \quad (1)$$

where the  $n \times n$  symmetric mass, damping and stiffness matrices satisfy the definiteness properties  $M > 0$ ,  $C \geq 0$ ,  $K \geq 0$ ;  $z(t)$  is an  $n \times 1$  configuration vector,  $u(t)$  is an  $m \times 1$  control vector; and  $D$  is an  $n \times m$  control influence matrix. All quantities are considered real in Eq. (1). The structural eigenvalue problem associated with the  $z = \phi e^{\lambda t}$  solutions for the undamped free vibration special case of Eq. (1)

$$M\ddot{z} + Kz = 0 \quad (2)$$

$$\text{is } \det[M\lambda^2 + K] = 0, \Rightarrow \text{eigenvalues: } \{\lambda_i^2 = -\omega_i^2, i = 1, 2, \dots, n\} \quad (3)$$

$$[M\lambda_i^2 + K]\phi_i = 0, \Rightarrow \text{eigenvectors: } \{\phi_i, i = 1, 2, \dots, n\} \quad (4)$$

For this case, all eigenvalues ( $\lambda_i = \pm i\omega_i$ ,  $i^2 = -1$ ) are purely imaginary and eigenvectors are real. It is well known that the eigenvectors are orthogonal with respect to  $M$  and  $K$ ; we normalize these orthogonality conditions in the usual way [1] as follows

$$\phi_i^T M \phi_j = \delta_{ij} \quad \text{and} \quad \phi_i^T K \phi_j = \delta_{ij} \omega_i^2, i, j = 1, 2, \dots, n. \quad (5)$$

In matrix notation, the orthonormality conditions assume the familiar forms

$$[\Phi]^T M [\Phi] = [I], \text{ and } [\Phi]^T K [\Phi] = [\omega^2] \quad (6)$$

where the *modal matrix*  $[\Phi]$  contains the eigenvectors (normal mode shapes) as columns,  $[I]$  is the identity matrix, and  $[\omega^2] = \text{diag}\{\omega_1^2, \omega_2^2, \dots, \omega_n^2\}$  is the matrix of natural frequencies squared, ordered so that  $\omega_{i+1} \geq \omega_i$ . It is evident from Eq. (6) that  $[\Phi]^{-1} = [\Phi]^T M$ .

For many purposes, it is convenient to introduce a transformation of Eq. (1) into the modal state space associated with Eq. (2) as follows:

$$z = [\Phi]\eta, \quad \eta = [\Phi]^T M z \quad (7)$$

Use of Eqs. (6, 7) in Eq. (1) yields the modal space equation of motion

$$\ddot{\eta} + [\Phi]^T C [\Phi] \dot{\eta} + [\omega^2] \eta = [\Phi]^T D u \quad (8)$$

We now define the  $2n \times 1$  modal state vector as  $x = \text{col}\{\eta, \dot{\eta}\}$ , so that the  $n$  second order system of equations, Eq. (8), can be written as a system of  $2n$  first order equations in the standard form

$$\dot{x} = Ax + Bu, \text{ with } A = \begin{bmatrix} 0 & I \\ -[\omega^2] & -[\Phi]^T C [\Phi] \end{bmatrix}, \quad B = \begin{bmatrix} 0 \\ [\Phi]^T D \end{bmatrix} \quad (9)$$

We note that Eq. (9) is normally preferred, for problems in structural dynamics especially, to the common alternative (configuration) state vector  $s = \text{col}\{z, \dot{z}\}$ , with the corresponding differential equation

$$\dot{s} = \hat{A}s + \hat{B}u, \text{ with } \hat{A} = \begin{bmatrix} 0 & I \\ -M^{-1}K & -M^{-1}C \end{bmatrix}, \quad \hat{B} = \begin{bmatrix} 0 \\ M^{-1}D \end{bmatrix} \quad (10)$$

One issue should be obvious, but nonetheless is not universally appreciated, it is *material* to address which of Eqs. (1), (8), (9), or (10) is used to design feedback control laws. The algebraic equivalence of these equations is clear, but the modal space differential equations are more amenable to qualitative analysis and, as a consequence, it is easier to address such issues as order reduction, truncation, spillover, robustness etc., than is the case if one pursues control designs based upon configuration space equations. This is because the lower frequency modes are generally more accurately converged (when using, for example, a finite element discretization process to arrive at Eq. (1)) and are typically more important physically. Of course, generic developments addressed to Eqs. (1, 10) include Eqs. (8, 9) for appropriate specialization of the coefficient matrices.

In this chapter, we are primarily concerned with design of the constant  $m \times r$  gain matrix  $G$  for a linear feedback control law of the form  $u = Gy$ . We assume that sensors are available to measure the  $r \times 1$  output vector  $y$  which is linearly related to the modal state vector  $x$  according to

$$y = Sx = S_1\eta + S_2\dot{\eta} \quad (11)$$

We address the general case in which there are fewer actuators than the number of modes we wish to control ( $m < n$ ). It is important to note that introduction of real actuator hardware generally changes the mass and stiffness characteristics of the system, and also increases the order of the dynamical system (since the controller seldom directly commands force or moment, but, for example, voltage, in the case of a control moment gyro electric motor). Therefore, we note that having the number of actuators equal to the order of the controlled system can be assumed for the sake of idealized analysis, but cannot usually be realized, since the actuators themselves are dynamical systems. Obviously, the path to determine Eqs. (1) or an augmentation thereof, should include accounting for finite contributions of the apriori modeled actuators and sensors to  $M$  and  $K$ , and, at least in the "end game" of a controller optimization study, should account for the dynamics of the sensors and actuators. Furthermore, we feel that we must include the case of a relatively small number of actuators to control at least a moderately high-dimensioned system, because this pattern is present in many problems of current practical interest. The  $m=n$  case will remain, of course, a special case of the more general developments.

Substituting the feedback law  $u = Gy$  into Eq. (9), and using Eq. (11), the *closed loop system* becomes

$$\dot{x} = [A + BGS]x \quad (12)$$

The closed loop eigenvalue problem (associated with  $x = \psi e^{\lambda t}$  solutions of Eq. (12)) is

$$\det[A + BGS - \lambda I] = 0 \Rightarrow \text{eigenvalues: } \{\lambda_1, \lambda_2, \dots, \lambda_{2n}\} \quad (13)$$

$$[A + BGS - \lambda_i I]\psi_i = 0 \Rightarrow \text{right eigenvectors: } \{\psi_1, \psi_2, \dots, \psi_{2n}\} \quad (14)$$

where advantage can be taken of the fact that eigensolutions  $(\lambda, \psi)$  occur in complex conjugate pairs, for the  $A, B$  matrices of Eq. (9), and that the  $2n \times 1$  eigenvectors  $\psi_i$  have the following structure:

$$\psi_i = \text{col} \{\psi_i, \lambda_i \psi_i\}, \text{ where } \psi_i \text{ is an } n \times 1 \text{ complex vector.} \quad (15)$$

Consider the situation wherein a subset of the structural parameters are available for re-design. Let the structural design parameter vector be denoted  $p$ , the system matrices typically have an algebraic functional dependence upon  $p$ :  $M = M(p)$ ,  $C = C(p)$ ,  $K = K(p)$ ,  $D = D(p)$ ,  $S = S(p)$ , and as a consequence, the eigenvalues and eigenvectors depend upon  $p$ . Using methods of [2], it is straight-forward to determine the partial derivatives of the open loop, undamped eigensolution pairs  $(\omega_i, \phi_i)$  with respect to  $p$ , through differentiation of Eqs. (4, 5). These sensitivities can be propagated, by the chain rule, through differentiation of Eqs. (13, 14) to the analogous partial derivatives of the closed loop eigensolution pairs  $(\lambda_i, \psi_i)$ . Except for isolated events of repeated eigenvalues, the

eigenvalues and eigenvectors usually behave continuously, albeit nonlinearly, as a function of  $p$ . The vector  $p$  can, in principle, contain any combination of the system's mass, stiffness, damping, geometric parameters, actuator locations, etc., but we consider  $p$  to be the subset of those parameters actually available for re-design. Also, depending upon the design methodology being used, it is possible [3,23,46] to include the elements of the gain matrix  $G$  in the design vector  $p$ . Several nonlinear optimization methods have been developed [3,23,46] and used successfully to optimize controlled closed loop performance by simultaneously or sequentially re-designing selected structural, sensor, and actuator parameters.

For generality of the developments below, we will only selectively specialize our results to reflect the structure of  $A, B$ , e. g., Eqs. (9), to accommodate, for example additional equations to model actuator dynamics. Therefore, we assume that the dimension of our state space is  $N \geq 2n$ . Due to the complexity and nonlinearity of the *simultaneous* structure/controller design process, we first address the design of a linear state feedback controller, via minimization of quadratic criteria and via a recently developed class of *robust eigenstructure assignment* methods, for the case of a *specified* structure. Since the stability and response characteristics of a given structure are fully dictated by the closed loop eigenvalues and eigenvectors, we can cast the control design problem as a quest for some optimal gain matrix ( $G$ ) which generates a desirable set of eigenvalues and eigenvectors. In the case that we seek to impose a set of equality constraints upon the eigenvalues and eigenvectors (i., e., *eigenstructure assignment*), there is a recently developed theoretical foundation which underlies existence, uniqueness and computation of  $G$ . The principle existence issues are captured in a theorem due to Srinathkumar[4,47]:

**Eigenstructure Assignment Theorem.** *Given a controllable and observable dynamical system described by  $\dot{x} = Ax + Bu, y = Sx, u = Gy$ , {having  $N$  states,  $r$  sensors, and  $m$  actuators, with matrices  $B$  and  $S$  of full rank}, then through choosing appropriate values for the elements of  $G$ ,  $\max(m,r)$  closed-loop eigenvalues (of  $A + BGS$ ) can be assigned,  $\max(m,r)$  eigenvectors can be partially assigned, and  $\min(m,r)$  entries in each eigenvector can be arbitrarily assigned.*

Typically, for a controllable system, a given set of eigenvalues can be assigned by an infinity of  $G$  matrices, the remaining freedom in selecting  $G$  can be used to optimize the eigenvectors to achieve robustness or some other objectives. During the past decade, a number of eigenstructure assignment (or "pole placement") formulations and algorithms have been developed and demonstrated [5-12]. The algorithms available, up until very recently, have been restricted to application to very low order systems, due to various computational difficulties. The most recent literature emphasizes gain determination which imposes eigenvalue placement constraints and result in control robustness (low sensitivity of stability and/or performance measures with respect to modeling errors and disturbances), it is fortuitous that well-conceived concepts which seek out robust controls often leads to algorithms for gain computation which are numerically robust, as well. The reason for this good fortune lies in the fact that good conditioning of the modal matrix of closed loop eigenvectors has been found to be the crucial necessary condition for robustness of the numerical processes to determine the control gains as well as low

sensitivity of the resulting closed loop performance and stability indices. In the present chapter, we present several attractive concepts and associated algorithms for efficient determination of judicious gain matrices ( $G$ ), which are "good" from one of the three viewpoints:

- (i) guarantees stability of the nominal unperturbed plant, and maximizes a measure of controlled system robustness (equivalently, minimizes an appropriately defined sensitivity measure).
- (ii) satisfies property (i), and also satisfies prescribed constraints on placement of the closed loop eigenvalues and eigenvectors.
- (iii) satisfies conditions (ii), subject to constraints on average control energy and average state error energy.

For perspective and contrast, we first review briefly, in the following section, more familiar optimal control methodology (based upon minimizing a quadratic performance measure in the time domain). We also present a generalization of the classical developments which are more attractive computationally. Several of the results developed are subsequently used in the *multi-criterion optimization* discussions. From one viewpoint, the commonly applied steady state (i.e., constant gain) optimal linear-quadratic regulator is just one (of many) ways to parameterize a family of stable feedback controllers. We believe that the indirect connection (i.e. through the Riccati equation and solution of the closed loop eigenvalue problem) of the weight matrices in a performance index, to the robustness properties and eigenvalue placement are significant practical disadvantages of the conventional quadratic regulator in comparison to the *robust eigenstructure assignment* methods we discuss below. We develop eigenstructure assignment methods which, in essence, exchange the solution of the algebraic nonlinear Riccati equation for solution of strictly linear algebraic equations. Judicious use of numerically stable singular value decomposition methods lead to reliable algorithms. The implications for control of high order systems are most significant.

## Generalized Quadratic Regulators

The cornerstone of *modern* control theory, judging from the frequency of application, are linear, constant gain feedback controls determined by minimizing the index

$$J = \int_0^{\infty} (x^T Q x + u^T R u) dt, \text{ with weight matrices } Q = Q^T \geq 0, R = R^T > 0 \quad (16)$$

subject to satisfying  $\dot{x} = Ax + Bu$ . This is widely known as the linear-quadratic regulator (LQR) problem. The solution is determined from Pontryagin's Principle[13]; it requires computing the positive-definite  $P$  matrix which satisfies the algebraic Riccati equation

$$PA + A^T P - PBR^{-1}B^T P + Q = 0 \quad (17)$$

The associated optimal control gain matrix is then

$$G = -R^{-1}B^T P \quad (18)$$

The existence of the solution for  $P = P^T > 0$  is theoretically guaranteed for controllable systems, but existing algorithms [14,15] and computer implementations limit practical applications to systems of moderate order ( $< 100$ ), and of course, numerical difficulties may be encountered for even low dimensioned systems, depending upon the conditioning of the solution (which measures *how controllable* the system is, in a numerical sense). We now consider two recently developed generalizations of the quadratic regulator.

### Generalized LQR - Form 1:

Recently [16], the following generalized quadratic index was introduced

$$J = \int_0^\infty \begin{Bmatrix} x \\ u \end{Bmatrix}^T W \begin{Bmatrix} x \\ u \end{Bmatrix} dt, \text{ with } W = W^T = \begin{bmatrix} Q + N^T R N & N^T R \\ R N & R \end{bmatrix} > 0, Q = Q^T \geq 0, R = R^T > 0 \quad (19)$$

The Pontryagin necessary conditions (minimizing Eq. (19), subject to  $\dot{x} = Ax + Bu$ ) lead to the generalized Riccati equation

$$P\bar{A} + \bar{A}^T P - PBR^{-1}B^T P + Q = 0, \text{ where } \bar{A} = A - BN \quad (20)$$

and the optimal gain matrix

$$G = -R^{-1}B^T P - N \quad (21)$$

Reference [16] shows that an arbitrary real  $m \times n$  cross coupling weight matrix ( $N$ ) can be chosen without de-stabilizing the closed loop system. Notice that  $N$  is essentially a pre-feedback gain, so it is evident that some redundancy must exist. In particular, [16] investigated  $N = [UD^T\Phi \quad VD^T\Phi]$ , with  $U, V$  positive semi-definite  $m \times m$  matrices; this choice has been found attractive. We present results which demonstrate significant advantages can be realized in comparison to using the classical LQR developments.

### Generalized LQR - Form 2:

The second modification of the LQR problem, introduced in [16], is obtained by minimizing the quadratic index

$$J = \int_0^\infty \begin{Bmatrix} x \\ u \end{Bmatrix}^T W \begin{Bmatrix} x \\ u \end{Bmatrix} dt, \text{ with } W = W^T = \begin{bmatrix} Q + N^T R N + PBR^{-1}B^T P & N^T R \\ R N & R \end{bmatrix} > 0, \quad (22)$$

subject to  $\dot{x} = Ax + Bu$ . The motivation for the final term ( $PBR^{-1}B^T P$ ) in the 1,1 partition of  $W$  is that it results in an important simplification of the necessary conditions. In fact the the  $P$  matrix satisfies the (much simpler) linear algebraic Lyapunov equation

$$P\bar{A} + \bar{A}^T P + Q = 0, \text{ where, as before } \bar{A} = A - BN, \quad (23)$$

instead of the nonlinear algebraic Riccati Eq. (20). The optimal gain matrix is still given by Eq. (21). Notice that we choose the weights  $Q, R, N$ , and solve for  $P$  from Eq. (23), only then can we fully specify  $W$  in Eq. (22), since it depends upon  $P$ .

The weight matrices  $Q, R$ , and  $N$  should be parameterized in such a way as to guarantee their definiteness properties and the controllability of  $\bar{A}$ , this insures the existence of a solution for a positive-definite  $P$  satisfying Eq. (23). This problem is solved [16] by the Choleski factorizations

$$Q = L_1 L_1^T, \quad R^{-1} = L_2 L_2^T, \quad U = L_3 L_3^T, \quad V = L_4 L_4^T, \quad N = [UD^T \Phi \quad VD^T \Phi] \quad (24)$$

with

$$L_1 = \begin{bmatrix} q_{11}^2 & 0 & \dots & 0 \\ q_{21} & q_{22}^2 & \dots & 0 \\ \vdots & \vdots & \vdots & \vdots \\ q_{nn} & q_{nn} & \dots & q_{nn}^2 \end{bmatrix}, \quad L_2 = \begin{bmatrix} r_{11}^2 & 0 & \dots & 0 \\ r_{21} & r_{22}^2 & \dots & 0 \\ \vdots & \vdots & \vdots & \vdots \\ r_{m1} & r_{m2} & \dots & r_{mm}^2 \end{bmatrix},$$

$$L_3 = \begin{bmatrix} u_{11}^2 & 0 & \dots & 0 \\ u_{21} & u_{22}^2 & \dots & 0 \\ \vdots & \vdots & \vdots & \vdots \\ u_{m1} & u_{m2} & \dots & u_{mm}^2 \end{bmatrix}, \quad L_4 = \begin{bmatrix} v_{11}^2 & 0 & \dots & 0 \\ v_{21} & v_{22}^2 & \dots & 0 \\ \vdots & \vdots & \vdots & \vdots \\ v_{m1} & v_{m2} & \dots & v_{mm}^2 \end{bmatrix}. \quad (25)$$

The high dimensionality of the parameter space consisting of the above, or any complete, weight matrix parameterization has proven a significant obstacle to numerical implementations with fully populated weight matrices. In [16], we introduced a *minimum modification homotopy* strategy for tuning the above matrices and demonstrated successful implementations. This method is employed where appropriate in the numerical studies reported below. While the high dimensionality of the weight matrices creates difficult problems, the assignment of these matrices is essentially the same hurdle which faces users of the classical LQR developments. However, the overwhelming majority of the historical numerical implementations have been accomplished with diagonal weight matrices (often, simply using a scalar multiple of an identity matrix), due the expense of ad hoc searches in the weight matrix space. However, faced with actuator saturation constraints, eigenvalue placement constraints, and other practical issues, constrained searches for "judicious weights" are often necessary and have been widely used. While any positive-definite choices for the weight matrices satisfy (for controllable systems) the most important necessary condition of placing all closed-loop eigenvalues in the stable left-half plane, finding the *optimal* optimal regulator (vis-a-vis robustness, stability margins, etc.) generally forces one to deal with the perhaps uncomfortable truth that the LQR weight matrices are simply one elegant, and not especially convenient, parameterization of stable controllers. On the other hand, numerical experience suggests that there are typically broad regions in the weight space which give good control laws of moderate sensitivity.

While the above modification (Form 2) of the LQR does not eliminate the necessity to find judicious weight matrices, it evident that eliminating the Riccati equation in favor of the simpler Lyapunov equation is extremely useful, especially for high dimensioned applications, since the Riccati equation solution is by far the most computationally challenging part of the LQR design process. Thus the LQR approach can be pursued



without having to solve the Riccati equation, while at the same time retaining a more general family of weight matrices than the classical formulation. Numerical studies reported below and in [19] indicate that optimized, fully populated weight matrices lead to more flexible eigenvalue placement and robustness optimization than the classical LQR formulation. In [3,23], analytical methods are presented for computation of partial derivatives of the closed loop eigenvalues and eigenvectors with respect to structural parameters and weight matrix parameters, consistent with the above developments.

For controller design problems more naturally posed in the space of eigenvalues and eigenvectors of the closed loop system, the LQR approach is cumbersome, since the choice of weight matrices dictates "everything", and substantial computation lies between specification of these matrices and evaluation of the corresponding eigenvalues, eigenvectors, and robustness properties. Thus attempts to impose eigenspace or robustness constraints involves expensive nonlinear iterations in a high-dimensioned parameter space. While successful algorithms have been demonstrated, all known algorithms suffer from local versus global convergence and related difficulties. In view of these truths, it is natural to ask the question: "Is there a more direct way to parameterize a family of stable controllers, defining both the gain matrix and closed loop robustness characteristics of the system as explicit functions of the closed-loop eigenvalues and eigenvectors?" The affirmative answer to this question leads to eigenstructure assignment concepts [5-12], and in particular the methodology in the following section.

## Robust Eigenstructure Assignment

In this section, an approach is developed for defining judicious sets of objective closed-loop eigenvectors, consistent with the system dynamics and prescribed placement of the corresponding closed loop eigenvalues. These objective eigenvectors are usually not exactly achievable, so we make use of orthogonal projection and least square methods to find admissible eigenvectors near the desired eigenvectors. The most general developments apply to systems having arbitrary structure in the first order system matrices ( $A, B$ ), however, we develop specialized versions of the methods to take advantage of the structure introduced when we begin with a system of second order differential equations of the form of Eqs. (1) or (8).

### Sylvester's Equation

For the standard first order state space system ( $\dot{x} = Ax + Bu$ , with  $u = Gx$ ), the right eigenvalue problem, for the special case that  $S = I$  can be rearranged from Eq. (14) as

$$[A - \lambda_i I]\psi_i = BG\psi_i \quad (26)$$

or, defining the  $m \times 1$  vector  $h_i$  as

$$h_i = G\psi_i \quad (27)$$

then Eq. (26) is put in the form of Sylvester's equation

$$[A - \lambda_i I]\psi_i = Bh_i \quad (28)$$

The matrix equivalents of Eqs. (27) and (28) are

$$H = G\Psi \quad (29)$$

and

$$A\Psi - \Psi\Lambda = BH, \quad \text{with } \Lambda = \text{diag} \{\lambda_1 \dots \lambda_N\}. \quad (30)$$

We can assign eigenvalues and eigenvectors using Eqs. (29) and (30) by first choosing the desired closed-loop eigenvalue matrix  $\Lambda$ , then selecting the parameter matrix  $H$ . Eq. (30) can then be solved for the corresponding eigenvector matrix  $\Psi$ . Finally the corresponding gain matrix  $G$  is obtained through solution of Eq. (29). Unfortunately, an arbitrary choice for the  $H$  matrix does not usually generate an attractive set of closed loop eigenvectors; occasionally the eigenvectors are so poorly conditioned that computing an accurate  $G$  from Eq. (29) is not possible.

### Projection Concepts

Since an arbitrary selection of  $H$  is not appropriate, we consider here choices which have a high probability of generating attractive gain matrices. It is well-known[17] that the condition number of the closed loop modal matrix  $k(\Psi) = \|\Psi\| \|\Psi^{-1}\|$  is a measure of robustness(sensitivity) of the placement of the closed loop eigenvalues. Recent research [41,46], proves that the stable system  $\dot{x} = Ax$  remains stable in the presence of an arbitrary model error  $E(t)$  in  $\dot{x} = (A + E)x$ , if  $E$  satisfies the inequality

$$\|E\| \leq \max [-\text{Real}(\lambda(A))] / k(\Psi) \equiv \mu \quad (31)$$

Thus for fixed eigenvalue positions, minimizing  $k(\Psi)$  is equivalent to maximizing the system robustness. More generally, we use  $\mu$  in Eq. (31) as the robustness measure. This motivates our search for an  $H$  matrix to give as-small-as possible condition number  $k(\Psi)$ . An attractive algorithm results if we seek the  $H$  matrix which makes the  $\Psi$  matrix of closed loop eigenvectors lie as close as possible to a prescribed, well-conditioned matrix. Notice, if we select some target set of well-conditioned closed loop eigenvectors  $\hat{\Psi} = [\hat{\Psi}_1 \dots \hat{\Psi}_N]$ , then we can use Eq. (28), or equivalently Eq. (30) to solve for the  $\hat{H}$  which most nearly (in the least squares sense, for example) produces the desired eigenvectors  $\hat{\Psi}$ . Upon substituting this solution for the  $H$  matrix and re-solving Eq. (30) for  $\Psi$ , we will find  $\Psi \neq \hat{\Psi}$ , exactly, with the degree of approximation being problem dependent. However, the  $\Psi$  matrix lies as near  $\hat{\Psi}$  as possible (in the least square sense), and is typically well-conditioned. The gain matrix  $G$  calculated from solution of Eq. (29) with  $\Psi$  and  $\hat{H}$  will, however, place the eigenvalues exactly, to within arithmetic errors. We now address the crucial issue of how to select the target vectors  $\hat{\Psi}$ .

From Eq. (28), it is evident that the admissible eigenvectors are mapped from the  $m$  dimensioned column space of  $(A - \lambda_i I)^{-1}B$ . This space can be spanned by a unitary matrix  $U_i$ , so through appropriate choice of  $h_i$ , we can generate all admissible eigenvectors from the projection

$$\Psi_i = U_i h_i \quad (32)$$

Assuming the target eigenvectors are denoted  $\hat{\Psi}_i$ , then the  $h$  which minimizes the residual  $\|\hat{\Psi}_i - U_i h\|$  is given by

$$\hat{h} = U_i^H \hat{\Psi}_i \quad (33)$$

and so the feasible eigenvectors nearest  $\hat{\Psi}_i$  are obtained by substituting Eq. (33) into Eq. (32), which gives

$$\Psi_i = U_i U_i^H \hat{\Psi}_i \quad (34)$$

with the corresponding residual vector

$$\Delta_i = \hat{\Psi}_i - \Psi_i = (I - U_i U_i^H) \hat{\Psi}_i \quad (35)$$

There are several computationally stable algorithms available for calculation of the unitary basis matrices  $U_i$ , three being:

(i) construct the singular value decomposition (SVD[18]) of the matrix

$$(A - \lambda_i I)^{-1} B = [U_{1i} \ U_{2i}] \begin{bmatrix} \Sigma_i & 0 \\ 0 & 0 \end{bmatrix} \begin{bmatrix} V_{1i}^H \\ V_{2i}^H \end{bmatrix} \text{ and define } U_i = U_{1i},$$

(ii) construct the QR decomposition [19] of

$$(A - \lambda_i I)^{-1} B = [Q_{1i} \ Q_{2i}] \begin{bmatrix} R \\ 0 \end{bmatrix} \text{ and define } U_i = Q_{1i}, \text{ or}$$

(iii) construct the SVD of the matrix

$$B^* (A - \lambda_i I) = [U_{1i} \ U_{2i}] \begin{bmatrix} \Sigma_i & 0 \\ 0 & 0 \end{bmatrix} \begin{bmatrix} V_{1i}^H \\ V_{2i}^H \end{bmatrix} \text{ and define } U_i = V_{2i},$$

where  $B^*$  is the orthogonal complement of  $B$  (i.e.,  $B^* B = 0$ ).

For the calculations of the present discussion, we follow [16] and adopt the third approach, since it does not require inversion of  $(A - \lambda_i I)$ .

The above developments still do not tell us how to choose the  $\hat{\Psi}_i$  judiciously. Following [12,19], we state the following optimization problem:

$$\text{Find } \{\hat{\Psi}_i, i = 1, 2, \dots, N\}, \text{ to minimize } J = \sum_{j=1}^N \Delta_j^H \Delta_j \quad (36)$$

subject to

$$\hat{\Psi}_i^H \hat{\Psi}_j = \delta_{ij}, i, j = 1, 2, \dots, N \quad (37)$$

Unfortunately, solutions of this problem requires iterative numerical optimization; it can be attacked by nonlinear programming. To avoid this iteration (or to initiate it with an excellent starting solution), we seek to directly specify near-feasible and well-conditioned target eigenvectors  $\hat{\Psi}_i$ . We begin by arranging the  $N$  sets of unitary basis matrices into a global matrix  $S$  as

$$S = [U_1, U_2, \dots, U_N] \quad (38)$$

and take the singular value decomposition of  $S$  to obtain the SVD factorization

$$S = \hat{U} \Sigma V^H \quad (39)$$

where  $\hat{U}$ ,  $V$  are the left and right matrices of singular vectors and  $\Sigma$  is the diagonal matrix of singular values. We hypothesize that the left unitary vectors of  $S$  provides an attractive set of target eigenvectors, it remains to determine which of the column vectors

of  $\hat{U}$  should be assigned as  $\hat{\Psi}_i$ , to each of the  $N$  least squares problems of Eqs. (33) - (35). We summarize the algorithm as follows:

- Step 1. For  $i = 1, 2, \dots, N$ , compute a unitary basis matrices  $U_i$  which span the column space of  $(A - \lambda_i I)^{-1} B$ .
- Step 2. Find the left singular vectors  $\hat{U} = [\hat{u}_1, \dots, \hat{u}_N]$  of  $S$ , and define these as the set of target vectors:  $\{\hat{\Psi}_i = \hat{u}_i, \text{ for } i = 1, 2, \dots, N\}$ .
- Step 3. For  $i = 1, 2, \dots, N$ , determine the index  $k$  for the  $i$ th target eigenvector  $\hat{\Psi}_k$  to minimize  $|\Delta_i| = |(I - U_i U_i^H) \hat{\Psi}_i|$ , store this index in an array  $index(i) = k$ , and remove  $\hat{\Psi}_k$  from the set of target vectors.
- Step 4. Calculate the admissible eigenvectors as the least square projection
 
$$\Psi_i = U_i U_i^H \hat{\Psi}_k, \quad k = index(i) \quad (40)$$
- Step 5. Determine the  $H$  matrix and the gain matrix  $G$  by solving Eqs. (30, 29).

### Specializations for Second Order Equations

One conceptually attractive modification of the above for the case of mechanical systems described by Eq. (1), with  $N = 2n$ , is to select the open-loop eigenvectors as the target eigenvector set  $\hat{\Psi}_i = col\{\phi_i, \lambda_i \phi_i\}$ . For a general mass matrix and for general prescription of the closed loop eigenvalues, these target eigenvectors do not constitute a unitary set and are not guaranteed to be well-conditioned. However, numerical experience reveals that the associated gain matrices usually have a relatively small (but not generally a minimum) norm, and also the condition number of the closed loop modal matrix is relatively small (but again, not generally a minimum). The algorithm for this case is obtained by replacing Steps 1 and 2 by calculation of the open loop eigenvectors  $\phi_i$ , and the target vectors  $\hat{\Psi}_i = col\{\phi_i, \lambda_i \phi_i\}$ .

More generally, we wish to take full advantage of the structure of the eigenspace for the case of full state feedback and a mechanical vibrating system of the form of Eq. (1), it is not necessary to limit attention to selection of the open loop eigenvectors as the target vectors; there are obviously an infinity of other possibilities. We can specialize the above developments into a  $N = 2n$  dimensional state space, but can also work exclusively with  $n \times n$  modal matrices for the original second derivative system. Let the feedback matrix be partitioned into position and velocity gains as  $G = [G_1 \ G_2]$ , so the control is given by

$$u = G_1 z + G_2 \dot{z} \quad (41)$$

Equation (1) becomes

$$M\ddot{z} + C\dot{z} + Kz = D[G_1 \ G_2] \begin{Bmatrix} z \\ \dot{z} \end{Bmatrix} \quad (42)$$

and the associated eigenvalue problem has the form

$$[\lambda_i^2 M + \lambda_i C + K] \psi_i = D[G_1 \ G_2] \begin{Bmatrix} \psi_i \\ \lambda_i \psi_i \end{Bmatrix} \quad (43)$$

Analogous to the development of Sylvester's equation for first order systems, we define

$$h_i = [G_1 \ G_2] \begin{Bmatrix} \psi_i \\ \lambda_i \psi_i \end{Bmatrix} \quad (44)$$

For eigenvalues assigned to positions other than their open loop locations, the inverse of Eq. (43) exists and we can determine the admissible eigenvectors generated by the infinity of possible assigned eigenvalues and  $h_i$  parameter vectors as

$$\psi_i = [\lambda_i^2 M + \lambda_i C + K]^{-1} D h_i \quad (45)$$

Notice that enforcing the structure of the modal eigenvectors results in only an  $n \times 1$  vector  $\psi_i$  being parameterized by  $h_i$  instead of a  $2n \times 1$  vector  $\begin{bmatrix} \psi_i \\ \lambda_i \psi_i \end{bmatrix}$  for the equivalent first order development. Upon calculating well-conditioned admissible vectors  $[\psi] = [\psi_1 \dots \psi_n]$ , i. e., those nearest a target unitary set  $[\bar{\psi}]$  (we have used as targets the open loop eigenvectors and also, the left singular vectors from singular value decomposition of  $S$  from Eq. (38) with the new definition  $U_i = [\lambda_i^2 M + \lambda_i C + K]^{-1} D$ ), we can determine the least square solutions for  $h_i$  and the closest admissible  $[\psi]$ . We can then form the  $2n \times 2n$  modal matrix

$$\Psi = \begin{bmatrix} [\psi] & \overline{[\psi]} \\ [\psi]\Lambda & \overline{[\psi]}\Lambda \end{bmatrix}, \Lambda = \text{diag}(\lambda_1 \dots \lambda_n), \quad (46)$$

where  $(\bar{\phantom{x}})$  denotes the complex conjugate of  $(\phantom{x})$ ; the control gain matrix  $G$  is then obtained by solving the linear system  $H = G\Psi$ , where the  $m \times 2n$   $H$  matrix is constructed from the  $h$  parameter vectors as

$$H = \begin{bmatrix} h_1 & h_2 & \dots & h_n & \bar{h}_1 & \bar{h}_2 & \dots & \bar{h}_n \end{bmatrix} \quad (47)$$

For the special case that the number of actuators are assumed equal to the number of controlled modes ( $m=n$ ), and for the special case that the target eigenvectors are taken to be the open loop undamped eigenvectors, we have established[19] analytical and numerical equivalence of the above to eigenvalue assignment by independent modal space control (IMSC[20]). We demonstrate in subsequent numerical results of the present chapter that selecting the open loop eigenvectors as the target set, while attractive in many cases, does not generally lead to the smallest gain norm or the optimally conditioned closed loop eigenvalue problem, even for the  $m=n$  case.

The above developments can be generalized and extended, as in [12], to apply in principle to the case of output feedback. While output feedback algorithms via direct eigenstructure assignment have been developed and successfully tested, the existence of solutions is not generally guaranteed. The design of gain matrices for the general output feedback problem remains an area of ongoing research, iterations are usually required to

converge upon practical designs, and convergence is not guaranteed, even if the formal theoretical conditions for assignability are satisfied. Convergence of virtually all non-linear programming algorithms can be greatly enhanced by use of homotopy algorithms [21]; these approaches are also attractive, because they have been successfully demonstrated for simultaneous structure and controller design optimization. In optimization of regulator designs (for a specified structure), and especially in simultaneous structure/controller optimization problems, we must face the truth that there are typically several competing definitions or measures of optimality, and that a systematic methodology is needed to study the design tradeoffs between competing measures of optimality. This family of problems and recently developed approaches are reviewed in the following section.

## Multiple Criterion Optimization

As developed above, the closed loop eigenvalues and eigenvectors can be assigned to achieve direct control over the controlled systems time constants and robustness properties. It is evident that the  $H$  matrix is usually redundant, vis-a-vis imposing eigenvalue constraints, and therefore we were free to seek small condition numbers of the closed loop modal matrix to enhance robustness properties.

More generally, there are often many competing performance issues which play a significant role in practical applications. We seek a graphical method for displaying *tradeoff surfaces* to allow the control designer visual evaluation of the nature of multiple performance compromises implicit in a given controller design problem. We develop below a method for constructing such surfaces; each point on the surface corresponds to a numerical setting on the feedback gains. It is evident that implicitly we are seeking to determine and display *families* of optimal solutions (instead of optimizing a single *point* design), so that particular implementations can be selected with as much visibility of the macroscopic and microscopic performance tradeoffs as is possible. Following [45,16], the tradeoff: *robustness* versus *average control energy* versus *average state error energy* is judged to be of fundamental significance, therefore we concentrate upon developing methods to determine and display this multiple criterion tradeoff surface. In this development, *average* is taken to mean the *expected* value of a quantity, for a distribution of initial conditions having a specified covariance.

### Objective Functions and Their Derivatives

Consider a closed loop system described by Eq. (12) with  $S=I$ . Assume that the initial conditions are distributed with prescribed covariance  $E[x_0 x_0^T] = X_0$ . We define time *expected error energy* ( $J_s$ ) and the *expected error energy* ( $J_u$ ) as

$$J_s = E \left\{ \int_0^\infty x^T Q_s x dt \right\}, \text{ and } J_u = E \left\{ \int_0^\infty u^T Q_u u dt \right\}, \text{ with } Q_s = Q_s^T \geq 0, Q_u = Q_u^T \geq 0 \quad (48)$$

The  $Q$  matrices should be selected to make the integrands correspond to physical energy measures. These two integrals can be evaluated as shown below by solution of Lyapunov equations. Letting  $\Psi$  denoting the matrix of closed loop eigenvectors, then the corresponding modal state vector  $\xi$  is related to  $x$  and  $u$  by  $x = \Psi \xi$  and  $u = H \xi$ . The modal space closed loop system is

$$\dot{\xi} = \Lambda \xi, \text{ with } \xi_0 = \Psi^{-1} x_0, E[\xi_0 \xi_0^H] = \Psi^{-1} X_0 \Psi^{-H} \quad (49)$$

Equations (48) become

$$J_s = E \left\{ \int_0^\infty \xi^H \Psi^H Q_s \Psi \xi dt \right\} \text{ and } J_u = E \left\{ \int_0^\infty \xi^H \Psi^H Q_u \Psi \xi dt \right\} \quad (50)$$

As is developed in [19,45], these integrals are evaluated as follows

$$J_s = \text{trace}[(\Psi^{-H} P_s \Psi^{-1}) X_0] \text{ and } J_u = \text{trace}[(\Psi^{-H} P_u \Psi^{-1}) X_0] \quad (51)$$

where  $P_s, P_u$  are solutions of the Lyapunov equations

$$P_s \Lambda + \Lambda^H P_s + \Psi^H Q_s \Psi = 0 \text{ and } P_u \Lambda + \Lambda^H P_u + H^H Q_u H = 0 \quad (52)$$

The solutions are written in index form as

$$P_s(i,j) = -(\lambda_i^H + \lambda_j)^{-1} \psi_i^H Q_s \psi_j \text{ and } P_u(i,j) = -(\lambda_i^H + \lambda_j)^{-1} h_i^H Q_u h_j \quad (53)$$

The partial derivatives of the expected state and control energy indices with respect to the parameter vectors  $h_i$  are obtained by direct differentiation[19]. Denoting the derivative with respect to a parameter  $p_k$  by  $\Delta_k$ , the eigenvector derivatives are

$$\Delta_k \psi_i = U_i \Delta_k h_i \quad (54)$$

Clearly if we take  $p_k$  an an element of  $h_i$ , then  $\Delta_k h_i$  is a column of zeros and ones. The derivative of the inverse of the modal matrix, where needed, is obtained as

$$\Delta_k \Psi^{-1} = -\Psi^{-1} [\Delta_k \Psi] \Psi^{-1} \quad (55)$$

As a third performance measure (robustness), we adopt the condition number  $J_r$  of the closed loop eigenvectors. The condition number is easily computed and has been found to be a good measure of closed loop robustness. We use methods of [22] to compute the partial derivatives of the condition number with respect to  $h_i$ . Additional indices, such as structural mass, stiffness, and loading measures, can be introduced to accomplish structure/controller optimization tradeoffs [23]. In the numerical studies below, we report some of these tradeoffs for an example problem.

### Multiple Objective Optimization

As developed above, we have two or more performance indices (e.g.,  $J_s^*, J_u^*, J_r^*$ ) all of which we would like to minimize. Recognizing from the onset that these minimizations are almost certainly in competition, we approach the problem from a different perspective [19,45]. Suppose that we are following the eigenstructure assignment approach as developed above; we seek to optimize, in some sense, over all  $H$  matrices for a given set of closed loop eigenvalue locations. In lieu of optimization, we first direct attention to the problem of finding  $H$  to impose the equality constraints

$$J_s^* - J_s(H) = 0, s \rightarrow u, r \quad (56)$$

The values  $(J_s^*, J_u^*, J_r^*)$  are interpreted as "the best one could possibly hope for", or as design goals to be achieved as nearly as possible. Since an exact feasible solution of the problem likely won't exist, especially when aggressive, demanding goals are assigned, we begin by defining a *homotopy family* of neighboring problems with "portable" goals.

Specifically, we replace the  $(J_s^*, J_u^*, J_r^*)$  goals by a one parameter ( $\gamma$ ) family of goals as

$$\{\gamma J_s^* + (1-\gamma)J_s(H_{start})\} - J_s(H) = 0, \quad s \rightarrow u, r, \quad 0 \leq \gamma \leq 1 \quad (57)$$

Sweeping the homotopy parameter ( $\gamma$ ) from zero to unity gradually drives the portable goals from their values on the starting iteration toward the specified goals. Notice  $H_{start}$  is some arbitrary starting matrix, but most usually it is determined from an eigenstructure assignment procedure similar to that described above. Since there are typically more elements in  $H$  than the number of portable goal constraints, the corrections to  $H$  are underdetermined. For most of our implementations to date [3,6,9,23], we have used the minimum correction norm algorithm. This algorithm is a generalized Newton method which finds the minimum sum square modification of  $H$  on each iteration to satisfy the currently specified goals  $\{\gamma J_s^* + (1-\gamma)J_s(H_{start})\}$ . This process has the advantage that each iteration, for fixed  $\gamma$ , seeks a minimum change of the current design and thereby increase the likelihood of achieving convergence to solutions for the sequence of neighboring problems. Notice that the current portable goals can be assigned arbitrarily near a neighboring converged design by increasing  $\gamma$  adaptively based upon convergence progress. As  $\gamma$  is increased toward unity, it is evident that successful convergences mean that the design goals are being approached. In the event that  $\gamma$  cannot be advanced some small assign tolerance with a convergence failure due to competition between the goal constraints, the process is terminated. Of course in the event that  $\gamma$  can be increased to unity without a convergence failure, the design goals have been achieved; this unusual event usually motivates one to be more aggressive in assigning at least one of the goals  $(J_s^*, J_u^*, J_r^*)$  to a smaller value. The homotopy can be applied to sweep all goals simultaneously, or to one goal at a time (while treating the remaining goals as fixed equality constraints).

Utilizing these ideas, we have developed a nonlinear programming algorithm [19] to generate the family of solutions which can be interpolated to form multiple objective performance tradeoff surfaces. We seek to establish a surface in  $(J_s^*, J_u^*, J_r^*, H)$  space, each point of which corresponds to the  $H$  (or, implicitly, the  $G$ ) which optimizes robustness (e. g., minimizes the condition number  $J_r^*$ ) for fixed values of the expected state error energy and control energy  $(J_s^*, J_u^*)$ . The overall process is outlined as follows:

- Step 1. Select the robustness index as the primary objective function, optimize it over a prescribed region of  $(J_s^*, J_u^*)$  space with  $(J_s^*, J_u^*)$  constrained only by upper and lower bounds.
- Step 2. Initiating with the minimum  $J_r^*$  solution, define a neighboring grid of  $(J_s^*, J_u^*)$  values; the grid values are treated as a sequence of equality constraints, while  $J_r^*$  is minimized for each pair of fixed  $(J_s^*, J_u^*)$  points on the grid, specifically
  - 2.1. Set values for the goals  $(J_s^*, J_u^*)$  to a point on the selected grid.



2.2. Determine minimum norm corrections to  $H$  and sweep  $\gamma$  to drive  $J_r^*(\gamma)$  as small as possible, subject to the equality constraints

$$J_s^* - J_s(H) = 0, \quad J_u^* - J_u(H) = 0$$

Save the resulting family of converged solutions  $(J_s^*, J_u^*, J_r^*, H)$ , if the  $(J_s^*, J_u^*)$  grid is complete, then go to step 3, otherwise, move to the next point on the grid and return to step 2.1.

Step 3. Interpolate the converged  $(J_s^*, J_u^*, J_r^*, H)$  data to establish the multiple criterion tradeoff surface.

The convergence achieved in Step 1 is typically, but not always, on the boundary of the admissible  $(J_s^*, J_u^*)$  region. Also, convergence to local extrema sometimes occurs. Since the first optimization is used to establish the departure point for the construction of the performance tradeoff, it is obvious that this solution is crucial. Therefore, it is important to vary the starting  $H$  and take all obvious steps to increase confidence that the global optimum has been achieved. The family of local constrained optimizations at Step 2.2 should be done with small convergence tolerances to make the surface numerically uniquely defined. The density of points in the  $(J_s^*, J_u^*, J_r^*, H)$  space required for accurate interpolation of the performance surfaces is problem-dependent and is obviously controlled directly by the user-selected  $(J_s^*, J_u^*)$  grid. We suggest cubic spline interpolation between the converged points to approximate the surface. Prudent verifications should be done in which interpolated designs for  $H$  or  $G$  (e. g., midway between the points on the grid) are computed and used to verify that the closed loop system's actual stability and performance properties are interpolated with sufficient precision. We illustrate these ideas in the numerical studies discussed below.

## Numerical Examples of Robust Controller Design and Multiple Objective Optimization

### Definition of System Models for Example Sets I and II

In order to illustrate several issues associated with controller design via the LQR based formulations and the robust eigenstructure assignment algorithm, we present numerical results for two sets of models: i) Set I (various parameter values for a 6th order mass-spring system, Table 1) and ii) Set II (various reduced order models for a flexible space structure). The mass and stiffness matrices for the first set of examples are chosen as

$$M = \text{diag}[m_{11}, m_{22}, m_{33}], \quad K = k \begin{bmatrix} 2 & -1 & 0 \\ -1 & 3 & -2 \\ 0 & -2 & 2 \end{bmatrix}$$

and the open-loop eigenvalues for the second example are given in Table 2.

### Eigenstructure Assignment

To study the performance of the robust eigenstructure assignment algorithm, several models are selected from Set I, in particular, we choose four variations of the system's mass matrix. For these Set I cases, the number of control inputs are chosen equal to the number of modes (i.e.,  $D=I$ ). From the second set of examples, several reduced order (modal space) models are obtained by truncating at different mode numbers of increasing frequency. The specifications of all eight models and the desired eigenvalues for each model are given in Tables 1 and 2.

For these structural systems, we tested the projection method (See associated discussion Eqs. (32)-(47)) using as target vectors a unitary basis (Algorithm I) and using as target vectors the open-loop eigenvectors (Algorithm II), and finally, using the IMSC pole placement technique (Algorithm III [20]). We summarize the condition number of the eigenvector matrix and Frobenius norm of the gain matrix obtained by using each model in Tables 3 and 4. For the flexible structure, the result of the IMSC method is not reported since we elect to hold the number of controllers fixed ( $m=6$ ) and thus IMSC can not be rigorously applied to control  $> 6$  modes without introducing additional actuators.

As shown in Table 3, the identical results were obtained by Algorithms II and III for Models 1-4. For systems with same number of controllers as number of modes, Algorithm II is equivalent to the IMSC method, since the open-loop modal matrix (Model 1), the condition numbers obtained by all the three algorithms were exactly the same. For this case, Algorithm I, however, generated a different gain matrix and since the unitary basis vectors employed as target vectors in the projection step did not coincide with the unitary open-loop modal vectors. For Model 4, we summarize the two gain matrices as follows:

#### Algorithm I Gain Matrix (using unitary set of target closed loop eigenvectors):

$$G = \begin{bmatrix} -6.801 & 10.000 & 0.000 & 363.299 & 0.000 & 0.000 \\ 10.000 & -16.664 & 20.000 & 0.000 & 36.517 & 0.000 \\ 0.000 & 20.000 & 6.934 & 0.000 & 0.000 & 5.189 \end{bmatrix}$$

#### Algorithms II and III Gain Matrix (using open loop eigenvectors as target set):

$$G = \begin{bmatrix} 6.666 & -3.333 & 0.000 & 396.842 & -32.917 & -0.305 \\ -3.333 & 10.000 & -6.666 & -32.901 & -41.009 & -4.803 \\ 0.000 & -6.666 & 6.666 & -0.305 & -4.803 & 5.142 \end{bmatrix}$$

For all models of the first example set, Algorithm I performed superior or equal to the others in the sense that the resulting feedback system is less sensitive. The reason is that the conditioning of the open-loop modal matrices depend on the mass matrices. From these observations, we conclude that the open-loop modal matrix is not generally the optimal choice for target eigenvectors, vis-a-vis minimizing the gain norm or the robustness index, for systems with an arbitrary mass and stiffness matrices.

Test results for Models 5-8 are interesting since these are consistent with many practical systems which have a smaller number of actuators than the number of modes we wish to control. As shown in Table 4, Algorithm I performs better than Algorithm II as regards conditioning (robustness) of closed-loop eigenvectors.

**Table 1. Test Example Set I (Spring Mass Systems)**

MODEL* NO.	MASS MATRIX	DESIRED EIGENVALUES	
		Freq ( $\omega$ )	Damping ( $\zeta$ )
1	M = diag[1,1,1]	$\omega_1 = 1.44$	$\zeta_1 = \zeta_2 = \zeta_3 = 0.5$
		$\omega_2 = 4.47$	
		$\omega_3 = 6.92$	
2	M = diag[100,1,1]	$\omega_1 = 0.89$	$\zeta_1 = \zeta_2 = \zeta_3 = 0.5$
		$\omega_2 = 2.33$	
		$\omega_3 = 6.76$	
3	M = diag[1000,100,1]	$\omega_1 = 0.09$	$\zeta_1 = \zeta_2 = \zeta_3 = 0.5$
		$\omega_2 = 0.95$	
		$\omega_3 = 4.70$	
4	M = diag[10000,100,1]	$\omega_1 = 0.03$	$\zeta_1 = \zeta_2 = \zeta_3 = 0.5$
		$\omega_2 = 0.31$	
		$\omega_3 = 4.49$	

\* All the models have the same stiffness matrix

**Table 2 Test Example Set II (Flexible Space Structure)**

MODE NO.	OPEN-LOOP EIGENVALUE		DESIRED CLOSED-LOOP EIGENVALUE	
	Freq ( $\omega$ )	Damping ( $\zeta$ )	Freq ( $\omega$ )	Damping ( $\zeta$ )
1	$4.90 \times 10^{-4}$	.001	6.78	.70
2	$4.46 \times 10^{-4}$	.001	8.17	.70
3	$4.27 \times 10^{-4}$	.001	8.98	.70
4	$2.57 \times 10^{-4}$	.001	8.79	.70
5	$1.95 \times 10^{-4}$	.001	11.97	.70
6	$1.07 \times 10^{-4}$	.001	15.26	.70
7	22.36	.001	16.46	.70
8	20.49	.001	18.40	.70
9	20.86	.001	20.10	.70
10	42.28	.001	21.86	.70
11	42.28	.001	23.87	.70
12	61.95	.001	67.23	.70

**Table 3. Performance of Eigenstructure Assignment Algorithms  
on Set I Examples**

MODEL NO.	Algorithm I*			Algorithm II*		Algorithm III*	
	$k(\phi^o)^{**}$	$k(\phi^c)^{**}$	$ G _F$	$k(\phi^c)^{**}$	$ G _F$	$k(\phi^c)^{**}$	$ G _F$
1	6.92	9.26	50.91	9.26	19.83	9.26	19.83
2	7.10	9.04	68.39	10.39	45.08	10.39	45.08
3	20.79	10.08	121.79	22.31	128.96	22.31	128.96
4	72.94	31.79	367.04	73.46	402.12	73.46	402.12

\* Algorithm I - Projection method using unitary basis vectors  
as target closed-loop eigenvectors.

Algorithm II - Projection method using open-loop eigenvectors  
as target closed-loop eigenvectors.

Algorithm III - IMSC method

\*\* The superscript o and c denote open-loop and closed-loop, respectively,  $k(\cdot)$  denotes the condition number.

**Table 4. Performance of Eigenstructure Assignment Algorithms  
on Set II Examples**

MODEL NO.	No. of States and No. of Controls		Algorithm I*			Algorithm II*	
	n	m	$k(\phi^o)^{**}$	$k(\phi^c)^{**}$	$ G _F$	$k(\phi^c)^{**}$	$ G _F$
5	12	6	9600	31.	234,000	32.	208,000
6	16	6	9600	347.	786,749	461.	906,380
7	20	6	9600	8,342.	11,904,002	14,753.	7,913,951
8	24	6	9600	11,406.	5,920,422	25,495.	10,730,075

\* Algorithm I - Projection method based on unitary vectors.

Algorithm II - Projection method based on open-loop eigenvectors.

\*\* The superscripts o and c denote open-loop and closed-loop respectively.

**Table 5. Robustness Index Optimization**

ALGORITHM	STATE ENERGY $J_s$	CONTROL ENERGY $J_u$	ROBUSTNESS INDEX $J_r^*$
I. LQR (N=0)	3.0	0.368	3.270
I'. LQR (N≠0)	3.0	0.385	3.150
II. Modified LQR	3.0	0.842	3.050
III. Sylvester's Method	3.0	1.000	3.040

\*  $J_r$  is minimized subject to the inequalities  $0 \leq J_s \leq 3$ ,  $0 \leq J_u \leq 2$ .

### Multi-Criterion Eigenstructure Optimization

Multiple objective optimization and trade-off surface generation requires many nonlinear iterations and are computationally expensive processes. It is presently reasonable to carry out this conceptually attractive idea only for low to moderate order systems. To illustrate the ideas, we restrict our attention to the sixth order spring-mass system with the mass matrix,  $M = \text{diag}[1, 1, 2]$ , and the stiffness matrix scaling factor  $k=1$ . This sixth order model has two controllers, i.e., the control input matrix is given by

$$D^T = \begin{bmatrix} 1 & 0 & 0 \\ 0 & 0 & 1 \end{bmatrix}$$

For this system, we consider three feedback design algorithms: Algorithm A (generalized LQR in Form 1, Eqs. (19)), Algorithm B (LQR in Form 2, Eq. 22) and Algorithm C (Sylvester's method, Eqs. (29), (30)). For Sylvester's method, the closed loop eigenvalues are also considered design parameters and tuned in the optimization process, so that with this additional feature [16], the comparison of its performance with the two LQR algorithms will be consistent. For Algorithm A, we considered two cases: one with  $N=0$  (this reduces to the classical LQR), another with  $N \neq 0$ . The performance of each feedback design algorithm is compared for multi-criterion optimizations of three design objectives: expected state error energy, control energy and robustness measure (condition number of the eigenvector matrix).

Arbitrary initial design parameters are selected for Algorithm B and corresponding initial parameters for Algorithms A and C are generated so that the three algorithms are initiated with the same control gains and closed loop system. The parameter values at the beginning of the iterations are summarized below:

Design Parameters for Algorithm B:

$$L_1 = \text{diag}[\cdot 5^2, \cdot 5^2, \cdot 5^2, \cdot 5^2, \cdot 5^2, \cdot 5^2], L_2 = L_3 = L_4 = \text{diag}[1, 1]$$

Weight Matrices and Initial State Covariance Matrix:

$$Q_u = Q_s = X_0 = I$$

Homotopy Step Size and Convergence Limit:

$$\alpha_{i+1} = \alpha_i + 0.1, |\Delta p| < 10^{-3} \text{ convergence tolerance for each } \alpha_i.$$

Using the three step numerical algorithm described above, the optimization of the primary objective,  $J_r$  (condition number of eigenvectors), was first performed subject to satisfying the specified admissible region constraining equations for the state error energy and control energy:  $0 \leq J_s \leq 3, 0 \leq J_u \leq 2$ . The results of this step are given in Table 5, where it can be seen that the optimum  $J_r$ 's obtained by each algorithm occurred on the boundary of the feasible region at the same state error energy level  $J_s = 3.0$ , however the  $(J_u, J_r)$  values were different. Starting each algorithm at the point obtained by minimizing  $J_r$ , grids of neighboring points in the  $(J_s, J_u)$  space were defined. At each grid point,

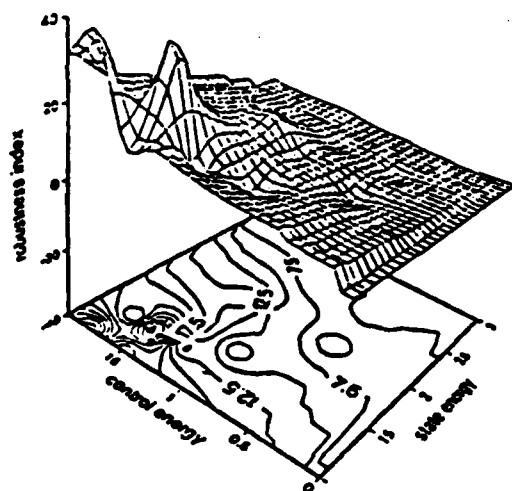


**Figure 1. Multi-Criterion Tradeoff Surface:  
Classical LQR Control ( $N=0$ )**

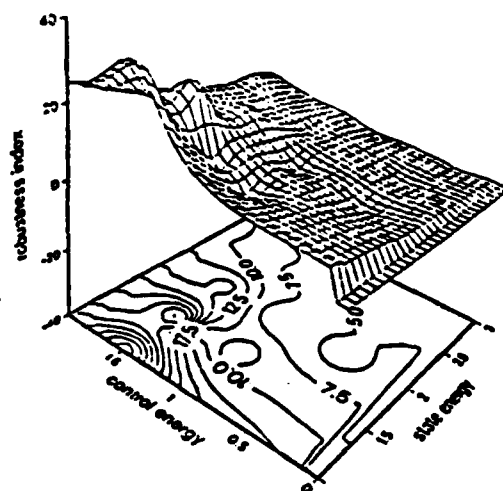


**Figure 2. Multi-Criterion Tradeoff Surface:  
Generalized LQR Control Form 1 ( $N \neq 0$ )**

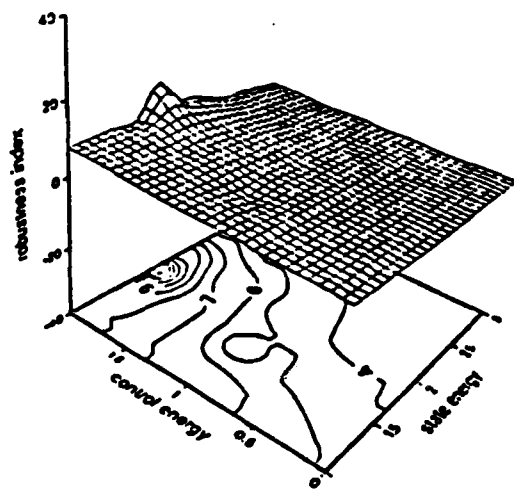


**Figure 3. Multi-Criterion Tradeoff Surface:  
Generalized LQR Regulator Form 2**

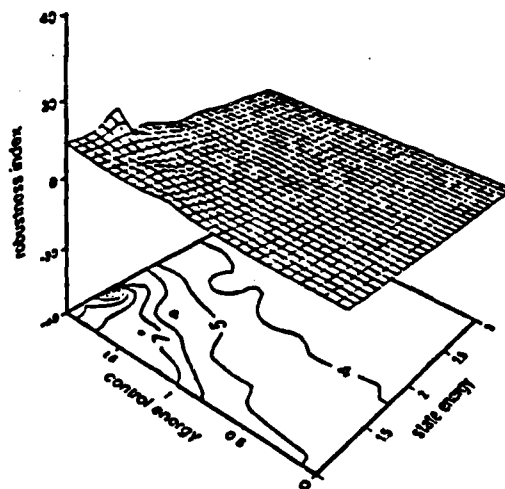


**Figure 4. Multi-Criterion Tradeoff Surface:  
Robust Eigentructure Assignment  
via Sylvester's Equation**

the primary objective  $J_r$  was optimized while constraining  $J_s$  and  $J_u$  to remain constant at a point on the grid, so that points on the surfaces of Figures 1-4 can be interpreted as constrained minima of the robustness index  $J_r$  (minimum  $J_r$  for fixed  $J_s, J_u$ ).

For all three algorithms, Figs. 1-4 show that the expected state error energy and robustness index are obviously competing each other for same control energy level. We also observe that there is a significant trade-off relation between control energy and the robustness index, especially for small state energy ( $J_s < 1$ ). As can be seen in Figs. 1-4, the surface generated by using the classical LQR (Algorithm A) is much more irregular than those of the others, which may be due to more nonlinear constraining equations, e.g., the nonlinear Riccati equation instead of linear Lyapunov equation. When only diagonal elements of the  $QR$  matrices were iterated, it was not possible to generate a complete trade-off surface since the accessible region in  $(J_s, J_u)$  space was found to be severely limited. Comparing Figs. 3 and 4, we conclude that the multi-criterion surfaces of Algorithms B and C are approximately the same. In fact, the Lyapunov equation can be viewed as a special type of Sylvester equation.

Several observations made from these numerical results are summarized as follows:

- 1) For all the cases, the expected state error energy and robustness index were found to be strongly competing objectives.
- 2) The LQR design with "cross-coupling" weights ( $N$  matrix) in the criterion produces more regular tradeoff surfaces and offers more choices of the feedback gains than that standard LQR design. However, the  $N$  matrix increases the redundancy in the sense that the number of weight parameters are increased compared to the number of elements in  $G$ .
- 3) For the cases studied, the modified LQR formulation and Sylvester's method performed approximately the same in the sense that both methods generated similar near-planar performance tradeoff surfaces, which are judged more attractive than the conventional LQR results. These two algorithms also are more easily implemented. An attractive feature of the Sylvester approach is the direct fashion in which the eigenvalues may be assigned to arbitrary points in the complex plane.

## Simultaneous Structure-Controller Design Optimization

The above developments all share the underlying assumption that the nominal structural design is being held fixed, i.e., the above developments are concerned with design of robust controllers for a *fixed* structural design. Recently [3,23,26,27,29,32,33,36-38,46] there had been considerable effort to unify structural design and controller design into a unified optimization problem. This research has met with some success, but it is fair to say that the unified methodology remains in an early stage of development. It is easy to extrapolate that there is a widespread need for this methodology since a trend is evident that extensive "paper studies" and optimization of preliminary structure and controller designs will precede most missions for large space structures.

This simultaneous structure-controller optimization is complicated by the following issues, relative to separate structure or controller optimization: (i) one must simultaneously consider several competing performance measures, (ii) the dimensionality of the independent and dependent parameter and/or function spaces is higher, there are typically many inequality constraints, and (iii) the simultaneous consideration of structural mass, geometry, and stiffness parameters along with sensor/actuator locations, and control law parameters inherently leads to highly nonlinear problems. Recently [23,32,33,38,46] progress has been made in developing an attractive nonlinear programming algorithm which has proven successful on a variety of problems. These algorithms combine the homotopy idea with Sequential Linear Programming (SLP). The motivation for using linear programming (LP) lies in the fact the (i) numerous inequality constraints are handled with ease, (ii) standard, reliable algorithms are available which are applicable to LP problems with several hundred unknowns [39,40,42,43], and (iii) it has been shown [32,39,40] to be competitive or superior to more popular penalty function approaches which use quasi-Newton or conjugate gradient correction schemes. For these reasons, we will overview the SLP approach and some recently obtained results.

### Unified Optimization Problem

We consider the closed loop, output-feedback controlled system of Eqs. (12)-(15). We address the most general situation wherein the  $d \times 1$  global structure/controller design vector  $p$  is given by

$$p = \text{col} \{m_1, \dots, m_{n_1}; s_1, \dots, s_{n_2}; a_1, \dots, a_{n_3}; g_1, \dots, g_{n_4}\} \quad (58)$$

with  $m = \text{col} \{m_1, \dots, m_{n_1}\}$ , structural model parameters,  $M=M(m)$ ,  $K=K(m)$ ,  $C=C(m)$

$s = \text{col} \{s_1, \dots, s_{n_2}\}$ , sensor location and model parameters,  $S = S(s)$

$a = \text{col} \{a_1, \dots, a_{n_3}\}$ , actuator location and model parameters,  $D = D(a)$

$g = \text{col} \{g_1, \dots, g_{n_4}\}$ ,  $= \text{vec}\{G\}$ , control gains,  $G = G(g)$

consider the situation where all independent and dependent constraint functions (e.g. eigenvalue constraints) are expressed as  $f(p) = f^*$ ,  $f \leq f^*$ ,  $f \geq f^*$ , all three possibilities are captured by the notation

$$f(p) \{ \leq, =, \geq \} f^* \quad (59)$$

The objective or desired values  $f^*$  are considered specified. In addition to performance bounds, eigenvalue constraints, and other dependent geometry constraints, Eq. (59) includes all structural constraints (i.e., negative thickness is not allowed), and requirements that sensors and actuators be located on the structure! Thus the dimension of Eq. (59) is often much higher than the  $p$  vector itself, even though only a subset of the inequalities are likely to be active at the final converged solution. In addition to the constraints of Eq. (59), we consider another set of dependent functions  $\{J_1(p), J_2(p), \dots\}$  to be performance measures which we are interested in extremizing subject to conditions of Eq. (59). Since we do not expect to be able to extremize minimize all functions simultaneously, we anticipate from the onset the necessity of tradeoff studies. In particular, we consider three performance objectives:



$$I \text{ minimize eigenvalue sensitivity } = J_1 = J_1(p) = \sum_{i=1}^n \sum_{j=1}^d \left| \frac{\partial \lambda_i}{\partial p_j} \right|^2 w_{ij}, w_{ij} > 0 \quad (60)$$

$$II \text{ maximize Patel/Toda robustness } = J_2 = J_2(p) = \max [Re(-\lambda)] / k(\psi) \quad (61)$$

$$III \text{ minimize total mass: } J_3 = J_3(p) = \text{total mass} \quad (62)$$

To simplify the SLP discussion below, we will use  $J$  to refer to any one of the  $J_i$  unless we need to be specific.

### Sequential Linear Programming (SLP)

We begin by defining a homotopy to replace constraint objectives by portable constraints, Eq. (59) is replaced by

$$f(p) \{ \leq, =, \geq \} (1 - \gamma) f(p_{start}) + \gamma f^* \quad (63)$$

Obviously as  $\gamma$  is swept from zero to unity, we define a family of neighboring objectives which initiate at  $f(p_{start})$ , associated with our starting design vector ( $p_{start}$ ), and terminating with the prescribed objective  $f^*$ . Clearly we have  $p = p(\gamma)$ , if we seek to minimize  $J = J(p)$  subject to Eq. (63), we suppress the dependence of  $p$  on  $\gamma$ , for notational convenience. Without loss of generality, we seek to maximize  $J(p)$ .

Equation (63) and  $J(p)$  can be linearized about the current  $p$  vector to obtain the following local linear optimization problem

$$\text{Maximize } \sum_{j=1}^d \frac{\partial J}{\partial p_j} \Delta p_j = \left\{ \frac{\partial J}{\partial p} \right\}^T \Delta p \quad (64)$$

$$\text{Subject to } \left[ \frac{\partial f}{\partial p} \right] \Delta p \{ \leq, =, \geq \} (1 - \gamma) f(p_{start}) + \gamma f^* - f(p) \quad (65)$$

$$-\epsilon \leq \Delta p \leq \epsilon \quad (66)$$

Equation (66) is a step size constraint (notice  $\epsilon$  has positive elements and is an assigned vector, Eq. (66) holds element-by-element). In [23,46], the above problem is arranged in standard form for using the Simplex Linear programming algorithm, as implemented in [43]. By slowly sweeping  $\gamma$  from zero to unity and iteratively solving the above linear program to convergence for each  $\gamma$ , we have a nonlinear programming method which applies to the family of problems under consideration. In [32], the above approach is compared to more popular nonlinear programming (penalty function methods using the CONMIN quasi-Newton algorithm); it is shown to be superior vis-a-vis reliable convergence. We now consider an illustrative example due to Lim[46] and Junkins [23].

### Numerical Example of Structure/Controller Design via SLP

Figure 5 shows a two-body problem consisting of a rigid body with a flexible beam attached by a torsional spring. The nominal configuration is specified in Tables 6 and 7.

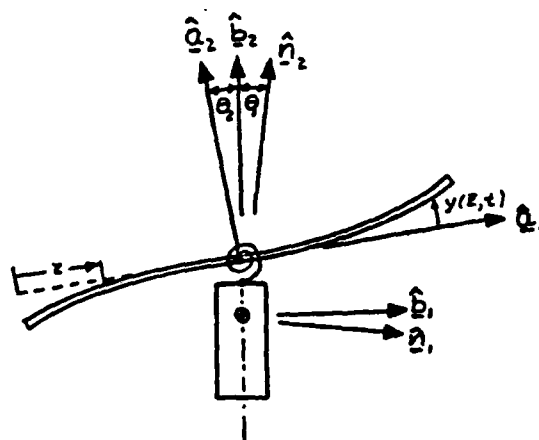


Figure 5 Two-Body Structure

Table 6. Nominal Design Variables

DESIGN VARIABLE	SYMBOL	VALUE
actuator 2 location	$a_1$	5m
actuator 3 location	$a_2$	10m
actuator 4 location	$a_3$	15m
stiffness of torsional spring	$k$	500 n-m/rad
thickness of flexible beam	$t_F$	.1m
Young's modulus of beam	$E$	$.1482 \times 10^9 \text{ N/m}^2$
mass density of rigid body	$\rho_R$	$300 \text{ kg/m}^3$
output gain elements:		
	$G(1,1), G(2,1), G(3,1), G(4,1)$	-1
	all other $G(i,j)$ elements	0

Table 7. Fixed structural parameters

PARAMETER	SYMBOL	VALUE
width of rigid body	$w_R$	1m
thickness of rigid body	$t_R$	3m
depth of rigid body	$d_R$	2m
width of flexible beam	$w_F$	20m
depth of flexible beam	$d_F$	1m
mass density of flexible beam	$\rho_F$	$1799 \text{ kg/m}^3$
sensor 1 location	$s_1$	3m
sensor 2 location	$s_2$	7m
sensor 3 location	$s_3$	13m
sensor 4 location	$s_4$	17m

Table 8. Open loop and desired closed loop damped frequencies and damping factors

MODE	OPEN LOOP		DESIRED CLOSED LOOP	
#	$\omega_d \text{ (rad/s)}$	$\zeta$	$\omega_d^* \text{ (rad/s)}$	$\zeta^*$
1	.0056	.4819E-10	.1	.7
2	.2803	.1402E-5	.3	.1
3	.3443	.1718E-5	.45	.1
4	1.241	.6204E-5	1.0	.05
5	1.768	.8839E-5	1.5	.05
6	3.981	.1990E-4	4.0	.05
7	5.004	.2502E-4	$> \omega_d^* + .1$	.02
8	8.295	.4147E-4	unconstrained	.02
9	9.902	.4951E-4	unconstrained	.02
10	14.34	.7171E-4	unconstrained	.02

**Table 9. Lower, upper and local step size bounds on design parameters**

PARAMETER	SYMBOL	VALUE
lower bounds on actuator location	$a_1^l, a_2^l, a_3^l$	0m
upper bounds on actuator location	$a_1^u, a_2^u, a_3^u$	20m
lower bounds on spring stiffness	$k^l$	5 N-m/rad
lower bound on beam thickness	$t_F^l$	.01m
upper bound on beam thickness	$t_F^u$	2m
lower bound on beam stiffness	$E^l$	.1480x10 <sup>9</sup> N/m <sup>2</sup>
upper bound on beam stiffness	$E^u$	.1496x10 <sup>9</sup> N/m <sup>2</sup>
lower bound on rigid body density	$\rho_R^l$	50 kg/m <sup>3</sup>
upper bound on rigid body density	$\rho_R^u$	1000 kg/m <sup>3</sup>
local step size bounds:		
actuator location	$\Delta a_1, \Delta a_2, \Delta a_3$	.1m
spring stiffness	$\Delta k$	30 N-m/rad
beam thickness	$\Delta t_F$	.01m
beam stiffness	$\Delta E$	.1x10 <sup>5</sup> N/m <sup>2</sup>
rigid body density	$\Delta \rho_R$	40 kg/m <sup>3</sup>
gain elements $i=1,\dots,4; j=1,\dots,12$	$\Delta G(i, j)$	10
frequency separation between mode 7 and 6	$\Delta \omega_{76}$	.1 rad/s

**Table 10. Computer execution times for various subproblems**

SUBPROBLEM	CP secs. (CYBER 170)
real, nonsymmetric left and right eigenvalue problems (20x20) using IMSL routine EIGRF	2.67
Solution of linear program (55 variables, 83 constraints) using IMSL routine ZX4LP	22.73
Compute eigenvalue derivatives $\frac{\partial \lambda_i}{\partial p_j}; i=1, \dots, 6; j=1, \dots, 55$	5.05
Compute second eigenvalue derivatives $\frac{\partial^2 \lambda_i}{\partial p_k \partial p_j}; i=1, \dots, 6; j=1, \dots, 55; k=1, \dots, 55$	159.06

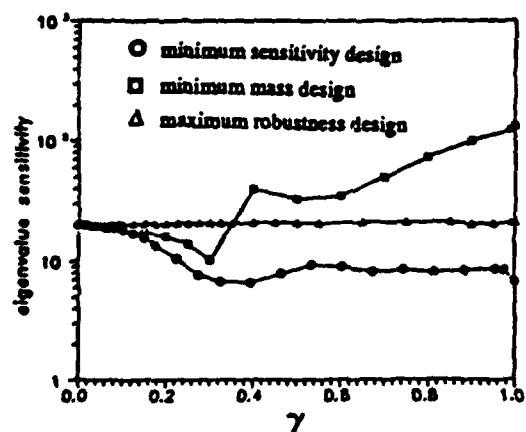


Figure 6 Convergence of Eigenvalue Sensitivity

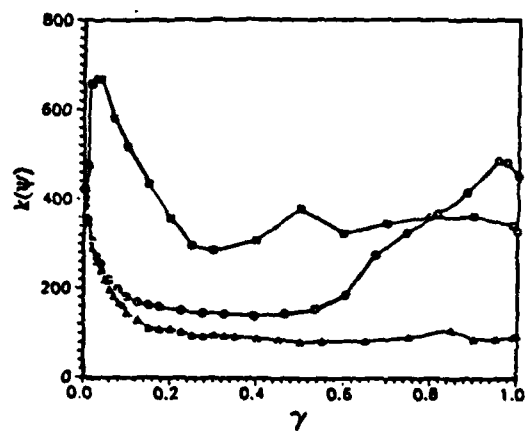


Figure 7 Convergence of Condition Number

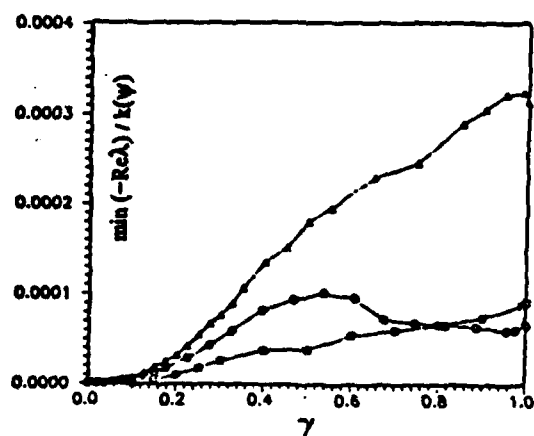


Figure 8 Convergence of Robustness Index

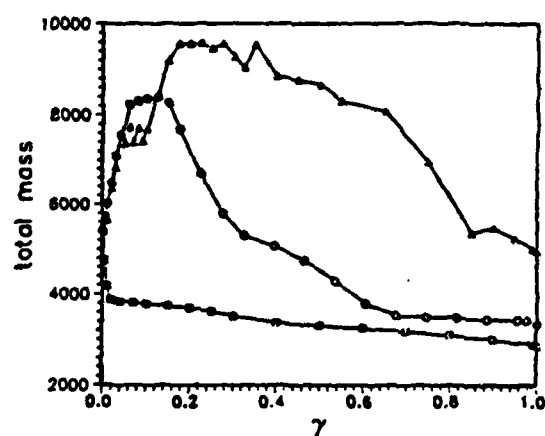


Figure 9 Convergence of Total Mass

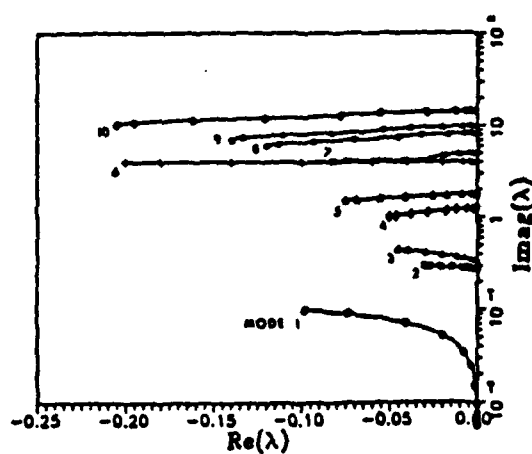


Figure 10 Closed Loop Eigenvalue Locus

**Table 11. Converged Parameters for Three Designs**

CASE I: Minimum Eigenvalue Sensitivity

CASE II: Maximum Stability Robustness Design

CASE III: Minimum Mass Design

CASE	$a_1$	$a_2$	$a_3$	$k$	$t_F$	$E$	$P_R$
I	4.924	7.878	14.72	1443	.0841	.1480E+9	51.22
II	4.797	8.924	15.48	1481	.0939	.1496E+9	262.1
III	4.087	9.795	14.75	2315	.0709	.1494E+9	50.0

**Table 12. Actual Robustness of Three Designs**

PARAMETER		PERCENT VARIATION CAUSING INSTABILITY		
		MASS DESIGN	SENSITIVITY DESIGN	ROBUSTNESS DESIGN
ACTUATOR LOCATIONS	$a_1$	6%	12%	16%
	$a_2$	1.5	9	8
	$a_3$	2.4	4	4
STRUCTURAL PARAMETERS	$k$	4	6	98
	$t_F$	3	5	10
	$E$	8	14	31
	$P_R$	6	24	28
SELECTED CONTROL GAINS	$G(1,1)$	9	9	67
	$G(1,3)$	12	50	28
	$G(2,8)$	43	31	91
	$G(3,9)$	38	51	25
	$G(4,11)$	24	8	31
55 PARAMETER AVERAGE		13%	18%	37%

Six pairs of position and velocity sensors and located on the structure, four linear motion pairs are located on the beam (Table 7) available for re-design iterations. An angle and angular-velocity measuring sensor pair is fixed to the rigid body and another to the beam mid-span. Four actuators are assumed, one torquer acts on the rigid body, the other three torquers act on the beam with their stations available for optimization. There are a total of 55 design variables free for optimization (the  $4 \times 12 = 48$  elements of the output feedback gain matrix, plus the 7 sensor, actuator, and model parameters of Table 6).

Table 8 shows the nominal system's open-loop eigenvalues for the first ten modes and some arbitrarily selected eigenspace constraints we wish to impose. Table 9 provides the additional set of inequality conditions imposed to establish Eq. (59). We considered the three performance measures of Eqs. (60) - (62) and established three separate design problems. For each case, we extremized one of the three indices, but calculated the other two for evaluation purposes.

Design I (minimum eigenvalue sensitivity) has a performance measure which involves a sum square of eigenvalue first partials. Obviously forming Eq. (64) requires eigenvalue second partials. We used the formulation of [2,3] to compute these by analytical means. As is evident in Table 10, the second partial derivative computation dominates the solution time, even in comparison to the cost of solving the linear program.

The results of the three optimizations are summarized with reference to Tables 11, 12 and Figures 6-11. Notice in Table 11 that the three sets of structural design and control gain parameters all satisfy the inequality bounds of Table 9, but the three designs are quite different. Figures 6-10 show the convergence of important quantities during the optimization/constraint enforcement process (as  $\gamma \rightarrow 1$ ). Each point on these curves represent the converged results from the SLP algorithm with  $\gamma$  held fixed. In Figure 6, it is obvious that the minimum sensitivity design I converged to a point one to three orders of magnitude less sensitive (measured locally by Eq. (60)) than the sensitivity of the maximally robust (II) and minimum mass designs (III). In Figures 7 and 8, notice that the small condition number and large robustness index are well correlated, as one would expect. Notice for  $\gamma$  small that the minimum sensitivity designs and maximum robustness designs are very close together. This is because eigenvalue sensitivity obviously dominates robustness when some eigenvalues are near the imaginary axis (the eigenvalue trajectories begin, for  $\gamma=0$ , near open-loop positions on the imaginary axis). Notice, the obvious tradeoff between robustness and mass. The mass of the minimum mass design was 2853 kgs, compared to the nominal design of 5398 kgs, the minimum sensitivity design of 3336 kg and the maximum robustness design of 4952 kg. The robust design, not surprisingly, converged to the thickest beam, the most massive rigid body and the largest Young's modulus of the three designs.

A crucial question is now considered, is the Robust Design II *really* more robust? We investigate this question by sweeping the 55 parameters away from their respective converged values (for the three designs) and record the variation for which one of the eigenvalues loci first enters the right-half plane. Table 12 summarized the three sets of

calculations. It is obvious that the actual robustness to these (highly structured) variations is most significantly increased. In [23,46], additional details are presented showing which modes were least stable (to the 55 parameter variations), consideration of a second Patal/Toda robustness measure, and a discussion of the computer implementation.

## Concluding Remarks

In this chapter we have presented significant methods for design of robust full state feedback controllers for *fixed structures*. We have also given some results for simultaneous optimization of structures and output feedback controllers. Enhanced convergence of iterative processes is achieved through the use of homotopy methods. A multi-criterion approach is followed throughout to display the multidimensional nature of optimal control. Performance tradeoff surfaces are presented which provide an attractive means for generating a family of designs displaying inherent tradeoffs between robustness, small control errors, and small controller inputs. The favorable consequences of robustness optimization upon actual robustness is studied through generation of multi-parameter root locii. Numerical examples are given which provide a basis for optimism for future development and implementations.

## Acknowledgements

This work has been the outgrowth of research sponsored by AFOSR (contract No. F49620-86-K-0014DEF), the support of A.K. Amos is greatly appreciated. Recent collaboration with Martin Marietta Aerospace (L. Morine, D. Wilks, et al.) have provided an educational opportunity to implement the robust eigenstructure algorithms to control the Rapid Retargeting and Precision Pointing experiment. We have also benefited significantly from on-going sharing of results and joint work with Dr. J.N. Juang (NASA Langley Research Center) and Dr. K.B. Lim (Kentron, Hampton, Va.).

## References

- [1] Meirovitch, L., Computational Method in Structural Dynamics, Sijthoff and Noordhoff, 1980, Rockville, Maryland, U.S.A.
- [2] Plaut, R.H. and Huseyin, K., "Derivatives of Eigenvalues and Eigenvectors in Non-Self-Adjoint Systems," AIAA Journal, Vol. 11, No. 2, pp. 250-251, Feb, 1973.
- [3] Bodden, D.S. and Junkins, J.L., "Eigenvalue Optimization Algorithms for Structure/Controller Design Iterations," AIAA Journal of Guidance, Control, and Dynamics.
- [4] Srinathkumar, S., "Eigenvalue/Eigenvector Assignment Using Output Feedback," IEEE Transactions on Automatic Control, Vol. AC-23, No. 1, 1978, pp. 79-81.
- [5] Brogan, W.L., Modern Control Theory, Quantum Publishers, Inc., New York, New York, 1974, pp. 311-315.
- [6] Bhattacharyya, S.P. and deSouza, E., "Pole Assignment via Sylvester's Equation," Systems and Control Letters, Vol. 1, No. 4, Jan. 1982, pp. 261-263.
- [7] Cavin III, R.K. and Bhattacharyya, S.P., "Robust and Well-Conditioned Eigenstructure Assignment via Sylvester's Equation," Journal of Optimal Control Applications and Methods, Vol. 4, 1983, pp. 205-212.
- [8] Potter, B. and D'Azzo, J.J., "Algorithm for Closed-Loop Eigenstructure Assignment by State Feedback in Multivariable Linear Systems," Int. Journal of Control, Vol. 27, No.6, 1978, pp. 943-947.
- [9] Moore, B.C., "On the Flexibility Offered by State Feedback in Multivariable Systems Beyond Closed-Loop Eigenvalue Assignments," IEEE Transaction on Automatic Control, vol. AC-21, 1976 pp. 689-692.
- [10] Kautsky, J., Nichols, N.K. and Van Dooren, P., "Robust Pole Assignment in Linear State Feedback," Int. Journal of Control, Vol. 41, No. 5, 1985, pp. 1129-1155.
- [11] Wonham, W.M., "On Pole Assignment in Multiinput, Controllable Linear Systems," IEEE Transactions on Automatic Control, Vol. AC-12, 1976, pp. 660-665.
- [12] Juang, J-N, Lim, K. B., and Junkins, J.L., "Robust Eigensystem Assignment," preprint of a paper submitted to 1987

AIAA Guidance and Control Conference, Dec. 1986.

- [13] Pontryagin, L.S., Boltyanskii, V.G., Gamkrelidze, R.V., and Mishchenko, E.F., The Mathematical Theory of Optimal Processes, Interscience Publishers, Inc., New York, 1962.
- [14] Potter, J.E., "Matrix Quadratic Solution," SIAM J. of Applied Mathematics, Vol. 14, No. 3, May 1966, pp. 496-501.
- [15] Laub, A.J., "A Schur Method for Solving Algebraic Riccati Equations," IEEE Transactions on Automatic Control, Vol. AC-24, No. 6, Dec. 1976, pp. 913-921.
- [16] Rew, D.W., and Junkins, J.L., "Multi-Criterion Approaches to Optimization of Linear Regulators," AIAA Paper No. 86-2198-CP, J. of the Astronautical Sciences, to appear, Aug. 1986.
- [17] Wilkinson, J.H., The Algebraic Eigenvalue Problem, Oxford University Press, Oxford, 1965.
- [18] Dongarra, J.J., Moler, C.B., Bunch, J.R., and Stewart, G.W., LINPACK Users' Guide, SIAM Publication, Philadelphia, 1979.
- [19] Rew, D.W. and Junkins, J.L., "Robust Eigenstructure Assignment by a Projection Method: Application to Multi-Criterion Optimization," preprint of a paper submitted to 1987 AAS/AIAA Astrodynamics Conference, Feb. 1987.
- [20] Oz, H. and Meirovitch, L., "Optimal Modal-Space Control of Flexible Gyroscopic Systems," Journal of Guidance and Control, Vol. 3, Nov.-Dec. 1980, pp. 220-229.
- [21] Junkins, J.L. and Dunyak, J.P., "Continuation Methods for Enhancement of Optimization Algorithms," Presented to 19th Annual Meeting, Society of Engineering Science, University of Missouri, Rolla, Oct. 1982.
- [22] Freudenberg, J.S., Looze, D.P. and Cruz, J.B., "Robustness Analysis Using Singular Sensitivities," Int. Journal of Control, Vol. 35, No. 1, 1982, pp. 95-116.
- [23] Lim, K.B., and Junkins, J.L., "Robustness Optimization of Structural and Controller Parameters," paper No. AIAA-87-0791-CP, presented at AIAA 28th SDM Conference, Monterey, CA, April 6-8, 1987.
- [24] Balas, M.J., "Trends in LSS Control Theory: Fondest Hopes, Wildest Dreams," IEEE Transactions on Automatic Control, Vol. AC-27, No. 3, June 1982, pp. 522-535.
- [25] Bekey, I. and Naugle, J.E., "Just Over the Horizon in Space," Astronautics and Aeronautics, May 1980, pp. 64-76.
- [26] Khot, N.S., et al., "Optimal Structural Modifications to Enhance the Optimal Active Vibration Control of Large Flexible Structures," 26th Structures, Structural Dyn., and Materials Conf. Orlando, FL, April 15-17, 1985.
- [27] Junkins, J.L., Bodden D.S. and Turner, J.D., "A Unified Approach to Structure and Control System Design Iterations," Fourth International Conference on Applied Numerical Modeling, Tainan, Taiwan, Dec. 27-29, 1984.
- [28] Haftka, R.T., et al., "Sensitivity of Optimized Control Systems to Minor Structural Modifications," 26th Structures, Structural Dynamics and Materials Conference, Orlando, FL, April 15-17, 1985.
- [29] Junkins, J.L. and Rew, D.W., "A Simultaneous Structure/Control Design Iteration Method," American Controls Conference, Boston, MA, June 1985.
- [30] Dantzig, G.B., Linear Programming and Extensions, Princeton University Press, 1963.
- [31] Hadley, G., Linear Programming, Addison-Wesley Publishing Co., Inc., Reading, MA, 1962.
- [32] Horta, L.G., Juang, J-N and Junkins, J.L., "A Sequential Linear Optimization Approach for Controller Design," AIAA Paper 85-1971-CP, 1985.
- [33] Lim, K.B. and Junkins, J.L., "Minimum Sensitivity Eigenvalue Placement via Sequential Linear Programming," Proceedings of the Mountain Lake Dynamics and Control Institute, ed. by J.L. Junkins, Mountain Lake, VA, June 9-11, 1985.
- [34] Newsom, J.R. and Mukhopadhyay, "A Multiloop Robust Controller Design Study Using Singular Value Gradients," Journal of Guidance, Control, and Dynamics, Vol. 8, No. 4, July-Aug., 1985, pp. 514-519.
- [35] Howze, J.W. and Cavin, R.K., "Regulator Design with Modal Insensitivity," IEEE Transaction of Automatic Control, Vol. AC-24, No. 3, June 1979, pp. 466-9.
- [36] Raman, K.V., "Modal Insensitivity with Optimality," Ph.D. Dissertation, Drexel University, Philadelphia, PA, 1984.
- [37] Raman, K.V. and Calise, A.J., "Design of an Optimal Output Feedback Control System with Modal Insensitivity," AIAA Paper 84-1940, AIAA Guidance and Control Conference, Seattle, WA, Aug. 20-22, 1984.
- [38] Lim, K.B. and Junkins, J.L., "Optimal Redesign of Dynamic Structures via Sequential Linear Programming," Fourth International Modal Analysis Conference, Los Angeles, CA, Feb. 3-6, 1986.
- [39] Palacios-Gomez, R., Lasdon, L. and Engquist, M., "Nonlinear Optimization by Successive Linear Programming," Management Science, Vol. 28, No. 8, October, 1982, pp. 1106-1120.
- [40] Palacios-Gomez, R., "The Solution of Nonlinear Optimization Problems Using Successive Linear Programming," Ph.D. Dissertation, The University of Texas, Austin, TX, 1980.
- ⇒ [41] Patel, R.B. and Toda, M., "Quantitative Measures of Robustness for Multivariable Systems," Proceedings of JACC, San Francisco, TP8-A, 1980.
- [42] Noble, B. and Daniel, J.W., Applied Linear Algebra, Englewood Cliffs, NJ: Prentice-Hall, 1977.
- [43] IMSL Reference Manual, International Mathematical and Statistical Library, Inc., 1982.
- [44] Chen, C.T., Introduction to Linear Systems Theory, Holt, Rinehart & Winston, Inc., 1970.
- [45] Fleming, P., "Computer Aided Design of Regulators Using Multiobjective Optimization," preprint, University College of North Wales, November, 1986.
- [46] Lim, K.B., "A Unified Approach to Structure and Controller Design Optimizations," Ph.D. Dissertation, Virginia Polytechnic Institute and State University, Blacksburg, VA, 1986.
- [47] Sobel, K.M. and Shapiro, E.Y., "Application of Eigenstructure Assignment to Flight Control Design: Some Extension," AIAA J. of Guidance, Control, and Dynamics, Vol. 10, No. 1, Jan-Feb 1987, pp. 73-89.



## **ATTACHMENT 9**

# **An Identification Method for Flexible Structures**

AIAA No. 87-0745-CP

# **AN IDENTIFICATION METHOD FOR FLEXIBLE STRUCTURES**

*N. GLENN CREAMER  
JOHN L. JUNKINS*

TEXAS A&M UNIVERSITY  
COLLEGE STATION, TEXAS 77843

AIAA/ASME/ASCE/AHS  
28th STRUCTURES, STRUCTURAL DYNAMICS  
AND MATERIALS CONFERENCE

APRIL 6-8, 1987 / Monterey, California

## AN IDENTIFICATION METHOD FOR FLEXIBLE STRUCTURES

Nelson G. Creamer \*  
Texas A&M University  
College Station, Texas 77843

John L. Junkins \*\*  
Texas A&M University  
College Station, Texas 77843

### Abstract

A structural model identification method is developed for determination of the mass and stiffness matrices of an undamped structure along with the damping matrix of a lightly-damped structure. Utilizing measurements of natural frequencies, damping factors, and frequency response elements, a unique identification of the model is established through incorporation of the spectral decomposition of the frequency response function and the modal orthonormality conditions. Numerical simulations demonstrate the flexibility and potential of the proposed method.

### Introduction

Accurate knowledge of the mass, damping, and stiffness associated with a dynamical system is a key ingredient for correlating theoretical and experimental results and for designing active control schemes for vibration suppression and attitude maneuvering. Discretization of a linear continuous structure by means of finite element analysis (or other similar methods) yields the well-known mass and stiffness matrices. Although this discretization process is well defined, the resulting structural model will be only as accurate as the parameters and modeling assumptions used to characterize the structural

behavior. Also, determination of the damping matrix requires knowledge of parameters which may be difficult, if not impossible, to measure in the laboratory.

Methods for refining a priori structural models are readily available in the literature. References [1-6] address the identification of a set of physical/geometrical parameters using nonlinear least-squares and Bayesian estimation methods. The disadvantages of these methods are i) use of natural frequencies and/or mode shapes exclusively results in non-unique identification unless some parameters are "fixed" at their initial values and ii) convergence of the nonlinear estimation algorithms requires initial parameter estimates to be "close" to their true values. References [7-11] determine mass and stiffness matrix improvements to enforce exact agreement between theory and experiment. Again, use of modal information alone results in both non-unique solutions and physically unrealistic coupling. Reference [12] utilizes submatrix scale factors to improve the initial mass and stiffness matrices using modal information with the uniqueness problem once again surfacing. In references [13-15] a linear algorithm is used to identify the mass, damping, and stiffness matrices from forced time-domain response. Although there is no initial estimate required for the model and the uniqueness problem is in principle eliminated, the disadvantages are now i) the order of the resulting model is dependent upon the number of sensors used on the structure and ii) the parameter vector consists of every element of the highly redundant mass, damping, and stiffness matrices.

\* Research Associate, Aerospace Engineering

\*\*TEES Chair Professor, Aerospace Engineering  
Fellow AIAA

Copyright © 1987 by N.G. Creamer. Published by  
the American Institute of Aeronautics and  
Astronautics, Inc. with permission.

A method for identifying the mass, damping, and stiffness matrices of an undamped or lightly-damped structure using measured modal information and frequency response elements is developed in this paper. This method is designed to eliminate the problems described above and is simple to implement.

### Identification of Undamped Structures

Consider the classical second-order equations governing the motion of an undamped structural system,

$$M \ddot{u} + K u = f \quad (1)$$

where  $M$  and  $K$  are the  $n \times n$  mass and stiffness matrices,  $u$  is the  $n \times 1$  generalized coordinate vector, and  $f$  is the  $n \times 1$  generalized force vector. The initial estimates of the mass and stiffness matrices,  $M_0$  and  $K_0$ , are obtained from a standard discretization process (i.e. the finite element method). It is assumed that the following measurements, extracted from response of the actual structure, are available: (i) a set of  $m$  ( $\sim n$ ) natural frequencies  $\omega_i$ , (ii) a set of corresponding  $n \times 1$  mode shapes  $\bar{u}_i$  (or approximations from the initial structural model), and (iii) a small set of frequency response elements  $h_{jk}(\omega)$  measured throughout the frequency range of interest for the structure. The goal of the structural model identification method is to improve the initial mass and stiffness matrices such that the theoretical and experimental results are in agreement.

To begin, it is desirable to introduce the well-known spectral decomposition of the frequency response function,

$$\bar{h}_{jk}(\omega) = \sum_{r=1}^n \frac{(-i)^{j-k}}{\omega_r^2 - \omega^2} \quad (2)$$

where  $i_{jr}$  is the  $j$ th element of the  $r$ th mass-normalized mode shape which, in matrix form, satisfies

$$M \bar{u} = I \quad (3)$$

Since the true mass matrix is not known, an approximation to Eq.(2) must be utilized.

Introducing the relation

$$i_{jr} = \sqrt{\frac{2}{\omega_r}} \phi_{jr} \quad r=1,2,\dots,m \quad (4)$$

into Eq.(2), an approximation of the spectral decomposition can be written as

$$h_{jk}(\omega) = \frac{a_1}{\omega^2} + \sum_{r=1}^m \left( \frac{-i^{j-k} \phi_{jr} \phi_{kr}}{\omega_r^2 - \omega^2} \right) u_r + a_2 \quad (5)$$

In Eq.(5), the first term represents the contribution from any rigid-body modes ( $\omega_r = 0$ ), the last term represents an approximate contribution from high-frequency modes (outside the measured frequency range), and the  $u$ 's are to-be-determined modal normalization factors. By "sampling" throughout the frequency range of interest, Eq.(5) can be rearranged into the following standard linear least-squares format to identify the modal normalization factors,

$$\begin{Bmatrix} \bar{h}_{jk}(\omega_1) \\ \vdots \\ \bar{h}_{jk}(\omega_N) \end{Bmatrix} = \begin{bmatrix} \frac{1}{\omega_1^2} & L_{11} & L_{12} & \dots & L_{1m} & 1 \\ \vdots & \vdots & \vdots & \ddots & \vdots & \vdots \\ \frac{1}{\omega_N^2} & L_{N1} & L_{N2} & \dots & L_{Nm} & 1 \end{bmatrix} \begin{Bmatrix} a_1 \\ u_1 \\ \vdots \\ u_m \\ a_2 \end{Bmatrix} \quad (6a)$$

$$\text{where } L_{pq} = \frac{i_{1q} i_{pk}}{\omega_q^2 - \omega_p^2} \quad (6b)$$

Once the modal normalization factors have been determined, the orthonormality conditions that the mode shapes must satisfy can be written as

$$\begin{aligned} \bar{u}_i^T M \bar{u}_j &= \delta_{ij} / \omega_j \\ \bar{u}_i^T K \bar{u}_j &= \delta_{ij} \omega_j^2 / \omega_j \end{aligned} \quad (7)$$

To identify the true mass and stiffness matrices the following expansions are utilized [12],

$$\begin{aligned} M &= M_0 + \sum_{r=1}^p i_r M_r \\ K &= K_0 + \sum_{r=1}^q \phi_r K_r \end{aligned} \quad (8)$$

where  $M_r$  and  $K_r$  are the  $r$ th pre-determined mass and stiffness submatrices,  $\gamma_r$  and  $\delta_r$  are the to-be-determined  $r$ th mass and stiffness submatrix scale factors, and  $P$  and  $Q$  are the total number of mass and stiffness submatrices. The mass and stiffness submatrices can represent single finite elements or (more commonly) groups of common finite elements assembled into their corresponding global locations. The flexibility (and responsibility) in defining  $M_r$  and  $K_r$  in Eq.(8) is an important feature which can be used to exploit an engineer's insight explicitly. Substituting Eq.(8) into Eq.(7) and rearranging terms yields

$$\begin{bmatrix} -\tilde{\psi}_i^T M_0 \tilde{\psi}_i + \frac{1}{\alpha_i} \\ -\tilde{\psi}_i^T M_0 \tilde{\psi}_j \\ \vdots \\ -\tilde{\psi}_i^T M_0 \tilde{\psi}_j \end{bmatrix} = \begin{bmatrix} \tilde{\psi}_i^T M_1 \tilde{\psi}_i & \dots & \tilde{\psi}_i^T M_P \tilde{\psi}_i \\ \tilde{\psi}_i^T M_1 \tilde{\psi}_j & \dots & \tilde{\psi}_i^T M_P \tilde{\psi}_j \\ \vdots & & \vdots \\ \tilde{\psi}_i^T M_1 \tilde{\psi}_j & \dots & \tilde{\psi}_i^T M_P \tilde{\psi}_j \end{bmatrix} \begin{bmatrix} \gamma_1 \\ \vdots \\ \gamma_P \end{bmatrix} \quad (9a)$$

$$\begin{bmatrix} -\tilde{\psi}_i^T K_0 \tilde{\psi}_i + \frac{\omega_i^2}{\alpha_i} \\ -\tilde{\psi}_i^T K_0 \tilde{\psi}_j \\ \vdots \\ -\tilde{\psi}_i^T K_0 \tilde{\psi}_j \end{bmatrix} = \begin{bmatrix} \tilde{\psi}_i^T K_1 \tilde{\psi}_i & \dots & \tilde{\psi}_i^T K_Q \tilde{\psi}_i \\ \tilde{\psi}_i^T K_1 \tilde{\psi}_j & \dots & \tilde{\psi}_i^T K_Q \tilde{\psi}_j \\ \vdots & & \vdots \\ \tilde{\psi}_i^T K_1 \tilde{\psi}_j & \dots & \tilde{\psi}_i^T K_Q \tilde{\psi}_j \end{bmatrix} \begin{bmatrix} \beta_1 \\ \vdots \\ \beta_Q \end{bmatrix} \quad (9b)$$

where the second set of equations in Eqs.(9a) and (9b) are valid when  $i \neq j$ . Collecting Eq.(9) for each measured natural frequency yields a set of equations, linear in the unknown submatrix scale factors, which can be solved by a least-squares method provided that  $m(m+1)/2$  is greater than  $\max(P, Q)$ . Since Eq.(5) represents an approximation to the frequency response function, an iterative procedure can be used whereby the unmeasured natural frequencies and mode shapes are predicted from the present best estimate of the structural model and used in Eq.(5) in lieu of measurements.

#### Identification of Lightly-Damped Structures

If there is a small amount of damping present in a structure the structural identification method developed in the previous section can be used, in conjunction with matrix perturbation theory, to identify the mass, damping, and stiffness matrices. Consider the symmetrical state-space representation of Eq.(1) in the form

$$A \begin{bmatrix} \dot{x} \\ x \end{bmatrix} = B \begin{bmatrix} \dot{u} \\ u \end{bmatrix} + \begin{bmatrix} 0 \\ f \end{bmatrix} \quad (10a)$$

$$\text{where } A = \begin{bmatrix} -K & C \\ 0 & M \end{bmatrix} \quad B = \begin{bmatrix} 0 & K \\ K & 0 \end{bmatrix} \quad (10b)$$

If light viscous damping is introduced into the equations of motion in the form of the damping matrix  $C$ , the state-space representation is perturbed by the relation

$$B = \begin{bmatrix} 0 & I \\ K & 0 \end{bmatrix} + \begin{bmatrix} 0 & 0 \\ 0 & C \end{bmatrix} = B_0 + B_1 \quad (11)$$

where  $B_1$  becomes the perturbation matrix due to the presence of the light damping. A first-order perturbation solution to the free-response eigenvalue problem of Eq.(10) can be obtained to approximate the change in the eigenvalues due to the inclusion of the damping matrix [16].

Consider the eigenvalue problem

$$-\lambda_{0r} A_0 \phi_{0r} = B_0 \phi_{0r} \quad (12)$$

where  $A_0$  and  $B_0$  are  $2n \times 2n$  symmetric matrices and  $\lambda_{0r}$  and  $\phi_{0r}$  are the  $2n$  eigenvalues and eigenvectors. It is assumed that the eigenvectors are normalized such that

$$\phi_{0j}^T A_0 \phi_{0k} = \delta_{jk} \quad (13a)$$

$$\phi_{0j}^T B_0 \phi_{0k} = -\lambda_{0k} \delta_{jk} \quad (13b)$$

If small perturbations  $A_1$  and  $B_1$  are added to each matrix the resulting eigenvalue problem becomes

$$-\lambda_r A \phi_r = B \phi_r \quad (14a)$$

$$\text{where } A = A_0 + A_1 \quad (14b)$$

$$B = B_0 + B_1 \quad (14c)$$

$$\lambda_r = \lambda_{0r} + \lambda_{1r} \quad (14d)$$

$$\phi_r = \phi_{0r} + \phi_{1r} \quad (14e)$$

The eigenvalues  $\lambda_{1r}$  and eigenvectors  $\phi_{1r}$  represent small perturbations from their original values. Expanding Eq.(14a), utilizing Eq.(12), and neglecting second-order terms, yields the equation

$${}^T B_1 \dot{e}_{0r} + {}^T B_2 \dot{e}_{0r} = -{}^T A_1 e_{0r} - {}^T A_2 e_{0r} \quad (15)$$

$$- {}^T A_3 e_{0r}$$

Multiplying Eq.(15) by  $e_{0s}^T$  and utilizing Eq.(13) yields the relation

$$e_{0s}^T B_1 e_{0r} + e_{0s}^T B_2 e_{0r} = -e_{0s}^T A_1 e_{0r} - e_{0s}^T A_2 e_{0r} - e_{0s}^T A_3 e_{0r} \quad (16)$$

$$= -e_{0s}^T A_1 e_{0r} - \lambda_{1r} \delta_{rs}$$

It can be observed from Eq.(14) that if  $A_1$  and  $B_1$  are zero then  $\lambda_{1r} = 0$  ( $r=1,2,\dots,2n$ ) and  $e_{1r}$  becomes a scalar multiple of  $e_{0r}$ . In general,  $e_{1r}$  can be written as a linear combination of the vectors  $e_{01}, e_{02}, \dots, e_{02n}$ . To guarantee that  $e_{1r} = 0$  when  $A_1$  and  $B_1$  are zero it is assumed that the perturbation eigenvector has the form [16]

$$e_{1s} = \sum_{k=1}^{2n} c_{sk} e_{0k} \quad c_{ss} = 0 \quad s=1,2,\dots,2n \quad (17)$$

Using Eq.(17) in Eq.(16) and letting  $s=r$  results in an expression for the perturbed eigenvalues,

$$\lambda_{1r} = -e_{0r}^T [A_1 + B_1] e_{0r} \quad r=1,2,\dots,2n \quad (18)$$

In the sequel, it will be shown that Eq.(18) can be used as the central equation for identification of the damping matrix.

For a lightly-damped structure the frequency response function closely resembles that of the corresponding undamped structure except near the resonant conditions. Therefore, given a set of complex frequency response measurements from a lightly-damped structure, identification of the mass and stiffness matrices can be performed, as described in the previous section, by using the real components of the frequency response measurements and the imaginary components of the eigenvalue measurements. Again, this method will only be accurate for frequency response measurements away from the resonant conditions. Once the mass and stiffness matrices have been identified, the damping matrix can be determined as follows. First, the perturbed eigenvalues  $\lambda_{1r}$  are obtained by simply subtracting the undamped modeled eigenvalues  $e_{0r}$  from the measured eigenvalues  $\lambda_r$ .

$$\lambda_r = e_{0r}^T (\dot{e}_{0r} - \omega_{0r} e_{0r}) = i\omega_{0r} \quad (19a)$$

$$= e_{0r}^T (i\omega_{0r} - \omega_{0r}) \quad (19b)$$

where  $\omega_{0r}$  and  $\omega_r$  are the  $r$ th measured damping factor and damped natural frequency. To utilize Eq.(18) the eigenvectors  $e_{0r}$  must be normalized according to Eq.(13). In general, the form of the eigenvectors becomes

$$e_{0r} = \begin{Bmatrix} e_{0r} \\ i\omega_{0r} e_{0r} \end{Bmatrix} \quad (20)$$

where  $e_{0r}$  are the mode shapes from the identified undamped model, normalized with respect to the identified mass matrix. Therefore, using Eq.(20) in (13a) determines scale factors  $u_r$  necessary to normalize  $e_{0r}$  such that Eq.(13) is satisfied,

$$u_r^T e_{0r}^T i\omega_{0r} e_{0r} = \begin{bmatrix} -k & u \\ 0 & M \end{bmatrix} \begin{Bmatrix} e_{0r} \\ i\omega_{0r} e_{0r} \end{Bmatrix} = 1 \quad (21a)$$

$$\text{or } u_r (-e_{0r}^T k e_{0r} - \omega_{0r}^2 e_{0r}^T M e_{0r}) = 1 \quad (21b)$$

$$\text{or } u_r = -\frac{1}{2\omega_{0r}^2} \quad (21c)$$

The normalized eigenvectors  $\hat{e}_{0r}$  can now be written as

$$\hat{e}_{0r} = \frac{1}{\sqrt{2}\omega_{0r}} \begin{Bmatrix} e_{0r} \\ i\omega_{0r} e_{0r} \end{Bmatrix} \quad (22)$$

Expanding the damping matrix in a similar fashion to Eq.(8), and using Eqs.(22) and (19b) in Eq.(18) with  $A_1 = 0$  and  $B_1$  defined in Eq.(11), yields the relation

$$\lambda_r = i(\omega_r - \omega_{0r}) = -\frac{1}{2} \sum_{q=1}^Q e_{0r}^T C_q e_{0r} \quad (23)$$

where  $C_0$  is the initial damping matrix,  $C_q$  is the  $q$ th damping submatrix,  $\lambda_q$  is the  $q$ th damping submatrix scale factor, and  $Q$  is the total number of damping submatrices. Since the right side of Eq.(23) is real, only the measured damping factors  $\omega_r$  are used to identify the damping

Matrix. Perturbing Eq.(23) to solve for the submatrix scale factors yields the least-squares problem

$$\begin{bmatrix} -2\gamma_1 & \gamma_1^T C_0^* 0 \\ \vdots & \vdots \\ -2\gamma_m & \gamma_m^T C_0^* 0 \end{bmatrix} \begin{bmatrix} \gamma_1^T C_1^* 0 & \dots & \gamma_1^T C_Q^* 0 \\ \vdots & \ddots & \vdots \\ \gamma_m^T C_1^* 0 & \dots & \gamma_m^T C_Q^* 0 \end{bmatrix} \begin{bmatrix} \gamma_1 \\ \vdots \\ \gamma_Q \end{bmatrix} = \begin{bmatrix} \gamma_1^T C_0^* 0 \\ \vdots \\ \gamma_m^T C_0^* 0 \end{bmatrix} \quad (24)$$

where it is assumed that there are  $m (>0)$  measured damping factors. Solving Eq.(24) for the submatrix scale factors leads to the desired damping matrix. The advantages of this perturbation approach are twofold: identification of the damped equations of motion can be performed in configuration space without the need to solve the state-space eigenvalue problem, and the original damping matrix  $C_0$  need only represent the true damping matrix in the coupling of the elements (the original numerical values can be off by orders of magnitude).

#### Example 1

The mass and stiffness matrices are identified for the simple manipulator arm shown in Figure 1. The structure consists of two flexible appendages, rotational springs at the base and at the connecting joint, and a grip with mass and inertia.



Figure 1 Simple Manipulator Arm

The estimation process is initiated by approximate mass and stiffness matrices obtained by increasing the true mass properties by 10% and decreasing the true stiffness properties by 10%. The first five natural frequencies of the true model and the frequency response function representing the ratio of displacement at the joint to torque at the base are treated as measurements. To cast the model in

terms of mass and stiffness submatrices the following mass and stiffness element groups are chosen:

Mass: Group I Mass matrix contribution of appendage 1  
Group II Mass matrix contribution of appendage 2  
Group III Tip mass moment of inertia  
Group IV Tip mass

Stiffness: Group I Stiffness matrix contribution of appendage 1  
Group II Stiffness matrix contribution of appendage 2  
Group III Base rotational stiffness  
Group IV Joint rotational stiffness

The initial fractional modal energy contributions of each element group (obtained from  $\gamma_0^T M_r \gamma_0$  and  $\gamma_0^T K_r \gamma_0 / \omega_r^2$ ) are given in Table 1. It is apparent from examination of the potential energy distribution that the first two modes approximate those that would be obtained for a two degree-of-freedom model with rigid appendages and the higher modes represent the flexibility of the appendages.

A two step process was used to identify the structure. First, the three highest modes were used to identify mass element groups I, II, and III and stiffness element groups I and II. Then, the two lowest modes were used to identify mass element group IV and stiffness element groups III and IV. The free- and forced-response identification results (after two iterations) are provided in Table 2 and Figure 2, respectively.

#### Example 2

The mass, damping, and stiffness matrices are identified for the planar truss structure shown in Figure 3. Both internal (material) and external (atmospheric) light viscous damping is present, although there is no quantification of the amount of damping.

Copy available to DTIC does not permit fully legible reproduction

MODE	KINETIC ENERGY(%) OF MASS GROUPS				POTENTIAL ENERGY(%) OF STIFFNESS GROUPS			
	I	II	III	IV	I	II	III	IV
1	0.0	0.5	0.0	99.5	0.2	0.1	66.5	33.2
2	58.8	39.1	1.9	0.2	0.1	0.1	33.3	66.5
3	27.5	47.3	25.2	0.0	19.5	80.5	0.0	0.0
4	64.0	22.1	13.9	0.0	75.7	24.1	0.1	0.1
5	16.5	36.8	44.7	0.0	7.4	92.6	0.0	0.0

Table 1 Group Modal Energy Distributions

MODE	$\omega_n$	$\omega_{n0}$	$\omega_{nf}$
1	0.0230 rad/sec	0.0208 rad/sec	0.0232 rad/sec
2	1.062	1.0114	1.074
3	55.44	50.15	55.55
4	91.12	82.42	91.19
5	156.75	141.78	156.98

Table 2 Free-Response Identification Results

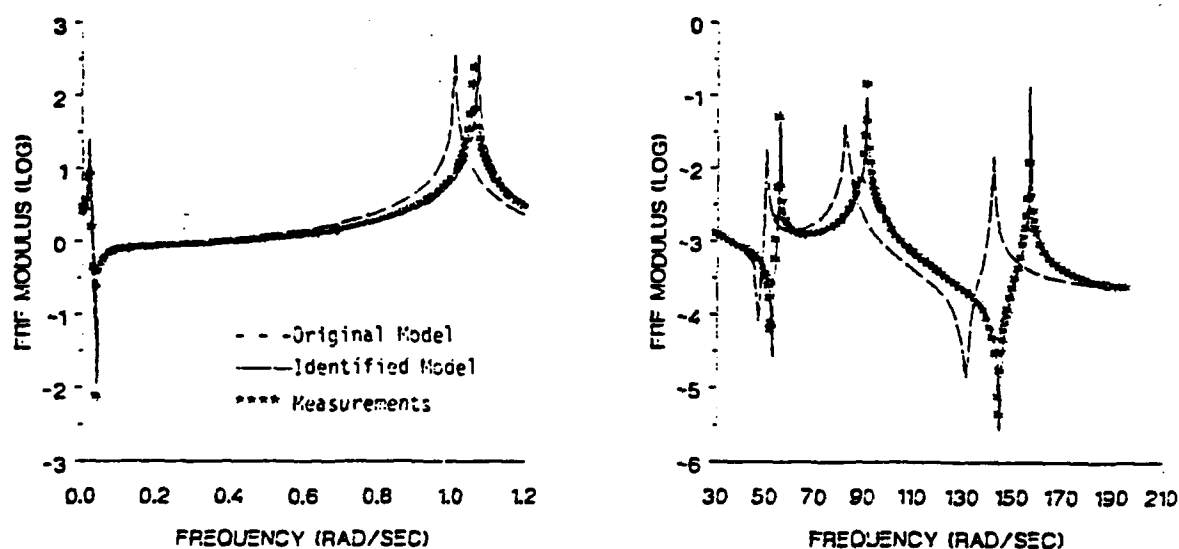


Figure 2 Forced-Response Identification Results





Figure 3 Planar Truss Structure

The measurement set consists of the first eight complex eigenvalues and transverse and longitudinal frequency response functions between points A and B. To cast the model in terms of submatrices, the following groups are chosen:

Mass and Stiffness: Group I 20 upper and lower bending elements  
Group II 20 diagonal bending/shear elements

Damping: Group I External viscous damping matrix  
Group II Internal viscous damping matrix

The mass and stiffness matrices are approximated initially by increasing the true mass properties by 10% and decreasing the true stiffness properties by 10%. The initial approximations of the external and internal passive damping matrices are only accurate in the coupling of the elements (the numerical values are off by orders of magnitude). The identification process requires two steps: (i) identification of the mass and stiffness matrices from the real components of the measured frequency response functions and the imaginary components of the measured eigenvalues, and (ii) identification of the damping matrix from the real components of the measured eigenvalues. The free- and forced-response identification results for the structure are presented in Table 3 and Figure 4, respectively.

### Conclusions

A method for identifying undamped and lightly-damped linear structures has been presented and successfully tested in two simulated examples. The advantages of the method are:

- 1) incorporation of measured frequency response functions provides a unique identification of the structural model,
- 2) all least-squares formulations are linear,
- 3) the consistency of the original model is maintained (no unmodeled coupling occurs as a consequence of the identification process),
- 4) use of submatrix scale factors limits the identification to a relatively small set of parameters,
- 5) for lightly-damped structures the identification can be performed in the (n) configuration space without the need to solve the (2n) state-space eigenproblem, and
- 6) for lightly-damped structures the original estimate of the damping matrix need only be accurate in the coupling of the elements (the numerical values can be off by orders of magnitude).

Further research efforts are currently being pursued on the effects of measurement noise in the simulated data and on application to an actual structure.

### References

1. Hendricks, S.L., Hayes, S.M., and J.L. Junkins, "Structural Parameter Identification for Flexible Spacecraft," AIAA Paper No. 84-0060, Presented at the AIAA 22nd Aerospace Sciences Meeting, Jan. 9-12, 1984.
2. Creamer, W.G., and S.L. Hendricks, "Structural Parameter Identification Using Modal Response Data," Proceedings of the Fifth VPI & SU/AIAA Symposium on Dynamics and Control of Large Flexible Spacecraft, VPI&SU, Blacksburg, VA, L. Meirovitch, ed., June 1985.
3. Collins, J.D., Hart, G.C., Hasselman, T.K., and B. Kennedy, "Statistical Identification of Structures," AIAA Journal, Vol. 12, No. 2, February, 1974, pp. 185-190.
4. Dobbs, M.W., and R.B. Nelson, "Parameter Identification of Large Structural Models - Concept and Reality," ASME Winter Annual Meeting, Boston, Massachusetts, November, 1983.

M.I.H	$\lambda$	$\lambda_0$	$\lambda_f$
1	-0.0869 + 6.76i	6.11i	-0.0870 + 6.80i
2	-0.0885 + 34.77i	31.45i	-0.0886 + 34.92i
3	-0.0895 + 87.22i	78.89i	-0.0895 + 87.41i
4	-0.1035 + 117.93i	106.67i	-0.1035 + 117.94i
5	-0.0904 + 157.11i	142.12i	-0.0904 + 157.12i
6	-0.0913 + 240.50i	217.54i	-0.0913 + 240.04i
7	-0.0924 + 333.88i	302.00i	-0.0923 + 332.64i
8	-0.1038 + 359.58i	325.25i	-0.1038 + 359.23i

Table 3 Free-Response Identification Results

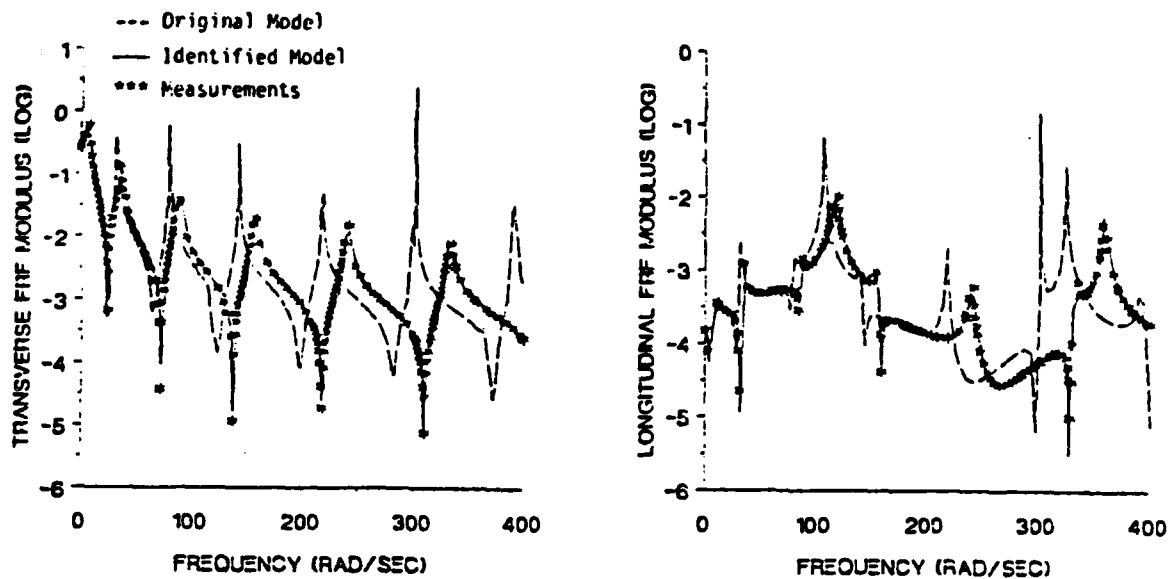


Figure 4 Forced-Response Identification Results

5. Hasselmann, T.K., "A Perspective on Dynamics Model Verification," ASME Winter Annual Meeting, Boston, Massachusetts, November, 1983.
6. Martinez, D.R., "Estimation Theory Applied to Improving Dynamic Structural Models," Sandia Report No. SAND82-0572, Sandia National Laboratories, Albuquerque, NM, November, 1984.
7. Berman, A., and W.G. Flannely, "Theory of Incomplete Models of Dynamic Structures," AIAA Journal, Vol. 9, No. 8, August, 1971, pp. 1481-1487.
8. Berman, A., and E.J. Nagy, "Improvement of Large Analytical Model Using Test Data," AIAA Journal, Vol. 21, No. 8, August, 1983, pp. 1168-1173.
9. Berman, A., "Mass Matrix Correction Using an Incomplete Set of Measured Modes," AIAA Journal, Vol. 17, No. 10, October, 1979, pp. 1147-1148.
10. Wei, F.S., "Stiffness Matrix Corrections from Incomplete Test Data," AIAA Journal, Vol. 18, October, 1980, p. 1274.
11. Chen, J.C., Kuo, C.P. and Garba, J.A., "Direct Structural Parameter Identification by Modal Test Results," 24th Structures Structural Dynamics and Materials Conference AIAA/ASME/ASCE/AAS, Part 2 of Proceedings, May 2-4, 1983.
12. White, C.W. and Maylum, B.D., "Eigensolution Sensitivity to Parametric Model Perturbations," Shock and Vibration Bulletin, Bulletin 46, Part 5, August, 1976, pp. 123-133.
13. Rajaram, S., "Identification of Vibration Parameters of Flexible Structures," Doctoral Dissertation, Virginia Polytechnic Institute and State University, Virginia, May, 1984.

## **ATTACHMENT 10**

# **Minimum Model Error Estimation for Poorly Modeled Dynamic Systems**

# **AIAA'87**

**AIAA-87-0173**

**Minimum Model Error Estimation  
for Poorly Modeled Dynamic Systems**

D. J. Mook, State Univ. of New York,  
Buffalo, NY; and J. L. Junkins,  
Texas A&M Univ., College Station, TX

**AIAA 25th Aerospace Sciences Meeting**

**January 12-15, 1987/Reno, Nevada**

For permission to copy or republish, contact the American Institute of Aeronautics and Astronautics  
1633 Broadway, New York, NY 10019

D. Joseph Mook\*  
State University of New York at Buffalo  
Buffalo, New York

and

John L. Junkins\*\*  
Texas A and M University  
College Station, Texas

### Abstract

A novel strategy (which we call "minimum model error" estimation) for post-experiment optimal state estimation of discretely-measured dynamic systems is developed and illustrated for a simple example. The method is especially appropriate for post-experiment estimation of dynamic systems whose presumed state governing equations are known to contain or suspected of containing errors. The new method accounts for errors in the system dynamic model equations in a rigorous manner. Specifically, the dynamic model error terms in the proposed method do not require the usual Kalman filter-smoother process noise assumptions of zero-mean, symmetrically distributed random disturbances, nor do they require representation by assumed parameterized time series (such as Fourier series). Instead, the dynamic model error terms require no prior assumptions other than piecewise continuity. Estimates of the state histories, as well as the dynamic model errors, are obtained as part of the solution of a two-point boundary value problem. The state estimates are continuous and optimal in a global sense, yet the algorithm processes the measurements sequentially. The example demonstrates the method and shows it to be quite accurate for state estimation of a poorly modeled dynamic system.

### Introduction

A large number of applications exist in the general area of "post-experiment" estimation, wherein estimates of the actual state histories of a dynamic system are obtained using an assumed state dynamic model and sets of discrete measurements. Applications are found throughout engineering, but are especially numerous in such aerospace problems as orbit estimation, attitude estimation, and post-flight trajectory estimation.

In general, both the dynamic model and the available measurements are imperfect. The motivation for applying an estimation algorithm is to combine the model-predicted state estimates with the available measurements in such a way as to obtain estimates of the state histories which are of higher accuracy and more complete than either

the model predictions or the measurements. If the estimation algorithm optimizes some performance index, typically based on the state estimate error, then the resulting state estimate is said to be optimal. In this paper, we propose a novel optimal estimation strategy, which includes both a new optimality criterion and a new algorithm for obtaining estimates based upon it.

The most commonly used estimation approach is the Kalman filter and numerous closely related strategies, originally developed by Kalman<sup>(1)</sup> and Kalman and Bucy<sup>(2)</sup>. In the keynote address to the 1985 American Control Conference, Gelb<sup>(3)</sup> points out that 2997 papers on Kalman filtering were published in the 15 years between 1969 and 1984, an average of 200 each year or 17 each month. The Kalman algorithms are well-suited for real-time estimation, due to their sequential processing structure and emphasis on the most recent data. Probably due to popularity and familiarity, Kalman filters are now routinely used for post-experiment estimation, normally accomplished via iterative post-processing of the filter estimate ("smoothing").

The various filter strategies use similar, although distinct, optimality criteria. The two most common are "minimum variance" and "maximum likelihood" criteria (see, e.g., Junkins<sup>(4)</sup>). In minimum variance estimation, a function of the trace (typically the trace itself) of the state estimate error covariance matrix is minimized. In maximum likelihood estimation, the most probable state estimate is found given the measurements. The important feature of these existing strategies is that they require estimation of the state estimate error covariance. In order to rigorously estimate the state estimate error, knowledge of both the model error and the measurement error is required. While measurement errors may be determined in numerous ways, model errors are generally unknown by definition (i.e., if one is aware of the model error, one corrects the model).

To the best of the current authors' knowledge (we admit that we have not read all of the pre-1969 nor post-1984 Kalman filter papers, let alone the 2997 published during 1969-1984), every filter strategy actually implemented numerically deals with the model error knowledge requirement by assuming that the model error is a symmetrically-distributed white noise sequence of known covariance, normally called "process noise" in the literature. We note that this assumption often has no theoretical basis, and that in fact, for physical systems, model errors are more often

\* Assistant Professor, Mechanical and Aerospace Engineering, Member AIAA

\*\* TEES Chair Professor of Aerospace Engineering, Associate Fellow AIAA

smooth functions resulting from typical model simplification assumptions such as linearization, ignoring of secondary effects or higher order terms, etc., or just plain ignorance.

In this paper, a new optimality criterion for determining state estimates is described. This criterion seeks to obtain the smallest estimate of model error subject to a "covariance constraint". It is based solely on assumed knowledge of the measurement error covariance, which, we claim, is far more likely to be accurately known than the model error and which, in any event, is also required in the filter strategies. We also present an optimal strategy ("minimum model error" estimation) for determining the state estimates which satisfy the optimality criterion. The algorithm is shown to be related to classical optimal control problems.

### General Problem Statement

The following generic problem statement for post-experiment estimation of a dynamic process is used as a starting point for the development of the method. Given a system whose state vector dynamics is modeled by the (linear or nonlinear) system of equations,

$$\dot{\mathbf{x}} = \mathbf{f}(\mathbf{x}(t), t) \quad (1)$$

where

$\mathbf{x}$  =  $n \times 1$  state vector

$\mathbf{f}$  =  $n \times 1$  model equations

and given a set of discrete measurements modeled by the (linear or nonlinear) system of equations,

$$\tilde{\mathbf{y}}_k = \mathbf{g}_k(\mathbf{x}(t_k), t_k) + \mathbf{y}_k, \quad k=1, 2, \dots, N \quad (2)$$

where

$\tilde{\mathbf{y}}_k$  =  $m \times 1$  measurement set at time  $t_k$

$\mathbf{g}_k$  =  $m \times 1$  measurement model at time  $t_k$

$\mathbf{y}_k$  =  $m \times 1$  gaussian distributed random sequence, with zero mean and known covariance,  $\mathbf{R}_k$

determine the optimal estimate for  $\mathbf{x}(t)$  (denoted by  $\hat{\mathbf{x}}(t)$ ), during some specified time interval  $t_0 \leq t \leq t_f$ .

### The Covariance Constraint Concept

In the present method, the optimal state trajectory estimate is determined on the basis of the assumption that consistent estimates of the state trajectories must match the available measurements with a residual error covariance which is approximately equal to the known measurement error covariance. This necessary condition is hereafter referred to as the "covariance constraint". The covariance constraint is imposed by requiring the following approximation to be satisfied:

$$[\tilde{\mathbf{y}}_k - \mathbf{g}_k(\hat{\mathbf{x}}(t_k), t_k)][\tilde{\mathbf{y}}_k - \mathbf{g}_k(\hat{\mathbf{x}}(t_k), t_k)]^T \approx \mathbf{R}_k, \quad k=1, 2, \dots, N \quad (3)$$

Thus, the estimated output  $\mathbf{g}_k(\hat{\mathbf{x}}(t_k), t_k)$  is required to fit the actual measurements  $\tilde{\mathbf{y}}_k$  with approximately the same error covariance as the actual measurements fit the truth. Otherwise, the estimate is statistically inconsistent.

Considerable flexibility exists in the application of the covariance constraint, Eq. (3). The interpretation of the "approximately equal" sign in Eq. (3) may be taken in a number of ways, no one of which is appropriate for all situations. For example, in the typical case where the measurement sets are all of the same physical quantities, and with the same nominal accuracy, it is appropriate to compare the averaged measurement-minus-estimate residual error covariance with a single prescribed measurement-minus-truth error covariance as

$$\frac{1}{N} \sum_{k=1}^N [\tilde{\mathbf{y}}_k - \mathbf{g}_k(\hat{\mathbf{x}}(t_k), t_k)][\tilde{\mathbf{y}}_k - \mathbf{g}_k(\hat{\mathbf{x}}(t_k), t_k)]^T \approx \mathbf{R} \quad (4)$$

where the subscript  $k$  has been dropped from the prescribed covariance to indicate that the measurement-minus-truth covariance is constant over all measurement sets.

The averaging of covariances over a number of measurement sets is applicable if any of the measurement sets are repeated during the time interval of interest. In some applications, there may be two or more distinct measurement subsets, each of which is measured numerous times. In these situations, an averaged covariance constraint in the form of Eq. (4) may be applied to each distinct measurement subset. An example of this type of application is the attitude estimation of a spacecraft, where numerous angular velocity and independent attitude angle measurements are made, but at different times and with different accuracy. An averaged covariance constraint for angular velocity measurements and a separately averaged covariance constraint for attitude angle measurements is appropriate.

The primary motivation for using an averaged covariance constraint is the reduction of the sensitivity of the approach to small sample statistical anomalies. If the covariance constraint is imposed individually on each measurement set, then obviously any measurements which deviate significantly from the assumed measurement error may cause unrealistic corrections to the state estimates. By averaging over a large number of measurements, the likelihood that statistical anomalies are affecting the estimates is reduced. We note in passing that the usual filter-smoother measurement processing equations are applied to each measurement sequentially, with the assumption that the measurement error covariance for that measurement is correct.

The estimate optimized by the averaged covariance constraint is in essence a global best fit, i.e., a batch estimate. In general, if a number of measurement sets are available simultaneously, as is the case in post-experiment estimation, batch processing is preferred over sequential filtering due to smoother estimates and generally higher accuracy. The advantages of sequential

filtering are found in real-time estimation, which is not the case under study here, and in the case of computation which is gained by processing the measurements sequentially. As is shown in a later section, we may accomplish a batch estimate via sequential processing of the measurements.

### The Minimum Model Error Concept

We begin by accounting for model errors by adding a to-be-determined unmodeled disturbance vector  $\underline{d}(t)$  to the right-hand sides of the original state model equations, Eq. (1), to produce the modified state governing equations,

$$\dot{\underline{x}} = \underline{f}(\underline{x}(t), t) + \underline{d}(t) \quad (5)$$

Next, the following cost functional is minimized with respect to  $\underline{d}(t)$ :

$$J = \sum_{k=1}^N [\bar{y}_k - \underline{s}_k(\hat{\underline{x}}(t_k), t_k)]^T R_k^{-1} [\bar{y}_k - \underline{s}_k(\hat{\underline{x}}(t_k), t_k)] + \int_0^T \underline{d}^T(\tau) W \underline{d}(\tau) d\tau \quad (6)$$

where

$W$  =  $n \times n$  weight matrix, determined so as to satisfy the covariance constraint as described shortly.

An algorithm for the minimization of Eq. (6) with respect to the unmodeled disturbance vector  $\underline{d}(t)$  is developed in the next section.

The functional  $J$  in Eq. (6) is the sum of two penalty terms. The first is a weighted sum of discrete terms which penalize the deviation of the predicted measurements (based upon the output computed using the estimated states) from the actual measurements. Minimization of this summation term drives the state estimates toward values which, when substituted into the measurement model, predict the actual measurements. The weighting  $R_k^{-1}$  on each of these penalty terms is the inverse of the associated measurement error covariance; thus, accurate measurements (small  $R_k$ ) are weighted more heavily than inaccurate measurements (large  $R_k$ ), as in weighted least squares or maximum likelihood estimators. The second term in  $J$  is an integral term which reflects the assumption that the amount of unmodeled effect to be added should be minimized, i.e., the original model should be adjusted by a minimal amount (we give the modeler the benefit of the doubt. While  $\underline{d}(t)$  may in fact be large, it should be as small as possible!). This is the origin of the title, "minimum model error" estimation.

The presence of  $\underline{d}(t)$  in the cost functional  $J$  produces somewhat ambivalent results. If the original state model equations contain significant errors, then the addition of large model correction terms should enable the estimate to better fit the measurements. Thus, the summation term in  $J$  is decreased. However, the addition of  $\underline{d}(t)$  increases the integral term in  $J$ . The proper balance between the two competing effects depends on the choice of  $W$ . The weight matrix,  $W$ , is

determined such that the covariance constraint is satisfied. Thus, we seek the smallest  $\underline{d}(t)$  which is consistent statistically with the measurements.

A typical plot of  $W$  versus the covariance constraint is shown in Fig. (1a). To keep the discussion simple, assume that a single state is being estimated, and that the measurements are of the state itself. Further assume that the dynamic model contains significant errors, i.e., the model-predicted state is substantially different from the actual state.

In Fig. (1a), the covariance constraint is represented by the point at which the measurement-minus-estimate variance is equal to the measurement-minus-truth variance (i.e., the known measurement error variance).

For large values of  $W$ , the model correction term  $\underline{d}(t)$  (the second term in  $J$ ) is penalized heavily compared with the measurement-minus-estimate residuals (the first term in  $J$ ). Consequently, large measurement-minus-estimate residuals are allowed. The state estimate is based primarily on the original model. The measurement-minus-estimate variance is large and essentially constant for a wide range of large  $W$ , since the model correction term  $\underline{d}(t)$  remains virtually zero. The measurement-minus-estimate variance is much larger than the measurement-minus-truth variance.

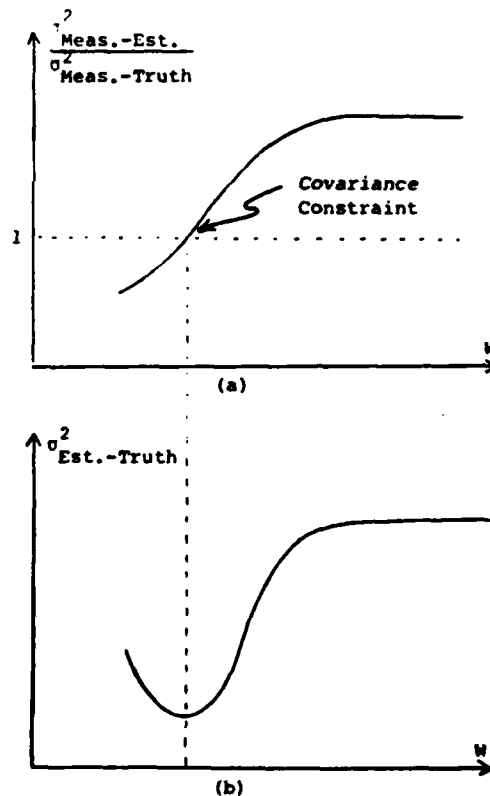


Fig. 1: Choosing  $W$  to satisfy the covariance constraint leads to an optimal state estimate.

However, if  $W$  is decreased, the model correction term is penalized relatively less heavily and the measurement-minus-estimate residuals are penalized relatively more heavily. For some sufficiently small  $W$ , the model correction term  $d(t)$  becomes nonzero and begins to correct the model prediction toward agreement with the measurements. The appropriate value for  $W$  is the one which allows enough model correction to cause the measurement-minus-estimate variance to match the measurement-minus-truth variance. If  $W$  is decreased below this value, the estimate matches the measurements too closely and becomes too affected by measurement noise.

In Fig. (1b), the actual estimate error variance (i.e., the truth-minus-estimate variance) is plotted versus  $W$ . Statistically, this variance is minimized when the covariance constraint is satisfied. If  $W$  is too large, the estimate is too far from the measurements. If  $W$  is too small, the estimate is too close to the measurements. When the covariance constraint is satisfied, the estimate matches the measurements with the same covariance as the truth matches the measurements. For the given model and particular sample of measurements, this is the optimal estimate, although the actual error covariance goes to zero only for an infinite set of measurements.

Fig. (1) represents typical results in a conceptual manner. However, like all strategies based on statistical interpretation, these results are affected by the particular sample of measurement errors in the available measurements. Although the measurement error covariance matrix,  $R_k$ , is assumed to be known, it is strictly valid only for an infinite number of measurements, so in practice it is an approximation. Thus, satisfaction of the covariance constraint is also an approximation. We note in passing that filter-type algorithms require assumed values for both the measurement noise and the model error noise (of course, this latter assumption presupposes that the model error is indeed simply noise). The present method eliminates the requirement for model error assumptions but retains the measurement noise knowledge assumption. The above qualitative discussion motivates the formalization and generalization of the ideas. These results follow.

#### Derivation of The Estimation Algorithm

In this section, the calculus of variations is used to develop an estimation algorithm for poorly modeled dynamic systems. The development is similar to the typical textbook developments of optimal control theory (see, e.g., Bryson and Ho<sup>(5)</sup> or Kirk<sup>(6)</sup>). However, the adaptation of these variational concepts to the development of an estimation algorithm represents a novel interpretation of the classical results. In particular, we encounter an unusual multi-point boundary value problem and find a novel solution process. Application of the covariance constraint is described in the next section.

We begin by giving the necessary conditions for the minimization of a functional, with respect to a vector function, which includes both discrete

and integral terms. Given the system of equations,

$$\dot{x} = f(x(t), u(t), t), \quad t_0 \leq t \leq t_f \quad (7)$$

where

$x$  =  $n \times 1$  state vector,  $x(t_0)$  specified

$f$  =  $n \times 1$  model equations

$u$  =  $p \times 1$  to-be-determined control vector

and a performance index defined as

$$J = \phi[x(t_f)] + \int_{t_0}^{t_f} L[x(t), u(t), t] dt \quad (8)$$

where

$\phi$  = penalty on the final state vector

$L$  = penalty reflecting the deviation of  $x(t)$  or  $u(t)$  from their desired trajectories.

the problem may be stated as: find a smooth, differentiable, unbounded  $u(t)$ , which minimizes  $J$ , subject to the differential equation constraint, Eq. (7).

The necessary conditions for the minimization of  $J$  in Eq. (8) are obtained by equating the variation of  $J$  to zero. These conditions, usually called "Pontryagin's necessary conditions", are given by (e.g., Rozonoer<sup>(7)</sup> or Kopp<sup>(8)</sup>) the  $2n$  differential equations,

$$\dot{\lambda} = f[x(t), u(t), t] \quad (9)$$

$$\dot{\lambda} = - \left[ \frac{\partial f}{\partial x} \right]^T \lambda(t) - \left[ \frac{\partial L}{\partial x} \right]^T \quad (10)$$

where  $\lambda(t)$  is the vector of costates; the  $p$  algebraic equations,

$$\left[ \frac{\partial L}{\partial u} \right]^T = - \left[ \frac{\partial f}{\partial u} \right]^T \lambda \quad (11)$$

and the  $2n$  boundary conditions,

$$x(t_0) = \text{specified} \quad (12)$$

$$\lambda(t_f) = \frac{\partial \phi}{\partial x} \Big|_{t=t_f} \quad (13)$$

The  $2n$  boundary conditions are split between  $n$  initial conditions on the states and  $n$  final conditions on the costates (classically called transversality conditions). Thus, Pontryagin's necessary conditions lead to a two-point boundary value problem (TPBVP). Numerous methods have been developed for the solution of TPBVP's; see, e.g., Vadali<sup>(9)</sup> or Keller<sup>(10)</sup>. Typically, the  $2n$  differential equations, Eqs. (9) and (10), must be integrated forward from the specified state initial conditions, Eq. (12), using "guessed" costate initial conditions. At the final time  $t_f$ ,



the integrated values of the costates are compared with the specified costate final conditions, Eq. (13). If the agreement between the integrated and specified values is inadequate, then the costate initial conditions must be adjusted and the integration repeated. This process is repeated until the agreement between the integrated final costates and the specified final costates is sufficient. Other forward/backward iteration schemes are given in Bryson and Ho<sup>(5)</sup>.

It is possible (see, e.g., Geering<sup>(11)</sup> or Mook<sup>(12)</sup>) to extend the basic Pontryagin's necessary conditions to account for terms in  $J$  at discrete times within the time domain. If the performance index is modified to the form,

$$J = \sum_{i=1}^I K_i(\bar{x}(t_i), t_i) + \int_0^T L[\bar{x}(\tau), \bar{u}(\tau), \tau] d\tau \quad (14)$$

then the necessary conditions are modified by the additional internal boundary conditions

$$\bar{\lambda}^T(t_i^+) = \bar{\lambda}^T(t_i^-) - \frac{\partial K_i}{\partial \bar{x}} \bigg|_{\bar{x}(t_i), t_i} \quad (15)$$

The resulting TPBVP now contains jump discontinuities in the costates at the times  $t_i$  associated with each internal penalty term. These jump discontinuities complicate the calculation of the partial derivatives of the final costates with respect to the initial states; these partial derivatives are frequently used as the basis for choosing corrections to the initial state estimates. However, the solution of the TPBVP is not the focus of the present work, so the TPBVP is assumed to be solvable in the discussion which follows.

Eq. (6) is clearly in the form of Eq. (14). The discrete penalty terms in Eq. (6) are given by

$$K_k = [\bar{y}_k - \bar{z}_k(\hat{\bar{x}}(t_k), t_k)]^T R_k^{-1} [\bar{y}_k - \bar{z}_k(\hat{\bar{x}}(t_k), t_k)] \quad (16)$$

Utilizing Eq. (15), the jump discontinuities in the costates due to this penalty term may be written

$$\begin{aligned} \bar{\lambda}^T(t_k^+) &= \bar{\lambda}^T(t_k^-) - \frac{\partial K_k}{\partial \bar{x}} \bigg|_{\hat{\bar{x}}(t_k), t_k} \\ &= \bar{\lambda}^T(t_k^-) + 2\bar{H}_k^T R_k^{-1} [\bar{y}_k - \bar{z}_k(\hat{\bar{x}}(t_k), t_k)] \end{aligned} \quad (17)$$

where

$$\bar{H}_k = \frac{\partial \bar{z}_k}{\partial \bar{x}} \bigg|_{\hat{\bar{x}}(t_k), t_k}$$

An algorithm for the implementation of the minimum model error approach now follows directly from the modified Pontryagin's necessary conditions. For a given  $W$ , the minimization of  $J$  in Eq. (6) with respect to  $\bar{g}(t)$  leads to the TPBVP summarized as:

$$\dot{\bar{x}} = f[\bar{x}(t), t] + \bar{g}(t) \quad (18)$$

$$\dot{\bar{\lambda}} = - \left[ \frac{\partial f}{\partial \bar{x}} \right]^T \bar{\lambda} \quad (19)$$

$$\bar{x}(t_0) = \text{specified (measured, estimated, etc.)} \quad (20)$$

$$\bar{\lambda}(t_0) = 0 \quad (21)$$

$$\bar{\lambda}(t_k^+) = \bar{\lambda}(t_k^-) + 2\bar{H}_k^T R_k^{-1} [\bar{y}_k - \bar{z}_k(\hat{\bar{x}}(t_k), t_k)] \quad (22)$$

$$\bar{\lambda}(t_f^+) = 0 \quad (23)$$

This algorithm, and the resulting state estimate, exhibits several desirable features of both batch and sequential estimation techniques. The state estimate is obtained by processing all of the available measurements, much like a batch estimator such as least squares. Thus, the estimate is optimized in a global sense. In addition, the state estimate is continuous, eliminating the state estimate jump discontinuities present in filter estimates. For many physical systems, jump discontinuities in the states are not possible; thus, jump discontinuities in the filter state estimates must be reconciled in an artificial manner. Obviously, the estimate of  $\bar{g}(t)$  is discontinuous at each  $t_i$ ; in essence, the discontinuities have been "pushed" up one order into the state derivatives. In addition to the batch algorithm-like advantages, the minimum model error algorithm calculations are based upon sequential processing of the measurements, which, like the filter algorithms, greatly reduces the memory requirements and eliminates the need for large matrix manipulations. From the standpoint of algorithmic calculations, the minimum model error technique shares advantages of both batch and sequential estimation techniques.

Eqs. (18)-(23) describe a TPBVP for a given value of  $W$ . Once the TPBVP has been solved, the state estimates are substituted into the measurement model  $\bar{z}_k$  to produce the predicted measurements for this value of  $W$ . If the errors between the predicted measurements and the actual measurements have the same covariance as the prescribed measurement error covariance, then the state estimate is consistent. If the prescribed measurement error covariance is larger than the error covariance matrix between the predicted and actual measurements, then the predicted measurements are too close to the actual measurements. Too much model correction has been admitted. Thus,  $W$  should be increased and the resulting TPBVP is solved for a new state estimate. If the prescribed measurement error covariance is smaller than the error covariance between the predicted and actual measurements, then the predicted measurements are not accurate enough. Too little model correction has been admitted, so  $W$  should be decreased, and the resulting TPBVP solved for a new state estimate.

Based on limited experience in applying this approach to a few example problems, a good starting value for  $W$  is the inverse of the measurement error covariance matrix. This value is also intuitively reasonable, but the final value of  $W$  is dependent on the model error, which is unknown a priori. The subsequent corrections to  $W$  may be automated using standard search procedures. We note that choosing an appropriate value of  $W$  is

similar to "tuning" a Kalman filter, with the important distinction that the choice of process noise in the tuning of a Kalman filter is rarely based on more than the user's artistry. In minimum model error estimation, the covariance constraint determines a necessary condition upon the acceptable choice of  $W$ . At the present, the uniqueness of  $W$  has not been resolved for multi-dimensional applications.

### Simple Scalar Example

To illustrate the application of the minimum model error approach, consider estimation of the state history of a scalar function of time for which noisy measurements are the only information available. No prior knowledge of the underlying dynamics is assumed. Thus, the system dynamic model equation is

$$\dot{x} = 0 \quad (24)$$

For simplicity, the measurements are direct measurements of the state itself, and the measurement noise is a zero mean gaussian process with a presumed known variance of  $\sigma^2$ .

Using the minimum model error approach, the system model is modified by the addition of a to-be-estimated unmodeled effect as

$$\dot{x} = 0 + d(t) \quad (25)$$

where  $d(t)$  represents the dynamic model error. The measurements are given as

$$\tilde{y}_k = x(t_k) + v_k, \quad k=1,2,\dots,M \quad (26)$$

where  $\tilde{y}_k$  is the measurement at time  $t_k$ ,  $x(t_k)$  is the true state at time  $t_k$ , and  $v_k$  is a zero-mean gaussian sequence of presumed variance  $\sigma^2$ . The cost functional to be minimized (see Eq. (6)) is

$$J = \frac{1}{\sigma^2} \sum_{k=1}^M (\tilde{y}_k - \hat{x}(t_k))^2 + \int_0^{t_f} d^2(\tau) W d\tau \quad (27)$$

where  $W$  is the to-be-determined weight on the integral sum-square model error term. The TPBVP which results from the minimization of  $J$  with respect to  $d(t)$  may be summarized as

$$\dot{x} = d(t) \quad (28)$$

$$\dot{\lambda} = 0 \quad (29)$$

$$\lambda(\cdot) = -\frac{\lambda}{2W} \quad (30)$$

$$\lambda(t_0^-) = \lambda(t_f^+) = 0 \quad (31)$$

$$\lambda(t_k^+) = \lambda(t_k^-) + \frac{2}{\sigma^2} (\tilde{y}_k - \hat{x}(t_k)) \quad (32)$$

where  $\lambda$  is the costate.

The algorithm proceeds according to the following steps:

1. Choose  $W$

2. Set  $\hat{x}_0 = x_0$
3. Integrate forward to  $t_f$ , accounting for the jump discontinuities in  $\lambda$  at each measurement time
4. Check: Is  $\lambda(t_f^+) = 0$ ? If so, go to step 7
5. Determine  $\frac{\partial \lambda(t_f^+)}{\partial x(t_0)}$ , then  $\Delta x(t_0)$
6. Adjust  $\hat{x}_0$  by  $\Delta x(t_0)$ ; go to step 3
7. Check the covariance constraint:
$$\frac{1}{M} \sum_{k=1}^M (\tilde{y}_k - \hat{x}(t_k))^2 \approx \sigma^2 ?$$
8. If the covariance constraint is not satisfied, go to step 1

The true state history for this example is taken as  $x(t) = \cos(t)$ . In Fig. (2), a set of 101 simulated measurements spanning the time interval  $t_0=0$  to  $t_f=10$  is shown. The measurements were simulated by adding a computer-generated gaussian random sequence to the true state as shown in Eq. (26). The nominal variance of  $v_k$  in Fig. (2) is 0.1, although the actual variance depends on the seed supplied to the random number generator. For the measurements shown, the actual error variance is 0.114, representing a typical error magnitude of approximately 0.34. The state itself has an average magnitude of 0.64, so that the typical measurement error in this example is more than 50% of the state (the signal to noise ratio is just under 2).

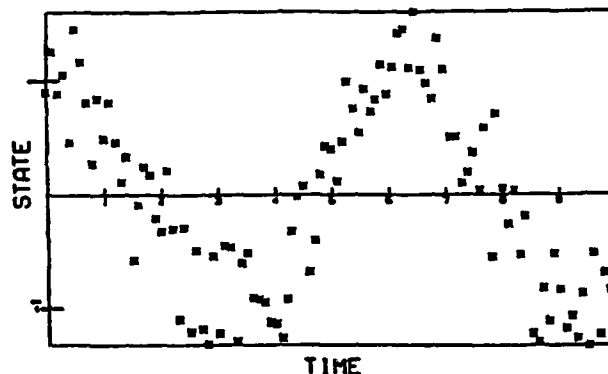


Fig. 2: Simulated Measurements  
Truth= $\cos(t)$ , Measurement variance=0.114

In Fig. (3), the minimum model error state estimate is shown along with the measurements and the true state history. Note that the state has been reconstructed to an error variance of .0085, considerably better than the measurement variance even in the total absence of a model. Note also that the model prediction variance (i.e., constant  $x=0$ ) is 0.717. Thus, the MME estimate error variance is 100 times smaller than the model error

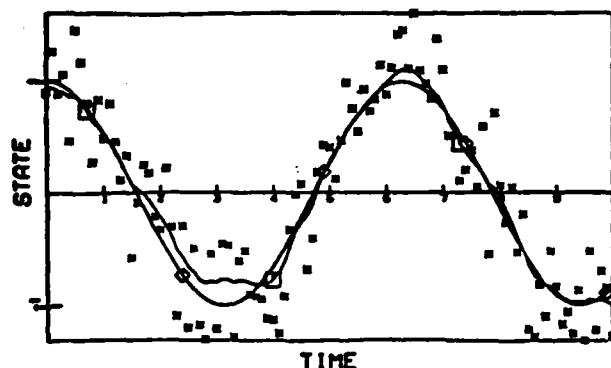


Fig. 3: \*Measurements,  $\diamond$  Truth, and  $\square$  State Estimate. Measurement variance is 0.114. Model variance is 0.717. Estimate variance is 0.0085.

variance and 15 times smaller than the measurement error variance. The optimal estimate is significantly more accurate than either the model or the measurements, which is the implicit objective of state estimation algorithms.

We note in passing that the usual filter strategies do not include mechanisms for correcting incorrect state dynamics models. Thus, the between-measurement filter predictions are based on integration of the original model. In the case of the present example, then, the filter estimate would consist of a discontinuous horizontal line, with jump discontinuities occurring at each measurement time.

#### Summary and Conclusions

In this paper, a new optimal state estimation method has been developed for the post-experiment state estimation of discretely-measured dynamic systems. The concept of a "covariance constraint" has been introduced as a necessary condition, marking a departure from the traditional criteria such as minimum variance or maximum likelihood estimation. The new method accounts for errors in the dynamic state model equations, and does not require or assume apriori knowledge of the dynamic model error. A minimum model error algorithm for obtaining state estimates which satisfy the covariance constraint is also derived. The method was demonstrated for a simple scalar problem, and the results indicate that the method is capable of obtaining very accurate state estimates in the presence of significant model error and significant measurement error.

With the exception of a few qualitative remarks, the method has not been compared to Kalman filter-smoother type algorithms. This omission is intentional, since (i) this paper serves to introduce the new method, and (ii) the comparisons should, for fairness, include a number of examples to permit systematic investigation of the several issues. This is a lengthy undertaking reserved for future papers. Several comparisons are done in Mook<sup>(12)</sup>. We note that if continuous, perfect measurements are available, the filters can obtain perfect estimates without a model, whereas sparse measurements rely heavily on the

dynamic model for the between-measurement estimates. Numerical comparisons must, by their very nature, be handled on an individual case basis. Nevertheless, minimum model error estimation is a potentially significant improvement for those situations in which the model error is large and the measurements are sparse and/or poor.

#### References

1. Kalman, R.E., "A New Approach to Linear Filtering and Prediction Problem," *Trans. ASME, J. Basic Engr.*, Ser. D, Vol. 82, pp. 34-45, 1960.
2. Kalman, R.E., and Bucy, R.S., "New Results in Linear Filtering and Prediction Theory," *Trans. ASME, J. Basic Engr.*, Ser. D, Vol. 83, p. 95, 1961.
3. Gelb, A., "Dual Contributions of Optimal Estimation Theory in Aerospace Applications," Keynote Speech to the 1985 American Control Conference.
4. Jenkins, J.L., *An Introduction to Optimal Estimation of Dynamical Systems*, Sijthoff and Noordhoff, Alphen aan den Rijn, The Netherlands, 1978.
5. Bryson, A.E., and Ho, Y.C., *Applied Optimal Control*, Blaisdell, Waltham, Mass., 1969.
6. Kirk, D.E., *Optimal Control Theory*, Prentice-Hall, Englewood Cliffs, NJ, 1970.
7. Rozonoer, L.E., "L.S. Pontryagin Maximum Principle in Optimal System Theory," *Avionika i Telemekh.*, Vol. 20, 1959. Also in *Optimal and Self-Optimizing Control*, R. Oldenburger, editor, M.I.T. Press, Part I, pp. 210-224; Part II, pp. 225-241; Part III, pp. 242-257; 1966.
8. Kopp, R.E., "Pontryagin Maximum Principle," Chapter 7 in *Optimization Techniques*, G. Leitmann, editor, Academic Press, New York, 1962.
9. Vadali, S.R., "Solution of the Two-Point Boundary Value Problems of Optimal Spacecraft Rotational Maneuvers," Ph.D. Dissertation, VPI and SU, December 1982.
10. Keller, H.B., *Numerical Solution of Two Point Boundary Value Problems*, Regional Conference Series in Applied Mathematics, No. 24, SIAM, 1976.
11. Geering, H.P., "Continuous-Time Control Theory for Cost Functionals Including Discrete State Penalty Terms," *IEEE Trans. AC*, Vol. AC-21, pp. 866-869, 1976.
12. Mook, D.J., "Measurement Covariance Constrained Estimation for Poorly Modeled Dynamic Systems," Ph.D. Dissertation, Virginia Polytechnic Institute and State University, 1985.

## **ATTACHMENT 11**

# **Ground-Based Testing of Large Flexible Spacecraft**

# GROUND-BASED TESTING OF LARGE FLEXIBLE SPACECRAFT

by

Roger C. Thompson

## ABSTRACT

Analytical and experimental results are presented concerning important topics in ground-based testing of flexible spacecraft. In particular, the concepts concerning testing of scale models is investigated, and the behavior of accelerometer sensor systems in the gravity field of Earth-bound laboratories is examined. For ground-based testing to be an acceptable and accurate basis for prediction of spacecraft behavior, we must address these issues.

Scaling down of large space system's to laboratory-sized models requires much more than simple proportional reduction of dimensions. In order to preserve the frequency response of the structure, point masses, structural masses, and the material itself must be scaled such that mass and stiffness elements are scaled by identical factors. Analytical results are presented for simple models.

Accelerometers, when operated under certain conditions in a gravity field may produce erroneous readings of structural accelerations, depending upon the orientation and frequency of the motion relative to the gravitational field. We investigate this phenomenon to determine how to predict the magnitude of the sensor errors. Experimental results for simple motion of rigid and flexible beams are presented.

### Acknowledgements

I wish to thank the Air Force Office of Scientific Research and the Air Force Astronautics Laboratory for their sponsorship of this work. The support and guidance of Dr. Alok Das was instrumental in the completion of this research. Furthermore, the assistance of Mr. Waid Schlaegel, Lt. Tim Strange, Lt. John Word, Lt. Greg Norris, and Mr. Angel Cruz of the Air Force Astronautics Laboratory was greatly appreciated.

I also wish to thank Drs. John L. Jurkins and S. R. Vadali for their assistance and for providing the opportunity for me to work on this project. Finally, I wish to thank Dr. Mark Norris for bringing the accelerometer problem to my attention, and for his assistance with the analytical derivations regarding the accelerometer responses.

## Introduction

Ground-Based testing of flexible spacecraft is required in order to verify the predicted behavior of many subsystems, and to analyze the global response of the structure, prior to placement in orbit. As satellites grow in size, complexity, and cost, we can ill-afford to proceed with launch plans without a more complete knowledge of how the spacecraft will react to controls, disturbances, and the environment of space. Consequently, we must rely on experimental measurements of system response, in the gravitational environment of ground-based laboratories, to predict the behavior of a structure under conditions experienced in orbit.

Laboratory testing of large space structures presents many problems that must be examined and compensated for, if possible. Because the environment of space can never be completely simulated in an earth-bound facility, we must usually test various systems individually. In this report, we present research efforts conducted at the Air Force Astronautics Laboratory (AFAL) regarding the vibrational response of large space structures. The research focuses on two distinct and unrelated areas. In the first, we examine the concept of developing laboratory-sized scale models of a structure such that the flexural response of the system is preserved; and in the second subject, we analyze the accelerometer measurement errors observed in experiments on the AFAL grid structure. Although unrelated, these two topics are important considerations when developing experimental procedures, and they illustrate some of the problems associated with ground-based testing of large flexible structures.

### Objectives of Dynamic Scaling

The principal objective of model scaling is to produce a (usually) smaller replica of a structure that is proportional to the actual (full scale) object. However, when we consider dynamic effects in the scaling process, we introduce additional requirements the reduced size model must behave dynamically like the full sized structure. Stated in more formal terms, dynamic scaling is the process by which a scale model of an object is produced such that the frequency response of the model is identical to the frequency response of the original structure for all possible types of motion.

It is important to understand why we require the frequency response to remain "constant." A large, complex structure will exhibit vastly different behaviors, depending on the natural frequencies of vibration. At low frequencies, motion may be difficult to control, damping is often small, and spillover or excitation of multiple modes is quite common. As modal frequencies increase, the spillover effects are reduced, the flexural motions are generally much smaller, and passive structural damping begins to dominate such that the motion decays

much faster. Therefore, if we use a scale model, with higher modal frequencies than the structure as a means of testing the behavior, the results will contain significant errors if the frequencies of the model and the structure are dissimilar.

Producing scale models that behave as a large structure would behave is a concept of dimensional analysis [1-2], where dimensionless parameters that govern the behavior of any similar structure under similar conditions are identified. The Buckingham Pi Theorem is a method by which a complete set of parameters can be isolated; however, the time (frequency) parameters must often be scaled in order to achieve perfect similitude. As indicated above, this is inconsistent with the goal of our dynamic scaling experiments. Conflicts with the scaling laws are quite common [3-4], particularly with rate sensitive parameters such as viscoelastic materials and structural damping.

### Derivation of the Scale Factors

If the physical dimensions of a structure were to be scaled by some proportional constant, excluding the dynamic scaling considerations, the natural frequencies of the structure would be increased. For example, if we consider only the bending modes of a simple beam, we know that the natural frequencies are proportional to the structural properties such that

$$\omega_k \propto \sqrt{\frac{EI}{\rho AL^4}} \quad (1)$$

Where E is the Elastic Modulus of the material, I is the cross-sectional moment of inertia,  $\rho$  is the density of the material, A is the cross-sectional area, and L is the length of the beam. If the dimensions of the beam are scaled by a common factor (n), then the scaled quantities are given by

$$\tilde{I} = n^4 I \quad \tilde{A} = n^2 A \quad \tilde{L} = nL$$

and the natural frequencies of the scaled model will be

$$\tilde{\omega}_k \propto \sqrt{\frac{n^4 EI}{n^6 \rho AL^4}} = \frac{\omega_k}{n} \quad (2)$$

Therefore, we can see that either the elastic modulus or the mass density (or both) must be scaled in order for the frequency response to be preserved.

We develop the scaling parameters by introducing simple factors for quantities that define some property of the structure, where these parameters may not be independent of each other. Clearly, the spatial dimensions of the model must be proportional to the structure. As indicated by the derivation of Eq. (2), the Mass density and Elastic modulus also represent common parameters in the dynamic analysis of a structure. In



addition, we include a scale factor for point masses (a mass without significant spatial distribution). Although it is true that no actual construction of a structure can truly contain a point mass, such idealize fabrications are often used in analytical modeling, and we shall include the concept in the derivation.

By defining the scale factors of the spatial quantities, density, elastic modulus, and point masses as  $n$ ,  $r$ ,  $s$ , and  $q$  respectively, the "scaling laws" may be defined by

$$\begin{aligned}\bar{x} &= nx & \bar{y} &= ny & \bar{z} &= nz \\ \bar{\rho} &= r\rho & \bar{E} &= SE & \bar{m}_p &= qm_p\end{aligned}\quad (3)$$

From these definitions, other scaled quantities can then be determined. For example, altering the physical dimensions of a structure by a factor  $n$  automatically alters the cross-sectional moment of inertia by  $n^4$

$$\bar{I}_A = \int_{\text{Area}} \bar{d}^2 d\bar{A} = \int_{\text{Area}} n^2 d^2 (n^2 dA) = n^4 \int_{\text{Area}} d^2 dA = n^4 I_A \quad (4)$$

where  $d$  is the distance of the centroid of  $dA$  from an axis of an indicated reference frame. Similarly, it can be shown that "structural masses" and mass moments of inertia are scaled according to

$$\bar{m}_s = \int_{\text{Vol}} \bar{\rho} d\bar{V} = rn^3 m_s \quad (5)$$

$$\bar{I}_m = \int_{\text{Vol}} \bar{d}^2 (\bar{\rho} d\bar{V}) = rn^5 I_m \quad (6)$$

However, the mass moment of inertia of a point mass would be given by

$$\bar{I}_m = \bar{d}^2 \bar{m}_p = qn^2 I_m \quad (7)$$

Consider the situation such that the moment of inertia of a small "structural mass" about an axis whose distance is much greater than the dimensions of the mass distribution is compared with the moment of inertia of a point mass of equal magnitude about the same axis. In the limit as the distance from the axis continues to increase, the two expressions for the moment of inertia must be equal. Therefore, the values of the scale factors  $q$ ,  $r$ , and  $n$  are constrained such that

$$q = rn^3 \quad (8)$$

In addition to quantities that define the structure of the dynamically scaled model, applied forces and moments must also be dynamically scaled. Applying Newton's law for any mass, the scaled force is found to be

$$\tilde{F} = \tilde{m} \ddot{\tilde{r}} = qn m \ddot{r} = qn F \quad (9)$$

In a similar manner, applied moments can be shown to be scaled such that

$$\tilde{M} = \tilde{r} \times \tilde{F} = qn^2 M \quad (10)$$

Derivations of other computed scaling laws can then be found from Eqs. (3-10). As an example, consider how a linear spring would be specified for a laboratory model. The equation for a scaled spring is directly analogous to the unscaled governing equation.

$$\tilde{F} = \tilde{k} \tilde{x} \quad (11)$$

After substituting Eqs. (3) and (9) into Eq. (11) and collecting terms, the spring stiffness is found to be

$$qnF = \tilde{k} nx \quad \text{or} \quad \tilde{k} = qk \quad (12)$$

clearly then, the natural frequency of a spring mass system is preserved since both the mass and stiffness are scaled by identical factors.

Finally, we examine the scale factor of the elastic modulus in light of the definitions given by Eqs. (3) and (9). Beginning with the definition of the modulus of elasticity, we have

$$\tilde{E} = \frac{\tilde{\sigma}}{\epsilon} \quad (13)$$

where  $\tilde{\sigma}$  is the stress applied to a scaled structural element and  $\epsilon$  is the dimensionless strain. The stress is defined by

$$\tilde{\sigma} = \frac{\tilde{F}}{\tilde{n}} = \frac{qnF}{n^2 A} = \frac{q}{n} \sigma \quad (14)$$

Substituting Eq. (14) and the definition of the scaled modulus from Eq. (3) into Eq. (13) yields the constraint equation

$$s = \frac{q}{n} \quad \text{or} \quad s = rn^2 \quad (15)$$

Equations (3-15) do not define every quantification of material or structural behavior; however, the definitions given here are typically all that would be encountered in examining flexural vibrations of structures.

#### Verification of the Scaling Laws

Now that the derivation of the scaling laws are complete, the results can be tested through analysis of example problems. For simple continuous systems, exact solutions are known for bending, extension, and torsional modes of vibration; the scaled modal frequencies can be quickly compared with the known functions. For bending modes, the natural frequencies are proportional to the structural parameters such that

$$\omega_k \propto \sqrt{\frac{EI_A}{\rho AL^4}} \quad (16)$$

Substituting the scaled variables into Eq. (16), the frequencies of a model would be given by

$$\bar{\omega}_k \propto \sqrt{\frac{\bar{E} \bar{I}_A}{\bar{\rho} \bar{A} \bar{L}^4}} = \sqrt{\frac{sn^4}{rn^6}} \omega_k \quad (17)$$

Upon substituting the constraints given in Eq. (15) into Eq. (17), it can be easily shown that the scale factors cancel exactly, and the modal frequencies remain the same. Similar results are shown for extensional modes where

$$\omega_k \propto \sqrt{\frac{EA}{\rho AL^2}} \quad (18)$$

and for torsional modes where

$$\omega_k \propto \sqrt{\frac{GJ}{TJ^2}} \quad (19)$$

As a next step in the verification process, the scaling laws are applied to a system that must be solved numerically. Consider the simple uniform beam depicted in Fig. 1 with a point mass attached to the end. Only bending modes will be considered for this particular example. For the unscaled structure, the parameters are

$$\begin{aligned} L &= 2.74 \text{ m} & M_p &= 4.536 \text{ kg} \\ E &= 2.068 \times 10^{11} \text{ N/m}^2 & A &= 4.459 \times 10^{-5} \text{ m}^2 \\ \rho &= 7800 \text{ kg/m}^3 \end{aligned}$$

Numerically this problem is solved using the Assumed Modes Method [5] with a trial function given by

$$\phi_1(x) = 1 - \cos \frac{1\pi x}{L} - \frac{1}{2} (-1)^1 \left[ \frac{1\pi x}{L} \right]^2 \quad (20)$$

The calculated natural frequencies of the first three modes are then found to be

$$\begin{aligned} \omega_1 &= 0.206 \text{ rad/s} \\ \omega_2 &= 4.23 \text{ rad/s} \\ \omega_3 &= 13.8 \text{ rad/s} \end{aligned}$$

This entire process is then repeated for a scaled model with scale factors of  $n = 0.25$  and  $r = 1$ . The structural parameters of the reduced size model are then

$$\begin{aligned} L &= 0.685 \text{ m} & M_p &= 0.0709 \text{ kg} \\ E &= 1.2925 \times 10^{10} \text{ N/m}^2 & A &= 2.787 \times 10^{-6} \text{ m}^2 \\ \rho &= 7800 \text{ kg/m}^3 \end{aligned}$$

Using the same trial function, the natural frequencies determined from the mass and stiffness matrices of the dynamically scaled model are identical (within numerical precision) of the frequencies of the full scale example.

The next logical step in verifying the dynamic scaling laws is to consider all possible modes of vibration for a more complicated structure. We have used the NASTRAN code to generate the natural frequencies for a model consisting of a tripod configuration of flexible beams cantilevered to a rigid base plate, as shown in Fig. 2. A large point mass is located at the juncture of the beams, and all modes of vibration were considered. The results obtained from the analysis of this structure, with various scale factors, are not presented in this report; however, the natural frequencies of the scaled model equaled the natural frequencies of the full scale structure to within numerical precision.

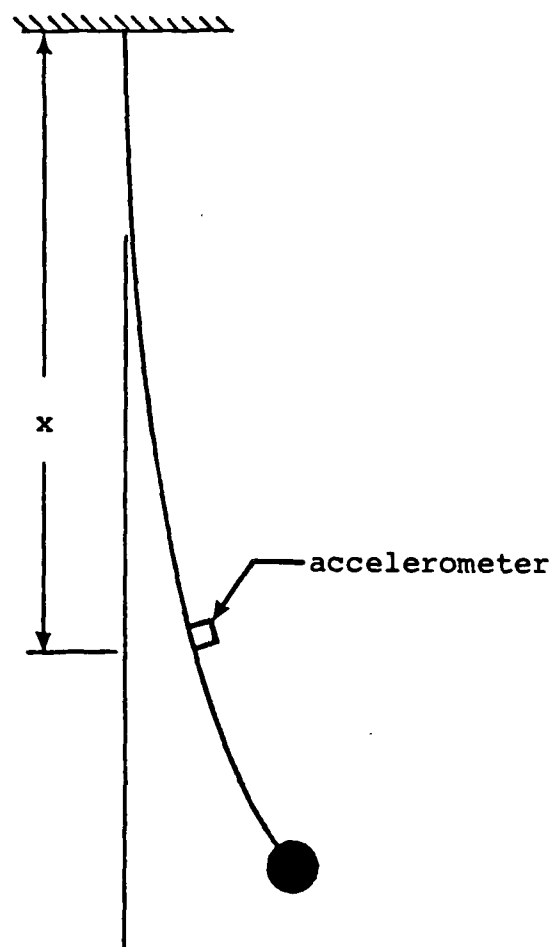


Figure 1. Flexible Beam with a Tip Mass

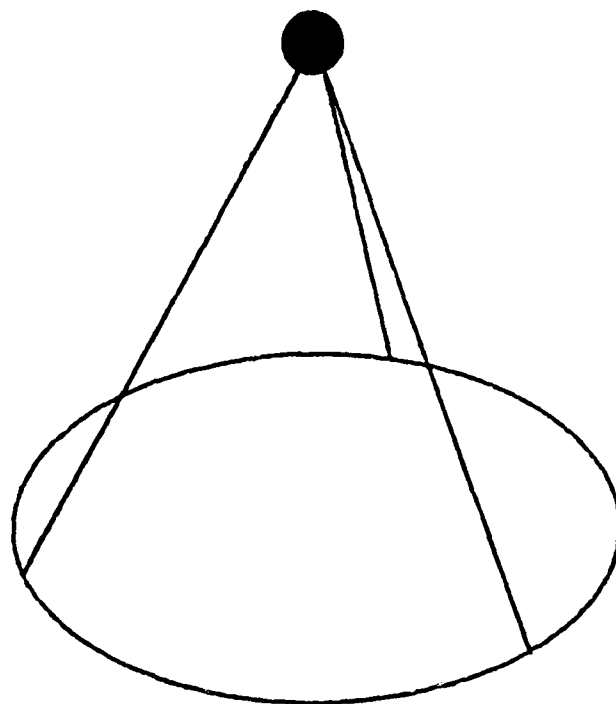


Figure 2. Tripod Configuration with a Tip Mass

### Experimental Verification of Scaling Concepts

The ultimate goal of this research effort was to verify experimentally the concepts of dynamic scaling of structures. Because the Air Force Astronautics Laboratory is considering a large structure constructed with thin-walled tubes for testing in their new facilities, it was important that we verify the dynamic scaling concepts using these components, if at all possible. The full-sized structure is to be a large tripod shaped article where the base of the tripod is mounted to a large truss structure. The composition of the truss elements and the tripod will be filament-wound, graphite-epoxy tubes. We proposed that our scaling experiments would test scale models of half, quarter, and one-eighth size. The material identification for each model, and some of the structural parameters are shown in Fig. 3.

Many problems were encountered in attempting to secure materials for the experiments. The full-sized structure is composed of thin-walled tubes. As we reduce the thickness of an already thin tube for each scale model, the components become unavailable due to manufacturing limitations. Furthermore, since the material must be scaled as well, it is even more difficult to find a specific size and material combination. For example, the quarter scale tin tube with a diameter to thickness ratio of 31.25 is virtually impossible to produce. Some manufacturers indicated that the product could be produced; however, the estimated cost prohibited any further consideration of that alternative.

Although plastic tubing is readily available, seldom is it used in structural components, so the material properties are not well known or vary considerably in the manufacturing process. We performed tensile tests on a number of representative tubes fabricated from materials such as PVC, fiberglass, acrylic, tubes for model aircraft/automobiles, and even drinking straws. None of these materials exhibited the correct properties (elastic modulus and density) required for a one-eighth scale model. Consequently, the experimental phase of this research was not completed.

### Accelerometer Measurement Error Experiments

A topic unrelated to dimensional analysis that was observed during tests on the AFAL grid structure is the phenomenon of phase-shifting of the output signal of accelerometers, or more precisely) the measurement errors induced in accelerometers due to motion in the gravity environment. A complete analytical treatment of the phenomenon is given [6] and is therefore not included in this report. However, to investigate the phenomenon and verify the analytical predictions, several experiments were conducted at the Large Space Structures Facility of the Air Force Astronautics Laboratory; consequently, the description of the experiments and the results are included in this report.

## DYNAMIC SCALING EXPERIMENT

### DYNAMICALLY SCALED CANTILEVERED TUBES

DESIRED SCALE FACTOR N	1	1/2	1/4	1/8
MATERIAL	GRAPHITE EPOXY	ALUMIN.	TIN	PLASTIC
DENSITY (KG/M3)	1600	2700	8000	1200
DENSITY SCALE FACTOR R	1	1.7	5	.75
LENGTH(METER)	2	1	1/2	1/8
OUTER DIA (CM)	5	2.5	1.25	.63
THICKNESS(MM)	1.6	.8	.4	.2
MATERIAL PROPERTY ( $E/\rho$ )	100	25	6-7	1-2
MASS LOADING (KG)	16	3.4	1.25	.023

Figure 3. Planned Dynamic Scaling Experiments



### Rigid Pendulum

The simplest structure that exhibits the accelerometer measurement errors is a simple rigid pendulum. The signed magnitude of the output signal of the accelerometer is given by [6]

$$a = \omega^2 - g/x \quad (21)$$

where  $x$  is the location of the accelerometer from the hinge point of the pendulum and  $\omega$  is the circular frequency of the pendulum. Clearly, the accelerometer output only approaches the true tangential acceleration of the pendulum as  $x$  becomes large. Furthermore, an accelerometer located at a distance  $x$  such that Eq. (21) is equal to zero (a nodal location), will have an output signal equal to zero, accelerometers located above the nodal location will indicate a reversed phase relative to accelerometers below the node point.

If the frequency of oscillation of a given pendulum is known, Eq. (21) can be used to predict the node location and to compensate for the measurement errors. At AFAL, we set up a simple experiment to determine the node location and compare the measured value with the predicted value. The pendulum consists of a rigid length of 2 inch wide channel-iron pinned to an aluminum block. The block, in turn, is bolted to a vertical surface, and the pendulum is allowed to swing freely. An accelerometer is attached to the pendulum and moved along the length of the pendulum until the output signal is zero. The results obtained in this experiment indicate an excellent correlation between the predicted and measured nodal locations, in light of the fact that this was a relatively crude experiment.

The natural frequency of the pendulum is 4.871 rad/s, the predicted node point is therefore 0.415 m, and the measured node point for this experiment was found to be 0.413 m. The discrepancy is less than 0.5%, which can be easily attributed to the manner in which the accelerometer location was determined.

### Free Vibration of a Flexible Beam

The second experiment used to investigate the accelerometer measurement errors examines the free vibration of a flexible beam. An aluminum strip 2 inches wide, 0.0625 inches thick, and 58 inches long is suspended vertically from a clamped end condition. Three accelerometers are mounted on the beam such that the uppermost accelerometer is above the nodal location (0.395 m from the clamp), the lower accelerometer is below the nodal location (0.7644 m below the clamp), and the middle

accelerometer is moved along the length of the beam until the signal strength is zero.

The analytical solution [6] indicates that the nodal location is given by

$$g \phi'_i(x) = \omega_i^2 \phi_i(x) \quad (22)$$

where  $\phi_i(x)$  is the  $i$ th eigenfunction of the transverse vibration of a uniform beam

$$\phi_1(x) = (\sin \beta_1 L - \sinh \beta_1 L) (\sin \beta_1 x - \sinh \beta_1 x) + (\cos \beta_1 L + \cosh \beta_1 L) (\cos \beta_1 x - \cosh \beta_1 x) \quad (23)$$

and  $\beta_1$  is determined from

$$\cos \beta_1 L \cosh \beta_1 L + 1 = 0 \quad (24)$$

For the first mode, the nodal location is determined to be  $x = 0.417$  m, and the measured natural frequency of the beam for mode 1 vibrations is  $\omega = 6.596$  rad/s.

The measured nodal location is found to be 0.418 m which is in excellent agreement with the predicted value; the error is less than 0.3%. Furthermore, the accelerometer signals, shown in Fig. 4, shows the zero output of accelerometer 2 and the phase shift between the output of accelerometers 1 and 3. Clearly, the analytical model predicts the signed magnitude of the accelerometer output very well. Based upon this information, a predictor for the accelerometers has been incorporated into the observer design for the AFAL grid experiments [6].

#### Forced Beam Response

Finally, the accelerometer nodal location for a forced flexible beam was determined experimentally. The experimental setup was the same as in the previous example except that a shaker was included to excite the structure at a frequency of 8.86 rad/s. The data has been collected and the measured nodal point has been determined to be 0.453 m from the cantilever point. Notice that the nodal location has shifted due to the artificial stiffness induced by the shaker. The analysis of this problem must be done numerically (by finite element methods) and is currently under way. The ability to predict the nodal locations and compensate for measurement errors for a forced response will be vitally important to active control experiments using accelerometer signals in the control loop.

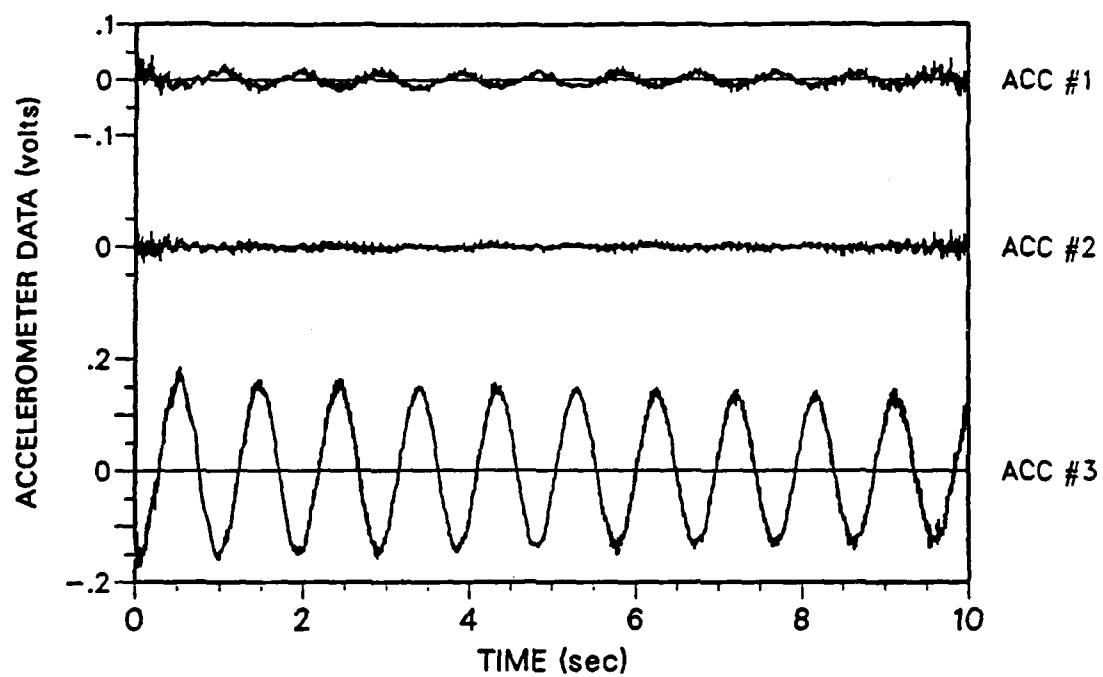


Figure 4. Free Response of a Flexible Beam

### Conclusions and Recommendations

Because of the prolonged search for the correct combination of materials and geometric configurations, the experimental phase of this research has not been completed. Although our search was not exhaustive, it is readily apparent that "off-the shelf" components for these experiments (with the single exception of aluminum tubing) do not exist. In order to verify the dynamic scaling concepts with experimental results, we propose that the experiments be conducted (initially at least) on cantilevered beams with solid cross-sections. For example, cylindrical rods or rectangular shapes could be used, since these components are much more readily available. In particular, the rectangular cross-sectional shapes can often be cut from sheet materials to any desired length and width. Because the scaling laws apply equally to any cross-sectional configuration, the specific article used in the experiments should be independent of the results.

With regard to the experimental research to be performed with the tripod structure, the aforementioned problems will continue to be an important issue. It may be necessary to further isolate the behavior that an experiment will be designed to investigate. For example, we may be interested only in the bending modes of a structure. Consequently the cross-sectional shape and area could be altered (in violation of the rules for dynamic scaling presented in this report) such that only bending mode frequencies remain unchanged. Obviously, this method will not allow the correct determination of nodal interactions and it is recommended only as a possible alternative for special cases. However, to completely investigate the behavior of a structure, it may be necessary to construct several different models where each is designed to aid the investigation of a specific type of behavior.

### References

1. Bridgman, P. W., Dimensional Analysis, Yale University Press, New Haven, 1963.
2. Goodier, J. N., Dimensional Analysis, Handbook of Experimental Stress Analysis, M. Hetenyi (Ed.), John Wiley and Sons, New York, 1950.
3. Shih, Choon-Foo, "Failure of Liquid Storage Tanks due to Earthquake Excitation," Ph.D. Dissertation, California Institute of Technology, Pasadena, California, 1981.
4. Morton, John, "Scaling of Impact Loaded Carbon Fiber Composites," 28th Structures, Structural Dynamics and Materials Conference, Monterey, CA, April 6-8, 1987.
5. Meirovitch, L. Computational Methods in Structural Dynamics, Sijthoff and Noordhoff, Rockville, Maryland, 1982.
6. Norris, M. A., Thompson, R. C., and Das, A., "Low-Frequency Response of Accelerometers for Observer Design in a Gravity Environment," unpublished paper submitted for review by the Journal of Guidance, Control, and Dynamics.

**Low Frequency Response of Accelerometers  
for Observer Design in a  
Gravity Environment**

## Low-frequency Response of Accelerometers for Observer Design in a Gravity Environment

M. A. Norris, R. C. Thompson and A. Das

Analytical and experimental results demonstrate that the dynamic effect of gravity degrades low-frequency accelerometer measurements. The motion of an accelerometer in a gravity field can cause the output signal to indicate a reversed phase relative to the actual acceleration of the point on the structure at which the sensor is mounted. The positions on the structure where the phase shift occurs are called accelerometer nodal locations, because the output of accelerometers located at these positions are theoretically zero. The effect is demonstrated analytically and experimentally using results from a pendulum and a two-dimensional grid structure. An observer is designed for the grid structure which uses the accelerometer measurements as input and compensates for the effect of gravity on the accelerometers. The observer performance including the dynamic effect of gravity on the accelerometer is compared to the performance of an observer using the output signal from the accelerometers without compensating for the gravity field degradation. The results show that the dynamic effect of gravity must be included in the observer design for low-frequency response estimates in a gravity environment.

### Introduction

Maneuver and vibration suppression strategies for flexible structures have received considerable attention in recent years. Numerous identification and control techniques have been proposed for active vibration suppression of large space structures (LSS) (Ref. 1-7). To test and evaluate the techniques, ground experiments must be performed to determine their practicality, performance and robustness.

The techniques require sensors to estimate the state of the structure to be used for identification and control strategies. Furthermore, in the test and evaluation phase, it is desirable to implement sensors that are suitable for space environment, so that the identification and control techniques can be evaluated using space-ready hardware.

A wide variety of sensors used to estimate the state of the structure include strain gauges, rate gyros, accelerometers, imbedded sensors, proximity sensors, and piezoelectric distributed (film) sensors. In this paper, we focus our attention on the application of accelerometers, and results are reported accordingly. We do not imply that any one type of sensor is more suitable than another. The accelerometer is advantageous for active vibration suppression of flexible structures due to its small size and low weight. In addition, the piezoelectric and piezoresistive accelerometers are becoming increasingly popular due to recent improvements in sensitivity to low-frequency response and in weight reduction.

We considered the applications of accelerometer measurements on a rigid-body and a two-dimensional grid structure in a 1-G environment. The ground experiments were conducted at the Air Force Astronautics Laboratory (AFAL) LSS laboratory. The AFAL experimental facility is used to verify and develop identification and control strategies for flexible structures (Ref. 8). Currently, structural vibrations are monitored using high-sensitivity, low-mass piezoelectric accelerometers and proximity sensors.

Initial results support the use of accelerometer measurements for ground-based testing of identification and control techniques. We consider the application where accelerometers are used to measure the



transverse vibration of the structure relative to static equilibrium. At low structural vibration frequencies in a gravity environment, the output of the accelerometers can provide unexpected results. The amplitude of the accelerometer output is dependent on the location of the accelerometer as one might expect. However, the relative motion of the accelerometer in the gravity field is interpreted as an acceleration of the structure and the output signal will include this additional component. For pendulum motion, the accelerometer output is decreased by the gravitational component and will be zero at a specific location on the pendulum. We call this location the accelerometer nodal location. For elastic motion of a structure, accelerometer nodal locations can be determined for certain modes of vibration, and predominantly occur in the lower modes of vibration. For the two-dimensional grid, the effect of gravity is to produce a 180 degree phase shift in the accelerometer output for the first mode of vibration, when comparing accelerometer outputs vertically above and below this nodal location.

This paper illustrates the dynamic effect of gravity on low-frequency accelerometer measurements, where the accelerometer translates and rotates in a gravity environment. The results are verified through analysis and experiment. The paper introduces the phenomenon by describing the accelerometer output for the case of pendulum motion. After introducing the equations of motion for flexible structures, the accelerometer nodal locations are determined analytically for elastic motion. To circumvent the gravity effect on the accelerometer output, an observer can be implemented as long as the mathematical model is an accurate representation of the structure. Furthermore, the observer

outputs are compared with and without the gravitational effect in the design and the outputs are compared using experimental data. In addition, analytical and experimental results using the two-dimensional grid structure illustrate the gravity effect.

#### Accelerometers in Pendulum Motion

We begin with the mechanical representation of a vibration measuring instrument as shown in Figure 1 (Refs. 9-11). The mass, damping, and spring stiffness of the instrument are denoted  $m$ ,  $c$ , and  $k$ , respectively. The displacement of the case, the displacement of the mass relative to the case, and the absolute displacement of the mass are denoted by  $y(t)$ ,  $z(t)$ , and  $x(t)$ , respectively, so that  $x(t) = y(t) + z(t)$ . The relative displacement  $z(t)$  is measured, which is used to infer the motion  $y(t)$  of the case. From Newton's second law, the equation of motion can be written as (Ref. 9)

$$m\ddot{x}(t) + c(\dot{x}(t) - \dot{y}(t)) + k(x(t) - y(t)) = 0 \quad (1)$$

which upon eliminating  $x(t)$  becomes

$$m\ddot{z}(t) + c\dot{z}(t) + kz(t) = -m\ddot{y}(t) \quad (2)$$

Note that the gravitational component of acceleration can be ignored as Eqs. (1) and (2) describe motion about the equilibrium position, where gravity is considered to be a static effect. The accelerometer parameters,  $m$ ,  $c$  and  $k$ , are designed such that  $\omega \ll \omega_n$ , where  $\omega$  and  $\omega_n$  denote the excitation frequency and the natural frequency of oscillation of the accelerometer, respectively. For harmonic motion of the case  $y(t)$ , it can be shown that Eq. (2) becomes (Ref. 11)

$$\omega_n^2 z \approx \omega^2 y \quad (3)$$

Hence, by measuring  $z$  and knowing  $\omega_n$ , the acceleration of the case  $\ddot{y} \approx -\omega_n^2 z$  can be determined.

Consider the case where the accelerometer rotates in a gravitational field (Fig. 2). As will become evident, gravity can no longer be considered a static effect. Using Newton's second law, Eq. (2) now has the form

$$m\ddot{z}(t) + c\dot{z}(t) + kz(t) = -m\ddot{y}(t) - mg\sin \theta(t) \quad (4)$$

We consider the case where the accelerometer is mounted to estimate the tangential component of acceleration along a rigid structure in pendulum motion. The tangential acceleration of the accelerometer casing is then  $\ddot{y} = \ell\ddot{\theta}$ , where  $\ell$  represents the radial distance from the accelerometer to the pendulum support. Using the small angle approximation  $\sin\theta = y/\ell$ , Eq. (4) becomes

$$m\ddot{z} + c\dot{z} + kz = -m(\ddot{y} + \frac{g}{\ell}y) \quad (5)$$

where we note that in pendulum motion, the angular displacement  $\theta(t)$  and the tangential acceleration  $\ddot{y}$  are harmonic with frequency  $\omega$ . It is now obvious that the acceleration due to gravity is no longer a static effect for small pendulum motion of the accelerometer. Hence, in the case of the accelerometer in pendulum motion, Eq. (3) becomes

$$\omega_n^2 z \approx (\omega^2 - \frac{g}{\ell})y \quad (6)$$

Equation (6) indicates that the dynamic effect of gravity is to reduce the output amplitude of the accelerometer. Figure 3 displays experimental results of three piezoelectric accelerometers mounted on a rigid bar in pendulum motion. The natural frequency of vibration of the pendulum, obtained experimentally, is  $\omega = 4.9$  rad/s. The three accelerometers are placed at locations  $\ell_1 = 0.34$  m,  $\ell_2 = 0.41$  m, and  $\ell_3 = 0.53$  m, respectively, along the rigid bar. Note that the output of the accelerometer at location  $\ell_2$  is nearly zero because  $\ell_2 \approx g/\omega^2$ , which designates the accelerometer nodal location for the

pendulum. In addition, note the 180 degree phase difference between the output of accelerometers located at  $x_1$  and  $x_3$ .

For structures in elastic vibration, the dynamic effect of gravity may also disturb the output of the accelerometers. For elastic motion, however, the relationship between the translation and rotation of the accelerometer is no longer kinematic as in the case of pendulum motion. In order to determine this relationship, we resort to the equations of motion. Indeed, accelerometer nodal locations for structures in elastic motion can be found using the equations of motion governing the structures, and they can be found for the modes of vibration individually. In the next section, we present the equations of motion for structures in elastic vibration.

#### Equations of Motion for Structures

The equations of motion of a flexible structure can be written in the form of a partial differential equation (Ref. 12)

$$\mathcal{L} u(P,t) + m(P)\ddot{u}(P,t) = f(P,t) \quad (7)$$

where  $u(P,t)$  is the displacement of point  $P$  in the domain  $D$ ,  $m(P)$  is the mass density and  $f(P,t)$  is the external force density. We consider the case in which the centrifugal forces can be ignored such that  $\mathcal{L}$  is a self-adjoint positive-definite differential operator representing the system stiffness. Moreover, we assume that structural damping and gyroscopic forces are small enough to be neglected. The displacement  $u$  must satisfy prescribed boundary conditions. Associated with Eq. (7), we have the eigenvalue problem

$$\mathcal{L} \phi(P) = m(P)\lambda_r \phi(P) \quad (8)$$

The solution to Eq. (8) consists of a denumerably infinite set of real eigenfunctions  $\phi_r(P)$  and associated real, positive eigenvalues  $\lambda_r$ , which

represent the mode shapes and square of the natural frequencies of oscillation, respectively. The infinite set of eigenfunctions are spatially orthogonal and can be normalized to satisfy the orthonormality conditions (Ref. 13). Using the expansion theorem (Ref. 13)

$$u(P,t) = \sum_{r=1}^{\infty} \phi_r(P) q_r(t) \quad (9)$$

and the orthonormality conditions, we can transform the equations of motion, Eqs. (7), into an infinite set of independent second-order ordinary differential modal equations

$$\ddot{q}_r(t) + \omega_r^2 q_r(t) = f_r(t) \quad (10)$$

where  $\omega_r^2 = \lambda_r$ ,  $\omega_r$  represent the natural frequencies of oscillation, and  $f_r(t)$  are modal forces given by

$$f_r(t) = \int_0 \phi_r(P) f(P,t) dD \quad (11)$$

#### Nodal Locations For Vibration-Measuring Instruments

In this section, we derive the accelerometer nodal locations for structures in elastic vibration, or nodal locations for any vibration-measuring instrument in which Eq. (4) holds. Before obtaining the nodal locations, we note that Eqs. (5) and (6) were obtained using the kinematic relation between the tangential and angular acceleration and assuming small motions of the pendulum about the static equilibrium position. For structures in elastic vibration, however, the relation between the acceleration  $\ddot{y}$  and the angular acceleration  $\ddot{\theta}(t)$  is no longer kinematic. To obtain the relation, we use the equations of motion of the structure.

In linear motion, the displacement of the structure is small enough so that we can assume that  $\ddot{y}$  coincides with the transverse

acceleration  $\ddot{u}_i = \ddot{u}(P_i, t)$  ( $i = 1, 2, \dots, m$ ) at a point  $P_i$  denoting the accelerometer location. Moreover,  $u_i$  represents the displacement from the static equilibrium position of the structure at a point  $P_i$ , so that  $\theta(t)$  in Eq. (4) represents any nominal rotation about the equilibrium point and is equal to  $u_i'$  ( $i = 1, 2, \dots, m$ ) as illustrated in Fig. (4), which is the local slope at  $P_i$  with respect to the static equilibrium position. Hence, Eq. (4) becomes

$$m\ddot{z}_i + c\dot{z}_i + kz_i = -m\ddot{u}_i - mg \sin(\alpha_i + u_i') \quad (12)$$

where  $z_i$  ( $i = 1, 2, \dots, m$ ) is the relative displacement of the  $i^{\text{th}}$  accelerometer and  $\alpha_i$  ( $i = 1, 2, \dots, m$ ) is a constant denoting the angle between the vertical and the tangent to the structure in equilibrium at accelerometer location  $P_i$ . We assume that  $\alpha_i$  ( $i = 1, 2, \dots, m$ ) can be computed from a static analysis. Using a small angle approximation in  $u_i'$ , Eq. (12) becomes

$$m\ddot{w}_i + c\dot{w}_i + kw_i = -m\ddot{u}_i - mg(\cos \alpha_i)u_i' \quad (13)$$

where  $w_i = z_i + mgs\sin\alpha_i/k$  ( $i = 1, 2, \dots, m$ ) denotes the motion of mass  $m$  in the accelerometer about its static equilibrium position. Note that for an accelerometer mounted vertically with  $\alpha_i = \frac{\pi}{2}$  in Eq. (13), the dynamic effect of gravity is negligible. The dynamic effect of gravity is greatest for values  $\alpha_i = 0$ .

The accelerometer is a vibration-measuring instrument designed such that the excitation frequency  $\omega$  is much smaller than the natural frequency  $\omega_n$  of the accelerometer  $\omega \ll \omega_n$ , so that inertia and damping forces in Eq. (13) may be neglected because they are quite small in comparison to the elastic spring force of the accelerometer. Hence, Eq. (13) becomes

$$a_i = -\omega_n^2 w_i = \ddot{u}_i + g(\cos \alpha_i)u_i', \quad i = 1, 2, \dots, m \quad (14)$$

where  $a_i$  represents the output of the  $i^{\text{th}}$  accelerometer. Using Eqs. (9), (10) and (14), the accelerometer output  $a_i$  is then

$$a_i = \sum_{r=1}^m \{ [g(\cos \alpha_i) \phi_r'(P_i) - \omega_r^2 \phi_r(P_i)] q_r(t) + \phi_r(P_i) f_r(t) \}, \quad i = 1, 2, \dots, m \quad (15)$$

where  $\phi_r'(P_i)$  represents the slope of the  $r^{\text{th}}$  mode of vibration at  $P_i$ . We consider the case of free vibration; i.e.,  $f_r(t) = 0$  ( $r = 1, 2, \dots$ ). At the accelerometer location  $P_i$  where  $g\phi_r'(P_i) = \omega_r^2 \phi_r(P_i)$ , the accelerometer output does not include the contribution to the acceleration of the  $r^{\text{th}}$  mode. Hence, nodal accelerometer locations exist for modes of vibration that satisfy  $g\phi_r'(P_i) = \omega_r^2 \phi_r(P_i)$ . Examining Eq. (15), for higher natural frequencies the effect of gravity may be negligible due to the domination of  $\omega_r^2$ , so that accelerometer nodal locations occur predominantly in the lower modes of vibration.

#### Observer Implementation

In this section, we develop an observer which uses as input accelerometer measurements. In general, the motion of a structure can be expressed as a linear combination of the lower modes of vibration because a large amount of energy is required to excite the higher modes. We consider a modal observer using only the lower modes of vibration.

The modal-state estimator has the form (Ref. 7)

$$\dot{\hat{\mathbf{y}}} = \mathbf{A}\hat{\mathbf{y}} + \mathbf{B}\mathbf{f} + \mathbf{K}(\mathbf{a} - \hat{\mathbf{a}}) \quad (16)$$

where  $\hat{\mathbf{y}} = [\hat{q}_1 \ \hat{q}_2 \ \dots \ \hat{q}_n \ \dot{\hat{q}}_1 \ \dot{\hat{q}}_2 \ \dots \ \dot{\hat{q}}_n]^T$  is the state estimate vector,  $\mathbf{f} = [f_1 \ f_2 \ \dots \ f_n]^T$  is the modal force vector,  $\mathbf{a} = [a_1 \ a_2 \ \dots \ a_m]^T$

and  $\hat{\underline{a}} = [\hat{a}_1 \ \hat{a}_2 \ \dots \ \hat{a}_m]^T$  are the m-dimensional accelerometer output and estimated accelerometer output vectors, respectively, and A, B are plant matrices given by

$$A = \begin{bmatrix} 0 & \vdots & I \\ -\Lambda & \vdots & 0 \end{bmatrix}, \quad B = \begin{bmatrix} 0 \\ \vdots \\ I \end{bmatrix} \quad (17)$$

Note that I is the nxn identity matrix, 0 is an nxn null matrix and  $\Lambda$  is an nxn diagonal matrix of eigenvalues corresponding to the lowest n modes of vibration. Furthermore, the matrix K is the observer gain matrix. If the system is treated as deterministic, Eq. (16) represents a Luenberger observer. If stochastic signals are considered, the gain matrix K may be designed to satisfy a Riccati equation in which case Eq. (16) represents a Kalman filter (Ref. 14). The associated output equation has the form

$$\hat{\underline{a}} = C\underline{v} + D\underline{f} \quad (18)$$

where C and D are mx2n and mxn dimensional matrices, respectively, and from Eq. (15) their entries are given by

$$\begin{aligned} C_{rs} &= 0, \quad D_{rs} = \phi_s(P_r), \quad r = 1, 2, \dots, m; \\ &\quad s = 1, 2, \dots, n \\ C_{rs} &= g(\cos \alpha_r) \phi_s'(P_r) - \omega_s^2 \phi_s(P_r), \quad r = 1, 2, \dots, m; \\ &\quad s = n+1, n+2, \dots, 2n \end{aligned} \quad (19)$$

A necessary condition for observability of the modal-estimator requires that the matrix C contain only n zero columns.

#### Analytical and Experimental Results

To determine the effects of gravity on the accelerometer measurements, an observer was implemented for the AFAL Grid structure (Ref. 8). The two-dimensional AFAL Grid structure is illustrated in Fig. 5. The observer was a modal-state estimator given by Eqs. (16) and



(17). The model used in the observer included the first four modes of vibration provided by a Nastran model of the Grid structure. To test the observer, both analytical and experimental results were considered. In the analytical tests, the free-response was used where the plant and observer model contained no damping. For the experimental tests, damping was added to the first mode of vibration of the observer model. The amount of damping was determined experimentally. The structure was excited using an electromagnetic shaker with frequency approximately equal to the first natural frequency of the structure, so that the response consisted mainly of the first mode of vibration. Four accelerometers  $a_i$  ( $i = 1,2,3,4$ ) and one shaker were placed as shown in Fig. 5, where the structure is suspended vertically so that  $\alpha_i = 0$  ( $i = 1,2,3,4$ ) in Eq. (19). The output equation for the observer is given by Eq. (18).

We consider two cases in the analysis. In the first, the plant simulation and observer are constructed without the gravitational effect and in the second, the dynamic effect of gravity on the accelerometers is included. In both cases, we use the free response where the initial conditions of the plant were designed such that the response consisted of the first mode of vibration only. Figure 6 shows the output of the observer when the gravitational effect is not included, so that  $g = 0$  in Eq. (18). Figure 7 includes the dynamic effect of gravity, where the phase shift between the accelerometer outputs is obvious. The poles of the observer were placed in the left-half of the complex plane so that the observer output converged to the plant response quickly. In addition, the simulation contained no noise, hence, the plant response is nearly identical to the observer output. In this manner, we

illustrate that the observer formulation given by Eqs. (16)-(19) does converge to the plant simulation. Comparison of Figs. 6 and 7 reveals that the dynamic effect of gravity is to cause a phase shift in accelerometer  $a_1$ . Moreover, Fig. 7 shows that the accelerometer nodal location for the first mode of vibration of the Grid exists between  $a_1$  and  $a_2$ , where these locations are illustrated in Fig. 5.

Figure 8 presents experimental data where the structures response mainly consisted of the first mode of vibration due to the resonance excitation of the shaker. Note the phase shift between  $a_1$  and the remaining accelerometer outputs. We use the steady-state accelerometer outputs shown in Fig. 8 as input to the observer. It was necessary to add damping to the first mode of vibration of the observer, due to the resonance excitation of the structure which is used as input to the observer through Eqs. (16) and (18). Furthermore, the damping added was experimentally observed for the first mode of vibration. The observer gains were computed using the solution of a Riccati equation with appropriate values for the noise intensities of the shaker and accelerometers, so that the observer is actually a Kalman filter.

For the experimental tests, we consider two cases. In the first, the observer was constructed by ignoring the gravitational effect on the accelerometer output using  $g = 0$  in Eq. (19). In the second case, the dynamic effect of gravity on the accelerometer output is included. The steady-state output for the observer design ignoring gravity is shown in Fig. (9). Note that the observer predicts the accelerometer outputs to be in-phase, similar to Fig. 6. To predict the phase-shift in accelerometer  $a_1$ , we must include the dynamic effect of gravity on the accelerometers in the observer. The steady-state observer output

including gravity is shown in Fig. 10. In this second case, the observer predicts a phase shift in accelerometer  $a_1$ , which is compatible with the experimental data. Comparing Figs. 8 and 10, we note that the amplitudes of the accelerometer outputs predicted by the observer do not match the experimental data. This is due to the disagreement between the model and the actual structure. Namely, the damping in the actual structure has been experimentally observed to be nonlinear. Moreover, the additional dynamics of the shaker are not included in the Nastran model. We recognize that the attachment of the shaker to the structure alters the natural frequencies and mode shapes of the system. Consequently, a more accurate observer model should include the additional dynamic constraints caused by the shaker.

#### Conclusions

Analytical and experimental results demonstrate the low-frequency response of accelerometers in a 1-G environment. It is concluded that for low-frequency response measurements, the dynamic effect of gravity on the accelerometer response cannot be ignored. The effect is demonstrated experimentally for pendulum motion and elastic vibration of the AFAL two-dimensional Grid structure. Furthermore, the results of analysis and experiment show that accelerometer nodal locations exist and predominantly occur in the lower modes of vibration. An observer is formulated to include the dynamic effect of gravity on the accelerometer measurements and is compared to an observer which ignores the effect of gravity. The observer is constructed for the AFAL Grid structure, and experimental results indicate that the dynamic effect of gravity on accelerometer measurements should be included in the observer design.

### Acknowledgements

Research sponsored by the Air Force Office of Scientific Research/AFSC, United States Air Force, under Contract F49620-87-R-0004. The United States Government is authorized to reproduce and distribute reprints for governmental purposes notwithstanding any copyright notation hereon.

In addition, the authors acknowledge L. Carter of the Aerospace Engineering Department, Virginia Polytechnic Institute and State University, Blacksburg, VA, for programming the simulations and generating some of the figures.

### References

1. Proceedings of the First VPI&SU/AIAA Symposium on Dynamics and Control of Large Structures, Blacksburg, VA, June 1977.
2. Proceedings of the Second VPI&SU/AIAA Symposium on Dynamics and Control of Large Structures, Blacksburg, VA, June 1979.
3. Proceedings of the Third VPI&SU/AIAA Symposium on Dynamics and Control of Large Structures, Blacksburg, VA, June 1981.
4. Proceedings of the Fourth VPI&SU/AIAA Symposium on Dynamics and Control of Large Structures, Blacksburg, VA, June 1983.
5. Proceedings of the Fifth VPI&SU/AIAA Symposium on Dynamics and Control of Large Structures, Blacksburg, VA June 1985.

6. Proceedings of the Sixth VPI&SU Symposium on Dynamics and Control of Large Structures, Blacksburg, VA, June 1987.
7. Balas, M. J., "Active Control of Flexible Systems," Journal of Optimization Theory and Applications, Vol. 25, No. 3, 1978, pp. 415-436.
8. Das, A., et. al., "Experiment and Parameter Estimation of Flexible Structures," Second NASA/DOD CSI Technology Conference, November 17-19, 1987.
9. Meirovitch, L. Elements of Vibration Analysis, McGraw-Hill, New York, N.Y., 1986.
10. Vierck, R. K., Vibration Analysis, Harper & Row, New York, N.Y., 1966.
11. Doebelin, E. D., Measurement Systems, McGraw-Hill, New York, N.Y., 1966.
12. Meirovitch, L. and M. A. Norris, "Parameter Identification in Distributed Spacecraft Structures," The Journal of the Astronautical Sciences, Vol. 34, No. 4, October-December, 1986, pp. 341-353.
13. Meirovitch, L., Computational Methods in Structural Dynamics, Sijthoff & Noordhoff, The Netherlands, 1980.
14. Junkins, J. L., An Introduction to Optimal Estimation of Dynamical Systems, Sijthoff & Noordhoff, The Netherlands, 1976.

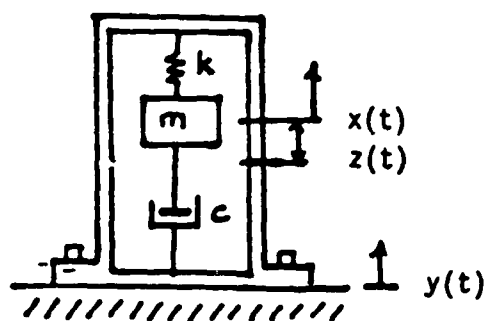


Fig. 1. Vibration Measuring Instrument

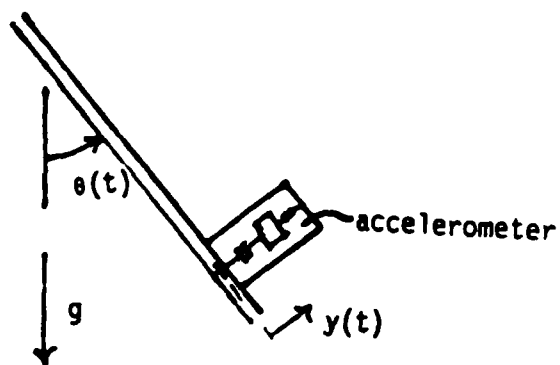


Fig. 2. Accelerometer in Pendulum Motion

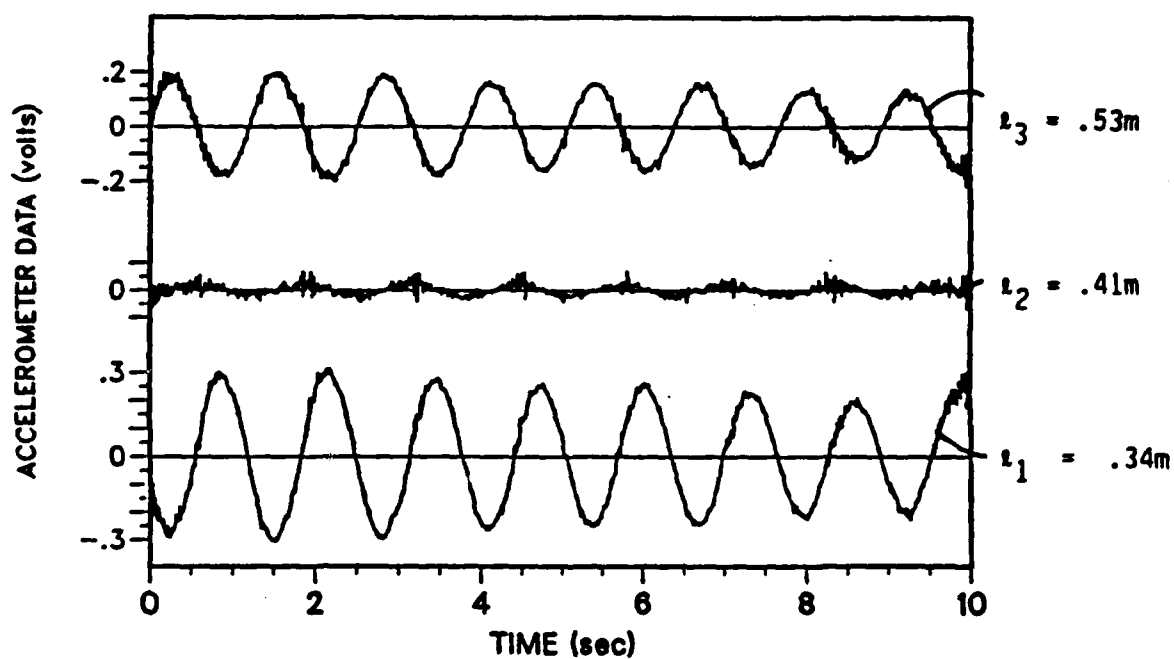


Fig. 3. Accelerometer Outputs For Pendulum Motion

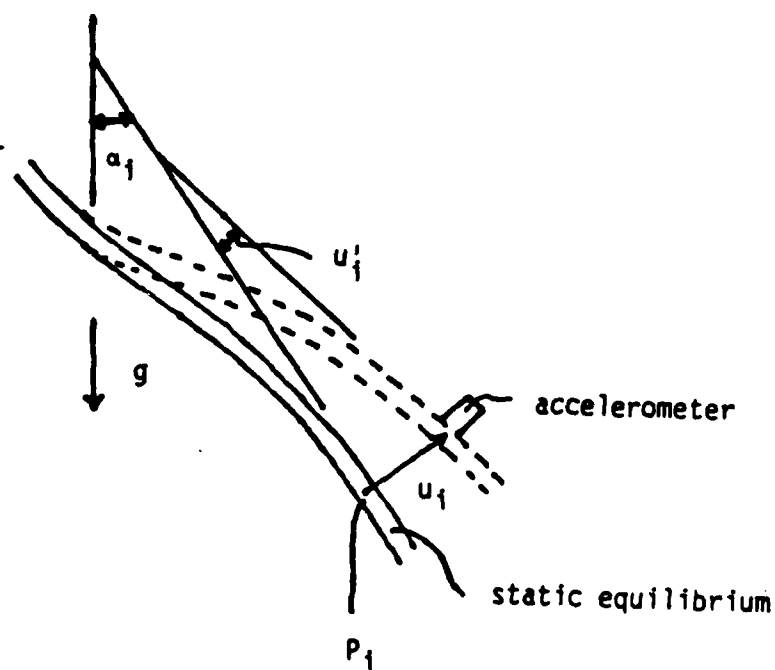


Fig. 4. Accelerometer Mounted on a Flexible Structure in 1-G.

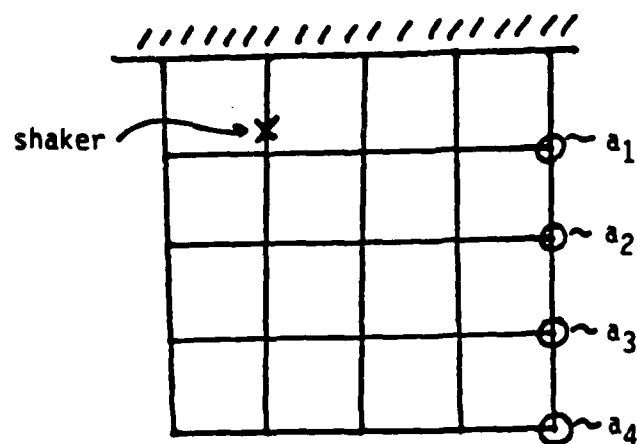


Fig. 5. AFAL Grid Illustration

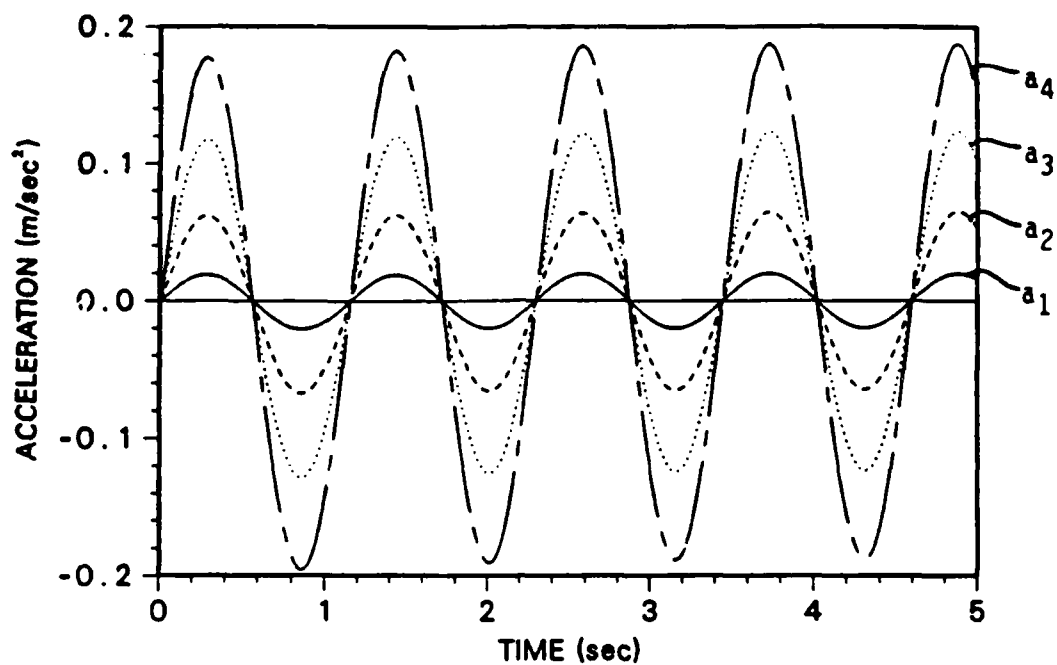


Fig. 6. Analytical Observer Response: Gravitational Effects Not Included.

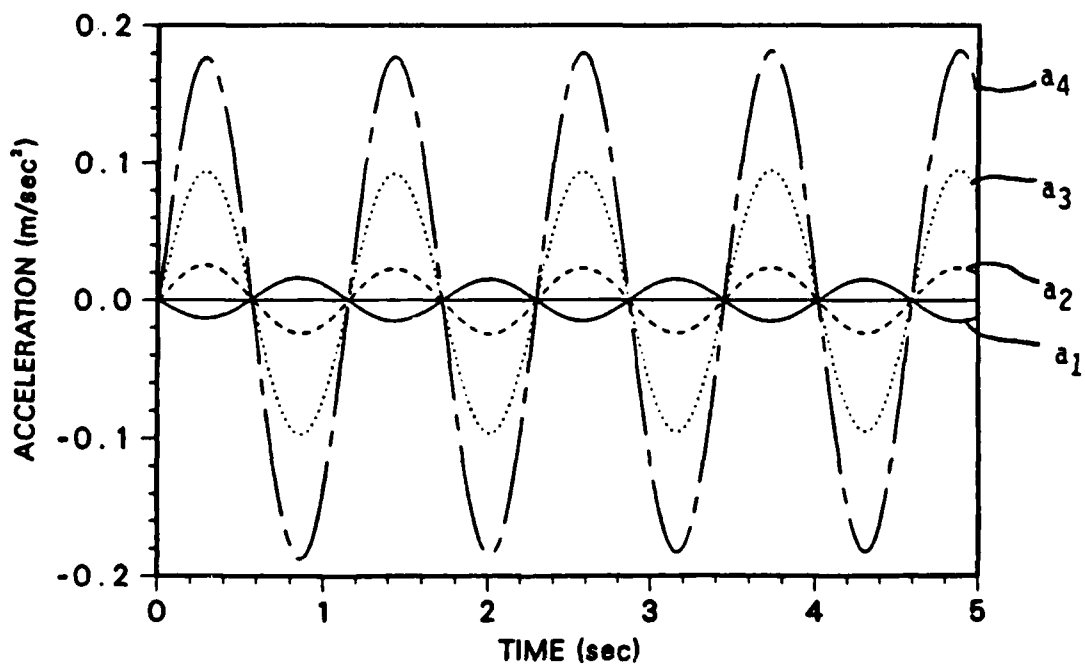


Fig. 7. Analytical Observer Response: Gravitational Effect Included.



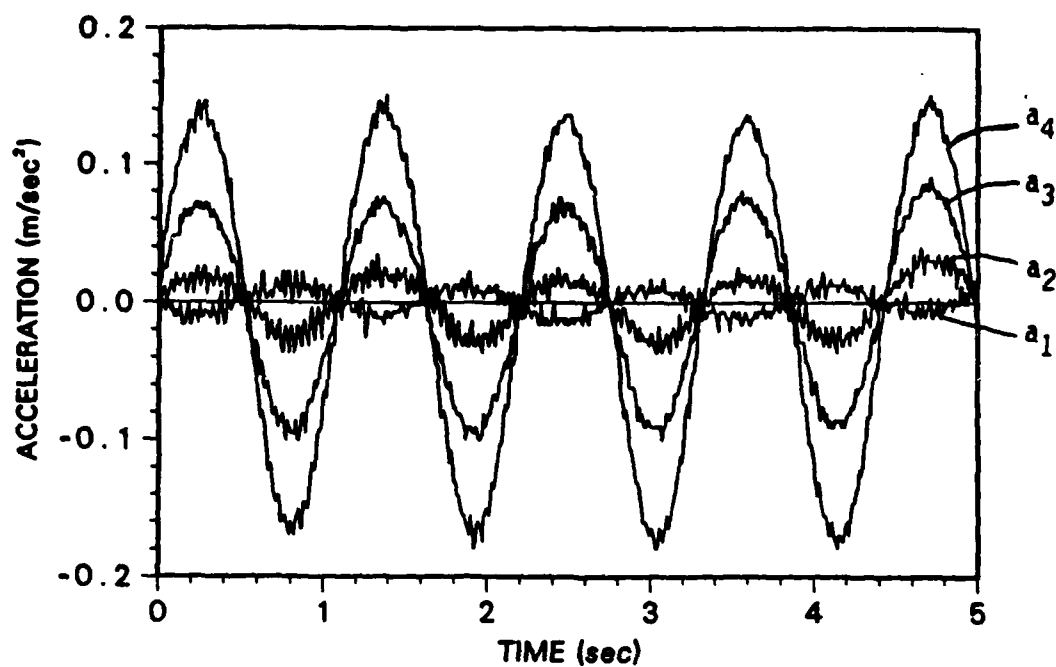


Fig. 8. Experimental Grid Response to Resonance Excitation of Mode 1.

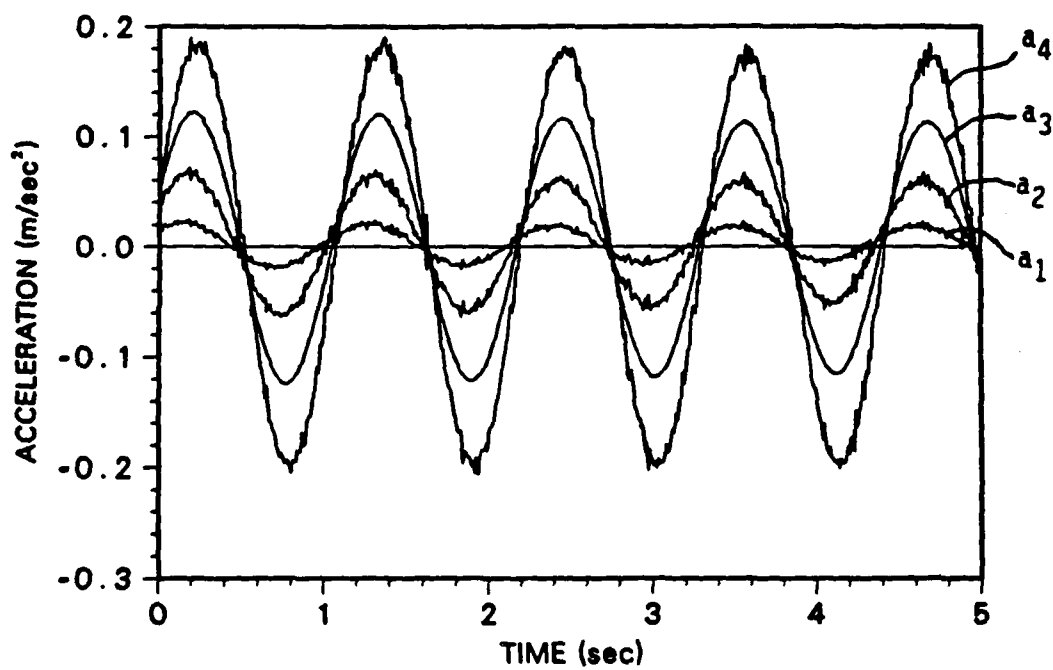


Fig. 9. Experimental Observer Response: Gravity Not Included.

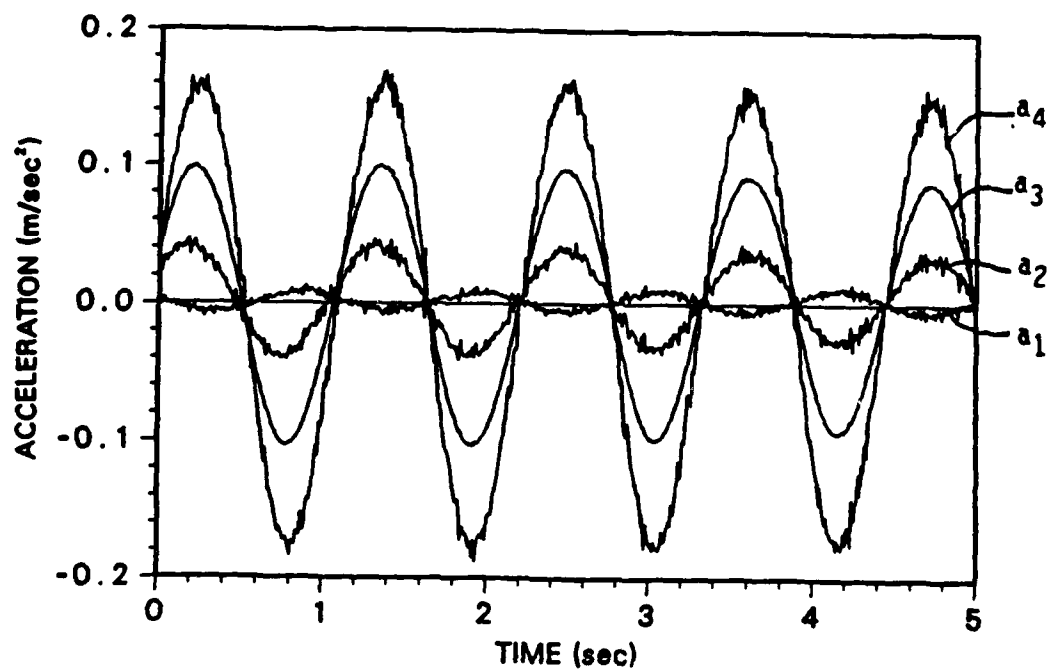


Fig. 10. Experimental Observer Response: Gravity Included.